



21283/931A 3750 PCT

IN THE UNITED STATES PATENT AND TRADEMARK OFFICE

In re application of:

ZHENGHE HAN et al.

Serial No: 10/541,296

Filed: July 6, 2005

For: SURFACE MODIFICATION
METHOD IN FABRICATING HIGH
TEMPERATURE SUPER
CONDUCTIVE DEVICES

Art Unit: 1793

Examiner: Paul A. Wartalowicz

APPEAL BRIEF

Honorable Commissioner of Patents & Trademarks
P.O. Box 1450
Alexandria VA 22313-1450

Dear Sir:

This is an appeal from the Final rejection dated April 13, 2009, from the Examiner of Group Art Unit 1793 rejecting the claims 1 through 13 and 15 through 18 of the above-identified patent application.

REAL PARTY IN INTEREST:

The party named in the caption of the brief is the inventor; however, the inventor has assigned all of his right, title and interest to Applied Superconductivity Research Center, Tsinghua University who is now still the owner of this invention and this patent application.

RELATED APPEALS AND INTERFERENCES:

To the best of Appellant's and Appellant's legal representatives' or Assignee's knowledge, there are no Appeals or interferences which will directly affect or be directly affected by or have any bearing on the Board's decision in this pending appeal.

STATUS OF THE CLAIMS:

A. Rejection of the Claims on Reference Grounds:

1. The Examiner has rejected the claims 1, 5, 9, 10 through 13 and 17 under 35 USC 102 as being anticipated by or, in the alternative under 35 USC 103 as being obvious over Hebard stating that Hebard teaches a process wherein a superconductor material is treated at the claimed energy and incidence angle wherein the ions are chosen from the claimed elements and an ion beam generator by the prior art of Hebard is substantially similar to plasma sputtering.

2. The Examiner has rejected the claims 1 through 4, 6, 8, 10 through 13 and 16 under 35 USC 102 as being anticipated by or, in the alternative, under 35 USC 103 as being obvious over Reade et al. stating that Reade et al. teaches a method for ion texturing superconductor devices wherein the materials to be textured include MgO, YSZ, nickel alloys, etc. wherein an ion beam at the claimed energies and claimed angles are disclosed and plasma sputtering is the same as an ion beam.

3. The Examiner has rejected the claims 1, 5, 9, 10 through 13 and 17 under 35 USC 103 as being obvious over Hebard in view of Desu et al. and Kroger stating that Hebard discloses all of the present invention except for plasma sputtering in an argon plasma; Desu et al. teaches a method of etching a thin film utilizing ion beam etching, plasma etching and sputtering etching and it is the Examiner's opinion that plasma sputtering is substantially the same thing or equivalent to sputtering etching; Kroger teaches that it is well known to treat substrate with sputter etching in an argon plasma; and it would have been obvious to one of ordinary skill in the art to modify Hebard in view of the teachings of Desu et al. and Kroger.

4. The Examiner has rejected the claims 1 through 4, 6, 8, 10 through 13 and 16 under 35 USC 103 as being obvious over Reade et al. in view of Desu et al. and Kroger stating that Reade et al. teaches a method for ion texturing superconducting devices utilizing an ion beam; Desu et al. teaches

sputtering etching which in the Examiner's opinion is the equivalent of plasma etching; Kroger teaches a method for making a superconductor wherein it is known to treat the substrate with super etching in an argon plasma; therefore, it is the Examiner's opinion that Applicant's invention would be obvious over Reade et al. in view of Desu et al. and Kroger.

5. The Examiner has rejected the claims 15 and 18 under 35 USC 103 as being obvious over Hebard in view of Chu et al. stating that Hebard discloses all of the present invention except for annealing; Chu et al. teaches a method of making superconductors wherein the superconductor is annealed after ion texturing for the purposes of restoring crystallinity; and it would have been obvious to one of ordinary skill in the art to modify Hebard in view of the teachings of Chu et al.

6. The Examiner has rejected the claim 7 under 35 USC 103 as being obvious over Reade et al. in view of Doi et al. and Shindo et al. stating that Reade et al. fails to teach texturing superconductors; Shindo et al. teaches a method of making a solar cell where it is known to texture the claimed semiconductors; Doi et al. teaches to utilize GaAs as a substrate for a superconductor; and it would have been obvious to one of ordinary skill in the art to modify Reade et al. in view of the teachings of Shindo et al. and Doi et al.

7. The Examiner has rejected the claims 15 and 18 under 35 USC 103 as being obvious over Hebard in view of Chu et al. and Desu et al. or Kroger stating that the combination thereof discloses all of Applicant's invention.

8. The Examiner has rejected the claim 7 under 35 USC 103 as being obvious over Reade et al. in view of Doi et al. and Shindo et al. and Desu et al. or Kroger stating that the combination would be all of Applicant's invention.

B. Claim 14 has been canceled without prejudice.

STATUS OF THE AMENDMENT:

Applicant filed a Response on July 13, 2009 to the Final Rejection dated April 13, 2009. The Response was entered and considered by the Examiner but an Advisory Action was issued on July 27, 2009 maintaining the rejection of the Final Office Action.

SUMMARY OF THE CLAIMED SUBJECT MATTER:

The present invention comprises a method for surface modification in the manufacture of high temperature superconducting devices as claimed by claim 1 and a high temperature superconducting device as claimed by Appellant's claim 17 (see page 6, lines 3-34). In the method the surface of a material is bombarded with a particle beam having energy to increase the smoothness of the material surface and change the microstructure of the processed material (see page 7, lines 1-3) and generating a particle beam by a plasma sputtering device with energy in the range of 5-50,000 eV (see page 7, lines 4 and 5). In addition the material may be a metal material such as Ni, NiO, Ni alloy, Cu, Cu alloy, Ag, Ag alloy, Fe, Fe alloy, Mg and Mg alloy (see page 7, lines 12 and 13), a semiconductor material such as Si, Ge, GaAs, InP, InAs, InGaAs, CdS, GaN, InGaN, GaSb and InSb (see page 7, lines 15 and 16) and any one of an oxide material such as SrTiO₃, LaAlO₃, Y₂O₃, RuO₂, CeO₂, MgO, ZrO₂, SiO₂, Al₂O₃ and YSZ (see page 7, lines 17-18). Still further, the material may be any super conducting material such as YBa₂Cu₃O_{7-δ}, REZ₂Cu₃O_{7-δ}, Bi-Sr-Ca-Cu-O and TI-Ba-Ca-Cu-O (see page 7, lines 18-20).

REFERENCES CITED:

A. Hebard (U.S. 4,966,885)

Applicant has carefully reviewed Hebard and respectfully submits that Hebard (US 4966885) discloses a method for producing an article comprising a thin film of a planar metal oxide superconductor, and the thinning the film comprises exposing the film to an ion beam. In contrast thereto, Applicants invention uses one beam from a plasma sputtering device. Still further, Applicant respectfully submits that Hebard does not disclose or suggest that the particle beam is generated by a plasma sputtering device; and the method of amended claim 1 is different from the cited Hebard and has advantages thereover. Particularly,

compared with an ion beam, the plasma sputtering can be performed on a larger area of the material surface, and is much more effective to increase the smoothness of the material surface and change the microstructure or internal defect of the processed material. Compared with an ion beam gun for providing the ion beam, the plasma sputtering apparatus is simpler, can be installed more easily, is at much lower cost and is suitable for mass industrial production.

B. Reade et al. (U.S. 6,809,066)

Applicant has carefully reviewed Reade et al. and respectfully submits that Reade et al. (US 6809066) discloses a method of ion texturing a noncrystalline surface, and the exposing the noncrystalline surface to at least two ion beams to texture the noncrystalline surface. In contrast thereto, Applicants invention uses one beam from a plasma sputtering device. Still further, Applicant respectfully submits that Reade et al. does not disclose or suggest that the particle beam is generated by a plasma sputtering device; and the method of amended claim 1 is different from Reade et al. and has advantages there over. Particularly, compared with an ion beam, the plasma sputtering can be performed on a larger area of the material surface, and is much more effective to increase the smoothness of the material surface and change the microstructure or internal defect of the processed material. Compared with an ion beam gun for providing the ion beam, the plasma sputtering apparatus is simpler, can be installed more easily, is at much lower cost and is suitable for mass industrial production.

C. Desu et al. (U.S. 5,873,977)

Appellant has carefully reviewed Desu et al. and respectfully submits that Desu et al. teaches a method of etching a film utilizing sputtering etching to remove material (see column 3, lines 42-53). However, sputtering etching removes surface material and is not the equivalent of the plasma sputtering of Applicant's invention because the main purpose of plasma sputtering is to increase the smoothness of the material surface and change the microstructure or internal defect of the processed material rather than to mainly remove material from the surface, which is the main purpose of sputtering etching.

D. Kroger (U.S. 4,536,414)

Appellant's careful review of Kroger indicates that as admitted by the Examiner it teaches sputter etching but in an argon plasma. Again, Appellant respectfully submits that sputter etching is not the same as plasma sputtering or the equivalent thereof since its main purpose is to remove material (as is admitted by Desu et al. at column 3, lines 42-53) and does not function in the manner of the plasma sputtering of Applicant's invention.

E. Chu et al. (U.S. 6,251,835)

In addition, Appellant has carefully reviewed Chu et al. and respectfully submits that while it may teach a method of making superconductors, it teaches a method of first smoothing the HTS surface by gas cluster ion beams (GCIB) bombardment followed by annealing in a partial pressure of oxygen to re-grow the damaged surface layer. However, the ion beam technique utilized to generate the GCIB (column 1, line 7) is different from the plasma sputtering in Appellant's invention as mentioned above. Accordingly, Appellant respectfully submits that Chu et al. does not function in the manner of Appellant's invention.

F. Doi et al. (U.S. 6,316,391)

Still further Appellant has reviewed Doi et al. and respectfully submits that Doi et al. teaches superconductive substrates that have a curved structure, but does not teach a manufacturing or modification thereof. Also, Appellant respectfully submits that Doi et al. does not teach that GaAs can act as a substrate for high temperature superconductors. Still further, Appellant respectfully submits that Doi et al. does not function in the manner of the plasma sputtering of Appellant's invention.

G. Shindo et al. (U.S. 5,738,731)

Appellant has reviewed Shindo and respectfully submits that it relates to the production of solar cells which are not a semiconductor in the sense of Appellant's or Reade's invention. Still further Shindo uses a plurality of beams and not one beam as in Appellant's invention.

GROUND OF REJECTION TO BE REVIEWED ON APPEAL:

A. The claims 1, 5, 9, 10 through 13, and 17 are rejected under 35 USC 102 as being anticipated by or, in the alternative, under 35 USC 103 as being obvious over Hebard and it is Appellant's position that Hebard does not disclose each and every element of Appellant's invention as claimed and/or all of the elements of the claimed invention are not obvious from the teachings of Hebard.

B. The claims 1 through 4, 6, 8, 10 through 13 and 16 are rejected under 35 USC 102 as being anticipated by or, in the alternative, under 35 USC 103 as being obvious over Reade et al. and it is the Appellant's position that all of the elements of the claimed invention are neither shown by or suggested by Reade et al.

C. The claims 1, 5, 9 10 through 13 and 17 are rejected under 35 USC 103 as being obvious over Hebard in view of Desu et al. and Kroger and it is Appellant's position that the combination suggested by the Examiner is not only not Appellant's invention but also would not have been suggested to one of ordinary skill in the art.

D. The claims 1 through 4, 6, 8, 10 through 13 and 16 are rejected under 35 USC 103 as being obvious over Reade et al. in view of Desu et al. or Kroger and it is Appellant's position that the combination suggested by the Examiner is not only not Appellant's invention but also would not have been suggested to one of ordinary skill in the art.

E. Claims 15 and 16 are rejected under 35 USC 103 as being obvious over Hebard in view of Chu et al. and it is Appellant's position that the combination suggested by the Examiner is not Appellant's invention.

F. Claim 7 is rejected under 35 USC 103 as being obvious over Reade et al. in view of Doi et al. and Shindo et al. and it is Appellant's position that the combination suggested by the Examiner is not only not Appellant's invention but also would not have been suggested to one of ordinary skill in the art.

G. The Examiner has rejected the claims 15 and 18 under 35 USC 103 as being obvious over Hebard in view of Chu et al. and Desu et al. or Kroger and it is Appellant's position that the combination suggested by the Examiner is not only not Appellant's invention but also would not have been suggested to one of ordinary skill in the art.

H. The claim 7 is rejected under 35 USC 103 as being obvious over Reade et al. in view of Doi et al. and Shindo et al. and Desu et al. or Kroger and it is Appellant's position that the combination suggested by the Examiner is not only not Appellant's invention but also would not have been suggested to one of ordinary skill in the art.

GROUPING OF THE CLAIMS:

The claims in each group stand or fall together.

ARGUMENT:

A. The rejection of claims 1, 5, 9, 10 through 13 and 17 under 35 USC 102 as being anticipated by or, in the alternative, under 35 USC 103 as being obvious over Hebard

It is the Examiner's position that there is no structural difference between the particle beam of the prior art and the particle beam of Appellant's invention, namely plasma sputtering. However, Appellant respectfully submits that there are basic differences which are generally acknowledged by science and technology researchers. A detailed description of these two different concepts can be found in the two books in this research field namely: "Thin film processes", by John L. Vossen and Werner Kern, New York, Academic Press, 1978, and "Glow discharge processes", by Brian Chapman, New York, Wiley, 1980 (copies of which are enclosed herewith).

Appellant respectfully submits that in Hebard, cited by the Examiner, the ion beams are produced by ion guns, also referred to as ion sources. However, in Appellant's invention, plasma sputtering is carried out by plasma sputtering systems. Appellant respectfully submits that these two techniques, ion beam and plasma sputtering, are widely used for both sputtering and depositions. The energetic particles generated by the ion guns or plasma sputtering systems can knock atoms out of the surface of the target. While it can be concluded that sputtering and sputtering deposition have similar theory and systems with merely different purposes, Appellant respectfully submits that either sputtering or sputtering deposition, the two techniques, ion beam and plasma sputtering, are always strictly distinguished.

In particular, the plasma sputtering technique is usually carried out in a

vacuum system in which discharge occurs. In a conventional plasma sputtering system, a DC voltage is utilized, the material to be sputtered is made into a target which becomes the cathode of an electric circuit and has a negative voltage applied to it. The particles generated from the discharge gas are accelerated towards the target to produce the sputtering (see pages 187 through 188 of "Glow Discharge Processes" by Brian Chapman and pages 12 through 14 of "Thin Film Processes" by Vossen and Kern). For some materials, an AC voltage is required to accelerate the particles (see page 195 of "Glow Discharge Processes" by Chapman and pages 27 through 29 of "Thin Film Processes" by Vossen and Kern). Still further, the magnetic field effects are used quite a lot in sputtering systems, which provides advantages in sputtering rate, extendibility of operating range and so on. As a result, Appellant respectfully submits that different types of magnetically enhanced plasma sputtering systems, such as cylindrical magnetron sputtering, circular magnetron sputtering, planar magnetron sputtering, etc. are utilized. (see pages 260-270 in the book of "Glow discharge processes" by Brian Chapman and pages 76-170 in the book of "Thin film processes" by Vossen and Kern) Still further, plasma sputtering usually can effect a rather large area.

As can be seen from the references to Vossen, Kern and Chapman, when sputtering or sputter deposition is introduced, ion beam systems are always separate from the plasma sputtering system since the energetic particles are generated by special equipment, namely ion guns, in an ion beam system. In particular, Appellant respectfully submits that the ion gun is a device in which gas ions are produced, omitted, accelerated and focused as a rather narrow beam. Acceleration takes place mainly in the extracted region since this is usually where the greatest potential drop exists. The focus system of the ion sources can adjust the divergence of the ion beam. It can be concluded therefore that there are quite significant differences in the generation of the energetic particles between ion beam systems and plasma sputtering systems (see pages 175 through 189 in "Thin Film Processes"). Appellant respectfully submits that the ion beam sputtering usually treats smaller areas relative to plasma sputtering, depending on the diameter of the ion gun. The particles of the ion beam are better parallel focused and non-energetic while requiring a more expensive facility. Also, ion guns are relatively expensive and require lower pressure in a vacuum facility and some gases, such as oxygen should be avoided to protect the ion gun. Therefore, compared with an ion beam gun for providing the ion beam, the plasma sputtering apparatus

is simpler, can be installed more easily, is at much lower cost and is suitable for mass industrial production.

In view of the above, therefore, Appellant respectfully submits that ion beam systems are not the same or a substitute for plasma sputtering systems.

Therefore, Appellant respectfully submits that Hebard does not show or suggest the use of a particle beam generated by a plasma sputtering device for surface modification in manufacturing high temperature superconducting devices. Therefore, Appellant respectfully submits that this critical element of Appellant's invention is neither shown nor suggested by Hebard and the claims 1, 5, 9, 10 through 13 and 17 are not anticipated or obvious thereover.

B. The rejection of claims 1 through 4, 6, 8, 10 through 13 and 16 under 35 USC 102 as being anticipated by or, in the alternative, under 35 USC 103 as being obvious over Reade et al.

Appellant respectfully submits that Reade et al., similarly to Hebard discloses the use of an ion gun. Accordingly, Appellant respectfully submits that for all the same reasons as discussed above relative to Hebard, Appellant respectfully submits that a particle beam from a plasma sputtering system is not shown or suggested by Reade et al. therefore, Appellant respectfully submits that Reade et al. does not show or suggest each and every element of Appellant's invention and the claims 1 through 4, 6, 8, 10 through 13 and 16 are not anticipated by nor obvious over Reade et al.

C. The rejection of the claims 1, 5, 9, 10 through 13 and 17 under 35 USC 103 as being obvious over Hebard in view of Desu et al. or Kroger

In reply to this rejection, Appellant would like to incorporate by reference his comments above concerning Hebard. In addition, Appellant has carefully reviewed Desu et al. and Kroger and respectfully submits that each teaches plasma etching. Appellant respectfully submits that plasma etching is a special conception of a process that is carried out to take away a layer of a multi-layer structure or to make a layer thinner (see pages 244-252 of "Glow Discharge Processes" by Chapman). In contrast thereto, in Appellant's invention, while the plasma sputtering may result in some small amount of material being removed from

the surface, this is not the main purpose thereof. The plasma sputtering process is to make the surface smoother, or to change the material structure, or to reduce defects in the material and Appellant respectfully submits that none of these can be achieved utilizing a plasma or sputtering etching process. Still further, Appellant respectfully submits that in Desu et al., plasma etching is used to cause the etching of the thin film of ferroelectric material. Also, Appellant respectfully submits that in Kroger the sputtering etching results in a substantial improvement of the sub-gap current-voltage characteristic of the super conductive tunnel junction device (see page 4, column 4, line 1). Accordingly, Appellant respectfully submits that the plasma etching or sputtering etching of either Kroger or Desu et al. is different from the plasma sputtering in Appellant's invention.

In view of the above, Appellant respectfully submits that none of Hebard, Desu et al. or Kroger show, suggest or teach the utilization of a particle beam generated by a plasma sputtering device for surface modification in a manufacturing of high temperature superconductive devices. Therefore, Appellant respectfully submits that the claims 1, 5, 9, 10 through 13 and 17 are not obvious over Hebard in view of Desu et al. or Kroger.

D. The rejection of claims 1 through 4, 6, 8, 10 through 13 and 16 as being obvious over Reade et al. in view of Desu et al. or Kroger

Appellant would like to first incorporate by reference his comments above concerning Appellant's invention, Reade et al., Desu et al. and Kroger. Based upon Appellant's arguments above, Appellant respectfully submits that neither Reade et al., nor Desu et al. nor Kroger disclose the use of a particle beam generated by a plasma sputtering device for surface modification in manufacturing high temperature superconductive devices. Accordingly, Appellant respectfully submits that the combination suggested by the Examiner is not Appellant's invention.

E. The rejection of claim 7 under 35 USC 103 as being obvious over Reade et al. in view of Doi et al. and Shindo et al.

Appellant would like to incorporate by reference his comments above concerning Reade et al. and Appellant's invention. In addition, Appellant has carefully reviewed Shindo et al. and respectfully submits that it relates to the production of solar cells

and has nothing to do with superconductors. Still further, Appellant has carefully reviewed Doi et al. and respectfully submits that neither Shindo et al. nor Doi et al. teach the use of a particle beam generated by a plasma sputtering device for surface modification in manufacturing high temperature superconducting devices. Accordingly, Appellant respectfully submits that neither Reade et al., Doi et al. or Shindo et al. show or suggest the use of a particle beam generated by a plasma sputtering device for surface modification in manufacturing superconducting devices as claimed by Appellant's claim 7.

F. The rejection of claims 15 and 18 under 35 USC 103 as being obvious over Hebard in view of Chu et al.

Appellant would like to incorporate by reference his comments above concerning Appellant's invention and Hebard. In addition, Appellant has carefully reviewed Chu et al. and respectfully submits that an ion beam technique is utilized to generate the GCID (see column 1, line 57) which is different from the plasma sputtering of Appellant's invention as discussed above. Therefore Appellant respectfully submits that Chu et al. does not show or suggest the use of a particle beam generator by a plasma sputtering device for surface modification in manufacturing high temperature superconducting devices. Therefore, Appellant respectfully submits that neither Hebard nor Chu et al. disclose the use of a plasma beam generated by a plasma sputtering device for surface modification in manufacturing high temperature superconducting devices. As a result, Appellant respectfully submits that the combination suggested by the Examiner is not Appellant's invention as claimed by claims 15 and 18.

G. The rejection of the claims 15 and 18 under 35 USC 103 as being obvious over Hebard in view of Chu et al. and Desu et al. or Kroger

Appellant would like to incorporate by reference his comments above concerning Appellant's invention, Hebard, Chu et al., Desu et al. and Kroger. In addition, Appellant would like to point out that the art cited by the Examiner either does not disclose the use of a particle beam generated by a plasma sputtering device for surface modification in manufacturing high temperature superconducting devices or is from a divergent art which could not be looked at or considered by one of ordinary skill in the art. Accordingly,

Appellant respectfully submits that the elements of claims 15 and 18 would not only not be shown or suggested by the combination of Hebard, Chu et al. Desu et al. or Kroger, but also the combination of Hebard, Chu et al., Desu et al. or Kroger would not have been suggested to one of ordinary skill in the art.

H. The rejection of claim 7 under 35 USC 103 as being obvious over Reade et al. in view of Doi et al. and Shindo et al. and Desu et al. or Kroger

Appellant would like to incorporate by reference his comments concerning Reade et al., Doi et al., Shindo et al., Desu et al. or Kroger and respectfully submits that none of this art cited by the Examiner discloses the use of a particle beam generated by a plasma sputtering device for surface modification in manufacturing high temperature superconducting devices. Therefore, Appellant respectfully submits that the combination suggested by the Examiner is not only not Appellant's invention but also would not have been suggested to one of ordinary skill in the art.

CONCLUSION:

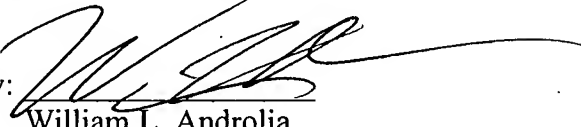
The finally rejected claims 1 through 13 and 15 through 18 of Appellant's application are respectfully submitted as clearly allowable for the reasons set forth below:

1. Claims 1 through 13 and 15 through 18 are not obvious nor anticipated by the cited art.
2. The allowance of claims 1 through 13 and 15 through 18 is earnestly solicited.
3. An oral hearing is not requested.
4. Pursuant to the telephone conversation with Mr. Pierce of the Board of Patent Appeals, submitted herewith are three (3) copies of the Appeal Brief and one (1) copy of each of "Thin film processes: by John L. Vossen and Werner Kern and "Glow discharge processes" by Brian Chapman.
5. Please charge the fee in the amount of \$270.00 (Fee Code: 2402) for filing the Appeal Brief to QUINN EMANUEL DEPOSIT ACCOUNT NO. 50-4367.

Please charge any additional costs incurred by or in order to implement this Appeal Brief or required for any requests for extensions of time to QUINN EMANUEL DEPOSIT ACCOUNT NO. 50-4367.

Respectfully submitted,

By:


William L. Androlia
Reg. No. 27,177

Quinn Emanuel Urquhart Oliver & Hedges, LLP
Koda/Androlia
865 South Figueroa Street, 10th floor
Los Angeles, CA 90017
Tel: 213-443-3000 Fax: 213-443-3100
E-mail: thomasedison@quinnemanuel.com

Certificate of Mailing

I hereby certify that this correspondence is being deposited with the United States Postal Service with sufficient postage as first class mail in an envelope addressed to:

Commissioner for Patents

P.O. Box 1450

Alexandria, VA 22313-1450, on

November 6, 2009

Date of Deposit

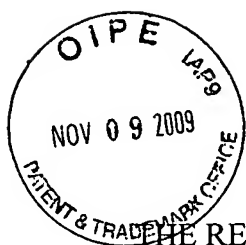
William L. Androlia

Name


Signature

11/6/2009

Date



THE REJECTED CLAIMS UPON WHICH APPEAL IS TAKEN:

Claim 1: A method for surface modification in manufacturing high temperature superconducting device, comprising the step of:

bombarding a surface of a preformed material with a particle beam having energy to increase the smoothness of the material surface and change the microstructure or internal defect of the processed material;

wherein the particle beam is generated by a plasma sputtering device; and the energy of the particle beam is in the range of 5-50000eV.

Claim 2: The method according to claim 1, wherein the material is MgO.

Claim 3: The method according to claim 1, wherein the material is CeO₂.

Claim 4: The method according to claim 1, wherein the material is a cold rolled Ni substrate.

Claim 5: The method according to claim 1, wherein the material is YBCO.

Claim 6: The method according to claim 1, wherein the material is any one of following metal materials: Ni, NiO, Ni alloy, Cu, Cu alloy, Ag, Ag alloy, Fe, Fe alloy, Mg and Mg alloy, purities of the alloy materials are more than 99% and alloying constituents of the metal alloys are at least 0.01wt.%.

Claim 7: The method according to claim 1, wherein the material is any one of following semiconductor materials: Si, Ge, GaAs, InP, InAs, InGaAs, CdS, GaN, InGaN, GaSb and InSb.

Claim 8: The method according to claim 1, wherein the material is any one of following oxide materials: SrTiO₃, LaAlO₃, Y₂O₃, RuO₂, CeO₂, MgO, ZrO₂, SiO₂, Al₂O₃ and yttria-stabilized zirconia (YSZ).

Claim 9: The method according to claim 1, wherein the material is any one of the following superconducting materials: $\text{YBa}_2\text{Cu}_3\text{O}_{7-\delta}$ ($0 < \delta < 0.5$), $\text{REZ}_2\text{Cu}_3\text{O}_{7-\delta}$ (RE is a rare earth element Z is an alkaline rare earth element $0 < \delta < 0.5$), Bi-Sr-Ca-Cu-O, TI-Ba-Ca-Cu-O.

Claim 10: The method according to claim 1, wherein the modification of the material is bulk, external or internal.

Claim 11: The method according to claim 1, wherein the surface of the material is monocrystalline, amorphous or polycrystalline structure.

Claim 12: The method according to claim 1, wherein the surface of the material is polished or unpolished.

Claim 13: The method according to claim 1, wherein the material is a substrate, a transition layer, a superconducting layer preformed in the process of manufacturing the superconducting device, or any combination of them.

Claim 14 (canceled).

Claim 15: The method according to claim 1, further comprising annealing the material bombarded with the particle beam, wherein the annealing temperature is in the range of 100-1500°C.

Claim 16: The method according to claim 6, wherein alloying constituents of the metal alloys are at least 0.1 wt.%.

Claim 17: A high temperature superconducting device, comprising:
a substrate; and
a high temperature superconducting film formed on the substrate,
wherein the high temperature superconducting film exhibits oblique cone topography characteristic after being bombarded with a particle beam having energy, wherein the particle beam is generated by a plasma sputtering device, and the energy of the particle beam is in the range of 5-50000eV.

Claim 18: The high temperature superconducting device according to claim 17, wherein the high temperature superconducting film is annealed after being bombarded with the particle beam, and the annealing temperature is in the range of 100-1500°C.

EVIDENCE APPENDIX

- 1 "Thin Film Processes" by John L. Vossen and Werner Kern, and
- 2 "Glow Discharge Processes" by Brian Chapman

RELATED PROCEEDING APPENDIX (none)

Glow Discharge Processes

SPUTTERING AND PLASMA ETCHING

Brian Chapman



201257610



A WILEY-INTERSCIENCE PUBLICATION
JOHN WILEY & SONS, New York • Chichester • Brisbane • Toronto

Preface

This book is based on a series of seminars held in 1978 and 1979. The seminars were intended to give some more insight into several practical glow discharge processes that are being increasingly used, particularly in the semiconductor industry. I hope that the text will serve as a useful general introduction to some of the scientific principles involved in these processes.

Glow discharges, like so many topics in science, are incompletely understood. Results are often misinterpreted, contradictory, or irrelevant. Glow discharge science has its own sub-language of special terms, with names that are often misleading, and with meanings which cannot be assumed to be constant from author to author! One can easily understand the need for the precision of scientific writing and sympathise with the conditions, provisos and double negatives of the author who is taking care not to make any definite statement which might be wrong. This is probably as scientific literature must be when one is close to the borders of knowledge and ignorance, but it is rather daunting to a newcomer to that particular branch of science.

Many of you will have had the experience of wanting to learn something about a particular area of science you're not familiar with, and so you go along for advice to the chap in your company or university who is considered the local expert. More often than not you come away with a list of references, in just about all of which it is assumed that you know the subject pretty well! And this is a particular problem in multi-disciplinary subjects such as sputtering where you are as likely to meet some electrical engineering phase angles as you are some organic chemistry.

This book is trying to be an introductory book. It attempts to thread a path through all the basic material you need before you can read the much more erudite reviews on the subject. In an effort to spare readers from attacks of mental indigestion, I have selected those aspects which appear to be more useful for first-time acquaintance, and even these are dealt with too briefly.

This text was written for readers with a wide range of backgrounds, and the emphasis is on concepts rather than on rigorous detail. I have usually restricted discussions to the general application of an idea, and have often ignored excep-

Copyright © 1980 by John Wiley & Sons, Inc.

All rights reserved. Published simultaneously in Canada.

Reproduction or translation of any part of this work beyond that permitted by Sections 107 or 108 of the 1976 United States Copyright Act without the permission of the copyright owner is unlawful. Requests for permission or further information should be addressed to the Permissions Department, John Wiley & Sons, Inc.

Library of Congress Cataloging in Publication Data

Chapman, Brian N

Glow discharge processes.

"A Wiley-Interscience publication."

Includes bibliographical references and index.

1. Sputtering (Physics) 2. Glow discharges.

I. Title. II. Title: Plasma etching.

QC702.7.P6C48 537.5'2 80-17047

ISBN 0-471-07828-X

Printed in the United States of America

10 9 8 7 6 5 4 3 2 1

Chapter 6. Sputtering

WHAT IS ALL THIS SPUTTERING NONSENSE ANYWAY?

A few years ago, a medical conference and a sputtering conference were taking place simultaneously at Imperial College. The conferees were as always demonstrating the well-known scientific phenomenon that conference systems tend towards a condition of being in the bar, where a well-oiled medic accosted a couple of the sputterers and demanded to know "What is all this sputtering nonsense, anyway?" "Well", replied one of the sputterers, "we're in a branch of the medical profession too, old chap — in speech therapy actually. Sputtering's a stuttering, you know, except our chaps say p . . . p . . . p . . . instead of . . . t . . . t . . .". The medic warmly thanked his newly-discovered professional colleague and hurried back to enthusiastically convey the freshly-gleaned information to his cronies.

The medic might have been a bit closer, though not very much, if he had looked in the dictionary. It seems that the word 'sputter' appeared in the English language (The Shorter OED, 1959) as early as 1598 and is adapted from imitative words 'sputteren' in Dutch and 'sputterje' in West Frisian. 'To spit it in small particles and with a characteristic explosive sound', says the dictionary; 'to utter hastily and with the emission of small particles of saliva, to sputulate in confused, indistinct or uncontrolled manner, especially from anger or excitement — His tongue was too large for his mouth; he stuttered and sputtered (1878)'.

Compared with the above, you may be disappointed with the type of sputtering I'm going to describe. I must confess that I have never heard the sound of uttering, although the sound of rotary pumps will ring in my ears forever. On the other hand, my type of sputtering is rather colourful!

INTERACTIONS OF IONS WITH SURFACES

Let us consider what happens when an ion approaches the surface of a solid (of the same or different material); the solid is usually called the *target*. One or all of the following phenomena may occur (Figure 6-1):

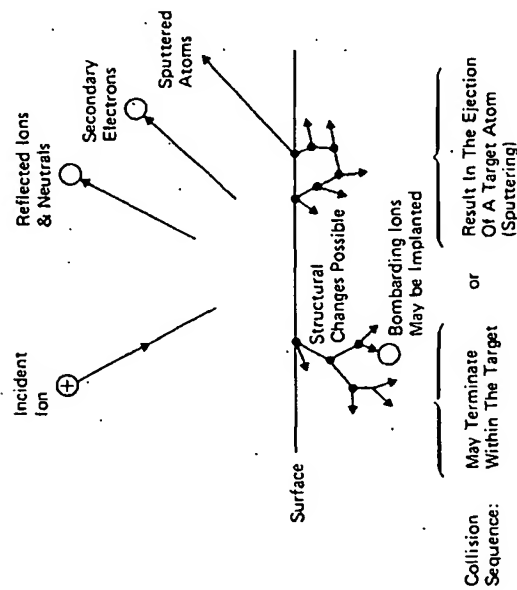


Figure 6-1. Interactions of ions with surfaces

- The ion may be reflected, probably being neutralized in the process. This reflection is the basis of an analytical technique known as *Ion Scattering Spectroscopy*, which enables us to characterize the surface layers of the material, and also tells us a lot about the fundamental ion-surface interaction.
- The impact of the ion may cause the target to eject an electron, usually referred to as a *secondary electron* (Chapter 4, "Secondary Electron Emission").
- The ion may become buried in the target. This is the phenomenon of *ion implantation*, which is already used extensively in integrated circuit technology for selectively doping silicon wafers with precisely controlled amounts and depth profiles of specific impurities, and is likely to find many other applications such as surface treatment of steels.
- The ion impact may also be responsible for some structural rearrangements in the target material. 'Rearrangements' may vary from simple vacancies (missing atoms) and interstitials (atoms out of position) to more gross lattice defects such as changes of stoichiometry (i.e. relative proportions) in alloy or compound targets, or to changes in electrical charge levels and

distributions, and are usually collectively referred to as *radiation damage*, which is a subject of great importance, particularly with relation to nuclear energy. Radiation damage can often be removed by annealing (heat treatment) but it is not always unwanted, and perhaps the alternative name of *altered surface layers*, used mostly to describe the stoichiometry changes, is more apt.

- The ion impact may set up a series of collisions between atoms of the target, possibly leading to the ejection of one of these atoms. This ejection process is known as *sputtering*.

The Mechanisms of Sputtering

In the energy range most relevant to sputter deposition, the interaction between the impinging ion and the target atoms, and the subsequent interactions amongst the latter, can be treated as a series of binary collisions. The sputtering process is very often compared to the break in a game of atomic billiards (Figure 6-2) in which the cue ball (the bombarding ion) strikes the neatly arranged pack (the atomic array of the target), scattering balls (target atoms) in all directions, including some back towards the player, i.e. out of the target surface. In the real process, the interatomic potential function (the variation of interatomic repulsion or attraction with separation distance) is rather different from the hard sphere billiard ball case, but nevertheless the billiard model is not too unrealistic.

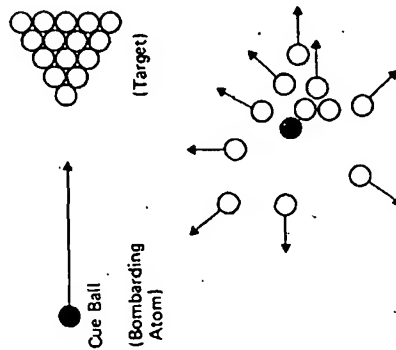


Figure 6-2. Sputtering – the atomic billiards game

It is implied in our description of the basic interaction that the incident particle could be either an ion or a neutral atom. Ions are normally used since they can easily be accelerated by an electric field, whereas neutrals pose a problem in this respect. Furthermore, the ions are likely to be neutralized anyway by the Auger emission of an electron from the target as the ion approaches, so that the impacting species are actually mostly neutral.

The series of collisions in the target, generated by the primary collision at the surface, is known as a *collision cascade* (Figure 6-1). It will largely be a matter of luck whether this cascade leads to the sputter ejection of an atom from the surface (which will require at least two collisions) or whether the cascade heads off into the interior of the target, gradually dissipating the energy of the primary impact, ultimately to lattice vibrations, i.e. heat. It's not surprising then that sputter ejection is rather inefficient, with typically 1% of the incident energy reappearing as the energy of the sputtered atoms.

The collision phenomena occurring in a target, often referred to as *target kinetics*, are a fascinating and important subject for study. They relate not only to sputter deposition and etching, but also to ion implantation and radiation damage. Life is rather short, however, and there is neither room in this book nor am I adequately informed to pursue the topic much further. But in this chapter we shall be looking at the applications of sputtering rather than the collision phenomena leading to sputtering, and fortunately we need consider only certain aspects of the process in order to do this. In the next section we shall look briefly and (unfortunately) superficially at some of the quantitative relationships involved in sputtering target kinetics.

Sputtering Target Kinetics

A generalized treatment of target collision phenomena would have to consider the detailed interatomic potential function, but fortunately the interactions in a sputtering target are sufficiently short range that we need consider interactions only between immediate neighbours (including the incident ion). A binary collision is characterized by the energy transfer function which we met earlier (Chapter 1, "Energy Transfer in Binary Collisions"):

$$S = \frac{4m_i m_t}{(m_i + m_t)^2}$$

where m_i and m_t are the masses of the colliding atoms. The sputtering process is the result of a series of such collisions. A detailed consideration and experimentation show that the binary model is a useful representation of the interactions under sputtering conditions.

A useful parameter that we shall encounter frequently is the *sputtering yield* S , defined as the number of target atoms (or molecules) ejected per

incident ion. From our model above, we would expect the sputtering yield to depend on the masses of the incident ion and the target atom, m_i and m_t respectively, and on the energy E of the incident ion. However, consider sputtering as the overall process of transferring energy from the incident ion to the sputtered atoms. Then, since the sputtered atoms can come only from the surface layers of the target, it is not just a question of transferring energy to the target atoms, but also that this energy should be transferred mostly to the surface layers. We would therefore expect the sputtering yield S to be proportional to the energy deposited in a thin layer near the surface, and this is determined by the *nuclear stopping power* $s(E)$; for low bombardment energies up to about 1 keV, an expression due to Sigmund (1969), which not surprisingly involves the energy transfer function, is

$$s(E) = \frac{m_i m_t}{(m_i + m_t)^2} E \times \text{constant}$$

and this is used to predict the following form for the sputtering yield S :

$$S = \frac{3\alpha}{4\pi^2} \frac{4m_i m_t}{(m_i + m_t)^2} \frac{E}{U_0}$$

Here U_0 is the surface binding energy of the material being sputtered, and α is a monotonic increasing function of m_t/m_i which has values of 0.17 for $m_t/m_i = 0.1$, increasing up to 1.4 for $m_t/m_i = 10$.

This expression for S predicts that the yield will increase linearly with E . In practice, this seems to be satisfied up to above 1 keV, above which S becomes relatively constant; Figure 6.3a is typical. It appears that the higher input energy is being distributed through a larger volume, so that the energy transmitted to the surface layers remains virtually constant. At very high energies, S even decreases as ion implantation becomes dominant (Figure 6.3b).

So our original expression for S is apparently valid only up to about 1 keV, and this is due to various assumptions about the atomic interactions. Above 1 keV, a modified interaction yields

$$S = 3.56\alpha \frac{Z_i Z_t}{(Z_i^{2/3} + Z_t^{2/3})} \frac{m_i}{(m_i + m_t)} \frac{s_n(E)}{U_0}$$

where $s_n(E)$ is a reduced stopping power and is a function of a reduced energy based on the actual energy, masses and atomic numbers Z_i and Z_t of the atoms involved. The interested reader is referred to Winters (1976) for further details.

The success of these theoretical models can be demonstrated by comparing experimental and theoretical results, with good agreement resulting in most cases. This is illustrated in Figure 6-4 for the case of argon on copper, which compares the yield predicted by the equation above, with experimental values.

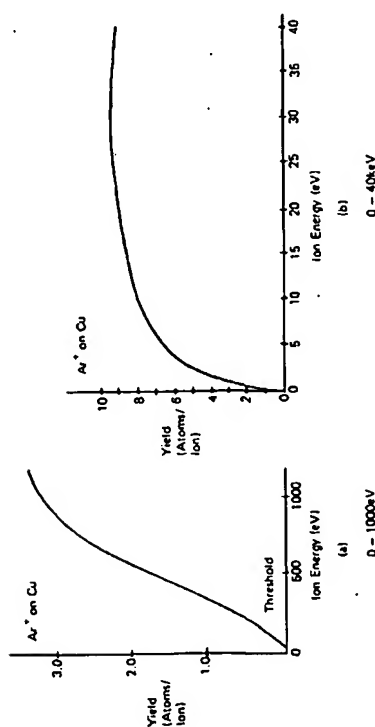


Figure 6-3. The variation of sputtering yield, for argon ions on copper, as a function of the ion bombardment energy (Carter and Colligon 1968)

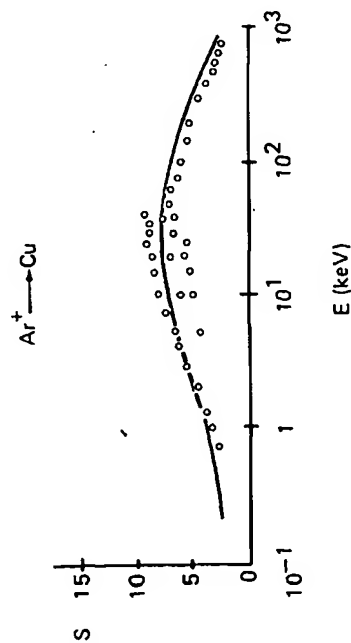


Figure 6-4. Theoretical (solid line) and experimental values for the energy dependence of the sputtering yield of copper in argon. Data from various authors; see Winters (1976)

It is apparent from examining the two sputtering yield expressions that we should no longer expect to find a maximum yield when $m_i = m_t$ as suggested by the energy transfer function alone. This prediction seems to be borne out in practice: Figure 6-5 shows the results obtained by Almen and Bruce (1961) for the sputtering of copper by inert gas ions over a wide range of ion energies.

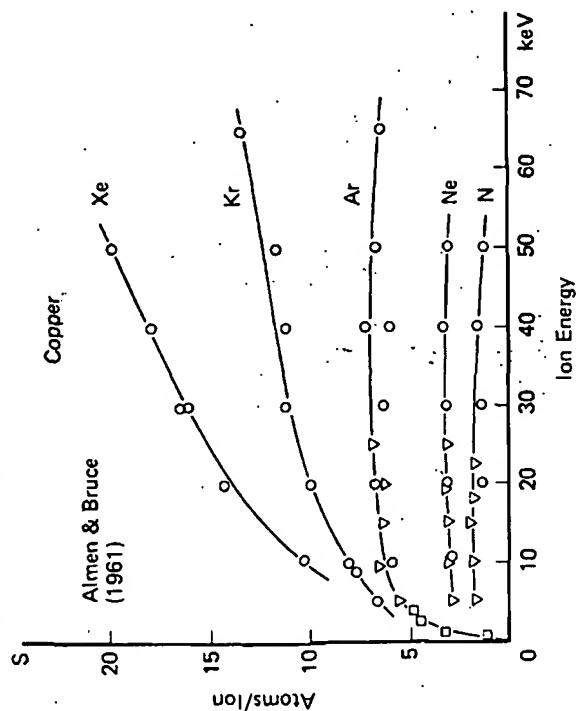


Figure 6-5. Sputtering yields of the noble gases on copper, as a function of energy (Almen and Bruce 1961)

These results show that the sputtering yield S obtained with xenon (atomic weight 131) is the largest of all these gases at all energies, even though the masses of krypton (83) and argon (40) are much closer to that of copper (64).

The high energy (> 1 keV) expression for S is reasonably successful at predicting the observed mass dependences but the low energy yield expression shows quite the wrong mass dependence. And indeed, the low energy model becomes quite incorrect for energies below 100 eV, which is an energy range which we shall discuss further in connection with bias sputtering.

The sputtering model which we used above shows only the general features of the process. A more accurate model is being developed and the interested reader should refer to the review articles by Wehner and Anderson (1971), Townsend and Kelly (1976), Winters (1976), and Kelly (1978). A realistic model is rather complex: for example, one has the pragmatic consideration that a sputtering target eventually becomes a mixture of the original target and the bombarding element embedded in or otherwise combined with it, so that one is no longer dealing with the sputtering of the original target. Never-

theless, we shall see that the simple ideas discussed above will be quite valuable when we consider later how the sputtering process is put into practice.

In the appendix to this chapter, we have shown more sputtering yield data, concentrating on typical sputtering ion energies and the usual sputtering gas, argon.

Summary of the Overall Process

Although we have looked a little at what's going on in the target, that knowledge isn't really essential to an understanding of sputter deposition. What we do need to know, however, is what the overall results of these target processes are (Figure 6-6):

- A target atom may be sputter ejected.
- The incident ion will either become implanted or be reflected, probably as a neutral and probably with a large loss of energy.
- The ion impact and the resulting collision cascade will cause an amount of structural reordering in the surface layers.
- A secondary electron may be ejected.

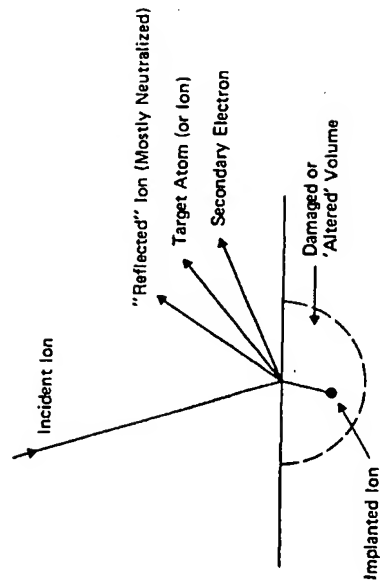


Figure 6-6. Summary of the target processes

These are just *possible* consequences of the impact; the possibilities will not generally occur in any specific ratio, nor even necessarily occur at all. We shall see shortly how each of these aspects of the sputtering process are manifested and/or utilized.

APPLICATIONS OF SPUTTERING

APPLICATIONS OF SPUTTERING

Sputter Etching

As we have already seen, the sputtering process essentially involves knocking an atom out of the surface of a target. By repeating this process over and over again, we can evidently *sputter etch* the target. We may wish to do this over the whole of the target surface, for example to clean it or to make it thinner, or selectively to generate a topographic pattern on the surface. We shall return to this application later in the chapter.

Sputter Deposition

The ejected atom can also be used. After ejection it can, under the right circumstances, move through space until it strikes and condenses on the surface of a receiver, which is known as a *substrate*. By repeating the process over and over, we can build up a coating of several or many atomic or molecular layers of target material on the substrate. The coating, which is generally less than about $1\ \mu\text{m}$, is called a *thin film*, and the process is known as *sputter deposition*; this process is currently the main application of sputtering.

Although I shall be frequently referring to the properties of thin films prepared by sputter deposition, there is no room here for a general treatment of thin film science, although the initial formation and growth stages are discussed below (in "Thin Film Formation"). The reader who has no background in this area is advised to read one of the several reviews on the subject (Berry, Hall and Harris 1968, Lewis and Campbell 1967, Chapman and Jordan 1968, Neugebauer 1970, Leaver and Chapman 1971; the last is very elementary).

Limitations of Sputtering

There are some devotees of sputtering who would claim that anything can be sputtered. There are others who would claim that if a material can't be sputtered then that material isn't worth bothering with!

These views are rather extreme, though it's certainly true that sputtering is a widely applicable and versatile process. How then do we decide whether to sputter? When it comes to specific applications and specific materials, there are so many factors to be considered that it would be misleading of me to generalize. However, ignoring my own advice, there are a few general restrictions. The capital expenditure for sputtering equipment is higher than for virtually all other coating processes. As a coating or etching process, it's too slow for some applications (for a review of the many other surface coating techniques available, see Chapman and Anderson 1974). Deposition rates are

typically 50 — 500Å per minute, and etch rates around 500 — 10,000Å per minute, although there are higher rate versions of the process available.

As we shall see, sputtering is carried out in partial vacuum and there are some materials which are incompatible with good vacuum practice, either due to their inherent properties or due to their products under the various types of bombardment involved in the process. Organic solids are frequently unable to withstand this bombardment, and completely degrade; the temperature rise alone is often adequate to produce this effect. On the other hand, it is remarkable that polytetrafluoroethylene, which has a long chain molecule and cannot possibly be sputtered intact, and which can easily be reduced to a carbonaceous mess at quite low temperatures, can nevertheless be sputtered to produce quite useful films with properties similar to those of the target.

The presence of the vacuum pumps also means that one frequently encounters problems when using target materials containing volatile components. The resulting films are often deficient in the volatile component, although this can sometimes be rectified.

To summarize, sputtering is a rather versatile process. It's applicable widely but naturally has some shortcomings and drawbacks. One is advised to read the published literature on specific applications and specific materials before becoming too enthusiastic.

We now begin to look at some of the details of the process by considering a dc sputtering system. Actually, most sputtering systems are rf driven, but it is helpful to first look at the dc counterpart.

A CONVENTIONAL DC SPUTTERING SYSTEM

In this section we shall meet briefly some ideas which are discussed in more detail later. This probably means that this will make more sense after you've read later sections. On the other hand, I think you should read this first so that you see the overall picture before we plunge into the detail.

How do we deposit thin films by sputtering? It's very informative to look at a conventional dc sputtering system (Figure 6-7) to see the elements used to turn the sputtering phenomenon discussed in the last section into a practical deposition process.

The material we wish to sputter is made into a *sputtering target* which becomes the cathode of an electrical circuit, and has a high negative voltage V (dc) applied to it. The target is nearly always solid, although powders and even liquids are sometimes used. The substrate which we wish to coat is placed on an electrically grounded anode a few inches away. These electrodes are housed in a chamber which is evacuated. Argon gas is introduced into the chamber to some specified pressure. The action of the electric field is to accelerate electrons

A CONVENTIONAL DC SPUTTERING SYSTEM

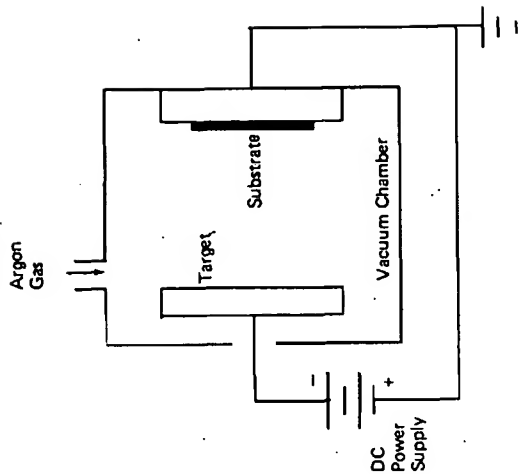


Figure 6-7. Schematic of a dc sputtering system

which in turn collide with argon atoms, breaking some of them up into argon ions and more electrons to produce the glow discharge that we discussed in Chapter 4. The charged particles thus produced are accelerated by the field, the electrons tending towards the anode (causing more ionization on the way) and the ions towards the cathode, so that a current I flows.

When the ions strike the cathode, they may sputter some of the target atoms off. They may also liberate secondary electrons from the target and it is these secondary electrons which are responsible for maintaining the electron supply and sustaining the glow discharge (Chapter 4, "Maintenance of the Discharge"). The sputtered atoms from the target fly off in random directions, and some of them land on the substrate (on the anode), condense there, and form a thin film.

The voltage V which is required to drive the current I through the system is a function of the system pressure p . The rate of thin film formation on the substrate will depend on the amount of sputtering at the target; this in turn will depend on the ion flux at the target and so (linearly) on the current. However, the amount of sputtering also depends on the sputtering yield S and so on the ion energy and hence on V , which determines the sheath voltage at

the target. The choice of sputtering pressure p and the implied choice of the V - I characteristic, are thus rather important and so we'll now look at the criteria used in selecting operating parameters and in deciding on the nature of the sputtering gas.

Choosing the Sputtering Gas

As we saw earlier, it doesn't really matter whether we use neutral atoms or ions as far as the actual sputtering process is concerned. However, it is easy to accelerate ions to the energies required by using an electric field and much more difficult to accelerate neutrals; so we normally use ions.

It's much easier to ionize atoms when they are in a gaseous state, and naturally the latter state is easier to achieve with materials already in a gaseous form at room temperature. So we use gases for our ion source. A glow discharge happens to be a particularly convenient method of producing a significant flux of gas ions.

We usually don't want the ions to react with the target or growing film, which therefore requires noble gas ions. We shall see later that some sputtering ions will become incorporated into the growing film and become trapped by the depositing film atoms. Since we are usually concerned with the purity of the film, we'd prefer these incorporated ions to be as innocuous as possible; this is another reason for using noble gas ions, with their closed shell electronic structures and (almost always) chemical inactivity. We saw earlier that the heaviest inert gas will give the highest sputtering yield (Figure 6-5). Radon ($Z = 86$) is the heaviest, but it is also radioactive. Xenon (54) and krypton (36) are next in line, but argon (18) is almost always used in sputter deposition because it is easily available and cheaper, and the sputtering yield is only a factor of about two down on xenon at sputter deposition energies. The cost of the sputtering gas is not usually a significant factor, though, because a cylinder may last a year in a small sputtering system. Most gas suppliers have several grades of argon; their standard grade is usually intended for applications such as argon arc welding, and is not pure enough for sputtering.

Choosing the Pressure Range

A vacuum system enables us to control the operating pressure inside the sputtering system. Operating pressure limitations are imposed by the requirements of both the glow discharge and of film deposition.

The glow discharge sets a lower pressure limit. The discharge is sustained by electrons making ionizing collisions in the gas. The number of ionizing collisions will decrease with decreasing gas density, and hence gas pressure, so that the discharge current (for constant voltage) will also decrease. This is shown for

A CONVENTIONAL DC SPUTTERING SYSTEM

a typical case in Figure 6-8. Below about 30 mtorr, the current (and hence ion flux at the target) and sputtering rate in a dc discharge become quite small.

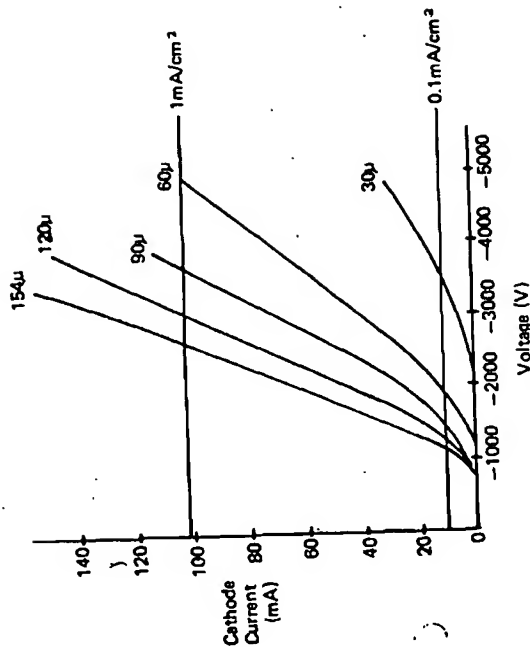


Figure 6-8. Typical I - V curves at different argon pressures using a $4\frac{1}{2}$ inch nickel cathode — area 103 cm^2 (Kay 1969)

A different problem arises at the other end of the pressure range. In the same way that electrons undergo collision, material sputtered from the target may collide with gas atoms on its way to the substrate, at a rate which will increase with increasing pressure; we discussed this in Chapter 1, "Probability of Collision". The result of the collision is to deflect the sputtered atom, sometimes back towards its parent, and hence decrease the deposition rate. This is demonstrated in Figure 6-9, which shows how the apparent sputtering yield of a nickel target (obtained by measuring its weight loss) decreases with increasing pressure due to sputtered nickel being backscattered in the gas phase and redeposited on the target. The mean free path (see Chapter 1) of the nickel is about 1 mm at 120 mtorr, so this result is expected. With increasing pressure, deposition becomes less a line-of-sight process and more a diffusion process. The scattering process becomes serious above about 100 mtorr, so that taking both of our limi-

SPUTTERING

tations into account, an overall operating range of about 30 – 120 mtorr is usual for dc sputter deposition. This isn't a very wide operating range, but at least the two limits haven't overlapped! Later we'll see modifications of the basic sputtering process which permit lower operating pressures.

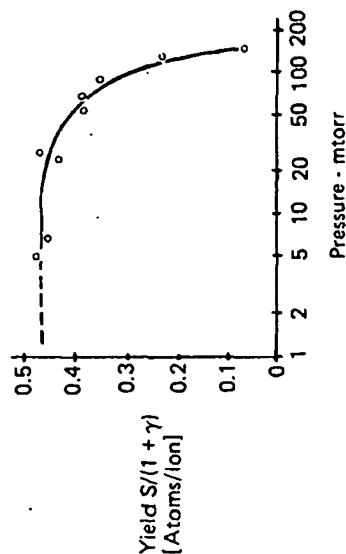


Figure 6-9. Variation of the apparent sputtering yield of nickel vs argon gas pressure; 150 eV ion energy (Laegreid and Wehner 1961)

Choosing Electrical Conditions for the Glow Discharge

We have an operating range of 30 – 120 millitorr, but what voltage and current should we use? To some extent that is Hobson's choice since, for each operating pressure, target material and sputtering gas, there is a specific voltage – current relationship. The V-I relationships at several pressures, for a nickel target sputtered in argon, are shown in Figure 6-8. Actually the target material isn't that important even though the secondary electron coefficient γ does vary from material to material. Table 6-1 shows the current densities obtained from various target materials under similar conditions, and the densities are very much alike, at least for this restricted case of conducting targets.

The sputtering rate of the target is determined by the flux of ions and energetic neutrals, and the sputtering yield. An ion current of 1 mA/cm² corresponds to a flux of 6×10^{15} singly charged ions per cm² per second. However, the target current also includes a secondary electron component, and the target bombardment flux is due to energetic neutrals as well as ions.

Figure 6-8 suggests that, by applying a high enough voltage, we could have any target current we want. But maybe that's the wrong approach. What ion

Table 6-1

Target current density as a function of target material and discharge gas. This data was acquired over a period of years and is presented to show that the target current density is relatively insensitive to target material and additive gases. Target voltage = -2000 V, gas pressure 70 mtorr, and interelectrode spacing ~4 cm. From Winters et al. (1977)

Target Material	Current Density (mA/cm ²)	Gas
Si	1.35	CF ₄
Si	1.25	CF ₄ + 6½% O ₂
Si	1.20	CF ₄ + 10½% O ₂
Si	1.05	CF ₄ + 16% O ₂
Si	1.15	CF ₄ + 22½% O ₂
Si	1.30	CF ₄ + 34% O ₂
Si	1.35	CF ₄ + 42% O ₂
Si	0.45	Ar
Mn ₂ Ge ₃	0.55	Ar
GdFe	0.69	Ar
CoNi	0.49	Ar
Ni	0.46	Ar
CoNi	0.42	Ar
Ti	0.43	Ar
V	0.43	Ar
Ag	0.49	Ar
C	0.41	Ar
Ta	0.63	Ar
Ni	0.56	Ar + 10% N ₂
Au	0.39	Ar + 10% N ₂
Au	0.51	Ar + 10% N ₂
W	0.51	Ar + 10% N ₂
W	0.49	N ₂
Ni	0.44	N ₂

energies should we use for sputtering? We saw earlier that the sputtering yield rises monotonically with ion energy up to several tens of keV, where it begins to decrease. This latter region, where we're getting less for more, is obviously not an energy bargain basement but what other criteria are important? A prime matter is that of safety. Electrically we'd like low voltages and because X-rays can be produced by fast ions and electrons, we ought to keep energies and voltages below 10 kV. Within this limit, many other criteria become important and so the material being deposited and the requirements made of it must be considered. The broad range, though, is usually determined by the fact that we will be restricted (if only economically) to a sputtering power supply of limited output. By varying the operating pressure of the sputtering system, we can change the V-I relationship of the discharge (within certain limits) whilst maintaining the same power input VI. So rather than consider only the sputtering yield S , we need to look also at the yield per energy input, S/E ; this is shown in Figure 6-10 for the case of xenon on copper, and in Figure 6-11 for argon on tungsten over a narrower energy range. These suggest a most efficient ion energy of a few hundred volts. Other materials would give similar results.

This dependence of S/E on E is not too surprising. Our sputtering kinetics model ("Sputtering Target Kinetics") suggested that S should increase linearly with E up to about 1 keV. If so, then S/E should be constant, and this seems to be the case except below about 100 eV, where the model begins to break down. Above 1 keV or so, the sputtering yield is fairly constant, so that S/E falls with increasing energy.

Several points, which are discussed in Chapter 4, have to be stressed. A V-I discharge relationship does not mean that the flux of sputtering particles at the cathode is equivalent to I , since some of the cathode current is carried by electrons, and some of the sputtering particles are neutral. It also doesn't mean that the sputtering particles will all have an energy of V electron volts: instead they will have a wide energy distribution with a maximum of V because they too (like the electrons) collide with gas atoms and usually slow down in the process.

Another way of saying all of the above is that not all of the VI power input goes into the target. Of course there is no general reason why we should try to get the maximum amount of sputtering per unit energy input, since there may be other more important criteria governing our choice of V-I such as a particular operating pressure or a low operating voltage.

The sputtering yield per unit energy input (S/E) data tell us that we shouldn't expect to sputter very rapidly below about 100 V and that the process is becoming very inefficient above 10 kV. In practice, a lower limit of about 500 V is used to achieve adequate current density, and an upper limit above 5 kV is rarely found necessary. Even with a sheath voltage of 500 V, the ion bombardment

energy is generally much lower because of charge exchange collisions in the sheath.

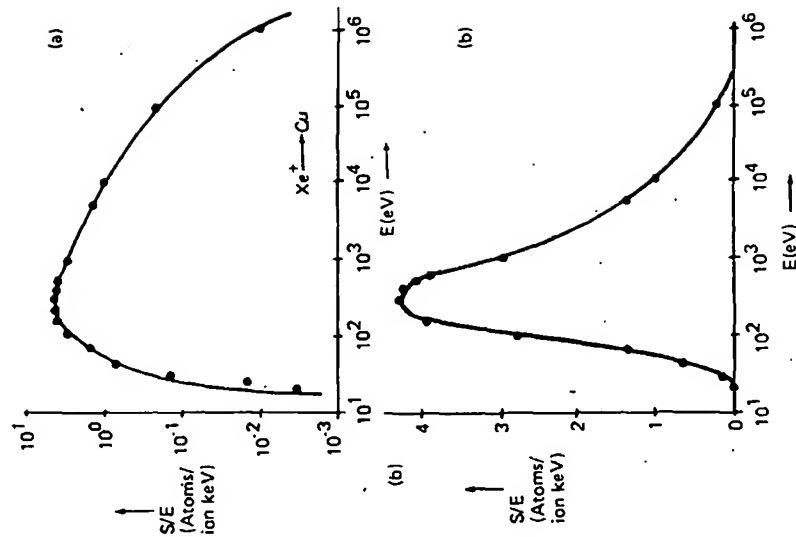


Figure 6-10. Variation of the sputtering yield per unit energy input of xenon on copper vs ion energy. Data from: Dupps and Scharman (1966), Almen and Bruce (1961), Guseva (1960), Wöhner (1962), Stuart and Wöhner (1962).

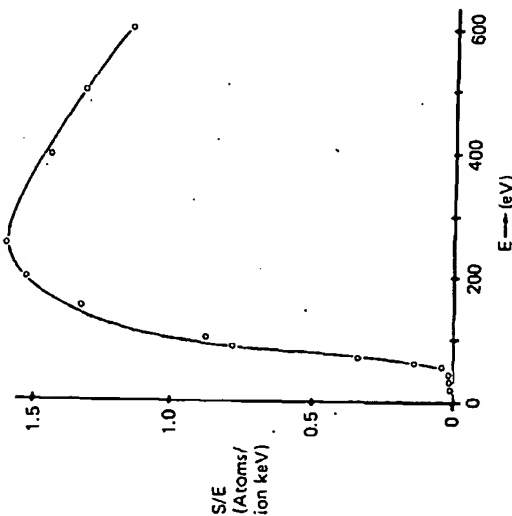


Figure 6-11. Variation of the sputtering yield per unit energy input for argon on tungsten vs ion energy. Data from: Stuart and Wehner (1962), Wehner (1962)

Summary

We have seen in outline how sputter deposition can be carried out in a dc system using a glow discharge as an ion source. The ions are usually of a noble gas which is introduced into the system and maintained at a pressure in the 30-120 millitorr range. The voltage required to maintain a glow discharge having a current density of $0.1 - 2.0 \text{ mA/cm}^2$ is usually in the range $500 - 5000 \text{ V}$.

In the next sections we shall look more closely at sputtering discharges so that we can better understand and control the sputter deposition process.

SPUTTER ETCHING AND DEPOSITION OF INSULATORS

In the previous discussion of a dc sputtering system, it was assumed that the target was conducting, or at least reasonably so. One wouldn't want to drop more than about 100 V across the target, so with typical numbers of 1 mA/cm^2 for the target current density and 0.5 cm for the target thickness, this sets a limit of $\rho = 2 \times 10^5 \Omega\text{cm}$, which is quite resistive. So some nominal insulators could be sputtered, but it isn't usually a very good solution because of problems such as stress developed in the target by the resistive heating there.

SPUTTER ETCHING AND DEPOSITION OF INSULATORS

Instead, two common ways of depositing insulating thin films are by *rf sputtering* and *reactive sputtering*.

RF Sputtering

The technique of rf sputtering uses an alternating voltage power supply at rf frequencies around 10 MHz, so that the sputtering target is alternately bombarded by ions and then electrons so as to avoid charge build-up. The rf discharge was discussed in some detail in Chapter 5, where we also looked at the choice of operating frequency, crystal controlled and self-excited oscillators, and matching networks. It also seemed that the rf discharge made more efficient use of the electron impact ionization, so that operating pressures could be practically extended down to 1 mtorr. Because the detail of the sheath mechanism is slightly different in the rf case, the sheath is still about 1 cm thick at 10 mtorr, and so the lower pressure leads to less ion energy attenuation due to charge exchange. The lower operating pressure also reduces the amount of scattering of material sputtered from the target (cf. Figure 6-9).

There are more subtle advantages: in dc sputtering systems, *arcing* is sometimes a problem, due to patches of dirt (with higher secondary electron coefficient), pockets of outgassing (higher pressure, higher j locally), or asperities (higher ϵ). These *unipolar arcs* (Maskrey and Dugdale 1966) can be quite troublesome, leading to the necessity of *conditioning* a sputtering target before general usage, by slowly increasing the applied power and sputtering (or evaporating) away the arc-forming defect.

These arcs are less likely to form in rf discharges because the field is maintained in one direction for less than one cycle, and reduces to zero twice in each cycle, making it more difficult for the arc to be sustained. Even so, target conditioning is still necessary.

With its various advantages, rf discharges are almost always used for sputtering purposes. The two principal exceptions are magnetron sputtering systems and ion beam sputtering systems; these are discussed later.

Reactive Sputtering

Reactive sputtering avoids the problem of target charging instead of solving it. A conducting elemental target is dc sputtered, and the sputtered material is combined chemically with a component from the gas phase, e.g. oxygen. In Chapter 7, we shall see how electron impact dissociation can turn the discharge into a chemically active environment. To illustrate the technique, silicon nitride can be produced by sputtering silicon in a dc (or rf) discharge containing nitrogen. Even when a compound target is rf-sputtered, reactive sputtering is often

used to restore the stoichiometry of the film. We shall return to this topic in "Deposition of Multicomponent Materials".

PRACTICAL ASPECTS OF SPUTTERING SYSTEMS

In the previous section, we dealt with some of the process conditions required for sputtering. Of course, there are many other practical considerations in making a sputtering system. This book is primarily about the glow discharge aspects of the process, and so such details are discussed only briefly.

Ground Shields

Looking into a sputtering system, one is immediately aware of several features (Figure 6-12). The target is surrounded by a *dark space shield*, also known as a *ground shield*. The purpose of this is to restrict ion bombardment and sputtering

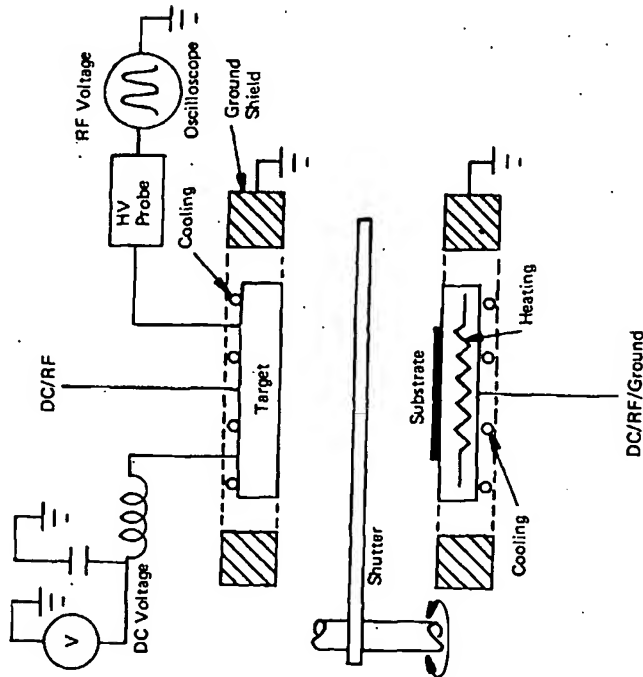


Figure 6-12. Schematic of a sputtering system showing ground shields, shutter, electrode cooling and heating, rf and dc voltage measurement

to the target only. Otherwise, the target backing plate, mounting clips (if any) and mechanical supports would also be sputtered and cause the film to be contaminated. In order to prevent ion bombardment of the protected regions, the space between the target and the ground shield must be less than the thickness of the dark space. From the descriptions of the glow discharge maintenance mechanisms in Chapters 4 and 5, we can see that this criterion is such as to prevent the establishment of a self-sustained discharge in the space between the target and the shield. Occasionally one finds that sharp points or patches of dirt cause local discharges or arcs, particularly with dc discharges, and these must be eliminated. Some possible ground shield arrangements are shown in Figure 6-13.

Since the thickness of the dark space decreases with pressure, the size of the gap between the target and shield sets an upper pressure limit for operating the system. In principle, the gap could be extremely small, but in practice this is limited by spurious discharges, and in the case of rf discharges, by increasing capacitive target-to-ground coupling as the gap is decreased. The dark space thickness also decreases with frequency, so systems operating above 13.56 MHz need to have correspondingly closer ground shields.

Many systems have the capability of applying electrical power to the substrate for the technique known as *bias sputtering* (q.v.). In this case, a ground shield is required around that electrode too.

Shutters

Figure 6-12 shows a shutter that can be rotated into place between the electrodes. This has its use during a *presputtering* period when the first few atomic layers of the target are removed by sputtering in order to clean it. During the time that the system is open to air to load or unload it, the target is liable to become contaminated by atmospheric pollution, by handling, or by chemical combination with the atmosphere to form an oxide or other compound. If this were left in place, the first period of sputtering would transfer the contamination to the substrate. This is avoided by interposing the shutter during that initial period, in order to prevent deposition on the substrate. For the same reasons, it is often extremely helpful to clean the substrate in the same way, and to do this immediately prior to deposition so that the surface does not become contaminated. So the ability to power the substrate is useful for this pre-sputter period as well as for applying bias during sputter deposition.

One has to be careful in the use of shutters. The operating pressure range of sputtering is such that the sputtered material makes many collisions in the gas phase, and so it can diffuse around shutters to an extent. This is in contrast to the use of shutters in high vacuum ($< 10^{-5}$ torr) evaporation where shutters block everything in the line of sight of the source.

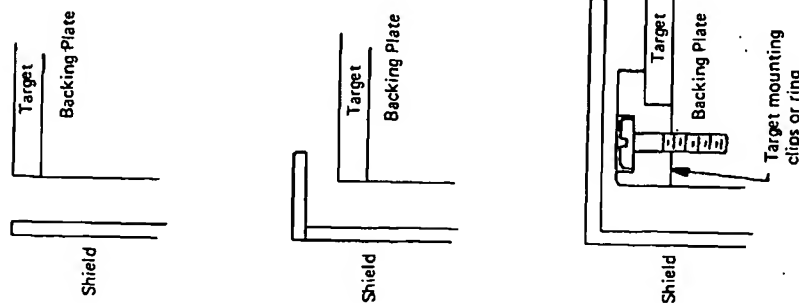


Figure 6-13. Some possible ground shield arrangements

Target Cooling

Returning to Figure 6-12 again, we see that the target is cooled. Sputtering is a very inefficient process, and most of the power input to the system appears finally as target heating. Such heating can become excessive — local temperatures of 400° C have been reported — and can lead to damage of the bonding between the target and the backing electrode, of the target itself, of associated

PRACTICAL ASPECTS OF SPUTTERING SYSTEMS

199

vacuum O-rings, etc. This is usually avoided by cooling the target with water or another suitable liquid. On the other hand, such cooling is a complexity and it can be avoided if the power input to the target is not too great. We have successfully run several systems without cooling; indeed, this probably contributed to their reliability. There are many of us who have suffered from water leaks and their consequences! Cooling systems seem to have a propensity for blocking up and then failing at their weakest point, usually a connection. As usual, nature likes to show her influence; aluminium seems to be attacked by recirculating water systems and algae seem to thrive in rf environments, both being causes of blockage. As a last resort against water leaks, Widmer (1978) has proposed a rather 'sweet' solution, using an electromechanical arrangement with a sugar 'fuse'!

Substrate Temperature Control

The temperature of the substrate surface is an important and yet difficult parameter to control. We shall see in the section on "Thin Film Formation" that the substrate temperature influences the formation stages of a thin film and its final structure, and in "Bias Techniques" how the temperature influences gas incorporation in the film. It is not terribly difficult to incorporate water cooling or even liquid nitrogen cooling into the substrate platform, although if the substrate platform is biased, one has to ensure that the liquid flow and its associated pipework do not cause a partial electrical short of the target by excessive resistive or capacitive coupling to ground.

Heating of the substrate platform can be achieved by circulating a hot liquid or by electrical resistance heating. If electrical isolation is required, the resistance heater can be decoupled with a suitable isolation transformer. The temperature is usually measured and controlled with a thermocouple feeding a power controller, and in this case the electrical isolation problem is a little more difficult since we need to preserve the thermoelectric emf of the couple whilst removing both the rf and dc offset components. The former may be removed by rf chokes; the latter is normally removed by using a thin insulator of mica or ceramic between the couple junction and the substrate platform or dummy substrate. In a dc sputter etch system, we have been able to successfully run the whole assembly of heater, thermocouple, and temperature controller at the dc target voltage by using a single isolation transformer at the power source, and this arrangement eliminated the need for electrical isolation (and consequent thermal isolation) between the thermocouple and substrate (Chapman et al. 1973).

There is an inherent problem in substrate temperature control in thin film deposition, whether by sputtering or evaporation. What we are really interested in is the temperature of the *surface* of the substrate rather than of its bulk, and it is difficult to measure even the latter, because of the thermal barriers inevita-

bly present, e.g. due to electrical isolation between the substrate and a thermocouple pressed down onto it, or due to thermal isolation between a substrate and the substrate platform. In this latter case, the problem arises because the substrate will generally make only three point contact to the substrate holder; it is sometimes possible to fill the intervening space with a suitable heat-conducting liquid or solid such as gallium, in order to heat-sink the substrate to the holder, but this is usually inconvenient and would be unacceptable in manufacturing processes.

The problem is exacerbated by the power input to the substrate from the glow discharge, which is liable to make the surface temperature greater than that of its bulk. The use of a thin film thermocouple evaporated onto the surface of the substrate has been proposed as a solution to this difficulty, but this is not very convenient. An alternative is to use an infra red thermometer that measures the infra red radiation emitted by the substrate; one needs to know the transmission characteristics of the window through which observation is made, but often this can be done empirically.

So it seems that measurement of the absolute substrate surface temperature is quite a difficult matter, although practically it is possible to reproduce the same conditions from run to run.

Electrode Voltage Measurement

Although many rf systems are controlled by the power input to the matching network and process chamber, some people prefer to measure and control with the target voltage since this eliminates the uncertain power losses in the matching network. It is more usual to measure the dc offset voltage, although the rf peak-to-peak is sometimes used. The dc voltage is normally obtained by filtering out the rf components with an LC circuit, as in Figure 6-12. The rf voltage waveform can be observed by using a high voltage probe (which is essentially a resistive network voltage divider) to reduce the rf signal to a suitable size for display on an oscilloscope. The probe is essentially a resistive or capacitive network voltage divider; if the ac and dc components of the waveform are required, the resistive type should be used. If only the rf peak-to-peak magnitude is required, a clamping circuit can be used, preferably immediately after the probe to avoid long leads carrying rf.

John Vossen has pointed out that when insulating targets are used, the dc offset voltage depends on leakage around the target edge to the backing plate; the unreliability of this can be avoided by using the peak-to-peak voltage. It is not clear to me why this leakage does not change the sputtering rate, if it really does change the target surface potential.

Whatever parameter is measured, care is required, both in safety and in interpretation. There are large rf currents flowing in the external circuitry, and the

SPUTTERING AS A DEPOSITION PROCESS

Inductance of even a straight piece of wire can become significant at radio frequencies. These combine to cause significant drops along current-carrying connecting cables, particularly that between the matching network and the target. One can observe these voltage changes with the probe . . . carefully. To obviate this problem, the probe should be attached to the back of the electrode.

All of the same considerations apply to the measurement of substrate voltage, which is almost always done in a bias sputtering system by measuring the dc offset of the applied rf.

At both electrodes, the sheath voltage is determined by the difference between plasma potential and electrode potential, as discussed in previous chapters. Christensen and Brunot (1973) have proposed a method of monitoring the sheath voltage continuously (their technique is discussed in Chapter 5) but this method has not been generally adopted. Target voltage is instead used to reproduce conditions rather than give absolute magnitudes.

SPUTTERING AS A DEPOSITION PROCESS

The current main application of sputtering is for the deposition of thin films.

Thin Film Formation

In sputter deposition, as with the other standard vacuum deposition process of evaporation, material arrives at the substrate mostly in an atomic or molecular form (Figure 6-14). The atom diffuses around the substrate with a motion determined by its binding energy to the substrate and is influenced by the nature as well as the temperature of the substrate. Energetically, the surface of the substrate is like an egg carton, with each of the depressions constituting a temporary resting point or *adsorption site* for the depositing and diffusing atoms. At each 'hop', the atom will either jump over the barrier into an adjacent site, or might even hop right out of the egg carton — i.e. re-evaporate. After a certain time, the atom will either evaporate from the surface or will join with another diffusing single atom to form a doublet, which is less mobile but more stable than the single atom. I like to think of two men (please insert your favourite ethnic group) tied together inside a giant egg carton, and trying to jump over the barriers into the adjacent depressions. The chance of them being well enough co-ordinated to jump together is extremely slim, so their mobility is severely limited, as is the chance of their 're-evaporation'.

The chance of forming the atomic pair will depend on the single atom density and hence on the arrival or deposition rate. In time, the doublets will be joined by other single atoms to form triplets, quadruplets and so on. This is the *nucleation* stage of thin film growth, leading to the formation of quasi-stable islands,

each containing tens or hundreds of atoms and typically having densities of $10^{19}/\text{cm}^2$. During the next, *island growth* stage, the islands grow in size rather than in number. Eventually they grow large enough to touch; this is the *agglomeration* or *coalescence* stage. From observations in the transmission electron microscope, it appears that the islands often display liquid-like behaviour during coalescence, and there are often crystallographic reorientations as a result of competition between the structures of the coalescing islands. Coalescence proceeds until the film reaches *continuity*, but this may not occur in some cases until the film is several hundred Angstroms in average thickness. During the coalescence stages, the film therefore typically consists of hills and valleys.

During the island stage, each island is usually single crystal or contains just a few crystals. On a polycrystalline substrate, the orientation of each island will be random, so that the resulting film is polycrystalline. On a single crystal substrate, the island orientations may be determined by the substrate structure so that growth and coalescence leads to a single crystal film. This is the phenomenon of *epitaxy* (Bauer and Poppa 1972).

If surface atoms are mobile, they have a greater opportunity of finding low energy positions, consistent with crystal growth, in the growing film. Mobility is enhanced by increased substrate temperature. But since it also takes time to find an energetically favourable lattice position, crystal growth is also encouraged by low deposition rates. Hence, on single crystal substrates, for each deposition rate there will be a temperature, the *epitaxial temperature*, above which single crystal films can be grown.

It is more likely that polycrystalline films on polycrystalline substrates will be required. During the island stage, each island will contain one or a few crystallites. The same mechanisms obtain as in single crystal growth, so that high substrate temperature and low deposition rate lead to large grains, low density of crystal defects, and large film thickness for continuity. The reverse (low temperature and high rate) associations are also generally true.

All of the relationships above were found for the comparatively simple case of deposition by vacuum evaporation. The structure of the growing film was found to be extremely sensitive to deposition conditions. Electron bombardment either prior to or during deposition was found to encourage film continuity and reduce epitaxial temperatures (Stirland 1966). Ion bombardment (Wehner 1962) and increased arrival energy of the depositing atoms (Chapman and Campbell 1969) also reduced the epitaxial temperature.

Life on the Substrate

The purpose of the preceding discussion was to illustrate the very sensitive dependence of thin film structure on growth conditions, even for deposition by

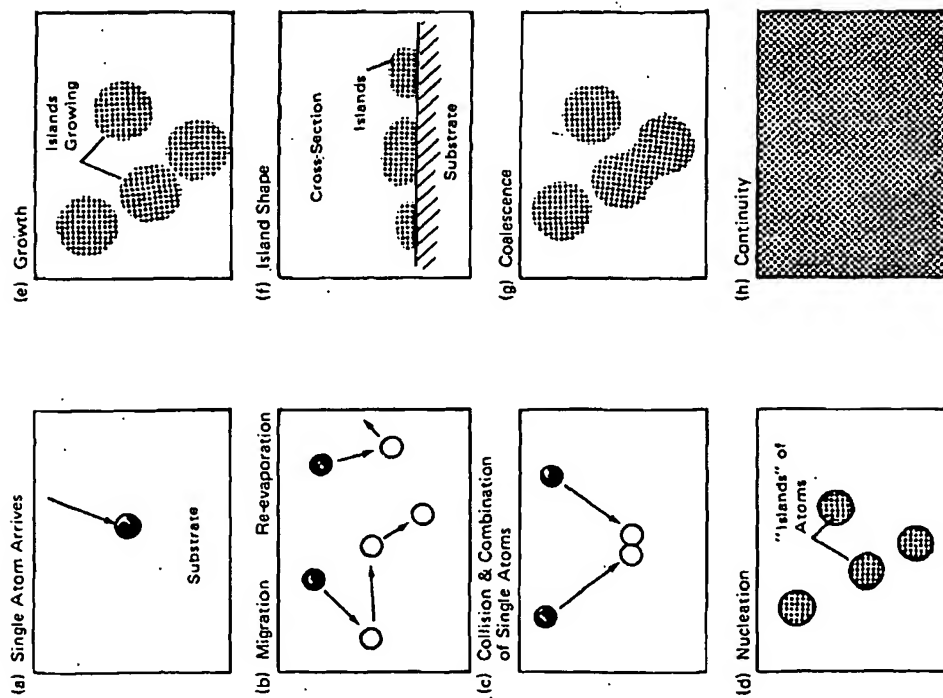


Figure 6-14. Formation of a thin film (Leaver and Chapman 1970)

SPUTTERING

evaporation. By contrast, the sputtering environment is extremely complex and has many variables.

Figure 6-15 shows a substrate on which we wish to deposit a sputtered film. We have seen that the nature and temperature of the substrate are important in determining the nature of the film. During thin film growth, the substrate and growing film will be subjected to many types of bombardment (Figure 6-16) which will now be described.

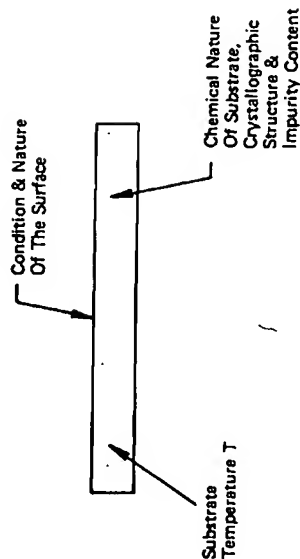


Figure 6-15. The influence of the substrate on thin film structure

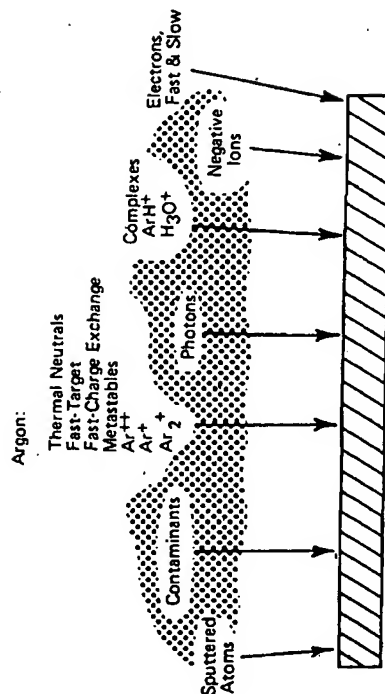


Figure 6-16. Particles bombarding the substrate in sputter deposition

Sputtered Atoms and Contaminants

Let's refer again to the example given in Chapter 1, "Monolayer Formation Time". A typical sputter deposition rate is one monolayer per second, i.e. $\sim 10^{-5}$ atoms/cm² second or 200 Å/minute for a 'typical' atom of about 3 Å diameter. A contaminant gas having a partial pressure of 10^{-6} torr will contribute a numerically equal flux at the substrate. Such contamination will be particularly effective if it is chemically active. The example in Figure 6-17 is from deposition by evaporation, at a higher rate (1200 Å/min) than the sputtering example, but the point is the same; the aluminium film begins to oxidize at an oxygen pressure $\sim 10^{-7}$ torr. We must remember that a contaminant partial pressure of 10^{-6} torr in a total sputtering pressure of 20 mtorr amounts to a contamination level of only 50 ppm! We are unlikely to achieve such a low level, and the contaminant flux will increase proportionately with its partial pressure. If the contamination results from an internal source such as outgassing from a heated substrate, then its partial pressure (which results from an equilibrium between the rates of introduction and pumping) can be minimized by maximizing the pumping rate and hence gas flow rate. (See Chapter 1, "Conductance"). But this expedient is ineffective if the contamination is introduced with the gas, indicating a vital need for pure sputtering gas.

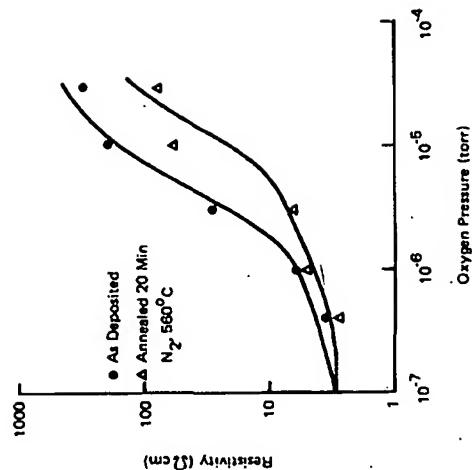


Figure 6-17. Room temperature resistivity vs oxygen pressure during evaporation of 5000Å aluminium films at 200° C and 20A/sec (d'Heurle et al. 1968)

Sputtering Gas Atoms — Fast and Slow

Compared with the fluxes of sputtered atoms and contaminants at the substrate, the flux of argon (or other sputtering gas) is truly enormous. At 20 millitorr, the argon flux would be about 10^4 times greater than the arrival rate of sputtered material. It would not be surprising, therefore, if argon were trapped in the growing film. Indeed, trapped argon is observed in sputtered films (Winter and Kay 1967), although not for the obvious reason. Winters and Kay evaporated a nickel film under similar conditions of argon pressure and deposition rate as for the sputtered films, but found that the argon content in the evaporated films was very much lower ($< 1\%$).

They determined the content of their nickel films by vaporizing the film and measuring the resultant gas evolution with a mass spectrometer. The argon content was measured as a function of substrate temperature (Figure 6-18) and total argon pressure (Figure 6-19). The temperature dependence is as expected; argon is likely only to be physisorbed, so is less likely to be initially adsorbed and more likely to be subsequently desorbed, with increasing substrate temperature.

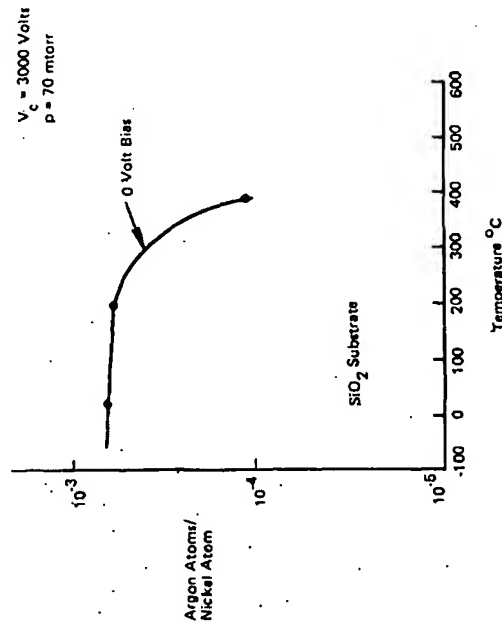


Figure 6-18. Argon content in sputtered nickel films as a function of deposition temperature (Winters and Kay 1967)

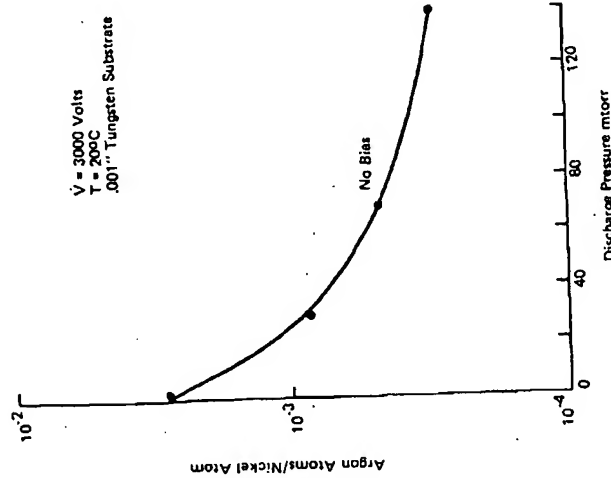


Figure 6-19. Argon content in sputtered nickel films as a function of argon discharge pressure (Winters and Kay 1967)

The pressure dependence (Figure 6-19) is rather interesting. The effect is ascribed to the small flux of high energy argon neutrals striking the substrate, rather than the large flux of thermal neutrals. Energetic argon ions striking the target are neutralized in the process and rebound as energetic neutrals. These energetic neutrals, arriving at the substrate, are likely to be embedded in the growing film; Comas and Wolicki (1970) have demonstrated how argon ions are entrapped in silicon, and fast neutrals are likely to behave in a similar way. Travelling across the sputtering chamber, the energy of these fast neutrals is attenuated by gas phase collisions and so their incorporation into the growing film (per unit film atom) decreases with increasing pressure.

One would expect fast neutrals to have a smaller collision cross-section than thermal neutrals. The existence of fast electrons and negative ions from the target similarly traversing the sputtering system without collision and bombarding

the substrate has been clearly demonstrated, as is discussed later. In the Winters and Kay work there is apparently an effect of the fast neutrals even at a pressure of 100 mtorr. Since there will be about one fast neutral leaving the target for each sputtered target atom, the measured argon content of $\sim 10^{-4}$ argon atoms per nickel atom at 100 mtorr (Figure 6-19) implies that at least this proportion reach the substrate with enough energy left to be adsorbed. Based on collision probabilities (Chapter 1), this is a little surprising, but one can't argue with the results. It is presumably a manifestation of the lower collision cross-section and pronounced forward scattering that one expects for higher energy particles (see Appendix 4).

Excited Neutrals

To return to Figure 6-16, we have so far been considering bombardment by ground state neutrals. A further source of bombardment is due to excited neutrals, of which metastables of the sputtering gas would be most abundant. These can presumably lose their potential energy at the growing film and hence influence its growth, although Kaminsky (1965) indicates that these metastables should be resonance ionized and Auger neutralized before they reach the substrate.

Positive Ions

In addition to these neutrals, there will be bombardment by charged particles. Argon ions will be the most abundant positive ions, with a flux of the order of $n\bar{n}/4$. The figure of $20 \mu\text{A}/\text{cm}^2$ from our example in Chapter 3 corresponds to a flux equivalent to a few tenths of a monolayer per second. There will also be ions of the sputtered material, produced both by electron impact ionization and by the Penning process of collision with metastables (Chapter 2, "Metastable Collisions"). These ions, and any others, will be accelerated across the sheath at the substrate. Under normal conditions, the sheath will be quite thin and there will be little attenuation of the ions due to collisions in the sheath.

Valuable information about ion bombardment at the substrate has been acquired via the work of John Coburn (1970 et seq.), who has been able to analyze the energy and mass of ions striking the substrate. His work is described in more detail in the section on bias sputtering. For now, we note that he was able to identify contaminant ions, the less abundant argon ion species such as Ar^{++} and Ar_2^+ , and also complex ions such as ArH^+ and short-lived ions such as H_3O^+ . (We discussed in Chapter 2 how ions can change their chemical identity as their electronic shell structure changes.) So we have to add these ions to our list in Figure 6-16.

SPUTTERING AS A DEPOSITION PROCESS

Negative Ions

Negative ions of the target material may form also. The space charge sheath established at the substrate will tend to repel and slow down these ions, but they will still reach the substrate if they are energetic enough (which will be so if they're formed at the target or in the target sheath). Negative ions at the substrate were detected by Koenig and Maisel (1970) in their work on sputtered quartz. Hanak and Pellicane (1976) have shown how fast negative ions from the target can sputter etch the substrate, and their findings have been confirmed more recently by the experimental work of Cuomo et al. (1978) and the theoretical work of Robinson (1979). Presumably, negative ions can also be formed from gas phase contaminants, although they would be energetic enough to reach the substrate only if they were formed in the target sheath.

Electrons

A major source of charged particle bombardment at the substrate is due to electrons. With a conducting substrate, the average current density will be about $1 \text{ mA}/\text{cm}^2$, which is equivalent to $6.25 \cdot 10^{15}$ electrons/ cm^2 second or a few electrons for each depositing atom. The majority of these electrons will be thermal electrons from the glow where they have energies of a few electron volts (Chapter 3), although only the more energetic of them will be able to surmount the sheath at the substrate. An insulating substrate on the anode in a dc discharge will charge up to floating potential and will receive a much smaller electron flux, equal to the ion flux.

In addition to these slow electrons, there will be bombardment by fast electrons. These electrons are emitted from the target by ion and other impact, are accelerated across the target sheath, and then travel across the sputtering system without making collisions, as described in Chapter 4. So they have energies equivalent to the sheath voltage. These electrons have been detected by Koenig and Maisel (1970); their results in an rf system, obtained by retarding potential measurements, are shown in Figure 6-20. Ball (1972), again using a retarding potential technique but in a dc system, obtained the results shown in Figure 6-21; these results suggest that a large fraction of the electrons striking the substrate have almost the full target sheath voltage, but it is not clear that an allowance was made for the transmission of the analyzer.

The energy spectrum of electrons bombarding the anode has also been measured by Leopoldo Guimarães (Chapman et al. 1974) using the apparatus shown in Figure 6-22. Typical results for the collector current as a fraction of the total current, using a copper target, are shown in Figure 6-23. For reasons involving the resolution and mode of use of the analyzer, these curves do not show electron flux against energy but rather power input to the substrate due to charged

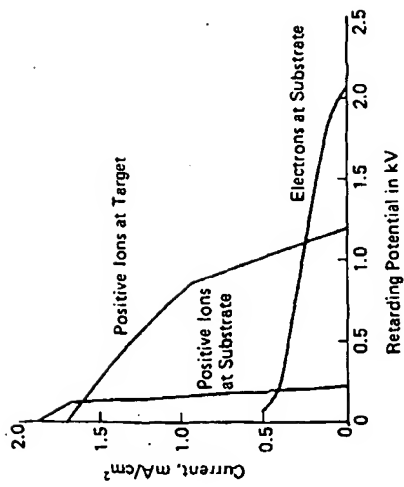


Figure 6-20. Electron and positive ion currents at substrate and target in an rf sputtering system (Koenig and Maisel 1970). Pressure ~ 5 mtorr. Maximum ion energy ~ equivalent dc sheath energy.

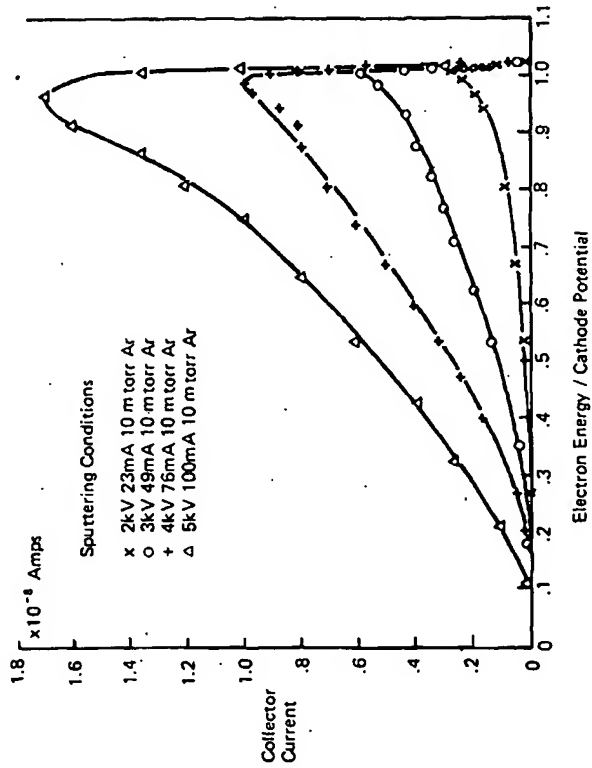


Figure 6-21. Energy spectra of secondary electrons arriving at the anode of a dc sputtering discharge (Ball 1972)

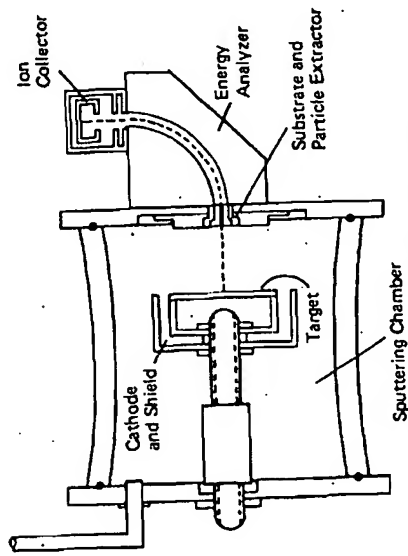


Figure 6-22. Energy analysis system for electrons on the substrate in dc sputtering (Chapman et al. 1974)

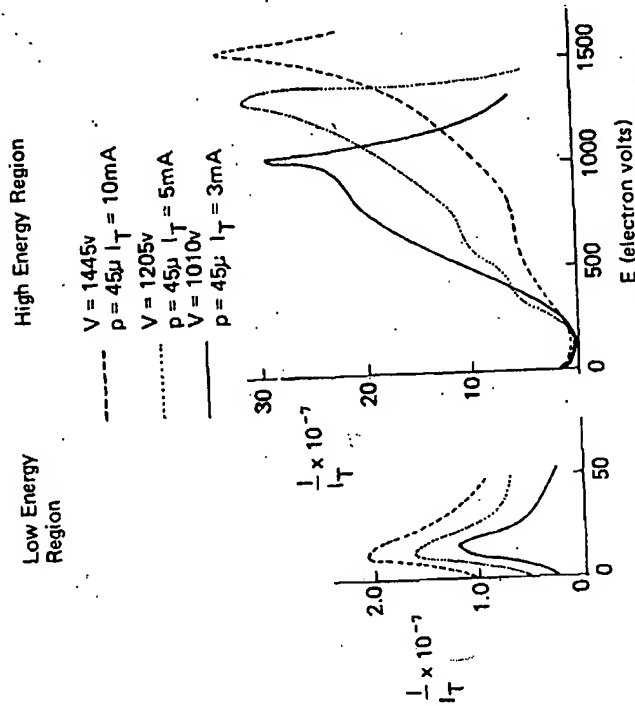


Figure 6-23. Energy spectrum for negative particles at the anode; note the different ordinate scales (Chapman et al. 1974)

particle bombardment versus particle energy, or, more precisely, $dP(E)/dE$ vs. E , where $dP(E)$ is the power carried to the electrode by particles with energies between E and $E + dE$. The flux distribution can be unravelled by noting that $dP(E) = E \cdot dN(E)$. The peak of the flux distribution occurs at quite low energy as expected, but there are a significant number of negative particles, which appear to be secondary electrons emitted from the target, that travel from the target to the substrate without making collisions, and hence travelling along the essentially straight field lines; we discussed these fast electrons in Chapter 4. This collision-free electron travel is presumably a manifestation of the total collision cross-section for electron scattering in argon (Figure 2-27) becoming quite small for electron energies above about 100 eV. However, although small in number, these electrons are responsible for almost all of the power input into the substrate. (The ion-electron recombination energy can also be considerable, amounting to 4.5 mW/cm^2 for an ion current component of 0.3 mA).

In the same series of experiments, a composite sputtering target of copper and glass (Figure 6-24) was used in an rf sputtering system. The glass had a much larger secondary electron coefficient than the copper. The electron emission pattern was directly observed by coating a glass substrate with a fluorescent material and placing this on the counterelectrode of the sputtering system, several inches from the target. It was then possible to directly observe changes in the

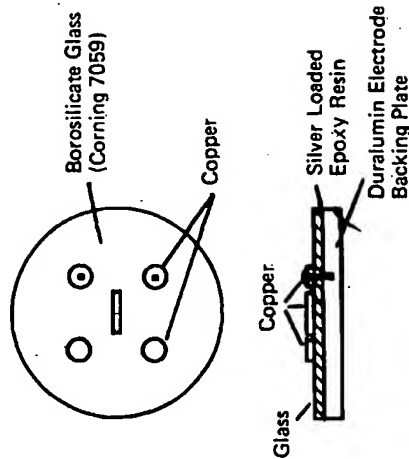


Figure 6-24. Composite sputtering target for secondary electron experiments (Chapman et al. 1974)

SPUTTERING AS A DEPOSITION PROCESS

electron bombardment pattern as the sputtering conditions were varied. The threshold for glowing was at several hundred volts, so that only fast electrons were detected by the screen. The screen glowed very brightly opposite the glass sections of the copper/glass target. Figure 6-25a is a photograph of the fluorescent screen taken at an angle of about 45° through the vacuum chamber wall. The pattern on the screen could easily be deflected with a weak magnetic field (Figure 6-25b), showing the particles to be electrons rather than much heavier (and hence more difficult to deflect) ions.

These fast electrons can have a major influence on the structure and properties of the growing film on the substrate. The large energy input causes a good deal of substrate heating, and there are more subtle effects due to the electron interaction with the surface, as discussed in "Thin Film Formation". These electrons have been observed to discourage as well as enhance thin film growth (Chapman et al. 1974).

Photons

The final type of bombardment that the substrate experiences is due to photons. Photons can be produced by ion or electron bombardment on any surface, and the photon can be as energetic as the ion or electron producing it, which therefore means a thousand electron volts or more in a sputtering system. Such energies put these photons in the soft x-ray class. Lower energy photons will also result from relaxation of excited atoms in the glow.

We have already discussed how photon bombardment can cause electron emission from a surface, and I would be surprised if these photons did not affect the growth of a film, as does every other type of energy input to the substrate. However, there appears to have been very little work on photon effects in thin film growth.

Radiation Damage: Creation and Removal

There is a recent paper by DiMaria et al. (1979) on neutral charge traps produced in silicon dioxide films, actually in a reactive ion etching system which is nevertheless very much like a sputtering system. By measuring the centroid of the damage, they concluded that this damage was due to soft x-rays rather than charged particle bombardments. This conclusion is consistent with the additional observation that similar damage could be produced with the substrate anywhere in the system; photons, being uncharged, bombard all surfaces within the system. DiMaria et al. also found more gross damage at the surface of their samples, which they concluded was due to energetic ion, neutral, and electron bombardment. Their results are consistent with the earlier work by Hickmott (1969), who studied radiation damage in rf sputtered SiO_2 films.

There is a general observation that metallization of semiconductor devices in conventional sputtering systems leads to radiation damage of various types (neutral traps, interface states, etc.). The magnitude of the damage increases with increasing sputtering target voltage. Probably a similar photon bombardment mechanism is responsible for the damage. In order to minimize the damage, magnetron sputtering devices using lower target voltages are currently used for metallization; it seems to be necessary to reduce the target voltage below 500 V. We shall be discussing magnetron sputtering systems later in the chapter. Inconsistent with this sputtering experience, DiMaria et al. have not found any significant energy dependence of damage, at least over the range 300 V - 800 V in their CF_4 reactive ion etching system.

The general phenomenon of radiation damage in thermally grown SiO_2 due to the various microcircuit fabrication processes of sputtering, plasma etching, ion beam implantation, and e-beam lithography, has been reviewed by Gdula (1977). A more recent application of rf discharges is the *rf annealing* process, a method of removing radiation damage (Ma and Ma, 1977), or at least a way of removing charge states. The process consists essentially of exposing wafers to a low pressure rf discharge of fairly low power, inside a barrel type plasma etching system. The gas composition does not appear to be critical. The annealing mechanism is postulated to be a plasma assisted electrical-thermal effect.

Bias Techniques

With so many particles bombarding the film, and with the sensitivity of the nucleation and growth processes to this bombardment, one would expect to be able to influence the properties of the film by changing the flux and energy of incident particles. It is difficult to directly modify the behaviour of the neutral particles, but the charged particles can be controlled by changing the local electric field, and this is the basis of the technique of *bias sputtering*.

Voltage Distribution in Bias Systems

Figure 4-4 showed the distribution of voltage in a dc diode system when a voltage of -2000 V was applied to the target. The plasma potential V_p was at +10 V in that example. Suppose that we now electrically isolate the substrate platform from ground and apply a negative potential of 50 V to it (Figure 6-26). Electrical ground at 0 V is still present as the conducting parts of the chamber walls and baseplate. The plasma potential likes to remain positive with respect to everything in the chamber and, to a first approximation, will be unaffected by the negatively biased electrode, so that V_p remains at +10 V (Figure 6-27).

If the applied bias is V_B volts, then a sheath of potential difference $V_p - V_B$, which would be 60 V in the example, will be established in front of the substrate

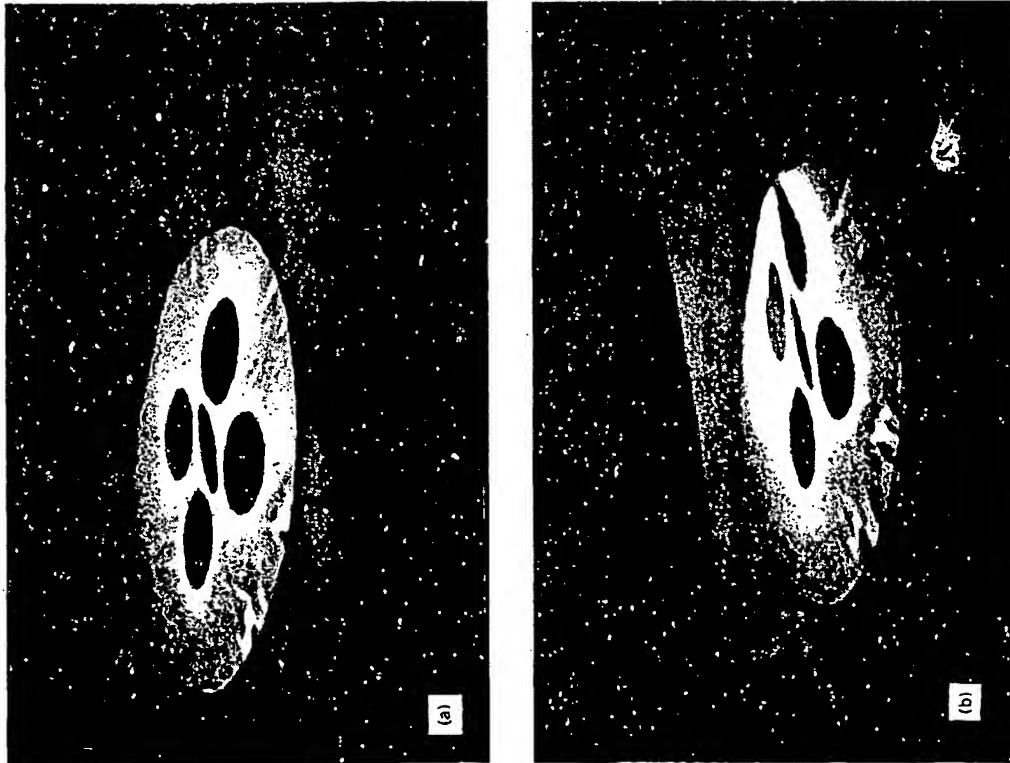


Figure 6-25. Fluorescence patterns on the counterelectrode screen
(a) without magnetic field
(b) with magnetic field
(Chapman et al. 1974)

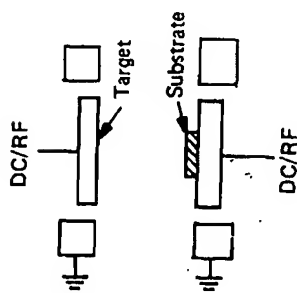


Figure 6-26. Schematic of a bias sputtering system

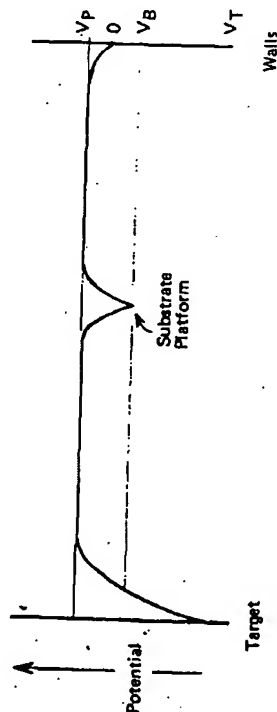


Figure 6-27. Potential distribution in a bias sputtering system

with polarity such as to accelerate positive ions onto the substrate. In effect, the substrate platform has become a secondary sputtering target. By this means, the flux and energy of all charged particles bombarding the substrate (Figure 6-16) can be modified. The energy of the ions striking the substrate would be equal to the energy with which they enter the sheath (which is usually small) plus the energy difference across the sheath, provided that there were no inelastic collisions en route. For small bias voltages, the sheath at the substrate will be thin enough that it will be collision free. For increasing bias voltage, the sheath thickness grows so that collisions may become important and attenuate the ion energy (Chapter 4, "Charge Exchange in the Sheath"). This means that the average energy of particles striking the substrate will increase less rapidly than the applied bias voltage. So a change in film properties as a result of bias sputtering may demonstrate the effects of a much smaller range of ion energies than is apparent.

SPUTTERING AS A DEPOSITION PROCESS

217

If we tried to apply a positive bias potential, then we would encounter the results already discussed in Chapter 4: the plasma potential would rise so as to try to maintain the sheath in front of the bias platform, and the functions of the original anode and the bias table would interchange. This has been observed experimentally by Orla Christensen (1975) in a paper concerned specifically with voltage distributions in bias sputtering. He points out that a positive bias can cause sputtering of the (original) anode and consequent contamination.

Coburn and Kay (1972) have measured positive bias potentials slightly (< 15 V) greater than the plasma potential, which implies that the sheath polarity has reversed. Although this result is not surprising for the very small probes that were used, and which would be limited by their small current-collecting surface areas, much the same result was found for very large positively biased probes. This unexplained result may have been due to the limited fast electron flux on the large probes due to their geometric shapes.

Bias — dc or rf?

An insulating substrate placed in a dc discharge will charge up to floating potential, and placing that substrate on a dc biased platform will not substantially change the situation until the substrate is coated with a conducting film, at which time the bias becomes effective. This situation can be changed by using rf bias, with the same rationale as for the sputtering of insulating targets. There is the same latitude in using dc or rf to power the main target, so that insulating films can be bias sputtered from insulating targets. The sputtering systems used become double ended. Figure 6-28 shows a system used for dc sputtering with rf bias. Systems with rf on both electrodes are probably more common.

It is usual, in both rf and dc bias sputtering systems, to measure the dc bias level with respect to ground. Although a more relevant parameter would be the sheath voltage — the plasma potential minus the bias potential — this is not easy to measure directly because of the relative inaccessibility (on a routine basis) of the plasma potential. The bias voltage is however a useful parameter to ensure reproducibility of the system.

It is probably true to say that, without the additional flexibility of bias sputtering, sputter deposition would be used to a much lesser extent than it is; the bias sputtering technique enables one to control so many film properties.

Control of Film Properties

Figure 6-29 shows how the resistivity of sputtered gold films can be controlled with the use of bias, reaching the bulk resistivity value for a bias of about -40 volts (this figure refers to the dc offset of the rf waveform — see Chapter 5).

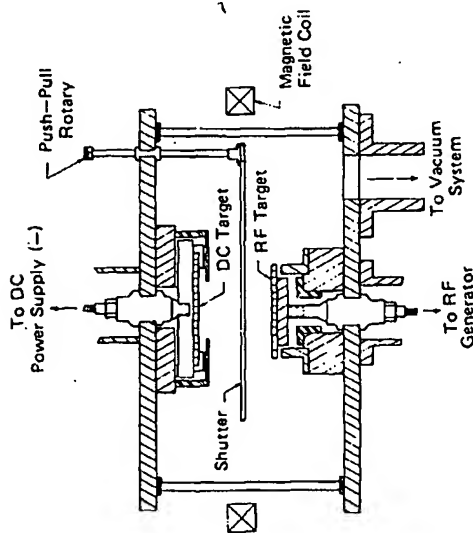


Figure 6-28. DC sputtering system with rf substrate bias (Vossen and O'Neill, 1970)

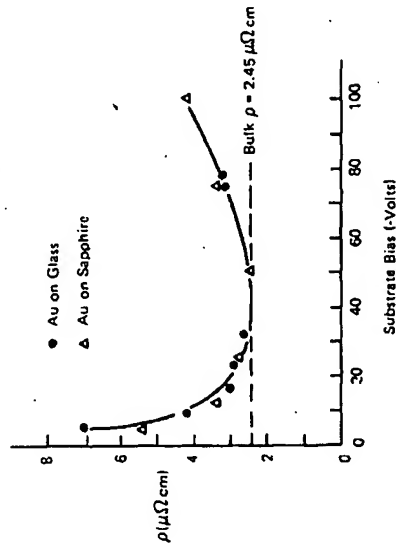


Figure 6-29. The variation of resistivity of 6000Å dc sputtered gold films versus rf substrate bias (Vossen and O'Neill 1968)

Similar behaviour of the resistivity change with bias for tantalum films is shown in Figure 6-30; this figure also illustrates the different effects of dc and rf bias discussed earlier in this section, with only the rf bias managing to achieve bulk resistivity.

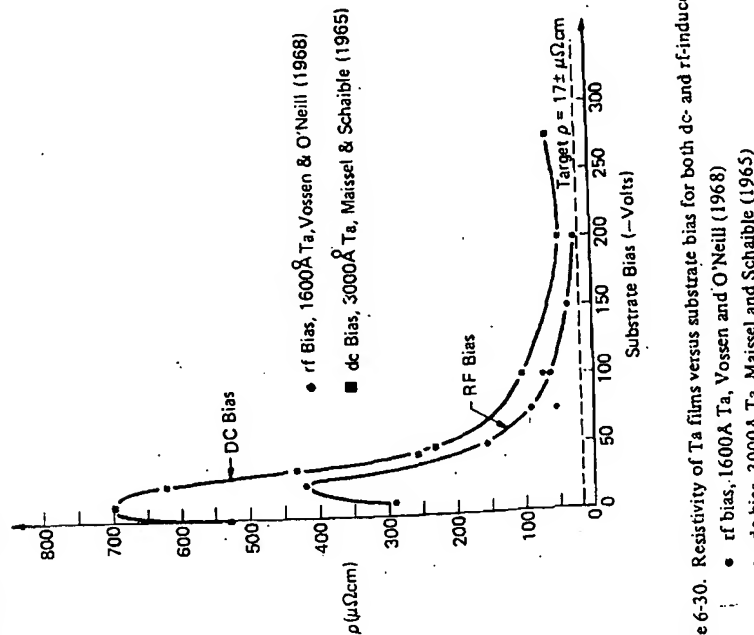


Figure 6-30. Resistivity of Ta films versus substrate bias for both dc- and rf-induced bias

But bias sputtering is not restricted to control of electrical resistivity. It seems as though any and every thin film property can be controlled with this technique. Figures 6-31 to 6-33 show how the electrical properties of sputtered SiO_2 films, the hardness of sputtered chromium films, and the etch resistance of sputtered silicon nitride films in buffered HF, can all be controlled by bias techniques — and there are countless other examples.

Control of Gas Incorporation

Earlier we saw that the sputtering gas can become incorporated into the growing film. The gas content also is a function of bias, and probably contributes to many other bias effects. Pursuing the work reported earlier, Winters and Kay (1967) measured the argon content of nickel films as a function of bias, and

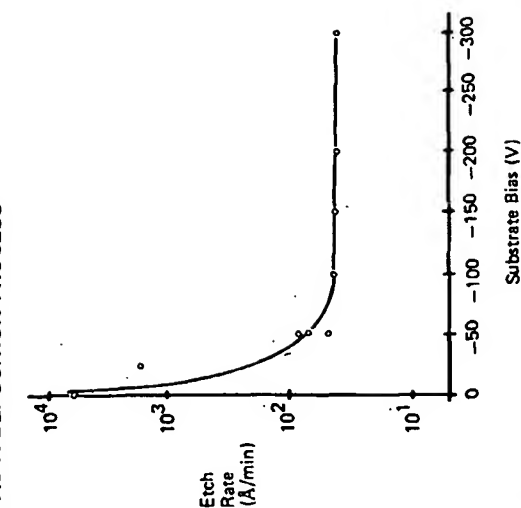


Figure 6-33. The etch rate of reactively sputtered silicon nitride films in buffered HF (Stephens et al. 1976)

their results are shown in Figure 6-34, with the 0-200 eV range clarified in the inset. The decrease in argon content observed is because incoming argon ions at these energies have a high probability of sputtering previously sorbed argon but only a small probability of sticking. However, as the bias voltage is increased, so is the energy of the incoming ions, and they are eventually energetic enough (at ~ 100 eV) to become embedded in the growing film; as soon as this effect dominates the sputtering effect, the argon content starts to rise again.

The growing film is also subject to resputtering by the incoming ions. However, you will recall from the discussion on sputtering target kinetics that the sputtering yield S drops rapidly below 100 eV, so at modest bias voltages of 50V or so, there will generally be little resputtering of the growing film itself; but with more than 100 V bias, resputtering can be significant. We shall return to this point in "Deposition of Multicomponent Materials".

Application of rf Bias

Probably the most common configuration for bias sputtering is with rf on the target and rf bias. This can be accomplished in various ways. A single power supply is normally used, and the rf power is split between the target and sub-

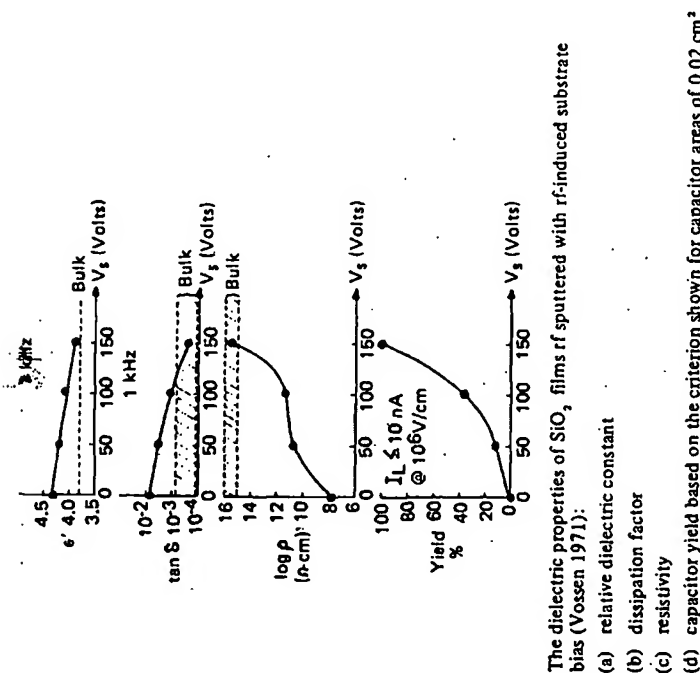


Figure 6-31. The dielectric properties of SiO_2 films rf sputtered with rf-induced substrate bias (Vossen 1971):

- (a) relative dielectric constant
- (b) dissipation factor
- (c) resistivity
- (d) capacitor yield based on the criterion shown for capacitor areas of 0.02 cm^2

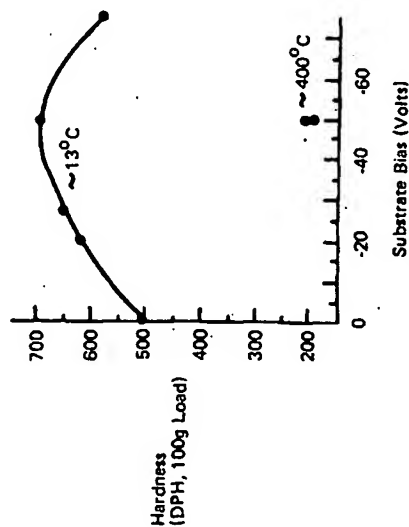


Figure 6-32. Influence of substrate bias voltage and temperature on hardness of sputter-deposited chromium (Patten and McClanahan 1972)

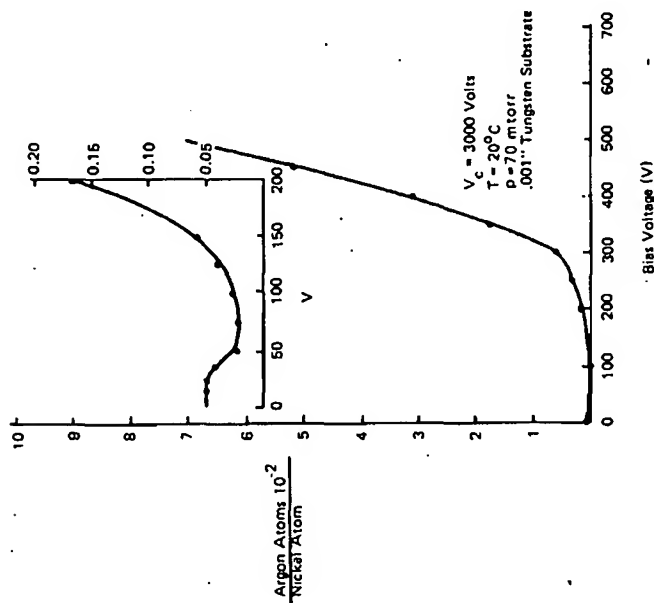


Figure 6-34. Argon concentration of sputtered nickel films, vs bias voltage (Winters and Kay 1967)

strate electrodes either in the matching network (for example with an autotransformer), or less frequently by inductive coupling (the *tuned substrate* system shown in Figure 6-35 and discussed in Chapter 5, "Equivalent Circuits of RF Discharges"), by capacitive coupling (Figure 6-36), or by using a controlled area ratio of electrodes — the *CARF* system discussed in Chapter 5, "Voltage Distribution in RF Systems". By contrast, systems with power more obviously applied to the bias platform are sometimes known as *driven substrate* systems. Keller and Pennebaker (1979) have analyzed the electrical properties of these various systems.

An alternative approach to the driven substrate system with one power supply is to use an rf power amplifier for each electrode with either a single common exciter or individual exciters. In the last case, exciters of nominally the same frequency (usually 13.56 MHz) are used, but they will never in practice be

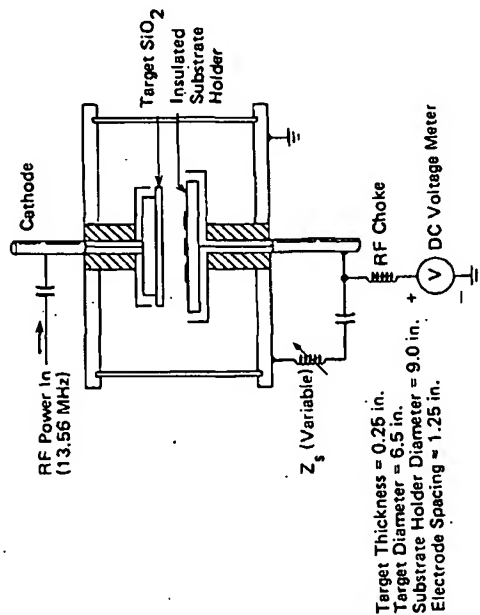


Figure 6-35. Experimental system for rf sputtering with substrate tuning (Logan 1970)

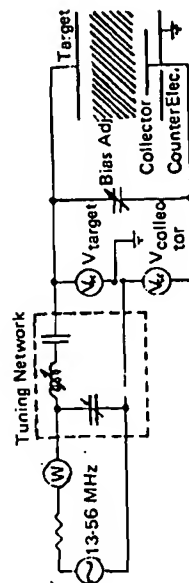


Figure 6-36. Circuit of RF sputtering diode with capacitive collector-to-target coupling (Christensen and Jensen 1972)

exactly the same, so that the phase angle between the two electrodes will continuously and regularly change. In all other cases, there will be a certain phase relationship between the two electrode sheaths that will be a function of operating conditions, cable lengths, and matching network settings. The effects of the phase relationship have been explored by Logan et al. (1977). The significance of substrate bombardment by fast secondary electrons from the target has been noted in the previous section. In rf sputtering with rf bias, these electrons will generally be decelerated by the substrate sheath to an extent determined by the phase of the sheath voltage as they enter. Logan et al. calculated and measured the maximum electron energy (Figure 6-37) and showed also how the threshold

SPUTTERING

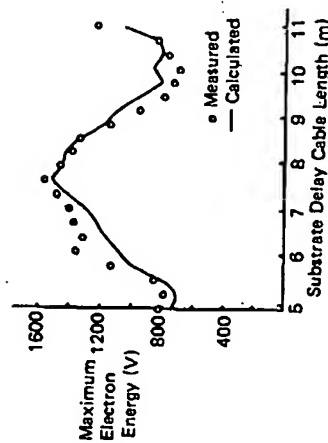


Figure 6-37. Maximum electron energy vs cable length, i.e. phase shift (Logan et al. 1977)

voltage of field effect transistor devices coated with sputtered quartz would be shifted during sputtering (Figure 6-38). The threshold shift increased with the maximum electron energy, and so could be phase controlled (which was achieved by varying cable lengths). As the maximum electron energy increased, higher annealing temperatures were required to anneal out the damage. Other parameters also might change with the phase angle.

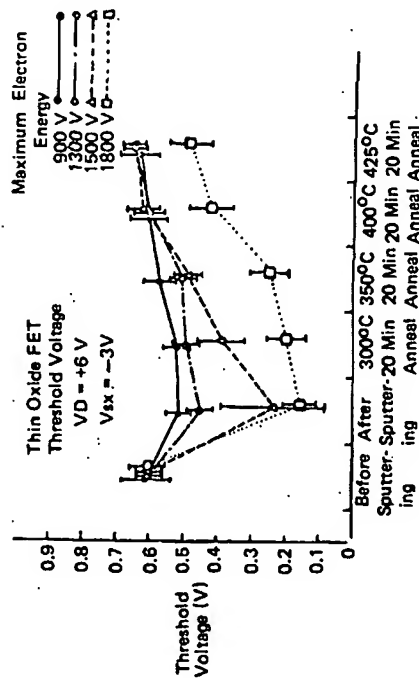


Figure 6-38. FET threshold voltage shift vs electron energy (Logan et al. 1977)

SPUTTERING AS A DEPOSITION PROCESS

Bias Sputtering Mechanisms

In a previous section, we saw that sorbed argon can be resputtered from the growing film by the bias sputtering technique. It is very common to find explanations for bias sputtering that describe how "... loosely-bonded material can be resputtered from the growing film by low energy ions". This may be an adequate explanation for the resputtering of weakly physisorbed gases, but it does not account for other commonly observed phenomena. As an example, sputtered chromium has a very high affinity for oxygen and tends to oxidize easily in the small amount of oxygen always present in a system; the use of bias sputtering can minimize this oxidation, even though the chromium-oxygen bond is very strong.

Winters and Kay (1972), in an extension of their earlier work on argon incorporation in thin films, studied the composition of films deposited in a gas mixture of argon and nitrogen. As a result of this study, they divided metals into three classes:

- metals which chemisorb molecular nitrogen and form a nitride, e.g. W.
- metals which do not chemisorb molecular nitrogen but still form a nitride, e.g. Ni.
- metals which neither chemisorb nitrogen nor form a nitride, e.g. Au.

Winters and Kay found that bias sputtering caused the nitrogen content of gold to increase, due to the increased sorption of nitrogen when the film was bombarded by energetic N_2^+ ions. However, although this same effect is present with the tungsten and nickel films, it is overshadowed by resputtering of the previously sorbed nitrogen, as it was for the tantalum films in pure argon at low bombardment energies. This rather surprising result is a consequence of the sputtering yield for nitrogen on tungsten being rather large. Winters and Kay maintain that there is adequate evidence to conclude that most chemisorbed gases have large sputtering yields and low thresholds; they suggest that this is a consequence of the poor mass fit in the energy transfer function $4m_1 m_2 / (m_1 + m_2)^2$ so that a struck chemisorbed atom cannot transfer its energy to the underlying substrate lattice. However, as we shall be discussing later in this chapter, there are examples in which a very thin metal surface layer, again having a poor mass fit to the substrate, has an anomalously low sputtering yield.

So it appears that bias sputtering can lead to either an increase or decrease in the concentration of gaseous species, depending on their surface adsorption characteristics which in turn control their sputtering yields. Winters and Kay also conclude that bias sputtering is unlikely to reduce impurity concentrations by more than a factor of 10, so that the biasing technique is not much of a substitute for good vacuum. However, Figure 6-39 shows how the nitrogen content

of metal films (unbiased) changes with the partial pressure of the nitrogen in the argon. Note that the nitrogen content of tungsten, which chemisorbs molecular nitrogen, decreases by less than a factor of 10 over four orders of nitrogen pressure change. So it may well be that, for tungsten and other class (a) metals, that biasing is very effective compared with decreasing the partial pressure of the contaminant.

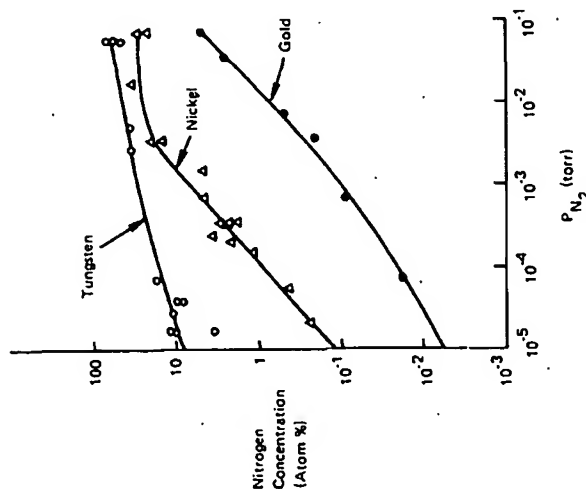


Figure 6-39. Nitrogen concentration in film vs partial pressure of nitrogen; $P_{\text{tot}} = 70$ mtorr, $T = 300$ K, target voltage = 3000 V, bias voltage = 0, and target - substrate distance = 4.5 cm (Winters and Kay 1972)

Winters and Kay make two other points. Firstly, they consider the effect of backscattering in the gas phase which tends to return sputtered material back to its substrate; they conclude that in many instances bias sputtering may be more effective in obtaining high purity films if the sputtering pressure is relatively high. Secondly, they note also that ion bombardment, and hence bias sputtering, also changes the physical appearance of a film. They had previously shown that

nickel films became much smoother as the bias voltage was increased from 0 V to 300 V. The topography of the film surface is important in determining its optical appearance, as light is scattered from surface features; we shall discuss more extreme examples of this later in the chapter. In Winters' and Kay's experiments, unbiased films of tungsten, nickel and iron looked dark grey or almost black, whilst biased films appeared metallic.

This last result emphasizes another point. Much of our discussion about bias sputtering so far has been concerned with the effect of bias on gas content. However, gas content is just one of many parameters which contribute towards the nature of a thin film. For example, the gold resistivity change in Figure 6-29 was apparently related to film density and not gas incorporation, and the tantalum resistivity modification in Figure 6-30 was due to a phase change. And other parameters such as the surface roughness or the hardness of a film may be important for a particular application.

Ion bombardment has many effects, some of which we are only now beginning to learn about; for example, in Chapter 7 we shall see how chemical reactions can be accelerated by ion bombardment. Changing the bias voltage will also change the power input to the film. The power due to ion bombardment can be considerable, and the consequent heating may be helpful or, as we shall see shortly, may lead to *grain growth* and other undesirable film features. We have also seen in earlier sections how fast electrons from the target can bombard the substrate. Increasing the bias on the substrate will tend to retard the electrons and lower their bombardment energy. Whilst this is always true in dc systems, the statement has to be restricted in rf systems depending on the phase of the sheath field seen by the fast electrons as they enter the substrate sheath. We discussed phase control in the previous section, and showed how it could be used to influence the threshold shift of FET devices during sputtered quartz deposition.

We would probably be correct to conclude that the control of the gas content of films is a significant role for biasing; but there are likely to be many other effects due to the flux and energy of ion and electron bombardment on the substrate. Some of these might be simple, such as thermal effects, and some might be more subtle influences on the nucleation and growth stages of the film. And in the next few sections we shall see how biasing can be used to control film topography by deliberately encouraging resputtering, but can also cause problems with multicomponent films by resputtering the film and causing a depletion of the component with the higher (or highest) yield.

There is no doubt that biasing can add enormously to the power of sputter deposition. As a broad generalization, it is likely that, no matter what particular film property you are interested in, it can be influenced by the bias sputtering technique. Try it and see!

Analysis of Charged Particle Bombardment at the Substrate

In earlier chapters, the work of Davis and Vanderslice (1963) has been mentioned. They identified the mass and energy of ions bombarding the cathode of a dc discharge, as a means of understanding some of the target sheath phenomena. John Coburn (1970) has used the same approach, but applied to the substrate platform, with and without bias. This application has been extremely fruitful, covering quite a range of topics, and in our energy-conscious world, Coburn has to be congratulated on getting such good mileage out of the technique!

The experimental arrangement is shown in Figure 6-40. Some of the ions bombarding the substrate plane pass through a small aperture into a differentially pumped low pressure region, where they are first energy analyzed and then mass analyzed.

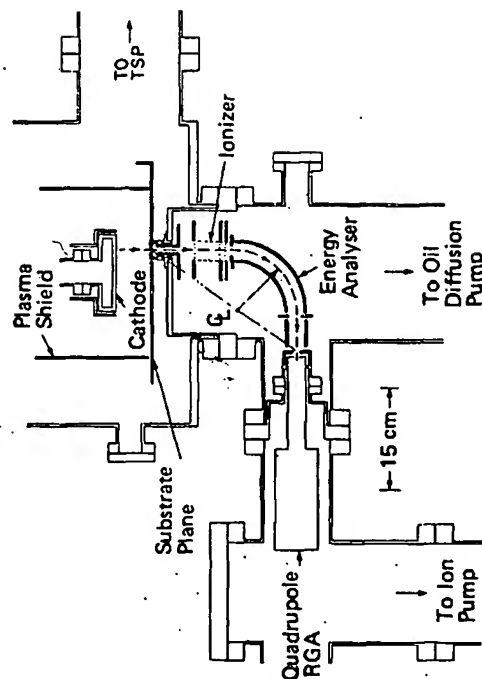


Figure 6-40. Experimental arrangement for the mass and energy analysis of ions bombarding the substrate plane (Coburn, 1970)

This arrangement can be used to identify the ion species at the substrate as a function of their energy. Figure 6-41 shows 2 spectra of ions from a system sputtering copper. These spectra differ as a result of the energy analyzer being set to admit different energies. In this case the difference was 1 eV; the bias voltage was -30 V. The figure shows some of the complex and contaminant ions referred to earlier in the chapter.

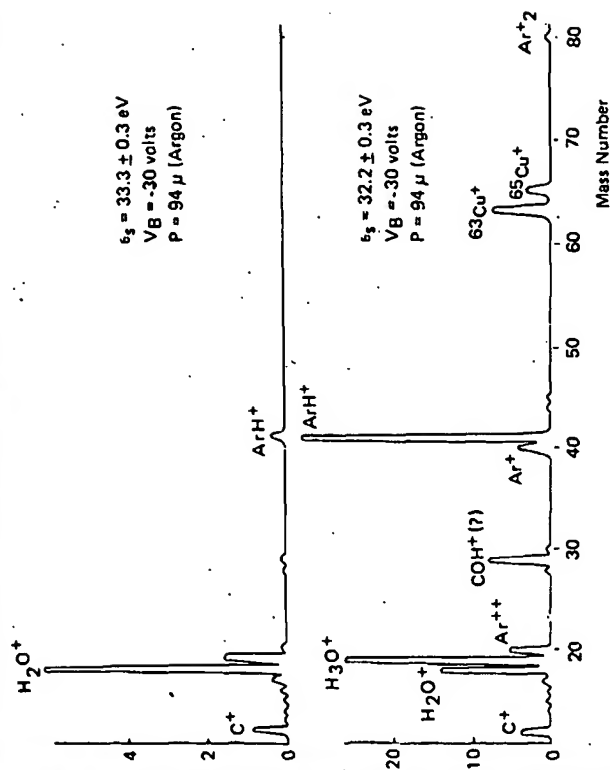


Figure 6-41. Mass spectra of positive ions from a dc discharge prior to sublimation pumping (Coburn 1970). Copper target -1000 V, cathode-bias table spacing 5cm, argon pressure 94 mtorr, bias voltage -30 V.

Upper trace: analyzer set to 33.3 ± 0.3 eV
Lower trace: analyzer set to 32.2 ± 0.3 eV

The mass/energy analyzer can also be used to measure the substrate sheath voltage (plasma potential minus substrate potential) by looking at an ion such as Ar_2^+ , which has a low cross-section for collisions in the sheath and a high mass so as to minimize energy modulation by the rf field as it crosses the sheath. The energy distribution will be strongly peaked at the sheath voltage. We have already discussed this application in Chapter 5.

Some of the sputtered target is likely to become ionized, particularly by the Penning mechanism of collision with a noble gas metastable, as discussed in Chapter 2: Copper has an ionization potential of 7.7 eV, well below the 11.6 eV metastable level of argon, and would be expected to be Penning ionized. Figure 6-41 clearly shows copper ions from the target.

The combination of an electron multiplier as an ion detector and a modern stable low-current amplifier, enables one to look at ion spectra with very high

gain. Figure 6-42 is a mass spectrum of ion bombardment on the substrate plane when a target half of copper and half of tantalum was sputtered in argon. In this case the energy analyzer was not used. If the ion fluxes from different mass numbers occur over a very wide range (in this case 6 orders of magnitude), the conventional approach is to take a series of spectra, with each subsequent spectrum having a gain increase of $\times 10$. Spectra for the Cu-Ta target example, taken by this means, are shown in Appendix 6, and are probably easier to interpret in that form. However, the series of spectra can also be taken in a single scan, with a useful savings in time, by using a logarithmic amplifier, as shown in Figure 6-42; actually this figure has a special non-linear logarithmic or *coburnithmic scale*.

The largest ion currents in Figure 6-42 come from argon as expected. But the logarithmic amplifier reveals Cu^+ , Ta^+ , and less abundant argon peaks at lower ion currents. For even smaller currents, less abundant isotopes and complexes appear, followed by contaminants such as Nb^+ and CH_3^+ . And so on. This expanded spectrum (and those in the appendix) show the sensitivity of the technique, and also illustrate one of the mixed blessings common to modern analytical techniques: the closer you look, the more you find.

Mass spectrometer data such as these have to be carefully interpreted, as the ion current magnitude cannot simply be equated with ion abundance; the quadrupole spectrum tends to underestimate higher mass ions, and its sensitivity also depends on ion energy.

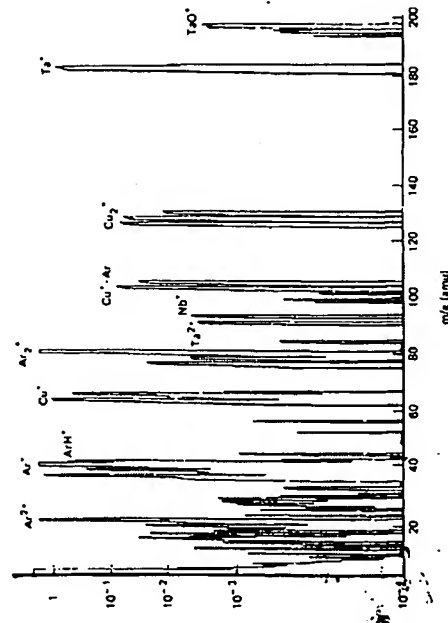


Figure 6-42. Ion mass spectrum at the substrate plane in an argon discharge sputtering copper and tantalum (Coburn 1979)

The mass/energy analyzer has been used by Coburn, by Coburn and Kay and other colleagues, for a variety of applications such as to measure the effects of discharge confinement on plasma potential, as described in Chapter 5, "Experimental Test of the Voltage Distribution Model". The sensitivity of the technique to the composition of a sputtering target makes it useful also as a technique for analyzing the composition in depth of the target as it is sputtered away. The technique is then called *Glow Discharge Mass Spectrometry (GDMS)*, and is one of a series of techniques for *depth profiling* a sample, as discussed later in "Sputter Etching". In GDMS, one can employ noble gases with higher metastable states so as to encourage Penning ionization of the target components and so enhance the sensitivity of the technique.

I suspect that mass/energy analysis will continue to be useful in glow discharge analysis. Essentially the same technique has been recently used by Komiya et al. (1977) to study vapour deposition using a hollow cathode glow discharge.

Bias Evaporation

So far we have been looking at the use of bias to control the properties of films deposited by sputtering. But the bias technique affects conditions at the substrate mostly, and in principle deposition could be by any technique, for example by evaporation. There are two manifestations of this combination, which are different in application rather than in concept. *Ion plating* is used primarily for high rate metal deposition with very large dc bias applied and is discussed further in the section on ion plating; *bias evaporation* is normally used with rf bias, with similar bias values as in bias sputtering.

Bias evaporation has been used by Vossen and O'Neill (1970) for the evaporation of aluminium. They suggest its use for any materials that recrystallize easily, and which would recrystallize under the energy input from a sputtering target. A schematic of the bias evaporation configuration is shown in Figure 6-43. Of course, to obtain any considerable amount of ion bombardment

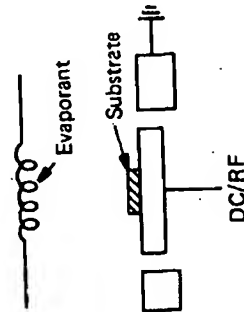


Figure 6-43. Schematic of a bias evaporation system

on the substrate, there must be a plentiful supply of ions, and these are obtained from a local glow discharge with substrate as target or part of the target. To obtain the discharge, the system is filled with argon to a pressure of a few millitorr.

Vossen and O'Neill reported several advantages of this technique over conventional evaporation. These advantages were in terms of being able to achieve almost bulk resistivity, ohmic contacts to silicon without sintering, reduced pinhole density, conformal coverage over severe substrate topography (which is discussed further in the section on that subject), and smoother films. To elucidate the latter, aluminium films generally have a tendency to form hillocks and to show microscopic pitting. With bias, these defects were less evident and reached a minimum at -400 V. For larger biases, the film started to show preferred $\{111\}$ crystallographic orientation, and the surface roughened as grain growth became evident, probably due to the heating effect of the ion bombardment. However, we must note that some of the improvements were probably a result more of the sputter cleaning of the substrate just prior to deposition rather than of the ion bombardment during it.

Bias Sputtering For Conformal Coverage

Bias sputtering can be used to control where a film is deposited, so as to ensure conformal coverage of surface topography.

Coverage of "difficult" surface topography, of which a perpendicular step is the epitome, has long been a problem and is responsible for many device failures, such as an open circuit in aluminium metallization on a silicon chip (Schnable and Keen, 1971).

Conformal coverage is difficult because surface features act effectively as masks and/or present little surface area to the deposition source. Changing the type of deposition source usually alleviates one of these problems only by accentuating the other (Figure 6-44). Vossen (1971) has demonstrated that neither rotating the substrate table nor using planetary rotation offers a proper solution and that the same is true of straightforward sputtering; however, it must be added that some people are satisfied with the use of planetary rotation, at least to the extent that it eliminates failures, which is not the same as saying that conformal coverage was achieved.

Seeman (1966) showed how it was possible to uniformly coat the inside walls of deep narrow trenches by dc bias sputtering. Logan et al. (1970) have used re-sputtering to obtain better edge coverage with sputtered quartz films. Vossen (1971) has shown how biasing can similarly overcome the problem of metallizing steep walls. The basic principle used to cover the side walls is to resputter already deposited material and redeposit this on the side walls. This is facilitated by the sputter ejection pattern being under-cosine (Figure 6-45) for low energy bom-

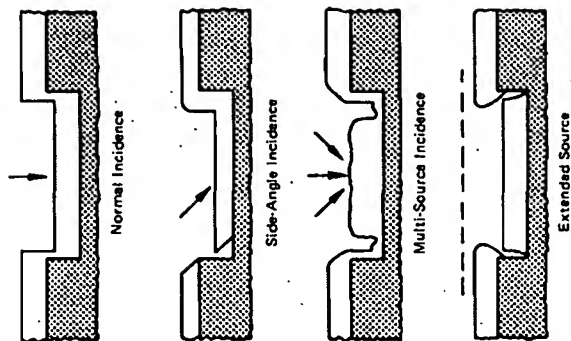


Figure 6-44. Defects arising as a function of source geometry during deposition of a coating to cover a steep step in a substrate (Kern et al. 1973)

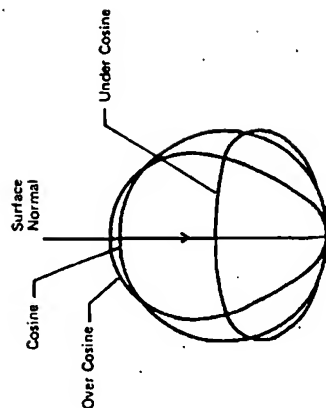


Figure 6-45. Angular distribution of particles from a polycrystalline target as a function of incident ion energy and direction (Kay 1962)

bardment; i.e. there is a tendency for material to be ejected sideways rather than outwards (cosine or over-cosine) as at higher energies. (The cosine law was initially derived from kinetic theory to describe the angular distribution of gas molecules bombarding a surface or leaving it. The result, which follows from an assumption of complete randomness of the motion of individual molecules, states that the number of molecules leaving the surface in a small element of solid angle $d\omega$ at an angle θ to the surface normal, is proportional to $d\omega \cos \theta$. The sputter ejection of atoms from a polycrystalline target is also a quasi-random process and tends to follow the same cosine law – to the extent already noted). As the bias voltage periodically varies, which it does (at mains frequency) for the usual rf or dc bias power supply to a greater or lesser extent (in this case, the greater extent is required – in other cases, we prefer to have a very small ripple), there is thus an effect which Vossen compares to a fireman hosing a wall up and down! There is little tendency for the material already on the side walls to be re-sputtered because the sputtering yield at virtually oblique incidence is practically zero (see later).

Vossen's experiments were performed using silicon substrates into which $6\mu\text{m}$ high vertical steps had been anisotropically etched. Figure 6-46 shows the varying distributions of platinum dc sputtered onto the silicon test wafer at various rf-induced bias voltages. As the bias voltage is increased, relatively more metal is resputtered on to the side walls. Similarly, for a given bias voltage a greater portion of material will be resputtered on to the side walls as the deposition rate is reduced. This is clearly a very useful technique for conformal coverage, but the parameters must be carefully chosen. In Figure 6-46, one sees again evidence of grain growth in the metal film. It is probably still true that people try to avoid having sharp corners rather than cope with them. Steep walls from etching processes can be turned into more gradual slopes by using 'taper control layers' (Kern et al. 1973) in wet chemical etching, or by using selective degradation of the photoresist in reactive ion etching, as described in Chapter 7, "Isotropic or 'Anisotropic' Etching?"

Finally in this section, we note the use of the bias technique to achieve not conformal coating, but almost its opposite – a deposited film with a planar surface, regardless of the topography of the substrate. This usage of bias sputtering for *planarization* (Ting et al. 1978) will be clearer after looking at the angular dependence of the sputtering yield, in "Sputter Etching".

Backscattering in Bias Sputtering

In an earlier section ("A Conventional DC Sputtering System – Choosing the Pressure Range"), we saw how molecules from a sputtering target can collide with gas phase molecules and be scattered, in some cases right back onto the target. This is a problem in bias sputtering, because the substrate backing plate

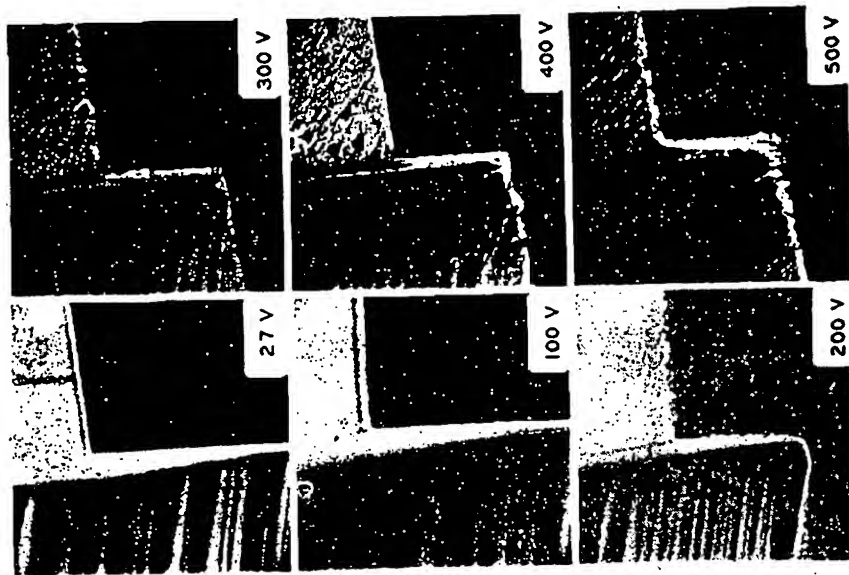


Figure 6-46. The thickness distribution of Pt coatings dc sputtered with various rf-induced bias voltages. The plane surface accumulation rate was held constant at 300 $\text{\AA}/\text{min}$ (Vossen 1971)

(Figure 6-26) will also be subjected to ion bombardment, and the resultant sputtering of the plate and backscattering in the gas phase can lead to backing plate material being deposited onto the substrate and incorporated into the growing film. A similar phenomenon of mixing would occur on composite targets, and would be important in sputter etching if not in sputter deposition. This problem has been investigated by Vossen et al. (1970). They placed 2.4 cm silicon wafers on various 15 cm diameter metal targets, principally Pt, in an rf diode sputtering system, with interelectrode separation of 5 cm. Using a dc level of ~ 700 V on the rf target, they found that the platinum concentration on the silicon reached an equilibrium value after about 10 minutes. This equilibrium value ranged from about 1 monolayer at 2.5 millitorr to about 4 monolayers at 20 millitorr, showed little spatial dependence except near the edges of the wafer (Figure 6-47), and increased monotonically with pressure although showing signs of saturation. The equilibrium value is presumably a balance between deposition by backscattering, and resputtering. In this work the target voltages used were more representative of sputter etching than of bias sputtering, but note that although sputtering of the backing plate would be much slower at the lower voltages used in bias sputtering, so also would resputtering from the substrate. Vossen et al. did vary the target voltage over the range 500 V - 1200 V, and found that the platinum coverage on the substrate increased from 2 monolayers to 4.5 monolayers as the voltage was reduced to the lower limit. It would be unwise to extrapolate these results down to the 50 V or so frequently used in bias deposition, because the sputtering yields of materials change so rapidly with energy at such values.

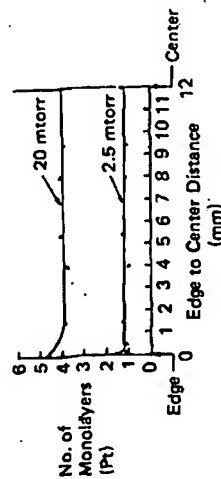


Figure 6-47. Typical wafer profiles; effect of argon pressure (Vossen et al. 1970)

The very clear lesson from these and similar results (Chang et al. 1973) is that one should use a backing plate which is at least compatible with the material being deposited, and may ideally be the same. The same message applies to the comparable situation in both types of diode plasma etching, as discussed in Chapter 7.

We shall return to the subject of backscattering in the section on 'Sputter Etching', where we shall also see that there can be some very unfortunate choices of backing plate material.

Deposition of Multicomponent Films

Most of our discussion to date has been concerned with the sputtering of single elements. But often multicomponent films are required, and these may be alloys, compounds, or a mixture of both. They can usually be prepared by sputtering from a single compound target, simultaneously from several different targets, by reactive sputtering, or by a combination of these techniques.

There are four stages that we have to consider, of the transport of an atom from a sputtering target to its incorporation into the thin film. These stages are sputter ejection from the target, transport through the gas, condensation onto the substrate, and stable incorporation into the film. We shall now consider these four stages.

Alloys

Let's consider initially the deposition of an alloy film, and specifically we'll think about deposition from a Ni:Fe target of uniform 80:20 composition. When we first start to sputter the target, we'll be removing the layer of metal oxide that is inevitably on the surface of the target. During this period, the shutter must be interposed between the target and the substrate to prevent condensation onto the latter. After some while, which will probably be in the 5 minute-30 minute time range, the sputtering system will have stabilized and the surface oxide will be removed, revealing the metallic alloy. In dc sputtering, the removal of the oxide will be accompanied by a corresponding change (usually a decrease) in the discharge current, since the secondary electron coefficient of the metal and the oxide differ. Even if rf sputtering is eventually to be used, the use of dc sputtering to determine the time required to remove the surface oxide, is often extremely helpful, and this of course can be applied to single element sputtering as well as multicomponent.

Now the metal alloy surface, initially having an 80:20 composition, is exposed. But nickel has a slightly higher sputtering yield than iron; for 1000 eV argon ions, it's 2.1 for nickel and 1.4 for Fe (see Appendix 6). So if we used ions of this energy, the nickel and iron atoms would be sputter ejected from the target in the ratio $80 \times 2.1 : 20 \times 1.4$; 86% of the atoms leaving the target would be nickel compared with 80% in the target. But this situation can't last for long, because a result of the preferential ejection of the nickel will be to cause the surface of the target to become enriched with iron. As this iron enrichment occurs, so the sputtering rate of iron atoms increases and of nickel atoms

decreases until they are again leaving in the ratio 80:20. Ultimately, in steady state, the departure rate from the target must equal the supply rate, which is the 80:20 alloy from the bulk of the target. In order to achieve this, in the present example, the surface composition would adjust to 72.7% Ni:27.3% Fe. During the period when the surface composition is stabilizing, the shutter must continue to be used to prevent condensation onto the substrate.

Two phenomena can prevent the steady state conditions described above, from being reached. The depletion of one element on the target surface (nickel in our example) will set up a concentration gradient of each of the elements at the surface, and this will encourage diffusion. In the case above, nickel will diffuse towards the surface and iron away from it; with enough diffusion, the initial 86:14 sputtering ratio could be maintained. Diffusion is minimized by keeping the target cold enough, and 'cold enough' will vary from alloy to alloy, of course.

Keeping the target cool will also offset another potential problem that can be encountered when sputtering multicomponent materials. If one of the elements or compounds has an appreciable vapour pressure at the target temperature reached, then it will evaporate from the target. Remember from Chapter 1, "Monolayer Formation Time", that a vapour pressure of 10^{-6} torr would correspond to an evaporation rate of about 1 monolayer per second. When the target has reached steady state, the shutter can be moved back and deposition can begin. Transport of the sputtered material from target to substrate will rarely be straight line travel. Even at the lowest sputtering pressures, collisions with the sputtering gas atoms will take place. As the pressure increases, transport becomes more like a diffusion process and some material is redeposited back onto the target. The redeposition does not affect the alloy composition because the target adjusts itself so that the *net* composition leaving the target is the same as the bulk. However, as the mfp of sputtered material decreases, more of it will eventually land on the walls and proportionately less on the substrate. There is no reason why the target atoms (Ni and Fe in the example) should have the same mfp, and so we should expect that the ratio of the Ni and Fe fluxes at the substrate will not be 80:20. On the other hand, the mfp values shouldn't be very different, so this will be only a small perturbation on the 80:20 value.

The next stage involves the condensation of the material onto the substrate. As we saw in the earlier section on "Thin Film Formation", an atom arriving at the substrate migrates around on the surface for a while, hopping from one adsorption site to another, until it either joins with another migrating atom to form a more stable pair, or it evaporates. The *condensation coefficient* is the proportion of the atoms arriving at the substrate that remains without evaporating, and this will be determined by the arrival rate, the bonding energy between adatoms and substrate, and the substrate temperature. In general, the condensation coefficient

SPUTTERING AS A DEPOSITION PROCESS

cient of each constituent of a multicomponent target will be different, causing an effective change in the composition of the depositing alloy.

Finally, the growing film will be bombarded by ions and so there will be a certain amount of resputtering of the growing film. As well as sputtering gaseous components from the film, the ion bombardment will sputter the solid components too. Since sputtering increases with increasing ion energy, such resputtering will be particularly effective under bias sputtering conditions. In the deposition of alloys, as at the target, the film will be depleted of the component with the higher sputtering yield. At the substrate, however, there will be no compensating mechanism.

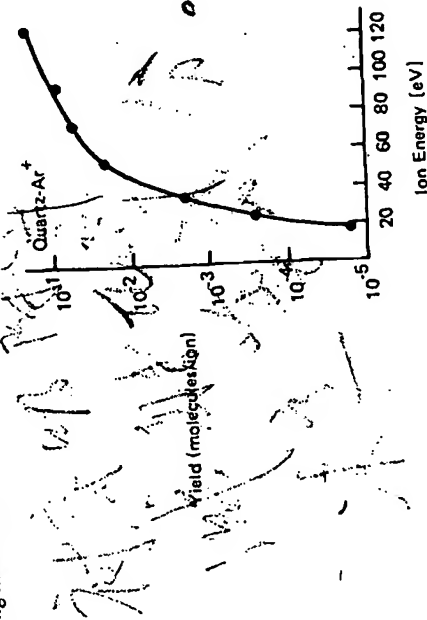


Figure 6-48. Sputtering yield of quartz in argon, in molecules per ion vs bombarding energy (Jorgensen and Wehner 1965)

Earlier in this chapter we have discussed sputtering primarily with rather energetic (~ 500 eV) ions. In bias sputtering, bias voltages of the order of 50 V are more common, and so low energy sputtering yield data becomes of interest. Figure 6-48 shows sputtering yield data for quartz in argon (Jorgensen and Wehner 1965). This data is typical also of the sputtering of metals, for which more yield data, obtained by Stuart and Wehner (1962) using an optical spectroscopic technique, is shown in Appendix 6. What is commonly observed is that the yield, which decreases linearly as the ion energy reduces from 1000 eV to 100 eV, starts to decrease much more rapidly somewhere below 100 eV; n.b. the logarithmic vertical axis in Figure 6-48. An apparent threshold is observed, although this is influenced by the sensitivity of the detection technique. Table 6-2 shows

SPUTTERING
Table 6-2 Threshold Energies (Stuart & Wehner 1962)

	Ne	Ar	Kr	Xe	Hg
Be.....	12	15	15	15	
Al.....	13	13	15	18	18
Ti.....	22	20	17	18	25
V.....	21	23	25	28	25
Cr.....	22	22	18	20	23
Fe.....	22	20	25	23	25
Co.....	20	25	22	22	
Ni.....	23	21	25	20	
Cu.....	17	17	16	15	20
Ge.....	23	25	22	18	25
Zr.....	23	22	18	25	30
Nb.....	27	25	26	32	
Mo.....	24	24	28	27	32
Rh.....	25	24	25	25	
Pd.....	20	20	20	15	20
Ag.....	12	15	15	17	
Ta.....	25	26	30	30	30
W.....	35	33	30	30	30
Re.....	35	35	25	30	35
Pt.....	27	25	22	22	25
Au.....	20	20	20	18	
Th.....	20	24	25	25	
U.....	20	23	25	22	27

the threshold data obtained by Stuart and Wehner, corresponding to a detection limit $\sim 10^{-5}$ atoms/ion. They observed no correlation between thresholds and energy transfer functions, and concluded that a binary sputtering model is inappropriate at these energies, in accord with more recent theories.

In a later section on "Sputter Etching", I shall describe some work by Tarnag and Wehner (1972) that shows how the sputtering yield of some thin film materials varies enormously according to the thickness of the film and the nature of the underlying substrate. There is very likely to be a comparable effect in bias sputtering, compounded if one is depositing a multicomponent film. Under such

SPUTTERING AS A DEPOSITION PROCESS

circumstances, sputtering yield data from homogeneous targets is probably of little relevance.

Taking all of these various effects together, we can see that the composition of a sputter deposited alloy film can be quite different from that of the target. However, the composition change should be reproducible for a given set of conditions, and so it becomes mainly a matter of choosing or fabricating a target of appropriate composition.

There are two other points to be noted. Firstly, a sputtering ratio of the two elements in the target holds for a particular ion bombardment energy. If that energy changes, e.g. by changing the target voltage or by changing the pressure, there will be a transition period while the target surface adjusts to a new steady state composition. Secondly, the composition of the deposited film can be changed somewhat by adjusting the bias voltage and other process parameters, but this means may be inconsistent with other process requirements. More flexibility may be attained by using two (or more) quasi-independent targets. One would then need to consider the deposition uniformity problems posed by the geometric constraints of this arrangement, as well as by the beam-like nature of electron and negative ion (if present) bombardment of the substrate. Nevertheless, this can be done successfully, with adequate confirmation from the deposition of multicomponent magnetic films.

Compounds

We now turn to consider the sputtering of a chemical compound target. Is this target sputtered as molecular species or as atoms? The general answer is both. The question has been studied by Coburn et al. (1974), who also cite several other papers where sputtered molecular species were detected.

Coburn et al. studied the rf sputtering of metal oxides. Using the ion sampling and analysis system that was described earlier in the section on bias sputtering, they have looked specifically at the relative numbers of atomic metal ions and dimeric metal oxide molecular ions arriving at the substrate plane. In some cases, ternary and more complex molecular ions were observed but always at very low intensities. Coburn et al. presented their data in terms of $\eta = MO^+/(M^+ + MO^+)$ for a series of metals M. They found that η was strongly influenced by the relevant M-O bond strength, as shown in Figure 6-49. Not surprisingly, more strongly bonded metal oxide ions were less likely to be disassociated. Whilst η is defined and measured for ions, one would expect this ratio to be at least indicative of the corresponding neutral species, and probably numerically not so different. Coburn et al. also found that η decreased significantly with increasing pressure, and since η at zero pressure is likely to be the best representation of the ion ratio leaving the target (there being no collisions in this hypothetical

Restoration of Stoichiometry

Given that a metal oxide target, and by implication any other compound target, is unlikely to be completely sputtered in a molecular form, it is not surprising that the stoichiometry of the resulting thin film will be different from that of the target, usually being deficient in the gaseous or other volatile species. For example, films from a quartz target sputtered in argon tend to be deficient in oxygen. This can be compensated for by sputtering in a mixture of 95% Ar:5% O₂ (Erskine and Cserhati 1978). The oxygen served to fully oxidize the sputtered film and so restore its stoichiometry. It can be particularly effective in doing this because the glow discharge environment provides energetic electrons to dissociate the molecular oxygen into its chemically more active atomic form.

We should note that we do not always want to achieve the stoichiometry of the equivalent bulk material. For example, Mogab et al. (1975) found that silicon nitride films which met their requirements were richer in nitrogen than the stoichiometric Si₃N₄.

Reactive Sputtering - Again

But if we are going to react a small amount of Si or SiO with O atoms, why not a lot? Indeed this can be done, and sputtered quartz films can be fabricated by sputtering a very pure elemental silicon target in a 50% Ar:50% O₂ mixture (Erskine and Cserhati 1978). This is the process of *reactive sputtering*, the chemical combination of the sputtered species and a component in the gas phase, that we usually try to avoid. Reactive sputtering can be used to promote total chemical conversion of the target material or, as in the previous section only to compensate for a deficiency in the film.

Quite small quantities of gas can be very effective and quite critical, so that careful partial pressure control, e.g. by mass spectrometry, is required. Note though, that although partial pressures of reactive gases can be very low, one still needs an adequate supply or flow of reactive gas. This requirement is discussed in more detail in the next chapter on "Plasma Etching". Oxygen and nitrogen are frequently used in reactive sputtering. In the discharge, molecular ions will be formed, and dissociation will lead to atomic ions and atomic neutrals in ground and excited states. Each of these species can play its role in the chemical conversion of the film.

The general situation will be rather complex and it is more fruitful to pursue specific cases. In principle, reactions could take place on the target, in the gas phase, and on the substrate. Target reactions result in one actually sputtering a compound target. These usually have a lower yield than elements, and result in the often observed reduction in deposition rate with added reactive gas.

Gas phase reactions suffer from the same problem of conserving energy and mo-

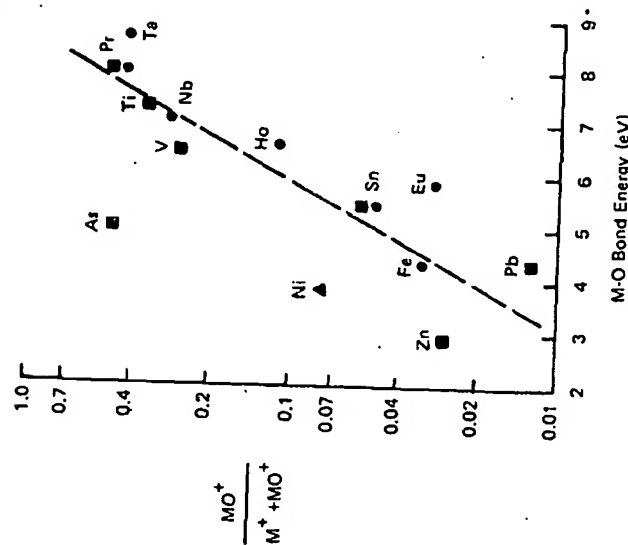


Figure 6-49. The dependence of $MO^+/(M^+ + MO^+)$, i.e. the relative ion flux of the dimer, on the bond energy M-O. Argon pressure 60 mtorr, rf power 100 watts at 13.56 MHz, target area 20 cm² (Coburn et al. 1974)

case), the η values shown would tend to underestimate the relative concentration of the sputtered molecular ion.

Figure 6-49 and other results indicate that the M-O bond strength is not the only factor influencing η . Coburn et al. propose that a molecular sputtering event is more likely to occur if the atom struck by the bombarding ion can transfer enough energy to its molecular partner that they can be ejected as a pair. The energy transfer function (Chapter 1, "Energy Transfer in Binary Collisions") tells us that this is more likely when the atom masses are similar, and in Figure 6-49 it is certainly the lighter metals, with smaller mass ratios compared to oxygen, that lie above the line and exhibit larger molecular ion fluxes than a direct dependence on the M-O bond would suggest. Finally, Coburn et al. demonstrate that the presence of contaminants such as water vapour, has a marked effect on the ratio η .

mentum that was discussed in Chapter 2. However, since there is in this case a molecular product, there is a chance that surplus energy will be absorbed into vibrational and rotational transitions, so such reactions should be much more likely than in atomic ion-electron pair recombination. On the other hand, there seems to be a general opinion that more reaction under these circumstances takes place on the substrate.

We have already discussed some of the various bombardments that go on at the substrate. We now add bombardment by reactive positive ions and neutrals to the list. Relevant work by Winters and Kay on the effects of the sorption characteristics of various gaseous and ionic species has already been cited. In the case of electronegative gases such as oxygen, we shall also have bombardment by fast oxygen negative ions formed in the target sheath or on the target itself. Then add substrate bias to confuse things!

There are all sorts of peculiar and interesting effects in reactive sputtering; they usually turn out to be due to some of the effects we have noted. For more practical information, see the review articles by Holland (1956) and by Mausel (1970), and the extensive bibliography by Vossen and Cuomo (1978).

SPUTTER ETCHING

Sputter etching is the name conventionally given to the process of removal of material from a surface by sputter ejection. There are several uses for the process other than as a prerequisite for sputter deposition, as we have already discussed.

Pattern Production

If material is selectively removed from a surface by using a suitable mask, then an etch pattern can be produced. The process of sputtering is fairly universal, so that the variety of wet chemicals used for the same process can be eliminated. Since sputtering results from bombardment by ions that move along electric field lines, and because field lines are always perpendicular to an equipotential surface, then etch profiles are inherently vertical in contrast to the isotropic profiles observed with wet chemical etching (Figure 6-50).

Sputter etching can be carried out in a conventional sputtering system with an *in situ* glow discharge, or with an externally generated ion beam. Ion beam sources are themselves glow discharge devices and are discussed in a later section. The change with an ion beam system is that the operating pressure can be much lower ($< 10^{-4}$ torr). There is then less chance of sputtered material (from the target or more importantly from the mask or target support) colliding in the gas phase and being backscattered onto the target. There is also a negligible flux onto

SPUTTER ETCHING

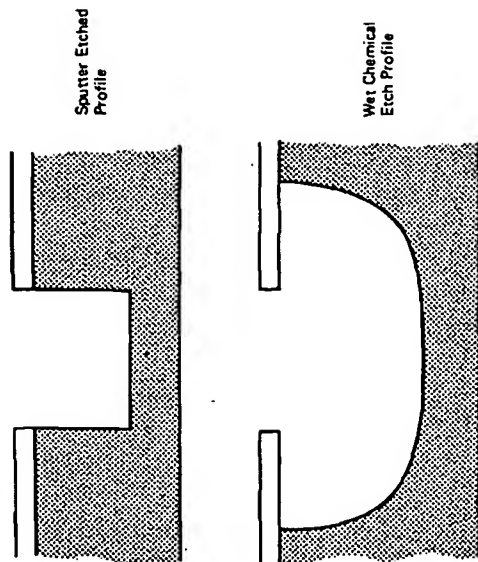


Figure 6-50. Etch profiles produced by sputter etching and by wet chemical etching.

the target of energetic neutrals produced by charge exchange. These fast neutrals are not affected by the electric field and therefore do not follow the field lines onto the target. They could lead to undercutting of the mask. In practice, there is a noticeable difference of directionality between results obtained in sputtering and ion beam systems. The difference is not that great, however; this may be due to pronounced forward scattering of the ions neutralized in the charge exchange process, so that the fast neutrals are more directional than one might at first suspect.

But even for ion beam systems, the sputter etch profile shown in Figure 6-50 is rather idealized. Two prime reasons for this are *mask erosion* and *trenching*. If the mask itself is also etched by the sputtering process, and this is always the case to some extent, then the final dimension of the opening in the mask will be greater than the initial dimension, leading to a tapered profile (Figure 6-51). The propensity of the mask to be sputter etched depends on its thickness and its profile. For etching of small dimensions of the order of microns, lithographically processed patterned photoresist materials are used. To achieve such resolution, the resists have thicknesses $\sim 1 \mu\text{m}$. The polymeric materials used for photoresists tend to sputter rather easily and also degrade under ion bombardment. Sometimes the heating effect of the glow causes *resist flow*, so that its profile changes. These effects combine to make resist masks prone to etch back during sputter etching.

(2410 p.p.m. 11/12/77)

There are much more resistant etch masks. Oxides generally have low sputtering yields, and alumina and magnesium oxide make good masks. But they are not photosensitive, so they must be patterned using more conventional photoresist

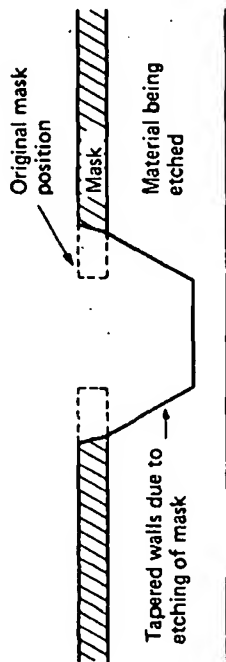


Figure 6-51. Etch profile resulting from mask erosion.

masks. The additional steps of oxide deposition and etching must be weighed against the reduced mask erosion.

Trenching is the enhanced erosion around the foot of an etched wall, leading to the 'molar' shape shown in Figure 6-52. It results from the increased flux of ions at the trenches due to reflection off the side walls of the etch pit, and perhaps also from material sputtered from the side wall onto the base of the pit.

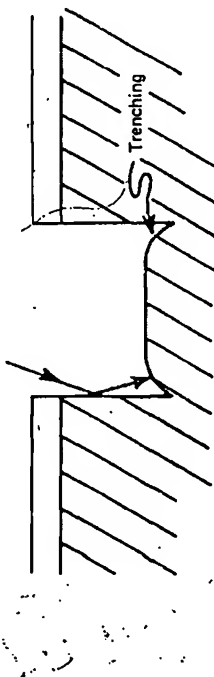


Figure 6-52. 'Trenching' in sputter etching

Several other phenomena control the topography of a sputter etched target. One concerns the redeposition of sputtered material. In the section on bias sputtering, we saw how some material is sputtered sideways, and this can be redeposited onto the side wall of another feature. This effect can be further illustrated by some results of Glöersen (1975). During the sputter etching of aluminium using a photoresist mask (actually in an ion beam system, but the principle is the same), sputtered aluminium is redeposited onto the side wall of the resist. After processing, the resist is chemically removed, leaving a wall of metal around the original resist position.

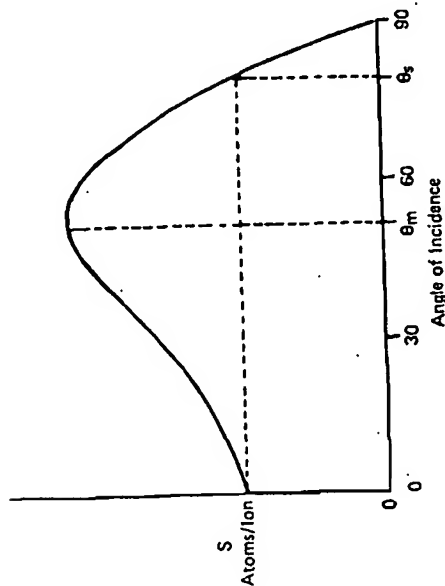


Figure 6-53. Variation of sputtering yield with angle of incidence (with respect to the target normal)

Another phenomenon related to etch topography depends on the angular dependence of sputtering yield. Figure 6-53 is a generalization of the effect; there are many specific examples, e.g. Wehner (1959), Cheney and Pitkin (1965), Glöersen (1975). Normal (in the angular sense) sputter ejection due to normal ion incidence requires 180° reversal of the momentum; this is not very likely and accounts for the low energy efficiency of the sputtering process. As the angle of incidence increases, so does the sputtering yield, again for momentum considerations. This is accompanied by the sputter ejection angular distribution becoming pronounced in the direction of specular reflection. Ultimately the yield goes to zero at 90° incidence, resulting in a maximum yield somewhere between 0° and 90° depending on the target material, and the ion identity and energy. This angular dependence has several consequences. One is the formation of *facets*. Figure 6-54 shows two surfaces being etched, one normal to the ion beam and the other at angle θ . If we consider sections of each surface that present the same cross-sectional area A to the incoming beam, then we can see that the etch rates in the direction of the beam, R_0 and R_θ respectively, will be proportional to the sputtering yields at the relevant angles of incidence. Although the inclined surface is subjected to a lower flux of ions, this is irrelevant because the volume of material removed depends on the *cross-sectional* area and the etch rate.

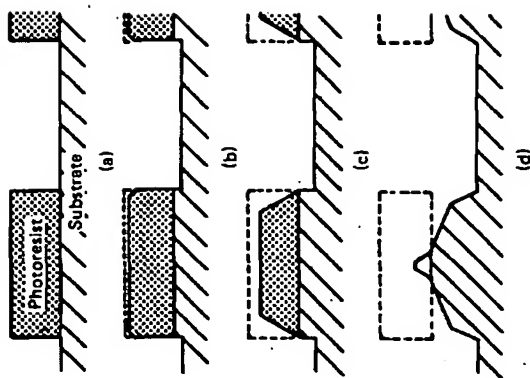


Figure 6-55. A simple model depicting the stages in the ion beam etching of grooves using a photoresist mask. (a) The photoresist cross-sections prior to initiating ion beam etching. (b) The onset of facet formation in the photoresist. (c) The photoresist facet intersects the original substrate surface plane. (d) After etching further, the facet in the photoresist propagates laterally thereby exposing additional substrate to ion beam etching and consequent facetting (Smith 1974)

Etch Topography

A phenomenon related to facetting is that of *cone formation*. The root of this can already be seen in Figure 6-55 where the resist has the shape of a truncated cone. The earliest observations of cones occurred nearly 40 years ago (Cuenther-schulze and Tollmien 1942), and there are now a large number of reports of cones on a variety of metals and semiconductors (Wehner 1959, Stewart and Thompson 1969, Nobes et al. 1969, Haufler 1971, Wilson and Kidd 1971, Bayly 1972, Tsong and Barber 1973, Robinson and Kaufmann 1979). Explanations and computer simulations (Catana et al. 1972) of these artifacts are based on the angular dependence of the sputtering yield, and show how structural faults or impurities can develop into cones. Although the phenomenon is frequently referred to as cone growth, this is a misnomer since the cones do not grow but instead result from not etching.

The interest in cone growths is also due to the observation by Wehner and Hajicek (1971) that cones could be developed on pure copper surfaces by depositing a very low flux of molybdenum at the same time the copper is being etched in

SPUTTERING

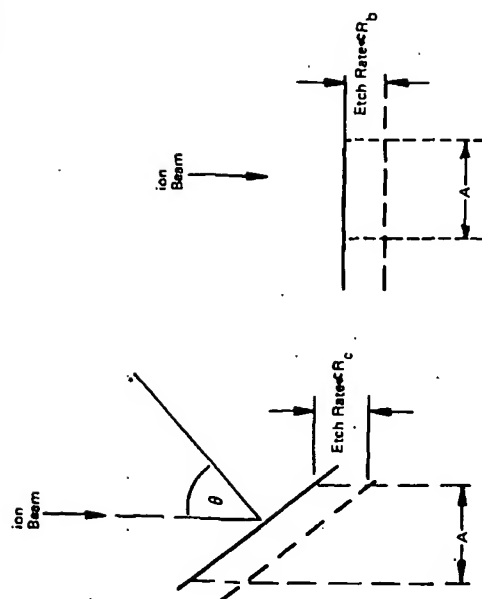


Figure 6-54. The etch rate parallel to the ion beam is proportional to the sputtering yield at the same incidence angle.

The phenomenon of facetting, which is illustrated in Figure 6-55, usually starts on corners which always have some rounding, and therefore present a variety of incidence angles to the incoming ions; in bias sputtering systems, the effect is pronounced due to the field concentrations occurring at sharp corners. A facet will develop for the plane which has the highest sputtering yield and etch rate ($\theta = \theta_m$ in Figure 6-53), as the more slowly etching planes are consumed. The effect is then transferred to the substrate but at a different angle corresponding to θ_m for the substrate material. A second material, photoresist in the figure, is not necessarily required and any artifact on the target surface can promote the facetting.

The mechanism for the *planarization process* (Ting et al. 1978) used to encourage the formation of a planar thin film over a non-planar substrate, is related to the mechanism of facetting, but has the additional complication that etching and deposition are occurring simultaneously.

Folks involved in ion beam etching use the angular dependence of yield to take care of trenching and other phenomena, and often use non-normal incidence and planetary rotation to achieve the required results (Leq 1979). Neither of these tricks is possible in glow discharge sputter etching since ion bombardment is controlled by the glow discharge, which follows the target and hence ensures normal ion incidence.

a conventional sputtering discharge environment. The effect is attributed to the low sputtering yield of the molybdenum and to its high surface diffusion mobility. Also using an in situ glow discharge, we carried out similar experiments using copper and tungsten and found, for example, that cone shape and density are very dependent on the structure of the original copper substrate; Figure 6-56 is of two copper specimens prepared side-by-side under identical etching/deposition conditions, and Figure 6-57 is also of copper but under slightly different conditions. The rounding of the cones which is evident, particularly in Figure 6-57, is probably due to the non-normal incidence of some sputtering particles which results from an in situ glow discharge.

As well as having interesting electrical properties, cones also produce optical effects. For example, a high density of closely spaced cones produces so much light scattering that the surface resembles matt black velvet, a condition that could be easily confused with gross contamination, and has resulted in at least several sputtering targets being dispatched to Valhalla (no, not the IBM location) and diffusion pump oils cursed, in both cases unjustly!

~~Chertin~~ ^{to} the Cu/Mo cone system, Tarnag and Webner (1972) made an interesting Auger study of the deposition of molybdenum onto various metal surfaces, and its subsequent sputter removal. The equivalent of 12 monolayers of Mo were deposited onto tungsten, copper, gold, and two grades of aluminium under conditions of complete condensation, and were then removed by sputter etching. The surface coverage was monitored throughout by Auger analysis. Results are shown in Figure 6-58 as a function of the amount of molybdenum that would have been removed if the target had been Mo entirely. Mo appears to initially completely cover the W, and is then removed almost as though from bulk Mo. On the other metal substrates, deposition did not produce complete coverage. However, under ion bombardment, the coverage in these cases at first begins to rise as the Mo is spread more uniformly over the surface. There is then a slow decrease in coverage as the Mo is etched away. The sputtering yield of Mo atoms from Cu, Au, and Al is much lower than that of Mo from Mo, especially at low energies; 200 eV argon ions sputter Mo from Al with a yield three orders of magnitude lower than that for bulk Mo or bulk Al.

Some very peculiar surface structures have been reported by Oohashi and Yamanaka (1972) under simultaneous etching/deposition conditions. Rather than use a separate deposition source, their substrates were placed on a tantalum target, so that the tantalum was backscattered onto the substrate whilst the latter was being etched. Figures 6-59 shows some of the 'winding' patterns they obtained. Prof. Yamanaka kindly sent me photomicrographs of Cu, Al, Ag, C, Co, Mn, Au, Fe, Zr, Pt, Ni, Ti and Brass, all sputter etched similarly on a Ta target. Only the Cu showed classic cones, whilst the others displayed all sorts of strange topographies. Goodness knows how these fit into the cone formation theories!



Figure 6-56. Scanning electron micrographs of two copper surfaces, sputter etched with simultaneous low rate deposition of W (Chapman et al. 1973)

- (a) Bulk polycrystal Cu.
(b) Evaporated thin film Cu.



Figure 6-57. As Figure 6-56, but for an evaporated copper film, and under slightly different conditions

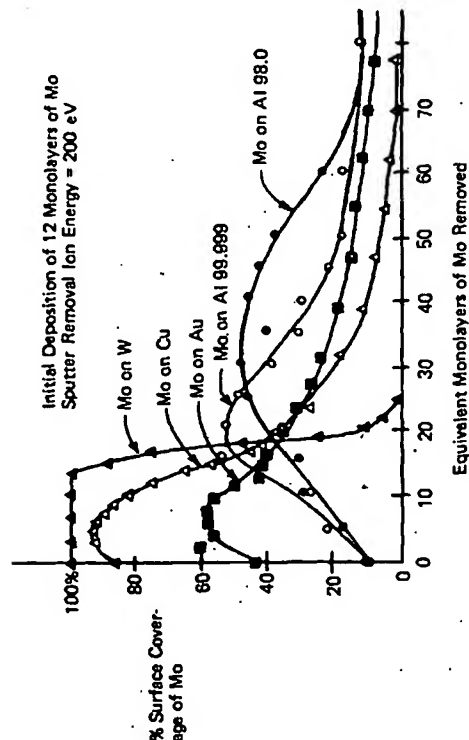


Figure 6-58. Surface coverage of Mo on various metal surfaces, subjected to Ar^+ bombardment. The coverage is shown as a function of time, measured in terms of the number of monolayers of Mo that would have been removed from a pure bulk metal Mo sample in the same time. (Tang and Wehner 1972)

Surface Analysis

There is now quite a range of techniques for analyzing surfaces, each with their specific advantages. They usually analyze a surface layer tens or hundreds of Angstroms in thickness, according to the penetration and escape depth of the particles involved in the specific analytical process. This is both an advantage in identifying the location of the analyzed section, and a disadvantage because the material beneath the surface layer is not analyzed.

This problem is eliminated by removing the surface layers sequentially, exposing deeper layers. This is usually done by sputtering, and the overall process is known as *depth profiling*. The sputter removal can either be part of the analytical process as in *SIMS* (Secondary Ion Mass Spectroscopy), or quite separate as in *Auger* analysis. In these latter cases, sputtering can either be continuous during analysis, or intermittent with analysis. Profiling techniques have been reviewed by Coburn and Kay (1974).

In all cases, one would like to be able to expose the sample by one atomic layer at a time. It should be clear from the discussions on alloy sputtering in "Deposition of Multicomponent Materials" and the preceding section on "Etch Topography" that layer-by-layer profiling of the substrate cannot be assumed,

and this adds enormously to the problems of surface analysis, which have been reviewed by Coburn (1976). Presumably one could, in principle, solve the problem by comparing the material actually leaving the surface with that remaining on it, for example by combining the results of simultaneous SIMS and Auger; but I'm sure that's horrendously difficult and I'm not aware that anyone has succeeded in doing it yet.

Surface Cleaning

Glow discharges can be used in several ways to clean the surfaces of materials, and this is usually done in situ immediately prior to another vacuum process such as deposition by sputtering or evaporation.

Glow-discharge cleaning involves placing the substrates to be cleaned in the glow so that they are bombarded by low energy ions and electrons. The precise energy of bombardment will depend on whether the substrates are insulating or conducting; whether the discharge is rf or dc excited (usually it's the latter), and whether the substrates are subject to high energy negative particle bombardment from the target sheath.

Beneficial results seem to result from this technique, particularly if the cleaning is carried out in an oxygen discharge (Hirai et al. 1966). Impurities are desorbed from the surface due to the ion and electron bombardment, or due to the heating associated with these bombardments. With the oxygen discharge, there will also be effective oxidation of organic impurities on the surface by atomic oxygen formed dissociatively in the discharge, and these oxides will generally be volatile. This is the *plasma ashing* process described in Chapter 7. There are also several reports of oxygen glow discharge cleaning improving the adhesion of subsequently deposited films, by modifying the substrate surface. Such effects could be due, though, to residual oxygen in the system forming an intermediate oxide layer at the interface. "Thin Film Adhesion" is discussed further at the end of this chapter.

The same glow discharge process is also used for treating certain polymeric materials prior to subsequent processing, e.g. before deposition of a coating onto a polymer. Apparently the action of the discharge is to change the surface structure of the polymer, creating dangling bonds and the like (Hall et al. 1968, Bersin 1974). Unfortunately I don't know much about this application.

As well as glow discharge cleaning, there is also *sputter cleaning* in which the material being cleaned is made the target of a sputtering discharge. The discharge could be rf or dc, with the former required for insulating materials. In this case, the target is exposed to energetic ions and, in the rf case, also to low energy electrons. In contrast to glow discharge cleaning, sputtering is encouraged and the target is cleaned by removal of its surface, contamination and target too!

SPUTTER ETCHING

In sputter deposition, sputter etching is commonly used to clean both target and substrate prior to deposition. Target cleaning by this technique is referred to as *presputtering*, which process is also used to heat the system and bring it to steady state, whilst protecting the substrate from deposition with a shutter (described in "Practical Aspects of Sputtering Systems"). The effectiveness of the shutter has been demonstrated by Chang et al. (1973) who showed, using several surface analytical techniques, that rf presputtering of a tungsten target for 10 minutes at about 10 mtorr produced no detectable damage or deposit on single crystal silicon wafers 3 cm away from the W target. A shutter was interposed about 5 mm above the wafers.

Similarly, substrates can be cleaned by sputter cleaning prior to deposition. Although glow discharge cleaning is effective for removing much contamination, it is ineffective in removing the native oxide layers or other compounds from metal or semiconductor surfaces. Removal of these layers is frequently necessary, particularly for electrical applications such as obtaining ohmic contacts.

Sputter cleaning of substrates is known by just that phrase, or alternatively as *back-sputtering*. In the same study already cited, Chang et al. rf back-sputtered silicon wafers on a tungsten plate, in argon for 10 minutes at 10 mtorr at a wafer bias voltage of -400 V. In this case, the shutter was about 2.5 cm above the wafers. They found that back-sputtering produced an amorphous contaminated layer of Ar, W, C and Si ≥ 3 monolayers, on the wafers. As in the results of Vossen discussed in "Bias Techniques", the W and C were backscattered from the substrate and concentrated near the edge of the wafers.

Clearly, the back-sputtering technique could have disastrous consequences if the wrong backing plate is used. In the work of Chang et al., the combination of the use of a tungsten backing plate with the bias sputter deposition of tungsten onto the silicon wafers, was very effective in preventing oxide formation at the wafer-film interface, whilst simultaneously promoting a mixed W-Si interface; tungsten is not an unwelcome contamination in this case.

Finally, the application of a positively biased probe in a discharge will raise the plasma potential, as we already know by now, and so will increase the energy of ion bombardment onto all grounded conducting surfaces in the discharge. This can be a useful cleaning technique, but must be recognized also as a potential source of contamination, since the sputtered material has to end up somewhere, usually on the substrate (Murphy, 1811).

Implications for Bias Sputtering

In the last few sections, we have been considering effects in sputter etching. Although one normally thinks of etching as a subtractive process at a target, we have to remember that the deposition which occurs on a substrate in bias

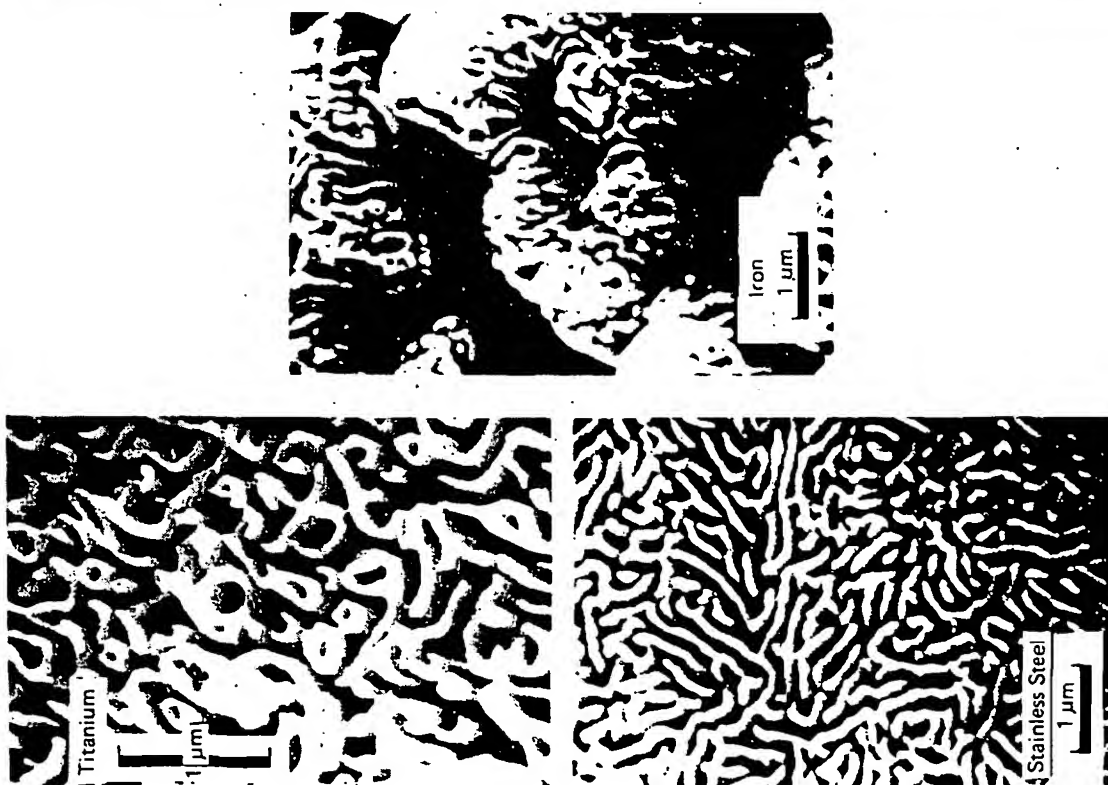


Figure 6-59. Scanning electron micrographs of sputter etched metal surfaces, showing the effect of backscattered tantalum (Oohashi and Yamanaka 1972)

SPUTTERING

sputtering is in fact the net result of deposition from the target and removal by resputtering due to ion bombardment. The bombardment leads to structural and compositional changes in the growing film; under certain circumstances, it can reduce the net deposition rate to zero or even make it negative — i.e. cause etching of the substrate.

SOME OTHER SPUTTERING CONFIGURATIONS

All of the discussion of sputtering systems so far has been about the cold cathode diode type of system. (Actually bias sputtering systems have three electrodes, but they are not generally referred to as triode systems). These systems need not be planar, and could have wire targets or other cylindrical symmetry as shown in Figure 6-60, which is from the review by Holland (1974). In all of these cases, secondary electrons are generated by ion impact at the target.

Enhancement of Ionization

In our discussion, in "A Conventional DC Sputtering System", about the range of operating pressure of a dc diode system, we found that a limitation was due to lack of electron impact ionization to sustain the discharge. There are two ways of combating this limitation, either by increasing the probability of ionization or by increasing the number of electrons, as follows:

- Using a magnetic field to increase the path length of an electron before it is collected or recombines on an electrode or wall.
- Using the ionization enhancement given by rf excitation.
- Injecting more electrons into the discharge by using a *hot filament* as an electron source.

Various configurations to enhance ionization are shown in Figure 6-61, which is also from Holland (1974).

Of this multitude of sputtering configurations, we have already discussed both dc and rf planar diode systems, with and without bias capabilities. In the following section we shall consider magnetic field effects in diode systems and the various types of magnetron systems. But first, a few words about hot filament triode systems are in order.

Hot Filament Discharges

The essential parts of a hot filament discharge system are the filament itself and the anode. The filament, which is normally tungsten or another refractory metal,

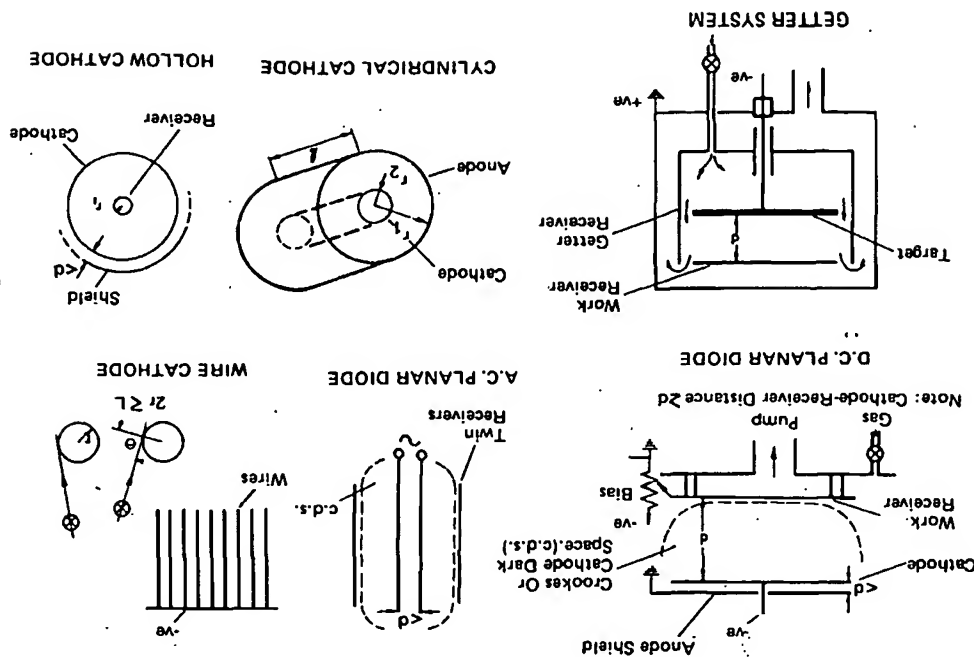


Figure 6-60. Cold cathode glow discharge sputtering systems (Holland 1974)

SOME OTHER SPUTTERING CONFIGURATIONS

is heated to incandescence, usually by the resistive heating ($I^2 R$) of a low voltage, high current ac or dc source. At such elevated temperatures, the filament can become a copious source of thermionically emitted electrons. Hence one refers to *hot filament cathodes*, as opposed to *cold cathodes* where the electrons are emitted by secondary emission.

The potential supply of current by thermionic emission is given by the

Richardson-Dushman equation:

$$j = AT^2 \exp \frac{e\phi}{kT}$$

where ϕ is the *work function* of the metal and A is a constant equal to 120 amp/cm² deg².

Usually the emission current from a filament will be severely limited by the electron space charge surrounding it, but with an anode located in the vacuum to withdraw the electrons, and a suitable gas introduced to a pressure of a few millitorr, a glow discharge can easily be generated. This discharge will be qualitatively the same as a cold cathode discharge, with sheaths formed at both cathode (the filament) and anode. What is distinctive about the hot filament discharge is that electron emission from the cathode is primarily by thermionic emission rather than by ion impact. Since the electron supply can be increased almost indefinitely, it is possible to generate low impedance discharges of several amperes with interelectrode voltages of just a few tens of volts. Pioneers in this area were surprised to be able to generate discharges with less than the ionization potential applied across the discharge, but they didn't know about non-uniform electric fields and two-step ionization processes. Hot filament discharges will work down to rather low pressures ($\sim 10^{-5}$ torr), particularly with the aid of a magnetic field, as is discussed in the following section.

The hot filament discharge is converted into a sputtering system by adding a target with an adequate dc or rf potential applied to it. The discharge is then the source of ions, and the potential on the target controls the ion energy and flux onto the target. This arrangement, shown in Figure 6-61d, is commonly known as a *triode sputtering system*. A substrate can be placed in a suitable position when thin film deposition is required.

Triode systems were very popular in earlier days of sputtering, particularly in the 50's and early 60's. The capability of quasi-independent control of discharge and sputtering process made this an attractive configuration, particularly to researchers, as did its ability to operate down to low pressures. These capabilities resemble those of ion beam sputtering. Triodes seemed to lose popularity in the mid 60's only to resurface around 1972 for several applications, partly because of their ability to sputter efficiently at low voltage and so avoid radiation dam-

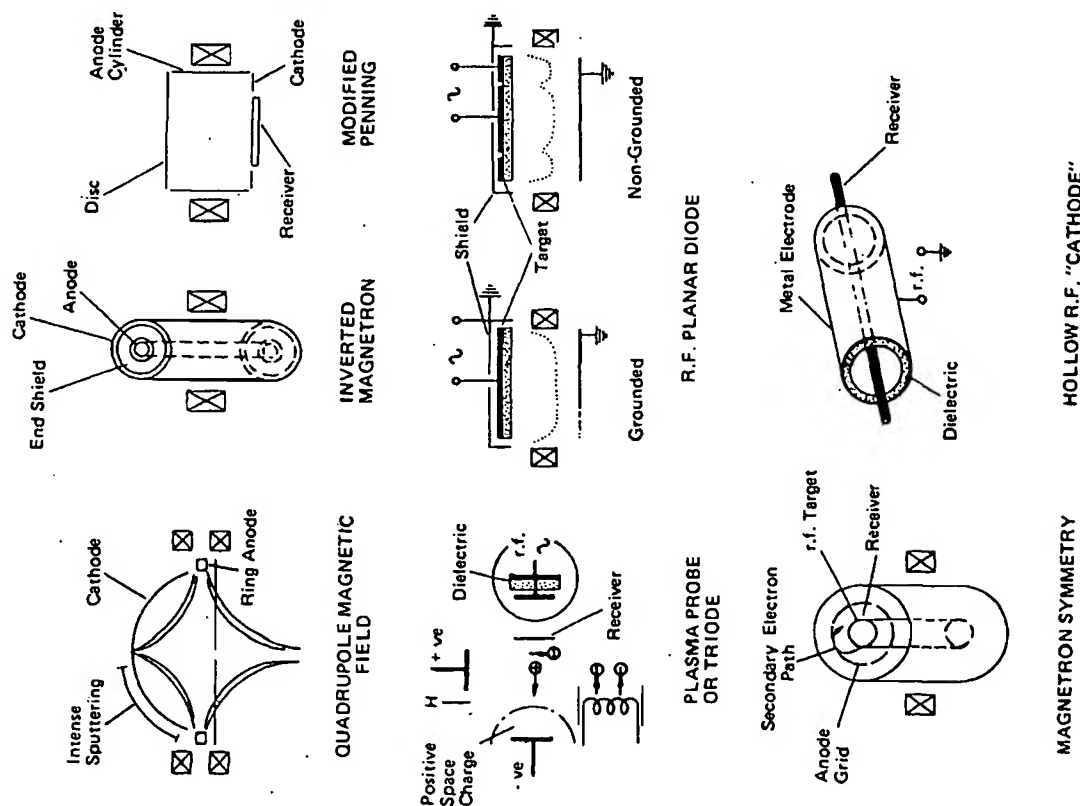


Figure 6-61. High vacuum and plasma probe sputtering systems (Holland 1974)

age, whilst maintaining adequate current density and deposition rate. An extensive analysis of a triode system has been made by Tisone and colleagues (see Tisone 1975). More recently, the hot filament triode system has been used as a high rate sputtering source, and for plasma etching by Chapman and Minkiewicz (1979) and Heiman et al. (1979).

MAGNETICALLY ENHANCED SPUTTERING SYSTEMS

Magnetic field effects are used quite a lot in sputtering systems. They give advantages in sputtering rate and extendability of operating range, and can reduce electron bombardment at the substrate. The problems of uniformity which sometimes arise, can be overcome in many cases.

The primary interaction between a particle of charge q and velocity v , and a magnetic field B , is to produce a force F on the particle of magnitude $F = Bqv$. The direction of the force is perpendicular to both the magnetic field and the velocity (Figure 6-62) and is better expressed in the vector form:

$$F = q \times v \times B$$

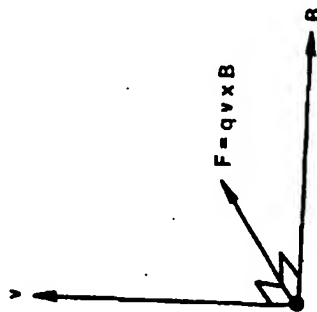


Figure 6-62. The electromagnetic force F is perpendicular to both v and B

This force will produce an acceleration that is inversely proportional to the mass of the charge. For the magnetic fields used in sputtering, which are typically 100 gauss, only the electrons will be affected; the ions are too massive. The purpose of using a magnetic field in a sputtering system is to make more efficient use of the electrons, and cause them to produce more ionization. In a conventional glow discharge, electrons are soon lost by recombination at the walls. To minimize this loss, there are two ways of using a magnetic field which are rather different in approach:

MAGNETICALLY ENHANCED SPUTTERING SYSTEMS

Axial Magnetic Fields

Axial magnetic fields are used in planar diode glow discharges and hot filament discharges for the purposes of increasing the path length of the electrons before they are collected by the anode, and of keeping electrons away from the vacuum chamber walls and hence reducing recombination. We shall illustrate the effect on the hot filament system introduced in the last section (Figure 6-63a). An electron travelling along the axis of the discharge will be unaffected, since B and v will be parallel and so their vector product will be zero. But suppose that the electron is travelling at θ to the magnetic field (Figure 6-63b). Then it will be subjected to a force $Bev \sin \theta$ perpendicular to the field. Provided that it doesn't make any collisions, the electron will then describe circular motion around B at a radius given by:

$$\frac{m_e(v \sin \theta)^2}{r} = Bev \sin \theta$$

$$\text{or} \quad \frac{m_e v \sin \theta}{Be} = r$$

Coupled with the velocity $v \cos \theta$ parallel to B , the general motion will be a helix (Figure 6-63c).

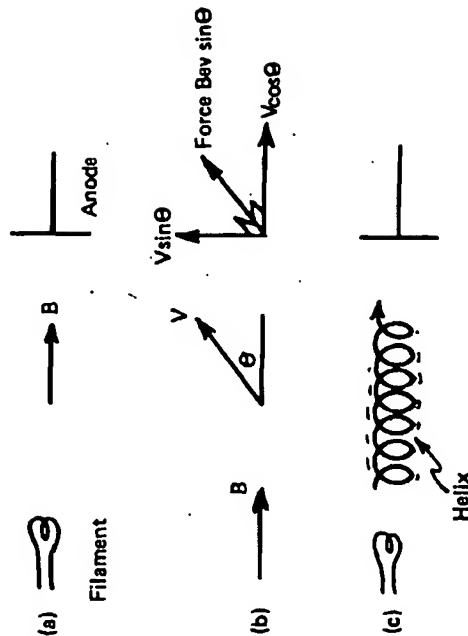


Figure 6-63. Effect of an axial magnetic field

- (a) hot filament discharge with axial magnetic field B
- (b) force on a particle with velocity v at θ to the axis
- (c) net motion of particle is helical.

SPUTTERING

After each revolution of the helix, the electron will return to the same radial position around the axis of the discharge. An effect of the magnetic field is therefore to reduce the net velocity of the electron towards the wall to zero, hence reducing wall recombination losses. A second effect of the helical path is to increase the total path travelled by an electron emitted from the filament on its way to the anode, thus enabling it to cause more ionization and excitation. These effects are very evident when the magnetic field is applied; the discharge is observed to be confined to a core which narrows with increasing magnetic field and brightens, indicating an increased electron density in the core.

A more complete analysis of this *magnetically confined* or *magnetically immersed* glow discharge would consider the spreading of the glow due to diffusion, balanced against the magnetic confinement. Similar calculations for electron beams are well developed (Hemenway et al. 1967). In the beam case, one has to consider the space charge expansion of the beam, but presumably these models could be developed to deal with the discharge situation.

Using magnetic field confinement in this way, hot filament triode systems, which normally can operate at a few millitorr by way of their effective thermionic electron sources, can extend their operating range down to about 10^{-5} torr. [The magnetic field can also have a considerable effect on the distribution of etching species in a hot filament triode plasma etching system, as shown by Chen et al. (1979).]

Axial magnetic fields are also used in the more conventional cold cathode diode sputtering systems described earlier. Again the effect can be used to lower the operating pressure or, probably more frequently, to increase the ion current and hence sputtering rate, at a constant pressure. Unlike the hot filament system, the substrate is normally on the anode in the cold cathode system. An effect of the magnetic field will be to constrict the discharge and perhaps cause non-uniform deposition on the substrates. One must be aware of these potential deleterious effects. Nevertheless, axial magnetic fields prove to be useful in many cases.

Magnetrons

Magnetron systems take the same philosophy one step further and attempt to trap electrons near the target so as to increase their ionizing effect. This is achieved with electric and magnetic fields that are generally perpendicular.

Consider the electron normally emitted with velocity v from a surface (Figure 6-64a) into a region of magnetic field B (into the paper in Figure 6-64a) and zero electric field. In a similar way to the axial magnetic field case, the electron will describe a semicircle of radius r given by $m_e v / Be$, providing it does not collide en route, and will return to the surface with velocity v . So the effect

MAGNETICALLY ENHANCED SPUTTERING SYSTEMS

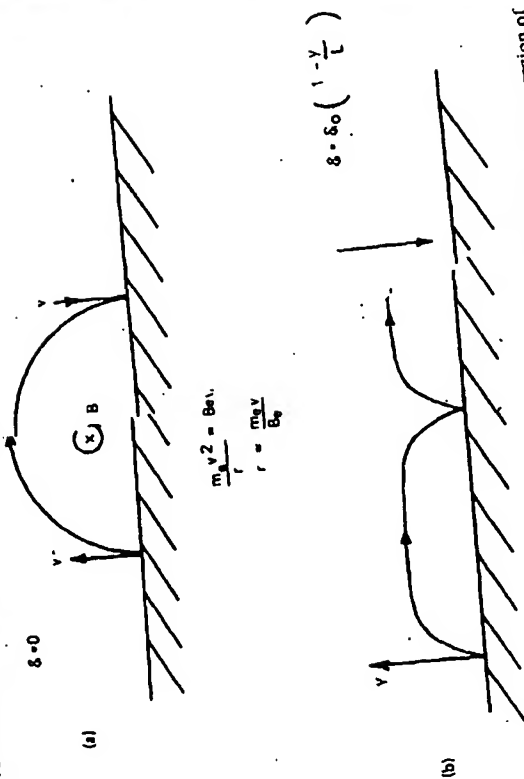


Figure 6-64. Motion of an electron ejected from a surface with velocity v into a region of magnetic field B parallel to the surface:

- (a) with no electric field
- (b) with a linearly decreasing field.

of the magnetic field is to trap the electron near the surface from which it was emitted.

To examine a situation which is closer to the magnetic sputtering application, Figure 6-64b is of a sputtering target where there is a strong electric field \mathcal{E} in the dark space above its surface, and again a magnetic field B parallel to the surface of the target. Let the electric field \mathcal{E} decrease linearly across the dark space of thickness L ; as we have seen earlier, this is a dependence frequently used for dark space fields, and although somewhat questionable, is quite adequate for the purpose of illustration. If y is the dimension away from the target, and the target surface is $y = 0$, then

$$\mathcal{E} = \mathcal{E}_0 \left(1 - \frac{y}{L}\right)$$

where \mathcal{E}_0 is the field at the target. Let x be the distance along the target surface from the point of emission of a secondary electron. This electron will be rapidly accelerated, initially away from the target by the strong normal electric field at

the surface. By comparison, we can assume that the electron emission velocity is zero. The equation of motion will then be:

$$\ddot{x} = \frac{Be\dot{y}}{m_e}$$

$$\therefore \ddot{x} = \frac{Bcy}{m_e}$$

$$\ddot{y} = \frac{e\mathcal{E} - Be\dot{x}}{m_e}$$

After substituting in the y dependences of \mathcal{E} and \dot{x} , the resulting differential equation can be solved to yield

$$y = \frac{e\mathcal{E}_0}{m_e\omega^2}(1 - \cos \omega t)$$

where

$$\omega^2 = \frac{e\mathcal{E}_0}{m_e L} + \frac{e^2 B^2}{m_e^2}$$

In the absence of the electric field, ω would be equal to eB/m_e . This is known as the *cyclotron frequency* and has the value $2\pi \times 10^6 B$ Hz, where B is in gauss.

In the absence of the emitting surface in this example, and in the previous example of an axial magnetic field, the electron would rotate around the field lines with the cyclotron frequency.

The addition of the electric field on the target changes the orbits from circular to cycloidal, provided the electron stays within the dark space. Since $r = m_e v / Be$, its instantaneous radius of curvature will decrease as it travels further from the target surface. If it enters the negative glow by straying further than L from the target, then it will describe circular motion in the electric field-free region there, before returning to the dark space.

The maximum excursion y_{\max} of the electron from the target, in the absence of collisions, can be found by equating the gain in kinetic energy to the loss of potential energy (Green and Chapman 1976):

$$\frac{1}{2} m \dot{x}_{\max}^2 = e(V - V_T)$$

where V_T is the negative target voltage and V is the potential at y_{\max} . But since $\ddot{x} = Be\dot{y}/m_e$ and $\dot{x} = Bcy/m_e$, then we can substitute into the energy balance equation to obtain:

$$y_{\max} = \left[\frac{2m}{B} \left[\frac{e}{e} (V - V_T) \right] \right]^{1/2}$$

Note that the form of the electric field has not been used in this derivation, so the result holds quite generally, both within and without the dark space.

The net result of all of this is that the electron is trapped near the target, provided it doesn't make any collisions, so the loss process of fast electrons going to the anode and walls is eliminated. If it does make collisions, the trapping won't be so effective, but on the other hand we want the electrons to make lots of ionizing collisions to sustain the glow, and the magnetron action enables them to do this before being lost to the anode.

The application of magnetic fields to enhance ionization in glow discharges seems to date back to Penning (1936), but their effective use in sputtering systems has been more recent. *Magnetrons* are originally valve (vacuum tube) devices for generating or amplifying high frequency signals, operating on the basic principles just discussed, but the name is now also applied to that group of sputtering devices using the same principle of crossed electric and magnetic fields.

Cylindrical Magnetrons

There are several types of magnetrons for practical sputtering applications. The earliest were probably those with cylindrical geometry and an axial magnetic field (Figure 6-65). With the inner cylinder as the target, the arrangement is known as a *cylindrical magnetron* or *post magnetron* (Thornton 1973, Wasa and Hayakawa 1969); this configuration has the ability to coat a large area of small substrates.

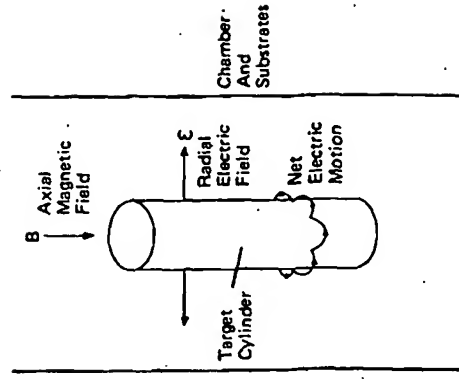


Figure 6-65. Cylindrical magnetron sputtering configuration (Green and Chapman 1976)

MAGNETICALLY ENHANCED SPUTTERING SYSTEMS

When the inside of the chamber becomes the target, the arrangement is known as an *inverted magnetron* (Gill and Kay 1965) and has a capability of depositing uniform thickness films over strangely shaped substrates placed along the axis.

Although electrons are constrained in their radial motion, there is little to restrict their axial motion and they can therefore 'walk' off the end of the target (Figure 6-66). These *end losses* can be prevented by various types of end-confinement (Thomson and Penfold 1978), to increase the effectiveness of the discharge.

Circular Magnetrons

The magnetron action can be achieved with other geometries, too. Figure 6-67 is a schematic of the *circular magnetron* due to Clarke (1971).

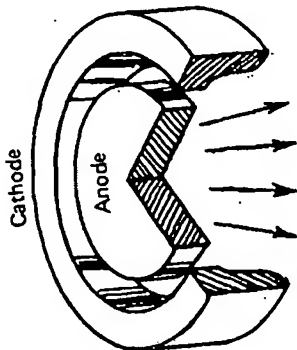


Figure 6-67. Circular magnetron sputtering configuration. Various cathode cross-sections are employed to minimize erosion problems.

The operating principle is the same as that of the cylindrical magnetron, but results differ in that, for example, the sputter ejected material has a pronounced forward direction (perpendicular to the anode); substrates are therefore usually placed on a rotating carousel to ensure good uniformity of film thickness. As with the other magnetrons, substrates are protected from the fast electrons which were very evident in the diode configurations, and this can be a big advantage when dealing with bombardment-sensitive substrates, such as some semiconductor devices. A disadvantage of circular magnetrons is that the localized erosion of the target causes deposition rates to change over a period of time, but this can be overcome to some extent by careful choice of the cathode shape. Magnetrons of this type have been reviewed by Fraser (1978).

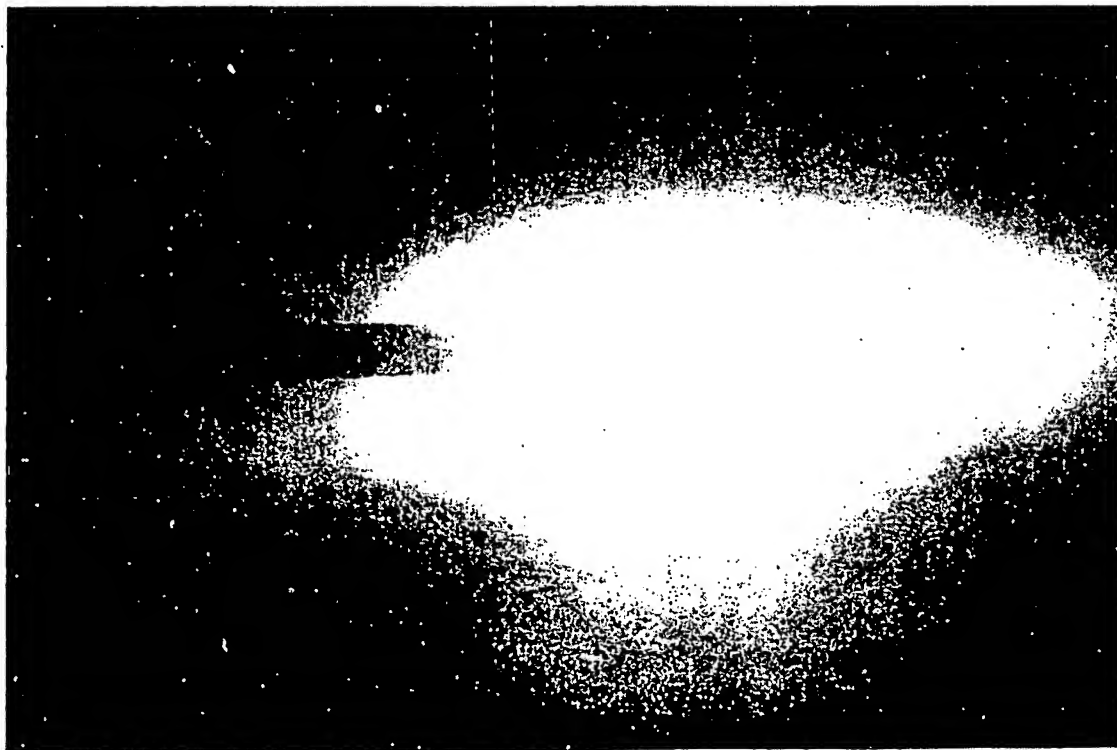


Figure 6-66. The extended glow shows that electrons are lost from the ends of the target (Green and Chapman 1975).

Planar Magnetrons

The third type of practical sputtering magnetron is the planar magnetron (Figure 6-68), which was first described in the literature by Chapin (1974). As with the circular magnetron, a 'looping' magnetic field is used, and this restricts the sputter erosion of the target to a 'racetrack' area. The geometry of the rectangular version of the planar magnetron makes it suitable as a line source with substrate motion again required for good uniformity. A circular configuration could also be used. The magnetic field causes very effective concentration of the glow (Figure 6-69) and the associated localized erosion of the target is again somewhat of a problem. Planar magnetrons have been reviewed by Waits (1978).

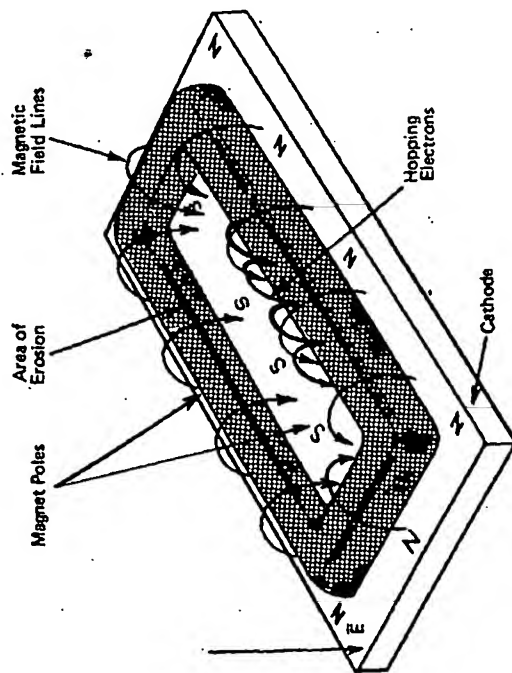


Figure 6-68. Planar magnetron sputtering configuration

General Comments

Magnetrons have proved to be very useful additions to the family of sputtering devices. They offer high deposition rates, with greater than one micron per minute being available if required. They also virtually eliminate bombardment of the substrate by fast charged particles; it is claimed that the heat input is reduced to the heat of condensation of the film (although it is not clear to me

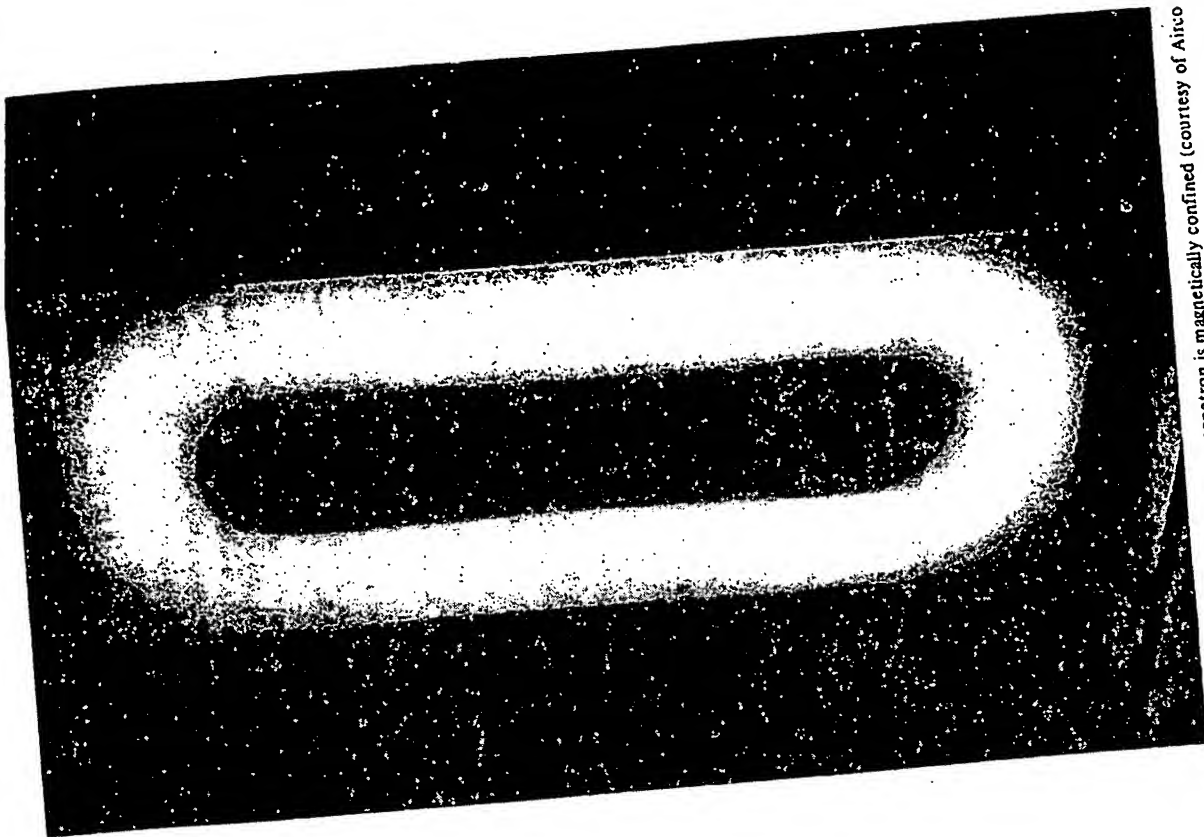


Figure 6-69. The glow in a planar magnetron is magnetically confined (courtesy of Airco Temescal)

how fast neutral argon bombardment — from ions neutralized and reflected at the target — is eliminated).

The disadvantages of magnetrons are of localized erosion of the target (although not in the cylindrical magnetrons), which causes deposition rates to vary with time and requires frequent replacement of the target, and of arcing. Magnetrons seem to be more susceptible to arcing than other types of sputtering system, and this is probably exacerbated by the high current, low voltage power supplies which are required to drive the low impedance discharges. Current densities may be up to 100 mA/cm², with 10 or 20 mA/cm² at a few hundred volts being quite typical. A 'unipolar arc', as described previously, can be established — for example by a small oxide patch of the cathode surface — and the arc can cause virtually the entire discharge current to be concentrated into the arc spot on the cathode. The huge power dissipation at the cathode causes the target to locally melt. Arcing of this type, although common to all magnetrons, is very clearly shown in the planar magnetron: *race track arcs* appear to be small particles that hop around the race track area of erosion (Chapin 1974) and are possibly evaporated clusters of target material which become charged by thermionic emission and then are driven by the qvB force. Arcing is particularly prevalent in reactive magnetron sputtering, presumably because of insulator formation on the target.

The sputtering of magnetic materials in a magnetron poses interesting problems because they tend to distort or even eliminate the field lines causing magnetron action. There are remedies for this problem, most of them proprietary.

Magnetron systems are usually dc powered, although rf versions are in use. The power dissipated at the target by the large ion currents involved causes considerable problems with target cooling, and these problems are considerably greater with insulators — which usually hinder heat flow as well as electrical flow.

For a general review of magnetrons and magnetic field effects in sputtering, readers are referred to the review by Thornton and Penfold (1978) and, for applications, to the papers presented at the magnetron sessions of the Annual Symposium of the American Vacuum Society — see, for example, *Journal of Vacuum Science and Technology*, Vol. 14, No. 1 (1977); Vol. 15, No. 2 (1978); and Vol. 16, No. 2 (1979).

ANALYTICAL AND MONITORING TECHNIQUES

There are now a whole range of techniques available for analyzing glow discharges, for process control, and for monitoring deposition rates.

Probe measurements for measuring plasma parameters have already been mentioned, and they are just one of a set of electrical techniques which also

ANALYTICAL AND MONITORING TECHNIQUES

includes double probes and propagation of microwave radiation through the glow (Thornton 1978).

Optical techniques are appealing as analytical tools because they do not interfere with the process at all, at least not when used in an emission mode. Spectroscopy of sputtering discharges has been developed by Greene and Sequeda-Osorio (1973) to give spatial resolution within the discharge. Not only the discharge gas but also elements from the targets can be detected in this way (Figure 6-70), which therefore offers a means of process control. Optical tech-

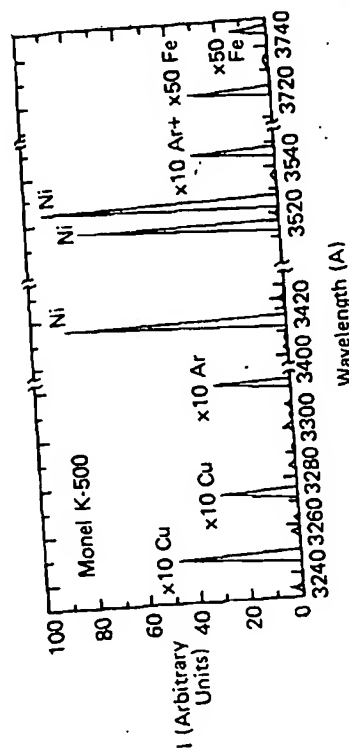


Figure 6-70. A portion of the emission spectrum from the discharge when sputtering Monel K-500 (a nickel-based heat resistant alloy) in argon (Greene et al. 1975)

niques have also been used to monitor emission from the growing film, by using a glass rod to transmit the emission to the monochromator (Ratinen 1973).

Optical techniques have been reviewed by Greene (1978). Mass spectrometry is also a valuable tool. The mass/energy analyzer of Coburn and colleagues has already been mentioned; more generally, mass spectrometry can be used to analyze the sputtering atmosphere and to control, for example, the partial pressure of active components in a reactive sputtering system.

Film deposition rates can be measured in situ by monitoring the change of frequency of a quartz oscillator as the mass of the film changes its characteristic frequency, with a resolution ~ 1 Å attainable. Other in situ techniques include monitoring the intensity of a light beam reflected from a growing dielectric film; the reflected-beam displays maxima and minima as its optical thickness increases (see Glang 1970). The infra red radiation from the film can be used to monitor its temperature.

ION BEAM SYSTEMS

The ion beam sources are operated at pressures above 10^{-4} torr. Some of the ions generated are accelerated and extracted by a series of grids. As we have already seen in Chapter 4, "Space Charge Limited Current", the current density j that can be extracted by a voltage V between two planes distance d apart, is given by the Child-Langmuir equation. For collisionless sheaths, this predicts $j \propto V^{3/2}/d^2$. With reasonable values for the separation d between two electrodes, current densities $\sim 1 \text{ mA/cm}^2$ at 1000 eV are obtained, and these are comparable to more conventional sputtering systems.

The extraction grids also serve as limiting pumping conductances so that a differential pressure can be set up and the process chamber can be operated at better vacuum, $< 10^{-5}$ torr, where molecular flow conditions obtain.

After extraction, the positively charged ion beam would expand due to Coulomb repulsion, and make the beam non-parallel. This is prevented by using a *neutralization filament* close to the source, consisting of a heated filament that thermionically emits electrons and neutralizes the beam. This also makes it possible to bombard insulators without them charging up.

Ion Beam Sputtering

For the purposes of sputter etching or sputter deposition, a noble gas ion beam is extracted from the ion source and used to bombard a target (Figure 6-71). The target can be used as a sputter deposition source to coat a substrate; this process is variously known as *ion beam sputter deposition*, *secondary ion beam deposition* (although the depositing material is un-ionized), and ambiguously as *ion beam deposition*. Alternatively the sputter etching of the target can be the main purpose, in which case the process is known as *ion beam etching*, and has been discussed earlier in the chapter.

The various differences between ion beam and glow discharge sputtering have been highlighted by Harper (1978), and can be summarized as follows:

- *For etching*, the control of the process is improved by: the parallel ion beam, the ability to control incidence angle, the ability to control beam current and energy independent of target processes, and the ability to sputter insulators without them charging up. In addition, the low process chamber pressure minimizes redeposition by gas phase scattering, and the monoenergetic ion beam permits study of ion impact processes, sputtering yields, etc.
- *For deposition*, the fact that the substrates are much more isolated from the glow discharge generation process minimizes unwanted heating of the substrate and minimizes fast electron bombardment. Because the substrates are not part of the electrical circuit, it is much easier to incorporate substrate heating, cooling, and process controls. The low operating pressure in the process chamber minimizes gas contamination of the growing film, particu-

SPUTTERING

ION BEAM SYSTEMS

In the beginning of this chapter, we decided that the ions used for sputtering purposes could be produced by an in situ glow discharge. Most of the discussion in this chapter has been about such systems. We have seen that the environmental conditions necessary to sustain the glow discharge can have a significant effect on the quality of the deposited films.

Ions can also be generated by an external *ion beam source*. This means that the substrate can be located in a virtually field-free high vacuum environment, and this has several implications for the growth of the film. A typical arrangement for ion beam sputtering is shown in Figure 6-71.

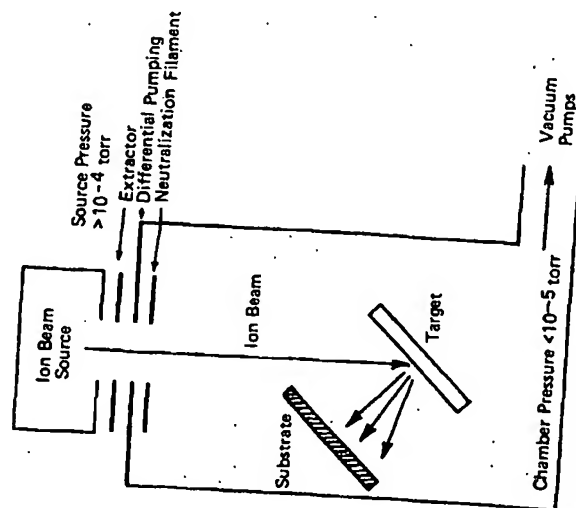


Figure 6-71. Typical configuration for ion beam sputter deposition

Ion Beam Sources

There are various ways of producing ions, but to achieve the current densities required for sputtering, one uses electron impact ionization in hot or cold cathode discharges. There are many source designs (Kaufman 1978), reflecting the wide interest in ion beam technology, of which sputtering is just one part.

larly since the vacuum pumps can operate with maximum conductance to the chamber and so minimize the partial pressure of contaminants. The low operating pressure also reduces energy-attenuating collisions of the sputtered particles en route from target to substrate. Weissmantel et al. (1972) have taken advantage of this environment to make in situ observations of sputter deposited film growth in the electron microscope.

I have not mentioned before (and perhaps should have) that sputtered particles are ejected with higher energies than are evaporated particles. The average energy from an evaporation filament at temperature T is of the order of kT and so would amount to 0.25 eV at 3000 K. For bombardment energies of 1 keV or so, the most likely sputter ejection energy is from 1 – 15 eV (Figure 6-72), with

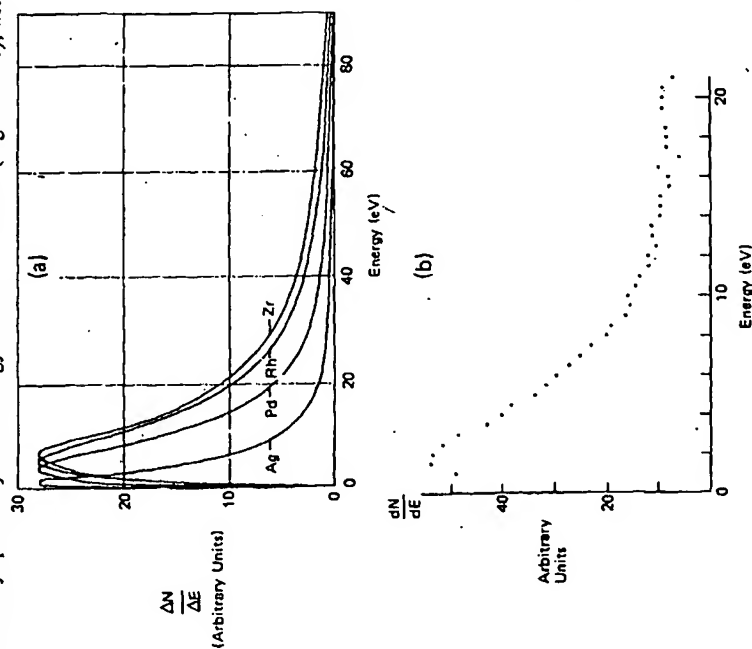


Figure 6-72. (a) Energy distributions for Ag, Pd, Rh and Zr under 1200 eV Kr^+ bombardment (Wehner and Anderson 1970). (b) Energy spectrum of neutral copper sputtered at 45° incidence and 45° ejection, by 3 keV Ar^+ (Lundquist 1978).

monotonically decreasing numbers of atoms having higher energies. In glow discharge sputtering systems, except at the lowest operating pressures, almost all of the ejection energy of the sputtered atoms will have been dissipated by collisions before the atoms reach the substrate. This will not be so with the pressures extant in an ion beam system. It has been suggested that the higher arrival energy of the atoms will lead to greater adatom surface mobility during the nucleation and growth stages of film formation. Single crystal films deposited in this mode have been observed to have lower epitaxial temperatures (Chapman and Campbell 1969).

Ion beam systems were used in the 60's to gain information about the basic processes in sputtering, and yielded information about sputtering yields, preferential sputter ejection from specific crystal axes of single crystal targets (which helped clarify sputtering mechanisms), sputter ejection energies, etc. Subsequently their use for sputter deposition waned, and work with such systems concentrated on high energy ion bombardment effects, of interest for ion implantation and radiation damage processes. Ion beam etching continued, but it was considered that ion beam sputter deposition was rather impractical in terms of capital cost and limited throughput. More recently, with the availability of large diameter ion beams (Laznovsky 1975) and a need for some specialized sputter deposition applications, there seems to be a renewed enthusiasm for ion beam sputtering processes.

Ion Beam Deposition

The sputter deposition process involves the condensation of low energy atoms onto a surface. Sputter etching uses high energy atoms or ions; although these may be incorporated in the bombarded surface, the net process is of etching. Ion beam deposition (also known as *primary ion beam deposition*) is the formation of a thin film by the direct deposition of ions, with the ion energies chosen to be low enough to ensure net deposition. Whereas the ion beam sputtering processes described above use a noble gas ion beam, ion beam deposition systems use a beam of the material to be deposited, and this is usually a metal; this requires special consideration of the ion source. The practical arrangement would be similar to Figure 6-71, with the target becoming the substrate.

Aisenberg and Chabot (1971) have used this technique to deposit highly adherent diamondlike carbon films, and have subsequently discussed the physics of the technique (Aisenberg and Chabot 1973). Their technique produced a beam of carbon and argon ions and neutrals. It is more representative of the philosophy of the process to use a charged particle beam, which can then be deflected and focused. The beam is also *mass analyzed* to produce a very pure, monoenergetic source of depositing ions. The beam energy chosen is determined

by the resulting film quality balanced against self-resputtering as the ion energy increases.

The difficulty of this process is in producing an adequate supply of ions. It is more difficult to produce ions of a solid to start with, and then their flux is limited by space charge limited extraction from the source (low voltage V leads to low current density j , for given d) and when adequate currents can be obtained, there will be problems of beam expansion due to space charge repulsion. It is usually found expedient to extract the ions at a high voltage and then to decelerate the beam. Amano and Lawson (1977, 1978) have used the technique for the controlled deposition of Pb^{+} and Mg^{+} , with deposition rates of 1000–3000 Å being deposited in 7 hours from a 10 μA beam at 24 eV.

Although an extremely slow process, ion beam deposition has a potential for very controlled deposition of very pure films, and might provide an alternative to molecular beam systems.

ION PLATING

Ion plating is a vacuum deposition technique that uses a glow discharge to modify the composition of the deposited film. The technique was introduced by Don Mattox in the mid-60's and has been more recently reviewed by him (Mattox 1973a) and by Carpenter (1974). The technique combines evaporation and sputtering. The substrate is made the cathode of a high voltage glow discharge, and this is used to initially sputter clean the surface of the substrate. Material is then evaporated onto the substrate from a resistively heated filament whilst still maintaining the discharge (Figure 6-73). As with bias sputter deposition and ion beam deposition, there is simultaneous deposition and resputtering,

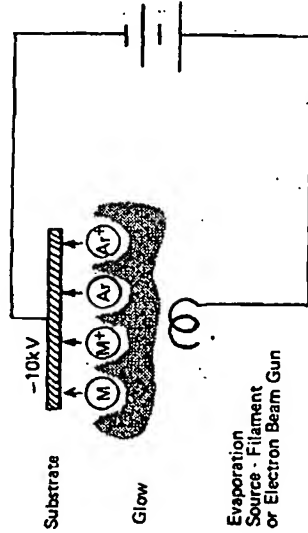


Figure 6-73. Ion plating configuration

ION PLATING

with the balance such as to ensure net deposition. Unlike those processes, deposition rates in ion plating are high enough that substantial resputtering can be tolerated. The technique encompasses bias evaporation which was discussed earlier, but is usually differentiated in terms of the accelerating voltages used at the substrate, being very much higher in ion plating than in bias evaporation.

When material from the filament is evaporated into the discharge, some portion of it will be ionized by the electric impact and (possibly) Penning processes that were described in Chapter 2. There are various reports of the degree of ionization attained, usually around a few per cent (Aisenberg and Chabot 1973). But we know that for a noble gas discharge, the degree of ionization is only about 10^{-4} , and apparently ion plating discharges can become self-sustaining without the noble gas, after the process is well underway (Kruténat and Gesick 1970). This can only occur if the evaporation rate is enough to maintain an adequate partial pressure of the evaporant. Under these circumstances, one has the opportunity of observing the emission from a gaseous metal discharge. This phenomenon can also be observed in high rate magnetron sputtering systems, and is very apparent in the colour original of Figure 6-66.

Remembering that sputtering at the substrate can reduce or even eliminate film deposition, then with several thousand volts applied to the substrate at pressures of a few tens of millitorr, film deposition will occur only if the evaporation rate is high. Ion plating is characteristically a high rate deposition process. High voltages are used in order to promote forward sputtering and implantation of the film into the substrate, and the elimination of this interface promotes excellent adhesion, as discussed in the later section on "Thin Film Adhesion". Figure 6-74 shows a depth profile analysis of an ion plated film, and one can see that the interface is spread over a considerable distance.

A secondary effect of the ionization is that the ionized material will follow electric field lines. Combined with the considerable gas phase scattering which occurs at the pressures used, and the high mobility of the deposited material due to the high substrate temperatures produced by the ion bombardment, conformal coverage of three dimensional objects can be achieved.

There is nothing unique about the use of an evaporation source, so that any source of material could be used, as pointed out by Mattox (1973a).

I suspect that ion plating has had a bigger effect on the use of vacuum deposition technology than might at first be clear. With the capability of achieving excellent film durability and high deposition rates up to several mils (1 mil = 25 μm) per minute, vacuum deposition is now used extensively in mechanical engineering applications, such as to resurface turbine engine blades and coat rotary engine surfaces (White 1973). High rate sputtering and other evaporation techniques also are being used for similar applications, which are far from the world of semi-conductor fabrication and illustrate the current wide utilization of glow discharge processes.

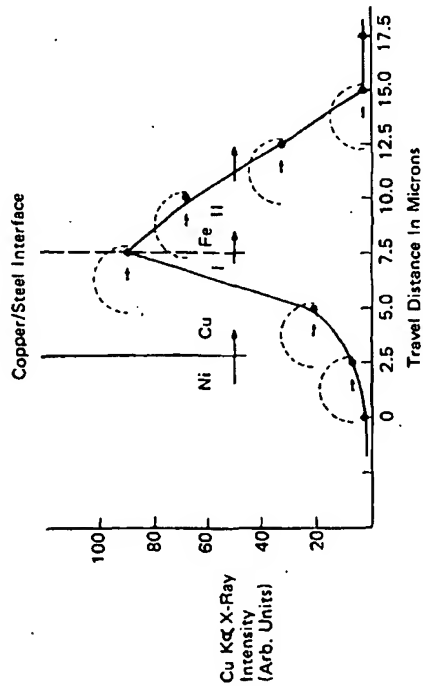


Figure 6-74. Depth profile of ion plated Cu on steel. The decreasing intensity of Cu (measured by electron microprobe) in region II corresponds to penetration into the substrate to a depth of 7-8 μm . The nickel layer was used for specimen support (Swaroop and Adler 1973).

ACTIVATED REACTIVE EVAPORATION

Activated reactive evaporation is another glow discharge process used primarily for mechanical engineering applications. The technique has been developed by Rointan Bunshah and colleagues; see Bunshah (1974).

Activated reactive evaporation follows the same principle used in reactive sputtering: a glow discharge is used to dissociate a gas into reactive components (see Chapter 2) which then combine with the growing film. Films of Y_2O_3 , TiN , TiC , VC , ZrC , HfC , NbC and TaC (and doubtless many others more recently) have been deposited at high rates (3-12 $\mu\text{m}/\text{minute}$) by evaporating the metal in a partial pressure of a few times 10^{-4} torr of O_2 , N_2 , or C_2H_2 . Coupled with high substrate temperatures, extremely durable coatings can be produced.

The configuration for activated reactive evaporation is shown in Figure 6-75. With the application of a field between the source and substrate, an activated reactive ion plating process could also be produced. The structure of thick coatings has been analyzed by Movchan and Demchishin (1969), who classify the structure of coatings into three zones according to the substrate temperature T and the melting point T_m of the coating. The first two zones are divided by $T/T_m = 0.3$, with the transition to the third zone taking place at higher temperature. Many desirable film qualities are achieved at higher temperatures.

THIN FILM ADHESION

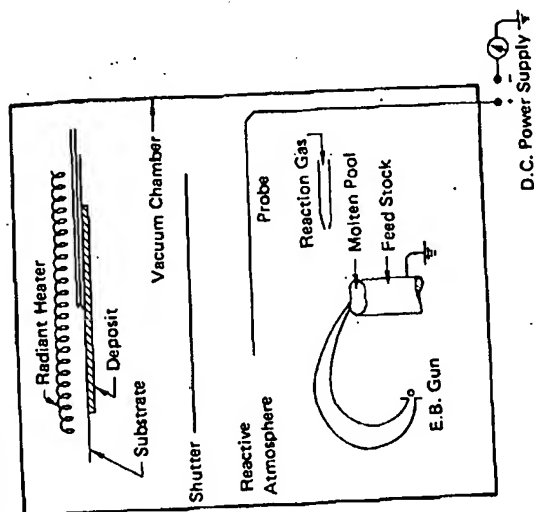


Figure 6-75. Schematic of the experimental arrangement for the activated reactive evaporation process (Bunshah 1974).

THIN FILM ADHESION

The topic of *thin film adhesion* has cropped up several times in the course of this chapter, as it inevitably does in any discussion of thin film deposition. Adhesion is one of the 'unloved' topics in thin film technology. The interaction between thin film and the substrate is in itself usually of little interest to those fabricating thin film structures, but unfortunately the quality of this interaction is a vital factor in determining the durability of the device. The extent to which it can do this depends largely on the bonding between the two. Inevitably, it turns out that some of the more interesting combinations of materials are incompatible in terms of adhesion. An understanding of thin film adhesion and how it can be controlled is therefore of considerable importance. But even after half a century or so, our knowledge of this topic is extremely limited and largely empirical. A major reason for this is the difficulty of measuring adhesion. Another reason is that confusion often arises over the usages of the words 'adhesion' and related rather undefined terms. In this section, *adhesion* will be used as a generic term describing how a film and substrate remain in contact, and *bonding* will refer to the specific interaction across the interface. As discussed in a review of thin film adhesion (Chapman 1974),

from a practical point of view one should really be concerned with the durability of the film-substrate combination, and this is a function of many more things than just the bonding.

There are various types of adhesion:

- The simplest of these is *interfacial adhesion*, in which the two distinct materials, film and substrate, meet at a well-defined interface.
- A second type is *interdiffusion adhesion*, which results from a solid state interdiffusion between the two materials or from solubility of one or both materials in the other. In this case, a discrete interface is replaced by a gradual and continuous change from one material to the other. The 'interdiffusion' can also be promoted artificially.
- A third type is *intermediate layer adhesion*. The film and substrate are bonded together via one or more layers of compounds of the materials with each other and/or with the environmental gases; oxides are particularly common. Again there is no single well-defined interface.
- All these different types of adhesion are further complicated in practice because substrate surfaces are never flat and some degree of *mechanical interlocking* takes place.

Methods of Influencing Adhesion

Although there are some film-substrate combinations which exhibit good adhesion, it usually turns out that a particular film-substrate system to satisfy certain functional requirements is poorly adherent! Sometimes the adhesion can be improved simply — for example, by cleaning the substrate surface so that the film and substrate really do contact: since vacuum deposition is an atomistic or molecular process, this is a real possibility, unlike the contact of two bulk materials. Solvent cleaning usually removes only oils and greases, leaving more tenacious materials such as surface oxides which may prevent interdiffusion. One can remove such deposits by chemical or sputter etching, but the problem then becomes how to deposit the film before the substrate is recontaminated, bearing in mind that a gas monolayer can form in 1 sec at 10^{-6} Torr. We shall return to this problem below. Nevertheless, Jacobsson and Kruse (1973) found that for ZnS on glass the critical load in their pull test of adhesion was nearly doubled if the glass was ion bombarded before film deposition. Butler (1970) also found improved adhesion of evaporated copper on glass if the substrate was glow discharge cleaned.

In the case of interdiffusion or compound interfaces, adhesion improvement can often be achieved by substrate heating. One has to be careful, however, that this does not produce adverse effects, such as grain growth. But this can usually

THIN FILM ADHESION

be avoided; e.g. reflective adherent films of aluminium on glass can be produced by evaporating a very thin layer of Al at a substrate temperature of 250° C, which is then reduced to 150° C for depositing the reflecting layer. Sometimes very little heating is required; gold can be evaporated onto silicon (provided the oxide surface is removed) at 50° C to produce excellent adhesion via a diffuse interface extending many atomic layers (Narusawa et al. 1973).

Intermediate layer adhesion occurs naturally for some materials, such as aluminium on glass (Bateson 1952). In other cases, intermediate materials may be introduced to advantage; Colbert et al. (1948a) have reported that metal films, strongly adherent to glass and other silica-containing substrates, can be produced using very thin intermediate layers of metallic oxides, sulphides, sulphates, selenates and phosphates, silver chloride, and magnesium fluoride. Many of these materials were produced in situ by oxidation of an evaporated material in an oxygen-containing glow discharge. Presumably, reactive deposition could also be used. A further patent (Colbert et al. 1948b) deals with the use of intermediate layers of lead compounds. In another specific example, the use of an intermediate layer of SiO₂ seemed even more effective in improving the adhesion of ZnS on glass than predeposition ion bombardment of the substrate (Jacobsson and Kruse 1973).

Intermediate oxide layers can also be achieved by depositing an oxygen-active metal (A) onto an oxide surface (BO), promoting the reaction $A + BO \rightarrow AO + B$ at the interface. Materials with large heats of oxide formation, such as titanium, molybdenum, tantalum, and chromium, are effective. A further metal layer, adherent to the intermediate material, can then be deposited. This is the basis of several multilayer systems, such as Ti - Au, Ti - Pd - Au, and Ti - Pt - Au (English et al. 1972).

Another version of the intermediate layer philosophy would seem to be particularly useful where substrate heating is restricted, e.g. with diffused semiconductor devices. The approach can be illustrated by its application to producing adherent tungsten on silica. A metallic cation having a different valence from the substrate silicon cation, such as aluminium or phosphorus, is introduced substitutionally into the surface layers of the substrate by diffusion or ion bombardment. This produces unsatisfied bonding of the oxygen anions in the substrate, and the tungsten can now be deposited by evaporation or sputtering and will chemically bond to the substrate (Cuomo et al. 1972).

The formation stages of a thin film, its initial nucleation and subsequent growth, should have an influence on the adhesion and cohesion failure mechanisms of a thin film — for example, those due to the presence of microcracks and voids. This aspect of adhesion and several others have been discussed by Mattox (1963-1973). One may expect that glow discharge and ion bombardment cleaning would have a further influence on nucleation and growth via the creation of deep adsorption

sites and other surface defects. Similarly, bias levels and several other deposition parameters will have a marked effect on film microstructure.

It is often stated that sputtered films are more adherent than evaporated films because the sputtered atoms are ejected from their target source with much more energy than those from an evaporation source as discussed in "Ion Beam Sputtering". However, the small mean free path in a glow discharge sputtering system probably means that this ejection energy is largely dissipated by collisions before material reaches the substrate. What are probably more important are the fast electrons from the target, and the field existing at the substrate due to the plasma potential which, as we have seen, is typically +50V with respect to the anode in rf sputtering and less in dc. Substrate bombardment by secondary target electrons may be quite significant since these electrons are responsible for a good deal of substrate heating, which will promote interfacial reaction and interdiffusion as well as influence nucleation; the associated charge will also have a marked effect on nucleation. The sheath field at the substrate will cause positive ion bombardment there, mostly by sputtering gas ions but also by sputtered target atoms which may become ionized by the Penning mechanism. This bombardment will tend to resputter material from the growing film and may also lead to forward sputtering and implantation (as discussed later), particularly if the energy of bombardment is increased by the application of a negative potential to the substrate; i.e. by using the biasing technique. However, one must ensure that the bias does not prevent adhesion-promoting oxide formation which might otherwise naturally occur (Maisel and Schaible 1965).

Mattox has also been responsible for the introduction of ion plating and its use in promoting good adhesion. As we saw in a previous section, ion plating basically consists of bombarding the substrate with high energy gas ions to sputter clean the surface and then of evaporating material through the plasma onto the substrate whilst still maintaining the ion flux, at least for an initial period. As a result, the substrate remains clean during deposition (cf. predeposition cleaning discussed earlier), its surface temperature is high (promoting interfacial reaction and interdiffusion), the growth of the film is modified because of surface bombardment, and some of the evaporated material becomes ionized, is accelerated onto the substrate, and may become implanted. Hence, similar to ion implantation, interdiffusion/adhesion may exist as a nonequilibrium state even when there is no mutual solubility. Mattox (1969) has suggested the term *pseudodiffusion* for this situation. Swaroop and Adler (1973) have reported a graded diffuse interface of 7 to 8 μm depth for ion plated copper on steel.

Similar thinking has led to the use of high energy ion bombardment to enhance adhesion. Perkins and Stroud (1970) have produced extremely adherent contacts by evaporating 300 Å of Ni onto glass and then bombarding with 100 keV argon ions. This is probably at least partly due to nickel atoms being forward sputtered

CONCLUSION

into the glass, which produces interdiffusion; one might also expect a similar mechanism to exist in ion plating and maybe even in bias sputtering to a lesser extent as a means of implanting un-ionized film atoms. Applications of ion bombardment to enhance adhesion have been reviewed by Stroud (1972).

Finally, a technique for increasing the adhesion of thin metal films to glass after deposition is due to Stuart (1969) and is reported by Butler et al. (1971). The back of the substrate is coated with a conductor and an electric field is applied; for copper, this is 1000 V/mm for 10 min at 200° C. The enhanced adhesion is thought to be due to an assisted diffusion of copper ions into the substrate. In the case of aluminium, an alumina layer grows at the interface as though the aluminium were being anodized with the glass as a solid electrolyte. Similar mechanisms may exist at the surface of an insulating substrate in bias sputter deposition.

CONCLUSION

In this chapter we have looked at some of the variations of the sputtering process. It is very clear, by looking at the current literature, that the range of applications of sputtering and the variations of the basic process, is extremely wide. However, these variations can usually be traced to the basic processes described in this chapter.

There have been no dramatic recent developments in sputtering, but there has been a continual improvement in the control of the process. There is also a considerable broadening in the fields of application: e.g. metals can be treated by an ion nitriding process in which the metal becomes the target of a nitrogen-hydrogen discharge so that the surface is hardened (Hudis 1973); the Davis and Vander-slice (1963) mass/energy analyzer was used to analyze the discharge. Continuity

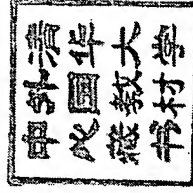
Over the next few years, we can expect to see a continuation of these trends.

THIN FILM PROCESSES

Edited by

JOHN L. VOSSEN WERNER KERN

*RCA Laboratories
David Sarnoff Research Center
Princeton, New Jersey*



20032214E



ACADEMIC PRESS, INC.

(Harcourt Brace Jovanovich, Publishers)

Orlando San Diego San Francisco New York
London Toronto Montreal Sydney Tokyo

5001411

COPYRIGHT © 1978, BY ACADEMIC PRESS, INC.
ALL RIGHTS RESERVED.
NO PART OF THIS PUBLICATION MAY BE REPRODUCED OR
TRANSMITTED IN ANY FORM OR BY ANY MEANS, ELECTRONIC
OR MECHANICAL, INCLUDING PHOTOCOPY, RECORDING, OR ANY
INFORMATION STORAGE AND RETRIEVAL SYSTEM, WITHOUT
PERMISSION IN WRITING FROM THE PUBLISHER.

ACADEMIC PRESS, INC.
Orlando, Florida 32887

ACADEMIC PRESS, INC. (LONDON) LTD.
24/28 Oval Road, London NW1 7DX

Library of Congress Cataloging in Publication Data

Main entry under title:

Thin film processes.

Includes bibliographical references.

1. Thin films. I. Vossen, John L. II. Kern,
Werner. Date 621.381'73 78-3348
TK7871.15.F3743
ISBN 0-12-728250-5

PRINTED IN THE UNITED STATES OF AMERICA

84 85 86 87 9 8 7 6

Contents

List of Contributors
Preface

ix
xi

Part I

I-1 Introduction

J. L. Vossen

References

5

Part II PHYSICAL METHODS OF FILM DEPOSITION

II-1 Glow Discharge Sputter Deposition

J. L. Vossen and J. J. Cuomo

I. Introduction 12
II. Physical and Chemical Effects of Ion Bombardment on Surfaces 14
III. Glow Discharges 24
IV. Equipment Configuration 31
V. Preconditioning of Targets, Substrates,
and Systems for Film Deposition. 41
VI. The Sputtering Gas 46
VII. Deposition with Simultaneous Ion Bombardment
of the Substrate and Growing Film 50
VIII. Rate and Uniformity of Deposition 61
IX. Conclusion 62
References 62

v

//-1

Glow Discharge Sputter Deposition

J. L. VOSSEN

RCA Laboratories
Princeton, New Jersey

J. J. CUOMO

IBM Thomas J. Watson Research Center
Yorktown Heights, New York

I. Introduction	12
II. Physical and Chemical Effects of Ion Bombardment on Surfaces	14
A. Emission of Neutral Particles—The Sputtering Yield	14
B. Emission of Other Particles	16
C. Emission of Radiation	20
D. Ion Implantation	20
E. Altered Surface Layers and Diffusion	21
F. Dissociation Processes	22
G. Chemical Sputtering	23
III. Glow Discharges	24
A. DC Glow Discharges	27
B. Low-Frequency AC Glow Discharges	27
C. RF Glow Discharges	29
D. Discharge Supporting Modes	31
IV. Equipment Configuration	31
A. Target Assemblies	33
B. Power Supplies	33
C. Instrumentation and Control	36
D. Substrate Heaters	37
E. Wall Losses	39
F. Shields and Shutters	39
G. Deposition Sources for Bias Sputtering and Ion Plating	39
H. Scale-Up Problems	40
V. Preconditioning of Targets, Substrates, and Systems for Film Deposition	41
A. Target Materials	41

11

B. Presputtering of Targets	42
C. Sputter Etching of Substrates	42
VI. The Sputtering Gas	46
A. Effects of Gas Species, Pressure, and Flow	46
B. Sources of Gas Contamination	46
C. Getter Sputtering	47
D. Reactive Sputtering	48
VII. Deposition with Simultaneous Ion Bombardment of the Substrate and Growing Film	50
A. Plasma, Floating, and Bias Potentials	50
B. Gas Incorporation and Desorption	58
C. Stoichiometry of Films	60
D. Physical Film Properties	60
VIII. Rate and Uniformity of Deposition	61
IX. Conclusion	62
References	62

I. INTRODUCTION

Over the past 20 years or so there have been numerous reviews of sputtering and sputtering processes for film deposition [1-15]. In this chapter we shall take a somewhat different viewpoint than those of most earlier reviewers. We shall attempt to treat this very complex subject from a process viewpoint. That is, we shall discuss the interactions of the process parameters to expose the many permutations and combinations that are available to control the properties of thin films.

Because there are so many interactions among parameters in sputtering systems, it is impossible to separate them completely. Thus, there are necessary, but regrettable references made to later sections throughout the chapter. In an attempt to minimize any confusion that this may cause, we shall give a brief, simple overview of the subject in this section before going to the more detailed discussions.

Figure 1 represents a greatly simplified cross section of a sputtering system. Typically, the target (a plate of the material to be deposited or the material from which a film is to be synthesized) is connected to a negative voltage supply (dc or rf). The substrate holder faces the target. The holder may be grounded, floating, biased, heated, cooled, or some combination of these. A gas is introduced to provide a medium in which a glow discharge can be initiated and maintained. Gas pressures ranging from a few millitorr to about 100 mTorr are used. The most common sputtering gas is argon.

When the glow discharge is started, positive ions strike the target plate and remove mainly neutral target atoms by momentum transfer, and these

II-1. GLOW DISCHARGE SPUTTER DEPOSITION

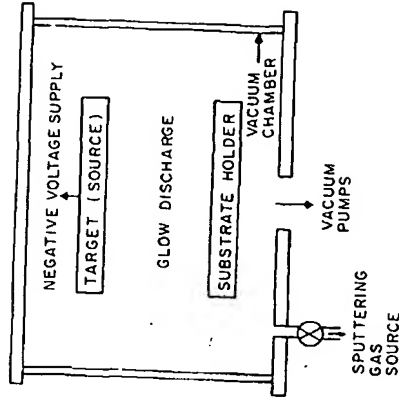


Fig. 1. Simplified cross section of a sputtering system.

condense into thin films. There are, in addition, other particles and radiation produced at the target, all of which may affect film properties (secondary electrons and ions, desorbed gases, x rays, and photons). The electrons and negative ions are accelerated toward the substrate platform and bombard it and the growing film. In some instances, a bias potential (usually negative) is applied to the substrate holder, so that the growing film is subject to positive ion bombardment. This is known variously as *bias sputtering* or *ion plating*. Initially, the term "ion plating" referred to a process in which the deposition source was a thermal evaporation filament instead of a sputtering target and the substrates were connected to a dc sputtering target [16], but it has sometimes been applied to any process in which the substrate is subjected to purposeful ion bombardment during film growth in a glow discharge environment [17].

In some cases, gases or gas mixtures other than Ar are used. Usually this involves some sort of *reactive sputtering* process in which a compound is synthesized by sputtering a metal target (e.g., Ti) in a reactive gas (e.g., O_2 or Ar- O_2 mixtures) to form a compound of the metal and the reactive gas species (e.g., TiO_2). Reactive sputtering is also used to replenish constituents of compound targets lost by dissociation. The reactive version of ion plating is sometimes known as *activated reactive evaporation* [18], but this terminology is more often applied to processes in which an evaporant passes through a glow discharge in transit to an electrically floating or grounded substrate. Reactive sputtering should not be confused with *chemical sputtering* in which the reactive gas (e.g., O_2) reacts with the target surface (e.g., C) to form volatile compounds (e.g.,

CO) that are pumped away [1]. Chemical sputtering is more properly related to ion etching processes (see Chapter V-2).

We shall consider in detail the complex interplay among target kinetics, glow discharge phenomena, substrate conditions, equipment configuration, etc. that bear on the ability to control the properties of thin films.

II. PHYSICAL AND CHEMICAL EFFECTS OF ION BOMBARDMENT ON SURFACES

In sputter deposition, surfaces subject to ion bombardment are usually considered as the source of material from which films are grown. In addition to the neutral (sputtered) material liberated from the bombarded surface which eventually condenses as a film, there are numerous other events that can occur at the target surface which may influence the growth of films profoundly. These include: secondary electron emission, secondary positive and/or negative ion emission, emission of radiation (photons, x rays), reflection of incident particles, heating, chemical dissociation or reaction, bulk diffusion, crystallographic changes, and reflection of some of the emitted particles back to the bombarded surface (backscattering). It should be noted that all of these same phenomena apply to sputter-etching processes (Chapter V-2) in which the workpiece is a sputtering target and to *substrates in most glow discharge deposition processes*. (As will be shown later, any material body immersed in a glow discharge acquires a negative potential with respect to its surroundings and must be considered a sputtering target.)

There have been several recent comprehensive reviews of the kinetics involved when a surface is ion bombarded [3, 6, 8, 12]. Therefore, we shall review them only briefly, emphasizing those target effects that can affect the way in which films grow.

A. Emission of Neutral Particles—The Sputtering Yield

The sputtering yield is defined as the number of atoms ejected from a target surface per incident ion. It is the most fundamental parameter of sputtering processes. Yet all of the surface interaction phenomena involved that contribute to the yield of a given surface are not completely understood. Despite this, an impressive body of literature exists showing the yield to be related to momentum transfer from energetic particles to target surface atoms. There is a threshold for sputtering that is approximately equal to the heat of sublimation. In the energy range of practical interest for sputtering processes (10–5000 eV), the yield increases with

incident ion energy, and with the mass and d-shell filling of the incident ion [19, 20].

The sputtering yield determines the erosion rate of sputtering targets; and largely, but not completely, determines the deposition rate of sputtered films. Several compilations of experimental sputtering yield and related data have been published [3, 5, 6, 21, 22]. All sputtering yields and related data should be used with caution. In glow discharge systems, bombarding ions are by no means monoenergetic, and it is not necessarily valid to use yield values for pure metals when alloys, compounds, or mixtures are sputtered. As will be shown, the sputtering yield of material A from a matrix of A + B is often very different from the sputtering yield of A from a matrix of A. Also, when sputtering yields of compounds are given, dissociation reactions are often ignored. Despite this, tabulations of sputtering yields are useful, if only to give a rough indication of the deposition or etch rate that might be expected for a given material. Tables I–III give a compilation of sputtering yields and relative film deposition

Table I
Sputtering Yield of Elements at 500 eV

Gas	He	Ne	Ar	Kr	Xe	Reference
Element						
Be	0.24	0.42	0.51	0.48	0.35	[23]
C	0.07	—	0.12	0.13	0.17	[23]
Al	0.16	0.73	1.05	0.96	0.82	[23]
Si	0.13	0.48	0.50	0.50	0.42	[23]
Ti	0.07	0.43	0.51	0.48	0.43	[23]
V	0.06	0.48	0.65	0.62	0.63	[23]
Cr	0.17	0.99	1.18	1.39	1.55	[23]
Mn	—	—	—	1.39	1.43	[23]
Mn	—	—	1.90	—	—	[24]
Bi	—	—	6.64	—	—	[24]
Fe	0.15	0.88	1.10	1.07	1.00	[23]
Fe	—	0.63	0.84	0.77	0.88	[25]
Co	0.13	0.90	1.22	1.08	1.08	[23]
Ni	0.16	1.10	1.45	1.30	1.22	[23]
Ni	—	0.59	1.33	1.06	1.22	[25]
Cu	0.24	1.80	2.35	2.35	2.05	[23]
Cu	—	1.35	2.0	1.91	1.91	[25]
Cu (111)	—	2.1	—	2.50	3.9	[26]
Cu	—	—	1.2	—	—	[27]
Ge	0.08	0.68	1.1	1.12	1.04	[23]
Y	0.05	0.46	0.68	0.66	0.48	[23]
Zr	0.02	0.38	0.65	0.51	0.58	[23]

Table I (Continued)

Gas	He	Ne	Ar	Kr	Xe	Reference
Nb	0.03	0.33	0.60	0.55	0.53	[23]
Mo	0.03	0.48	0.80	0.87	0.87	[23]
Mo	—	0.24	0.64	0.59	0.72	[25]
Ru	—	0.57	1.15	1.27	1.20	[23]
Rh	0.06	0.70	1.30	1.43	1.38	[23]
Pd	0.13	1.15	2.08	2.22	2.23	[23]
Ag	0.20	1.77	3.12	3.27	3.32	[23]
Ag	1.0	1.70	2.4	3.1	—	[27]
Ag	—	—	3.06	—	—	[28]
Sm	0.05	0.69	0.80	1.09	1.28	[23]
Gd	0.03	0.48	0.83	1.12	1.20	[23]
Dy	0.03	0.55	0.88	1.15	1.29	[23]
Er	0.03	0.52	0.77	1.07	1.07	[23]
Hf	0.01	0.32	0.70	0.80	—	[23]
Ta	0.01	0.28	0.57	0.87	0.88	[23]
W	0.01	0.28	0.57	0.91	1.01	[23]
Re	0.01	0.37	0.87	1.25	—	[23]
Os	0.01	0.37	0.87	1.27	1.33	[23]
Ir	0.01	0.43	1.01	1.35	1.56	[23]
Pt	0.03	0.63	1.40	1.82	1.93	[23]
Au	0.07	1.08	2.40	3.06	3.01	[23]
Au	0.10	1.3	2.5	—	7.7	[29]
Pb	1.1	—	2.7	—	—	[27]
Th	0.0	0.28	0.62	0.96	1.05	[23]
U	—	0.45	0.85	1.30	0.81	[23]
Sb	—	—	2.83	—	—	[24]
Sn (solid)	—	—	1.2	—	—	[30]
Sn (liquid)	—	—	1.4	—	—	[30]

rates. The latter have been normalized to the sputtering yields of pure metals [21]. All target materials are polycrystalline unless otherwise indicated.

B. Emission of Other Particles

1. Secondary Electrons

Since sputtering targets are held at high negative potentials, secondary electrons are accelerated away from the target surface with an initial energy equal to the target potential. As will be shown in Section III.A, these electrons help to sustain the glow discharge by ionization of neutral sput-

Table II

Sputtering Yield of Elements at 1 keV

Gas	He	N	Ne	N ₂	Ar	Kr	Xe	Reference
Element								
Fe	—	—	0.85	—	1.33	1.42	1.82	[25]
Fe	—	0.55	—	0.78	—	—	—	[3]
Ni	—	—	1.22	—	2.21	1.76	2.26	[25]
Ni	—	0.74	—	1.05	—	—	—	[3]
Ni	—	—	—	—	2.0	2.0	2.0	[26]
Cu	—	—	1.88	—	2.85	3.42	3.6	[25]
Cu	—	1.5	—	—	—	—	—	[3]
Cu	—	—	—	—	3.2	2.5	—	[27]
Cu (111)	—	—	2.75	—	4.5	4.65	6.05	[26]
Cu	—	—	—	1.95	—	—	—	[31]
Mo	—	—	0.49	—	1.13	1.27	1.60	[25]
Mo	—	0.16	—	0.3	—	—	—	[3]
Ag	1.8	—	2.4	—	3.8	4.7	—	[27]
Sn	—	—	—	—	0.8	—	—	[32]
W	—	0.18	—	0.2	—	—	—	[3]
Au	—	—	—	—	1.0	—	—	[32]
Au	0.3	—	2.1	—	4.9	—	—	[29]
Pb	1.5	—	—	—	3.0	—	—	[27]
Sn (liquid)	—	—	—	—	1.7	—	—	[30]
Au (111)	—	—	—	—	3.7	—	—	[33]
Au (100)	—	—	—	—	3.0	—	—	[33]
Au (110)	—	—	—	—	2.0	—	—	[33]
Au	—	—	—	—	3.6	—	—	[33]
Al (111)	—	—	—	—	1.0	—	—	[33]

tering gas atoms which in turn bombard the target and release more secondary electrons in an avalanche process. Upon arrival at the substrate, such energy as they retain after collisions in the gas is liberated in the form of heat [38-43]. Many of the secondary electrons are thermalized by collisions in the gas, but even at high gas pressures, a substantial number of electrons retain full target potential upon impact at the substrates [41, 42].

2. Secondary Ions

Most of the data on ion emission from solids due to primary ion bombardment is to be found in the literature of secondary ion mass spectroscopy (SIMS). Most of this literature deals with the formation and emission of positive ions. However, in glow discharge sputtering, it is highly

Table III
Miscellaneous Sputtering Yields

Material	Gas	Energy (keV)	Yield	Reference
Fe	Ar	10	1.0	[32]
Cu	Ne	10	3.2	[34, 35]
Cu	Ar	10	6.25	[34, 35]
Cu	Kr	10	8.0	[35]
Cu	Xe	10	10.2	[35]
Ag	Ar	10	10.4	[36]
Ag	Kr	10	14.8	[36]
Ag	Xe	10	15.5	[35, 36]
Au	Ne	10	3.7	[35]
Au	Ar	10	8.5	[32, 35]
Au	Kr	10	14.6	[35]
Au	Xe	10	20.3	[35]
Sn	Ar	10	2.1	[32]
Mg (0001)	Ar	5	3.13	[37]
Mg (10 $\bar{1}0$)	Ar	5	2.70	[37]
Mg (11 $\bar{2}0$)	Ar	5	1.64	[37]
Zn (0001)	Ar	3	11.22	[37]
Zn (0001)	Ar	4	11.43	[37]
Zn (0001)	Ar	5	12.65	[37]
Zn (11 $\bar{2}0$)	Ar	3	9.19	[37]
Zn (11 $\bar{2}0$)	Ar	4	10.07	[37]
Zn (11 $\bar{2}0$)	Ar	5	9.35	[37]
Zr (0001)	Ar	5	1.12	[37]
Zr (10 $\bar{1}0$)	Ar	5	1.56	[37]
Zr (11 $\bar{2}0$)	Ar	4	0.74	[37]
Zr (11 $\bar{2}0$)	Ar	5	0.64	[37]
Zr (11 $\bar{2}0$)	Ar	10	0.65	[37]
Cd (0001)	Ar	4	19.01	[37]
Cd (0001)	Ar	5	21.25	[37]
Cd (10 $\bar{1}0$)	Ar	4	15.86	[37]
Cd (10 $\bar{1}0$)	Ar	5	17.86	[37]
Cd (11 $\bar{2}0$)	Ar	5	13.58	[37]
PbTe (111)	Ar	0.5	1.4	[28]
GaAs (110)	Ar	0.5	0.9	[28]
GaP (111)	Ar	0.5	0.95	[28]
CdS (10 $\bar{1}0$)	Ar	0.5	1.12	[28]
SiC (0001)	Ar	0.5	0.41	[28]
InSb	Ar	0.5	0.55	[28]
TaC	Ar	0.6	0.13	[21]
Mo ₂ C	Ar	0.6	0.15	[21]

improbable that a positive ion generated at the target surface could escape the negative target field, so these are of little interest. Negative ions have been studied by SIMS to a lesser extent [44-53]. Negative ions result mainly from the sputtering of the anionic species of compounds [48-51] and high-electron-affinity constituents of alloys [53a,b]. Virtually no secondary negative ions are produced during inert gas ion bombardment of pure metal surfaces. Negative ions, like electrons, are accelerated away from the target toward the substrates, thus representing another source of substrate bombardment. Experimental evidence [54] shows that these ions actually arrive at the substrates as energetic neutrals, having suffered electron-stripping collisions in transit through the glow discharge.

3. Reflected Incident Particles

Some of the primary bombarding particles are reflected from the target surface. The literature of ion scattering spectroscopy (ISS) [55-62] contains most of the pertinent literature related to this effect. These reflected particles are neutralized and reflected as atoms, not ions. The amount of reflection is an inverse function of primary bombarding energy because this effect competes with ion implantation. As low primary energies, reflection fractions as high as 0.4 have been observed [56], whereas at high primary bombarding energies (>1000 eV) typical reflection fractions are of the order of 0.05. These particles represent still another source of substrate bombardment during film growth [43].

4. Desorption of Gases

Desorption of gases occurs even for very dense target materials. Initially, adsorbed gas layers on target surfaces are sputtered away, and then, depending on the nature of the target material, chemisorbed gases, occluded gases, and gases generated by decomposition of target compounds are released in that order [63-66]. For adsorbed gases there are marked peaks in the desorption rate at low energies (generally <200 eV) which have been attributed to local heating of the lattice in a radius of the order of 10 Å. Chemisorbed gases are truly sputtered [66]. It is these gases that usually leave the target initially as negative ions as noted above. Occluded gases are both sputtered and thermally desorbed. This is especially a problem with hot-pressed targets [67] and powder targets [68]. The effect of massive gas desorption from porous targets is to contaminate the sputtering gas and, hence, the deposited film. In addition, depending on the nature of the gas, it will have an effect on the film deposition rate (Section VIII.B).

C. Emission of Radiation

In this section, we consider the emission of radiation due to the sputtering process alone at the target surface—not to that contributed by the glow discharge.

1. Photons

Both ultraviolet (UV) and visible radiation are emitted from sputtering targets [69–76]. Sputtered metal and elemental semiconductor atoms leaving the target in an excited or ionized state undergo resonance- and Auger-type electronic transitions with subsequent photon emission characteristic of the metal being sputtered. Electronic transitions do not apply to compounds or glasses. In these cases the radiative process is simply due to the excited species of the sputtered atoms. Only semiquantitative data on this phenomenon have been reported, but the hierarchy of emission proceeds from low to high in the sequence: elemental targets, binary compounds, ternary compounds, etc., glasses. In the context of sputter deposition, this effect is mainly related to radiation damage to sensitive substrates by energetic UV photons. However, it has been used to advantage to monitor sputter deposition and etching rates (Section IV.C).

2. X rays

X rays characteristic of the target material are emitted from the target surface at energies up to that of the primary bombarding ions. These x rays also can damage surface-sensitive substrates. Also energetic secondary electrons originating at the target which arrive at substrates can generate x rays at the substrate surface. Tables of x-ray energies and excitation potentials [77] can sometimes be used to estimate the degree of damage that may be introduced by this effect.

D. Ion Implantation

Primary bombarding particles can embed into the target surface, become neutralized and trapped. A large body of literature exists on ion-surface interactions particularly those dealing with first-wall problems in fusion reactors. Even at relatively low bombarding energies [78–81] substantial implantation of the primary bombarding ions occurs (Fig. 2). When these ions lose their energy, they contribute to target heating and do not give rise to sputtering.

II-1. GLOW DISCHARGE SPUTTER DEPOSITION

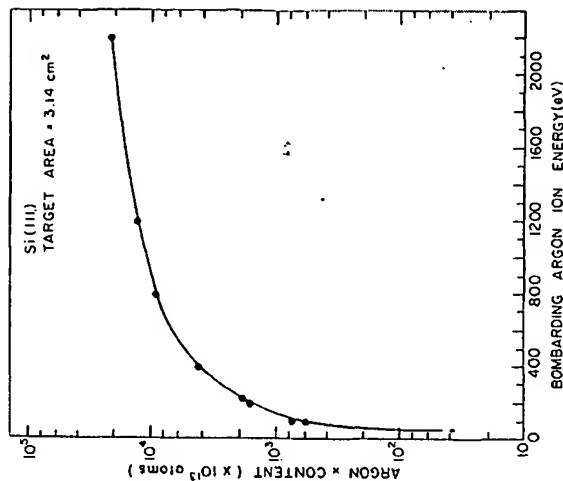


Fig. 2. Argon content of Si versus incident ion energy (after Comas and Carosella [78], with permission of The Electrochemical Society).

E. Altered Surface Layers and Diffusion

1. Multicomponent Targets

The bombardment of a multicomponent solid surface with ions or neutral atoms alters the chemical composition of the surface due to the difference in the sputter yield of the constituents [82]. The region of change is known as the altered layer. Upon initial bombardment of the surface the constituent with highest sputter yield is preferentially removed from the surface, enriching the surface layer in the lower sputter yield material until a steady state is reached. At steady state, the sputtered composition is that of the bulk target composition and the altered layer will recede uniformly with continued sputtering as long as the steady state conditions are maintained. Data on altered layers come from several areas: sputter deposition [83, 84], surface analysis [85, 86], and ion beam alteration of surface properties [86]. Empirical data were generated in attempts to quantify surface analysis techniques [86–91].

2. Yield

The surface composition alteration generally assumes yields of the components as in the elemental form [88], although it is has been shown [87] that some alloys have yields that are greater than those of either element by itself. For example, the yield of Cu from $\langle 100 \rangle$ Cu₃Au was found to be higher than from $\langle 100 \rangle$ single crystal Cu.

3. Steady State

The thickness of the altered layer has been explored in some detail for a variety of targets [83–85, 92–94]. Estimates for metal alloys have been a few tens of angstroms. For oxides the layer is much thicker (~ 1000 Å) [94].

4. Diffusion

Diffusion severely affects the altered layer thickness and the time to reach steady state. These can be due to ion-induced diffusion [87, 91, 94, 95], the ion mean range [93, 94], temperature driven surface diffusion [88], and enhanced diffusion due to the surface implantation of sputter-gas species [93, 95]. As noted in the previous section, surface diffusion will be affected by the phases present, grain size, and the nature of the species in the target. The temperature dependence of diffusion of the two phase Ag–Cu system was examined at 80 and 270°C [96]. Forty minutes sputtering time was required to reach steady state for the 80°C target while the 270°C target required about 200 min to reach steady state. In the 270°C experiment the target showed a definite reddish cast, the altered layer thickness was estimated to be about 1 μ m, and the films deposited were enriched in Ag. The difference in sputter yield ratios of Ni/Cu of 1.9 at room temperature [88] to that of 1.6 [96] at 300°C was attributed to diffusion in the target at 300°C.

5. Models

There have been numerous phenomenological models for the altered layer [83–85, 92, 93]. Due to the relationship between multicomponent sputter deposition and altered layer formation [96a] these will be considered in the section on multicomponent sputtering.

F. Dissociation Processes

1. Sublimation

Most of the energy of the incident ions at a sputtering target is transferred to the target surface as heat. When one or more of the target con-

stituents is volatile this can lead to sublimation from the target [97–99]. Even though the back surface of the target is directly cooled, substantial thermal gradients can arise with materials of low thermal diffusivity. This effect can lead to stoichiometric differences between the target and the deposited film. For fixed sputtering conditions, it is possible to compensate for this effect by purposely enriching the target in the volatile material [98].

2. Chemical Dissociation

Since most compounds have dissociation energies in the 10–100 eV range, it is not surprising that sputtering with keV ions results in chemical dissociation. Numerous studies in sputter-deposition systems have shown this by indirect [21, 97–104], but there is also a significant body of literature related to electron spectroscopy for chemical analysis (ESCA) that gives direct, quantitative evidence of this effect [105–107]. What is less obvious is the relationship between film stoichiometry and target bombarding potential. For example, in the case of binary oxide targets, films are, in general, less deficient in oxygen if the target potential is high than if it is low [11, 108–110]. This is because higher target potentials sputter more secondary oxygen ions that are accelerated toward the substrate where they can recombine to form the original compound. At low target potentials, these secondary ions have insufficient energy to survive the collisions encountered between the target and the substrate, and are lost to the vacuum pumps. If truly stoichiometric oxides, nitrides, sulfides, etc. are desired in the film, it is virtually always required to add O₂, N₂, H₂S, etc. to the sputtering gas to ensure stoichiometry by reactive sputtering. In some cases, sputtering with 100% reactive gas will still not result in stoichiometric films [100] because it is probable with weakly bonded compounds that reactive gas bombardment of the substrate will lead to preferential sputtering of the reactive gas rather than incorporation of it in a film [102, 106].

G. Chemical Sputtering

Chemical sputtering involves the reaction of an excited neutral or ionized gas with a surface to form volatile compounds [1, 111, 112]. This technique is mainly used for plasma treatment of organic surfaces and for etching in plasmas (Chapter V-2). However, it is sometimes a factor in film deposition [113]. When targets containing reactive anions (e.g., F⁻, Cl⁻) are sputtered, some of these anions are sputtered as secondary ions and accelerated toward the substrates where chemical etching reactions can occur. Etching of glass substrates, rather than film deposition, has

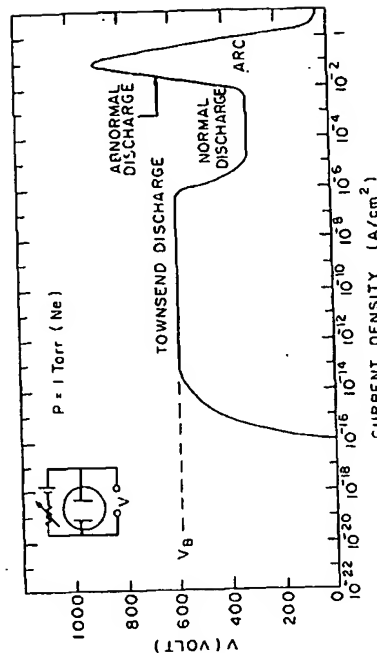


Fig. 3. The formation of a dc glow discharge.

the discharge. This region, the "abnormal glow," is the mode used in sputtering and virtually all other glow discharge processes. If the cathode is not cooled, when the current density reaches about 0.1 A/cm^2 , thermionic electrons are emitted in addition to secondary electrons, followed by a further avalanche. The output impedance of the power supply limits the voltage, and the low-voltage high-current arc discharge forms.

The foregoing represents a qualitative description of the various dc discharge modes. Several more quantitative reviews have appeared [114-117].

Crucial to the formation of an abnormal glow is the breakdown voltage V_B (Fig. 3). This voltage is mainly dependent upon the mean-free-path of secondary electrons and the distance between the anode and cathode. Each secondary electron must produce about 10-20 ions for the original avalanche to occur. If the gas pressure is too low or the cathode-anode separation too small, the secondaries cannot undergo a sufficient number of ionizing collisions before they strike the anode. If the pressure and/or separation are too large, ions generated in the gas are slowed by inelastic collisions so that they strike the cathode with insufficient energy to produce secondary electrons. This is a qualitative statement of Paschen's law which relates V_B to the product of gas pressure and electrode separation (Fig. 4). In most sputtering glow discharges, the pressure-separation product is well to the left of the minimum, thus requiring relatively high discharge starting voltages. In close-spaced electrode configurations it is often necessary to increase the gas pressure momentarily to start the discharge. Alternatively, an external ionizing source may be used (e.g., a Tesla coil connected into the chamber by a high-voltage feedthrough).

24 J. L. VOSSEN AND J. J. CUOMO
been observed during "sputter deposition" from targets of TbF_3 and TbCl_3 [113].

III. GLOW DISCHARGES

In this section, we give a brief account of glow discharge phenomena relevant to diode sputtering. The treatment of magnetron glow discharges is not included here; (see Chapters 11-2-11-4). The effects of these glow discharge phenomena on substrates are described in Section VII.

A. DC Glow Discharges

Figure 3 illustrates the manner in which a glow discharge is formed in a low-pressure gas with a high-impedance dc power supply. When a voltage is first applied, a very small current flows. This is due to the presence of a small number of ions and electrons resulting from a variety of sources (e.g., cosmic radiation). Initially, the current is nearly constant, because all of the charge present is moving. As the voltage is increased, sufficient energy is imparted to the charged particles so that they produce more charged particles by collisions with the electrodes (secondary electron emission) and with neutral gas atoms. As more charge is created the current increases steadily, but the voltage is limited by the output impedance of the power supply. This region is known as the Townsend discharge.

Eventually, an avalanche occurs. Ions strike the cathode, release secondary electrons which form more ions by collision with neutral gas atoms. These ions then return to cathode, produce more electrons that, in turn produce more ions. When the number of electrons generated is just sufficient to produce enough ions to regenerate the same number of electrons, the discharge is self-sustaining. The gas begins to glow, the voltage drops, and the current rises abruptly. At this point, the mode is called the "normal glow." Since the secondary electron emission ratio of most materials is of the order of 0.1, more than one ion must strike a given area of the cathode to produce another secondary electron. The bombardment of the cathode in the normal glow region self-adjusts in area to accomplish this. Initially, the bombardment is not uniform, but is concentrated near the edges of the cathode or at other irregularities on the surface. As more power is supplied, the bombardment increasingly covers the cathode surface until a nearly uniform current density is achieved. (This region of the glow discharge is used for voltage regulator tubes.)

After the bombardment covers the whole cathode surface, further increases in power produce both increased voltage and current density in

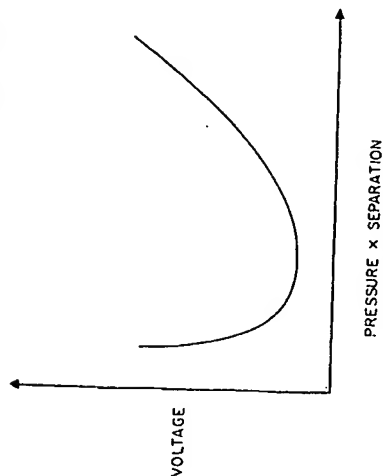


Fig. 4. Paschen's Law.

Figure 5 illustrates the luminous regions of a dc glow discharge, the voltage distribution, and the net space charge as a function of distance from cathode to anode. Adjacent to the cathode, there is a brilliant luminous layer known as the cathode glow. This is the region in which incoming discharge ions and positive ions produced at the cathode are neutralized by a variety of processes. This is also the region in which secondary electrons begin to accelerate away from the cathode. The light emitted is characteristic of both the cathode material and the incident ion.

Secondary electrons are repelled at high velocity from the cathode and start to make collisions with neutral gas atoms at a distance away from the cathode corresponding to their mean free path. This leaves a dark space which is very well defined. Since the electrons rapidly lose their energy by collisions, nearly all of the applied voltage appears across this dark space. The dark space is also the region in which positive ions are accelerated toward the cathode. Since the mobility of ions is very much less than that of electrons, the predominant species in the dark space are ions [118]. Acceleration of secondary electrons from the cathode results in ionizing collisions in the negative glow region.

The Faraday dark space and positive column are nearly field-free regions whose sole function is to connect electrically the negative glow to the anode. They are not at all essential to the operation of a glow discharge. In most sputtering systems, the anode is located in the negative glow and these other regions do not exist. The length of an unobstructed negative glow is exactly equal to the range of electrons that have been accelerated from the cathode [119]. When the negative glow is truncated,

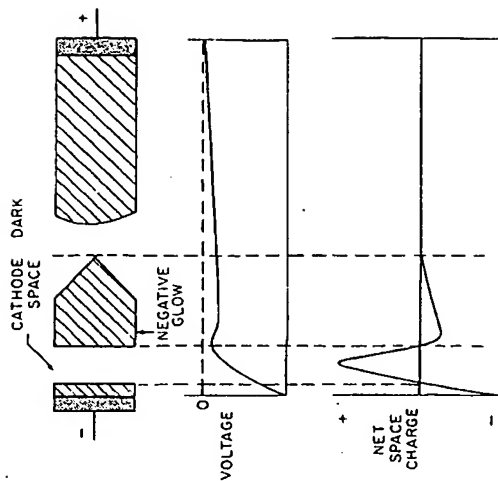


Fig. 5. Luminous regions, voltage and net space charge versus position in a dc glow discharge.

higher voltages must be applied to make up for the ions that would have been generated in the part of it that is blocked by the anode. In general, for uniform cathode bombardment, the anode should be located at least 3-4 times the thickness of the dark space away from the cathode. This distance, of course, is inversely related to gas pressure.

B. Low-Frequency AC Glow Discharges

Low-frequency ac glow discharges are not often used for sputtering. At frequencies up to about 50 kHz, ions are mobile enough so that there is ample time for a complete dc discharge to form on each electrode on each half-cycle. Thus, the discharge is basically the same as a dc discharge, except that both electrodes are alternatively cathode and anode (i.e., both are sputtered).

C. RF Glow Discharges

As the frequency of an applied ac signal is increased above 50 kHz, two important effects occur. First electrons oscillating in the glow space acquire sufficient energy to cause ionizing collisions, thus reducing the

dependence of the discharge on secondary electrons and lowering the breakdown voltage [120]. Second, the electrodes are no longer required to be electrical conductors since rf voltages can be coupled through any kind of impedance. Thus, it is literally possible to sputter anything. However, this does not imply that the films deposited will necessarily resemble the target (Section VII).

At typical rf frequencies used for sputtering (5–30 MHz), most ions are sufficiently immobile that one would expect negligible ion bombardment of the electrodes. In fact this is not the case. If one or both of the electrodes is coupled to the rf generator through a series capacitor, a pulsating, negative voltage will be developed on the electrode [121]. Owing to the difference in mobility between electrons and ions, the I - V characteristics of a glow discharge resemble those of a leaky rectifier (Fig. 6). Upon application of an rf voltage through the capacitor, a high initial electron current flows to the electrode. On the second half of the cycle, only a relatively small ion current can flow. Since no charge can be transferred through the capacitor, the voltage on the electrode surface must self-bias negatively until the net current (averaged over each cycle) is zero. This results in the pulsating negative potential shown in Fig. 6 [122]. The average dc value of this potential (V_d) is nearly equal to the peak voltage applied [123].

To obtain sputtering from only one electrode in an rf system, it has been shown [120] that the electrode which is to be the sputtering target must be an insulator or must be capacitively coupled to the rf generator and that the area of that electrode must be small compared to that of the directly coupled electrode. Also the ratio of the voltage between the glow space and the small capacitively coupled electrode (V_c) to the voltage between the glow space and the large directly coupled electrode (V_d) is

$$V_c/V_d = (A_d/A_c)^{1/2}, \quad (1)$$

where A_d and A_c are the areas of the directly and capacitively coupled electrodes, respectively. In practice, the directly coupled electrode is the system ground, including baseplates, walls, etc., and is quite large with respect to A_c . Thus, the average sheath potential (V_d) varies between the target electrode and ground as shown in Fig. 7. Clearly, to minimize bombardment of grounded fixtures, the area of all grounded parts should be very large by comparison to that of the target. We shall expand on this point further in Section VII.A.

Recently, Logan *et al.* [124] have described a total model for an rf sputtering system in which externally measured parameters can be put into a computer program to predict ionization levels, sputtering, material transport, and other bombardment effects in the system.

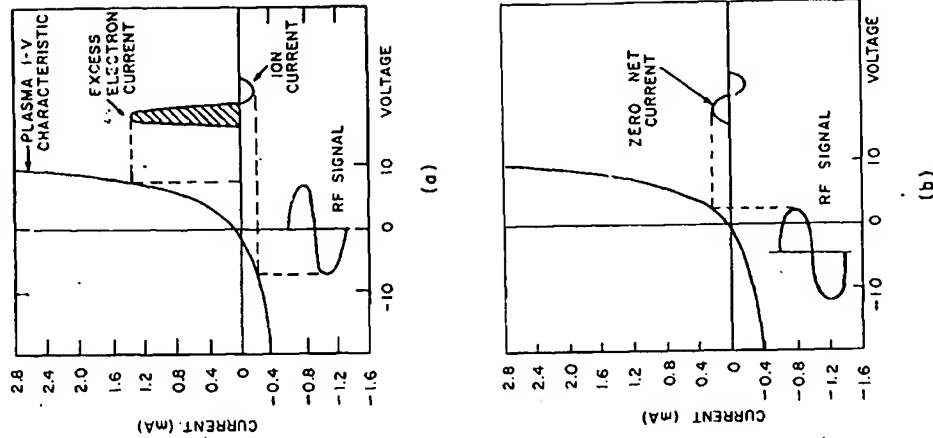


Fig. 6. The formation of a pulsating negative sheath on a capacitively coupled surface in an rf glow discharge (after Butler and Kino [121]).

D. Discharge Supporting Modes

Glow discharges are relatively inefficient ion sources. Only a few percent of the gas atoms in a glow discharge are ionized. Several techniques have been developed for increasing the ionization efficiency somewhat.

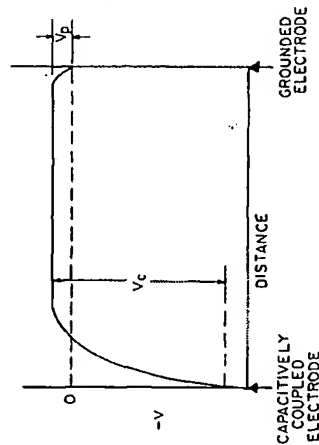


Fig. 7. Distribution of voltage in an rf glow discharge from a small, capacitively coupled electrode (target) to a large, directly coupled electrode.

These include axial and transverse magnetic fields, thermionic additions of electrons, and rf coils. The transverse magnetic field devices are described in Chapters II-2-II-4.

1. Axial Magnetic Field

A magnetic field normal to the target surface constrains secondary electrons to follow a helical, rather than straight-line path, the radius of which is given by

$$r = (mv \sin \theta) / eB, \quad (2)$$

where m is the electron mass, v the velocity, θ the angle of emission, e the electron charge, and B the magnetic flux density. The effect is to give electrons a longer path length for a fixed mean free path, thus increasing the probability of ionizing collisions before the electron reaches the anode. The magnetic field pinches the discharge in toward the center of the target, resulting in nonuniformity of film thickness. For relatively small targets (<20-cm diameter) the judicious use of low magnetic fields (10–50 G) can be used to improve uniformity by compensating for excessive edge bombardment (Section VII.F). For targets >20 cm in diameter, axial magnetic fields should be avoided.

2. Thermionic Support (Triode Sputtering)

In this technique, ions are generated in a low-voltage (~50 V), high-current (5–20 A) arc discharge between a thermionic filament and a main anode. The sputtering target is located in this main discharge and ions are extracted from it toward the target which can be powered either by a dc or

capacitively coupled rf source. This technique produces a very high ion density, allows operation at much lower pressures than a two-terminal glow discharge, and allows control of the target current density independent of the target voltage. However, it is not necessarily good practice to operate a sputtering system at low gas pressures (Section VI.A). The use of triode sputtering is mainly advantageous for sputter etching (Chapter V-2).

The main limitation of this technique is that it is difficult to scale up to very large sizes because of the difficulties involved in producing a large, uniform thermionic arc discharge. Numerous configurations have been described in the literature [125–132] and a complete analysis of such systems has been published by Tisone and co-workers [133–137].

3. RF Coil

Radio-frequency coils are sometimes employed in ion plating systems to increase the ionization efficiency at low gas pressure [138]. The evaporant passes through the coil in transit to substrates attached to a dc sputtering target. This increases the level of ionization of both the evaporant and the sputtering gas.

IV. EQUIPMENT CONFIGURATION

A. Target Assemblies

Electrodes to which the target material is attached and the counter electrodes to which substrates are attached have been designed in a variety of configurations [5, 9, 10, 16, 39, 97, 139–141]. For bias sputtering and ion plating, the counter electrode is a sputtering target assembly similar to the type used as deposition sources. There are four essential considerations in the design of target assemblies: heat dissipation, electrical isolation and contact, ground shielding, and materials of construction. A versatile assembly suitable for research is shown in Fig. 8. Several multitar- get arrangements have been described which are useful in sequential deposition of several materials (see, e.g., Cambey [141]).

1. Heat Dissipation

It is estimated [8, 9] that 1% of the energy incident on a target surface goes into ejection of sputtered particles, 75% into heating of the target, and the remainder is dissipated by secondary electrons that bombard and heat the substrates. The heat generated is usually removed by water cool-

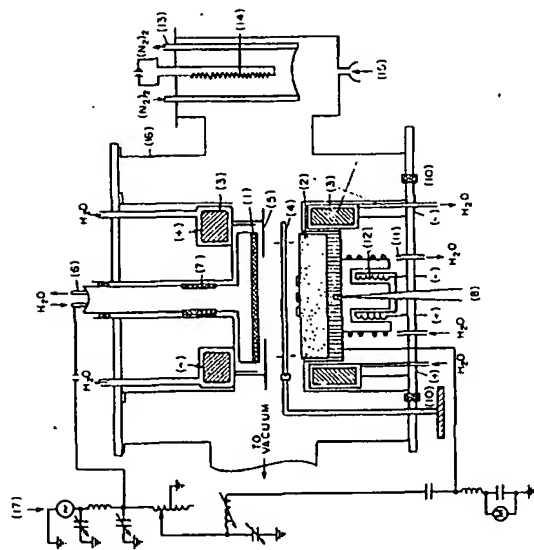


Fig. 8. Schematic of an rf sputtering apparatus. The components are listed as follows: (1) cathode target, (2) anode substrate holder, (3) cathode and anode magnets (water cooled), (4) shutter (SS), (5) cathode shield (SS), (6) cathode water cooling, (7) cathode isolation insulator, (8) substrate thermocouple, (9) substrates, (10) anode isolation insulator, (11) substrate cooling, (12) substrate heating, (13) liquid nitrogen cooled SS shroud, (14) T1 sublimation filaments, (15) sputter gas, (16) SS vacuum chamber, and (17) rf power supply matching network and substrate bias supply.

ing the backing plates to which the target or substrates are attached. Since targets are often soldered or epoxy bonded to the backing plates, the water-cooling channels should be designed so that water is forced through convolutions machined in the material. In this way, no hot spots can develop.

Substrates merely resting on a water-cooled plate are not in good thermal contact, and will be heated almost as much as if the plate were not cooled at all. In cases where substrate heating must be minimized, the substrates must be bonded to the cooled plate (Section IV.D) [142].

2. Electrical Isolation and Contacts

Isolation of the target assembly from grounded parts of the system usually involves a ceramic-to-metal seal with a sufficiently thick ceramic to minimize capacitive losses. Water lines must be isolated from ground by putting several meters of insulating tubing in series with both inlet and

outlet connections. Electrical connection from the power supply or matching network is made conveniently by bolting a strap to the water line on the back of the target assembly.

3. Ground Shields

To prevent sputtering of the target assembly itself, a ground shield is contoured around all surfaces at a distance less than that of the cathode dark space. In some cases, shields are placed over the outer rim of the target surface (e.g., to prevent clamping screws from sputtering). In these cases, focusing effects near the ground shield result in excessive erosion of the target [9].

4. Materials of Construction

Many materials have been used to construct sputtering target assemblies, the most common being stainless steel and copper. Stainless steel is highly corrosion resistant, but has very poor thermal conductivity. Copper usually must be gold plated for corrosion protection and is difficult to machine, but it is a good choice. Aluminum, unless it is perfectly protected from corrosion in the presence of water, is a very poor choice.

B. Power Supplies

1. DC

There are many requirements imposed on power supplies used for glow discharge sputtering. The output rating is determined by the size of the target and should be capable of delivering up to 10 W/cm^2 at voltages up to about 5 kV. (Note that this does not apply to magnetron sputtering which generally requires higher output power and current but lower voltage. See Chapters II-2, II-3, and II-5.) The actual power drawn from the supply depends on the process operating parameters (voltage, gas, and gas pressure) and on the secondary electron yield of the target surface. For most metals, the secondary electron yield is initially high and then decreases as surface oxides and other contaminants are sputtered away. Insulating surface contaminants give rise to arcing due to local dielectric breakdown. The power supply must be capable of withstanding these arcs without shutting down, but must be able to distinguish between these small arcs and catastrophic ones such as may happen if a flake of metal shorts the target to ground.

For relatively small targets (up to about 300 cm^2), the most commonly used type of dc supply involves an autotransformer-controlled high-volt-

age transformer that is magnetically shunted followed by a full-wave bridge rectifier. No smoothing filters are employed, but rf chokes should be used in series with the output to prevent high-frequency spikes (due to arcing) from damaging the bridge rectifier. Magnetic shunting of the power transformer leads to a high output impedance. In the event of a serious arc, the short circuit output current is limited by circulating the current in the transformer and the output voltage drops to zero [143]. This type of supply is limited in that the maximum usable voltage decreases rapidly as the rated output current is approached (Fig. 9).

For larger targets, saturable reactor power supplies are preferred because these are tolerant of arcs, even when operated with very high output currents [143]. They are, however, unstable when the output load is small (Fig. 10).

2. Low-Frequency AC

Power line frequencies are generally used only in processes in which both sides of a substrate are to be coated simultaneously by two targets facing each other. The power supply problems are basically the same as those with dc, except that no rectifiers are used and it is not necessary to use rf chokes in the output circuit.

3. RF (Crystal Controlled)

Most rf generators used for sputtering are crystal controlled to one of the "Industrial, Scientific, and Medical Equipment" (ISM) frequencies allotted by international agreement for unlimited radiation [144]. The fre-

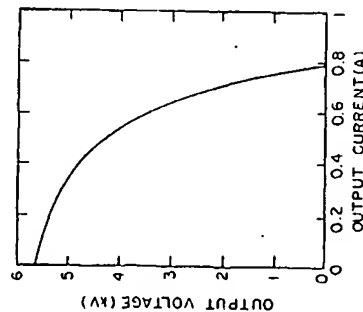


Fig. 9. Typical maximum output voltage and current for a magnetically shunted dc power supply rated at 2 kW.

II-1. GLOW DISCHARGE SPUTTER DEPOSITION

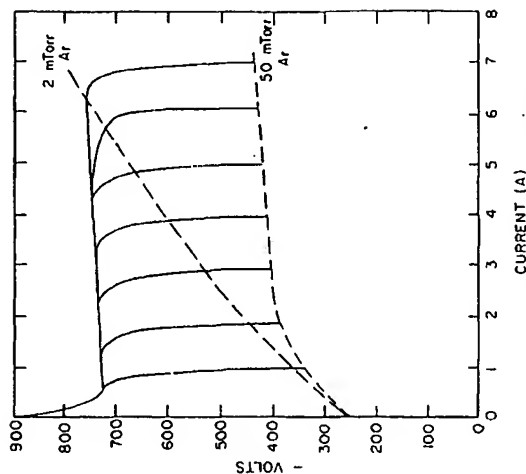


Fig. 10. Typical operating characteristics of a saturable-reactor dc power supply.

quencies and their tolerances most often used are 13.56 ± 0.00678 , 27.12 ± 0.0160 , and 40.68 ± 0.020 MHz.

Since the output impedance of these generators must be held constant (usually 50 Ω), and since the glow discharge impedance is much higher than this, a matching network must be situated physically close to the target assembly. A typical matching network for a single-ended sputtering system includes a variable-shunt capacitor, a variable-series capacitor, and a fixed inductor. The design of such matching networks are the same as for antenna matching to transmitters [145]. When bias sputtering is contemplated, the situation is more complex. Several manual and automatic circuits have been described for splitting the rf power from a single supply to control voltages and phase at two interacting targets in the same glow discharge [124, 146-151]. In some cases, the substrate target is directly driven, while in others substrate power is coupled through the discharge either by substrate tuning (i.e., inserting a matching network between the substrate target and ground) or by adjusting the system geometry and glow discharge to produce a high plasma potential (Section VII.A).

To prevent damage to the power supply (e.g., during an arc), the

power output tubes should be triodes rather than pentodes or tetrodes so that reflected power appears on the plate rather than the grids of the tubes.

4. RF (Self-Excited)

While crystal-controlled rf generators are most commonly used, variable-frequency, self-excited oscillators have advantages in some applications and have been used extensively [97, 152–157]. For output power up to about 1.5 kW, the usual circuit is a Hartley class-C oscillator. For higher power and/or for bias sputtering, in which the rf power must be split between the deposition and substrate targets, push–pull circuits are preferred. The output circuit is usually transformer coupled, and tuning is accomplished by varying the frequency with a capacitor across the primary of the transformer. If the output circuit is slightly over-critically coupled, one observes a very broad, flat-topped tuning peak as compared to the very high- Q output of crystal-controlled oscillators [157]. As a result of this, these generators are much more tolerant of arcs and other disturbances in the glow discharge. For bias sputtering, the secondary of the transformer is center tapped to ground and a series capacitor is inserted in both target legs. These capacitors act as voltage dividers and can vary the two target voltages independently and in a very smooth fashion. The major disadvantage of self-excited oscillators relates to the fact that their output impedance is quite high. Thus, flexible coaxial cables cannot be used to make electrical connection. Instead the generator must be physically close to the target(s) and connections must be made using rigid, air-dielectric coaxial pipes or some other kind of high-impedance connection, which often complicates the mechanical design of the system. As with all kinds of rf equipment, precautions such as shielding, power line filters, etc., should be taken to minimize radio frequency interference.

C. Instrumentation and Control

Depending on the application, one must be able to monitor voltage, current (dc), power (rf), and sputtering gas pressure. In rf glow discharges it is often useful to measure both the average dc self-bias voltage, the peak-to-peak voltage, the waveform, and the phase angle. Pressure measurements can be especially difficult. Thermocouple, Pirani, and high-pressure ion gauges can sometimes be used, but they are easily contaminated by reactive gases (leading to erroneous readings and drift), are not tolerant of rf fields if the output impedance of the sensing head is high, and are difficult to use when gas mixtures are employed (e.g., in reactive sput-

tering). The most suitable gauges for critical work are low-impedance capacitance manometers with temperature-controlled heads [158]. The membranes in these gauge heads suffer from mechanical hysteresis if they must be cycled from atmosphere to vacuum frequently, so it is advisable to include a shutoff valve between the head and the vacuum chamber to keep them under vacuum at all times.

Many processes are affected by gas flow throughput, which determines how fast impurities are flushed out of the system. In such cases, mass-flow meters should be included in the gas feed supply.

Langmuir probes are especially helpful in calibrating a system to determine plasma and floating potentials (Section VII.A), but they perturb and contaminate the discharge [159] so they should not be used for *in situ* monitoring.

Temperature measurements of anything in a vacuum system are difficult at best. If properly attached and of sufficiently low thermal mass, thermocouples or thermistors can be used [160], but they can also contaminate the system, and the pyrometer or potentiometer must be isolated from ground. Infrared pyrometers are quite useful [161]. Their main advantage is that no material must contact the substrates. However, they must be carefully calibrated for optical losses in the light path (windows, etc.), infrared emission from the glow discharge, and the emissivity of the coated and uncoated substrate surface.

If a given sputtering process is stable and relatively slow, deposition rates can be monitored by controlling conditions and deposition time. In-vacuum monitors (e.g., quartz microbalance) simply do not work because resputtering processes are different on the head than on substrates. Also, they are intolerant of rf fields (high impedance). The most successful techniques for rate monitoring have been optical emission and absorption spectroscopies [162–168], but they must be independently calibrated. These same spectroscopies along with mass spectroscopy are also useful for diagnosing glow discharge species of all kinds (ions, neutrals, molecular fragments, etc.) [169–181]. These techniques are especially useful in reactive sputtering.

D. Substrate Heaters

Given the fact that there is heat input to substrates from the glow discharge, control of substrate temperatures above ambient can be quite difficult. Both resistance (Fig. 8) and radiant heating (Fig. 11) have been used. The resistance heater is relatively massive and has a relatively slow thermal response time. The radiant heater can be used either to heat substrates in the holder shown directly or to heat a solid plate which has a

thermocouple embedded in it. Because of its machinability, high-thermal conductivity and resistance to warping, molybdenum is the preferred material of construction for the heated surface (plate or substrate holder). When rf is used, a decoupling network must be employed to prevent rf interference with the thermocouple controls and heat-input circuits (Fig. 11c).

As with substrate cooling, it is essential to make a good thermal contact between the substrate and heated holder. Ga or In-Ga eutectic can be used up to about 450°C if the substrate holder is made of molybdenum. At higher temperatures there are reactions of Ga or In-Ga with Mo. The Ga or In-Ga is best used at a temperature at which it is molten. Upon solidification the thermal mismatch between it, the substrate and substrate holder sometimes can crack the substrate or break the bond. For lower temperatures a thermally conductive grease has been employed which is a mixture of alumina powder and high vacuum grease [142].

E. Wall Losses

"Wall losses" is a generic term for any material body in a glow discharge which can act as a point of neutralization for ions. Ions cannot be neutralized in the gas phase because there is no mechanism which can dissipate the heat of the neutralization to conserve both momentum and energy. This can only happen at a surface. Thus, to obtain a uniform ion density across a target surface, all extraneous solid objects (e.g., vacuum chamber walls, support posts, etc.) should be kept well away from the target edges. How far away is far enough depends inversely upon the glow discharge gas pressure. For typical gas pressures (5–50 mTorr) a safe distance is about 10 cm.

F. Shields and Shutters

Dark-space shields around targets and shutters used for preconditioning targets and/or substrates are necessary objects which must be near the target. To minimize their effect on ion neutralization, they should be made as symmetric as possible with respect to the target. As will be shown in Section V.D, the materials from which shields and shutters are constructed are also important to avoid contamination of targets and/or films.

G. Deposition Sources for Bias Sputtering and Ion Plating

Bias sputtering or ion plating are film deposition processes in which substrates are ion bombarded (sputter etched) prior to and/or during dep-

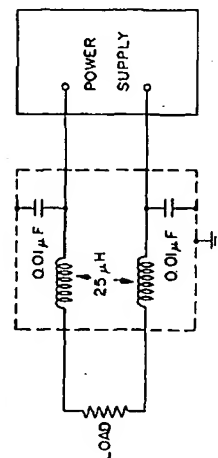
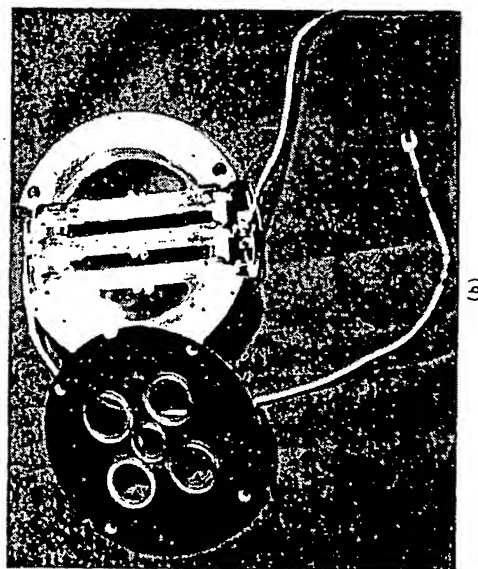
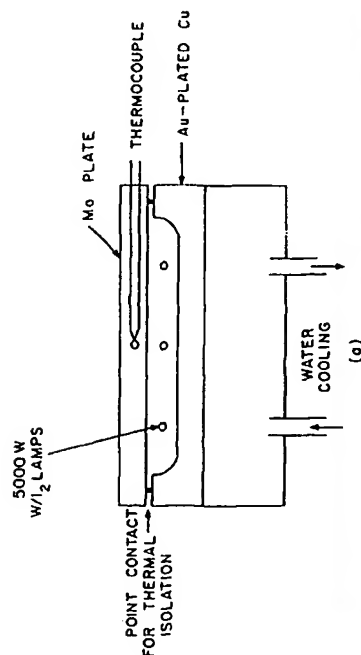


Fig. 11. Radiant substrate heater. (a) Cross section, (b) photograph, (c) rf decoupling network (courtesy of Silano and Leary [142]).

osition from a vapor source. Thus, the substrate holder is a sputtering target assembly which is usually the same type of assembly as a deposition target. However, depending upon the vapor source used, modifications to the substrate target assembly may be required. Vapor sources that can be used include dc or rf sputtering targets, magnetron sputtering targets of all types, resistance-heated filament, rf-heated or electron-beam evaporation sources, or gaseous reagents of the type normally used for chemical vapor deposition. Problems arise mainly with those vapor sources that require that the substrate target be up and the vapor source down in the system. When the reverse is true, the substrates merely rest on an appropriate backing plate, but if the substrates have to be supported against gravity, the substrate holders become a major problem because of contamination (Section V.D), and the nonuniform bombardment that occurs near sharp edges due to fringing fields. This is mainly a problem with thermal evaporation vapor sources in which the molten evaporant must be contained (as, e.g., in the hearth of an electron beam gun). Numerous inverted target assemblies for holding various kinds of substrates have been reported [182-187], all of which probably suffer from these problems to some extent.

H. Scale-Up Problems

Scaling up any deposition process from small laboratory equipment to large production is a very major problem. There are several examples in the literature [188-198a] of laboratory to production scale ups that range from larger bell jars to very large continuous machines. It is almost axiomatic to state that each production application must be treated as a special case, so it would be futile to present a detailed discussion of such systems here.

Most of the problems with large systems arise if they are not designed around the process. That is, if the deposition process is subordinated to a mechanical design, pumping considerations, etc., the process inevitably suffers. The major process-related factor in large sputtering systems is sputtering gas uniformity across large target surfaces to maintain uniform levels of target ion bombardment. Because of implantation of gases into the target and, in some cases, getting of sputtering gas by the target and/or growing films (e.g., in reactive sputtering), sputtering systems must be considered as vacuum pumps. In general, the sputtering gas must be introduced in several locations, and the main vacuum pumps must be located sufficiently far from the active sputtering region that uniform gas flow across large target surfaces is achieved. Particular attention must also be paid to other effects described earlier (wall losses, target shield-

ing, etc.). Systems intended for long operation between cleaning of fixtures must be carefully designed to assure that buildup of film material on system parts will not result in short circuits, arcs (due to flaking material), or jamming of moving parts (e.g., substrate carriers).

It is especially helpful if sputtering targets can be built into one of the walls of vacuum chamber, so that electrical and water-cooling connections can be made at atmospheric pressure. Otherwise one must face the formidable task of ensuring that high-voltage leads and water lines inside the vacuum chamber do not become part of the glow discharge.

V. PRECONDITIONING OF TARGETS, SUBSTRATES, AND SYSTEMS FOR FILM DEPOSITION

As a general rule, the best way to prepare a system for sputter deposition is to run the system first without substrates in exactly the way in which it will be run during the deposition. A preconditioning run of this sort may have one or more of several beneficial effects: (1) the target altered surface layer is established, (2) fixtures are outgassed by bombardment, and (3) fixtures are coated with the material to be deposited, minimizing subsequent contamination.

A. Target Materials

While it is possible to use virtually any kind of material as a sputtering target, for high purity work very dense targets are preferred. Sputtering can and has been done successfully from sintered, hot-pressed, powder, and liquid targets, but the highest purity work has been done with very dense targets (e.g., vacuum-cast or arc-melted materials). Hot-pressed and powder targets have been shown to be nearly limitless sources of gaseous contamination [67]. The major contaminant appears to be oxygen sorbed onto the raw powder surface prior to hot pressing. For oxides this is not a problem, but it can be severe for other materials depending upon the intended application and the tolerance of the desired film properties to oxygen contamination. Even getter sputtering cannot eliminate gaseous contaminants from films if they originate in the target because a large fraction of the contaminant is sputtered as negative ions, accelerated toward the substrate, and implanted in the growing film.

Targets are usually bonded to some kind of water-cooled backing plate. Target bonding must be done with great care to avoid contamination from the bonding material and/or failure of the bond due to nonuniformity and thermal fatigue. In general, epoxy bonds are not recom-

mended because of their poor thermal transfer properties and brittleness. Epoxy bonds usually lead to large amounts of organic contamination. Solder bonds with appropriate plating layers on the back of the target and the front of the backing plate are generally preferred [199].

B. Presputtering of Targets

Presputtering of targets is done to clean and equilibrate target surfaces prior to film deposition with a shutter usually located close to the substrates. For pure metal targets surface oxides are removed, the target surface is brought to thermal equilibrium, and the system is outgassed. The discharge current can be used as a monitor to determine when the system is equilibrated [200]. Initially, oxides with high secondary electron emission ratio are sputtered and background gaseous contaminants (especially H_2O) are being broken down, leading to high discharge current which gradually decreases as the contaminants are removed from the system and/or covered up with film material. When the discharge current falls to a constant value, presputtering can be terminated. Alternatively, glow discharge optical spectroscopy or mass spectroscopy can be used to determine the endpoint (Section IV.C).

When alloy or compound targets are used, one must establish the altered surface layer in addition to the phenomena noted above. The amount of time needed for this must be established empirically. Since there will be inevitably some resputtering of material deposited onto the shutter and subsequent return of some of this material to the target, the shutter must be kept at the same potential as that which the substrate will have when the shutter is removed. This means that shutters should not be grounded, and in some cases they should be biased. If this is not done, there will be a transient in resputtering as the shutter is removed which can change the composition of the first few monolayers of the film [83]. In general, all discharge conditions (voltages, pressure, etc.) should be the same as those used during the subsequent deposition.

C. Sputter Etching of Substrates

Practical methods for cleaning substrates prior to film deposition have been reviewed by Mattox [201, 202]. In this section, we shall restrict our discussion to sputter etching of substrates prior to film deposition, and assume that gross surface contaminants have been removed chemically or otherwise prior to putting the substrates into the vacuum chamber. If it is

not done properly, sputter etching can actually produce more surface contamination than was originally present on the substrate.

With glow discharge sputter etching, it is rarely possible to obtain an atomically clean substrate surface. In general, this is only possible in an ultrahigh vacuum system using ion beams followed by high-temperature annealing [203–208].

The first problem in glow discharge sputter etching relates to organic contamination. This may be on the surface as it is put into the vacuum chamber or may be adsorbed into the surface (e.g., from backstreaming vacuum pump fluids). In either case inert gas ion bombardment will polymerize the organic material [209] and render it very difficult to remove [21].

In most cases organic contaminants can be removed by chemical sputtering in O_2 [111, 112, 210]. Clearly, this will not be adequate if there is continuous backstreaming of pump fluids. If the contaminant is a silicone, this will leave a residue of SiO_2 . If the substrate is a metal, the O_2 discharge may oxidize the surface [211]. In both cases, a subsequent sputter-etch step in Ar can be used to remove these oxides.

The next problem that must be addressed is backscattering of material emitted from the target surface [11, 21, 200, 212–219]. When the substrate surface is heterogeneous (e.g., an integrated circuit consisting of Si and SiO_2 areas) and/or when the substrate rests upon a target backing plate of a material that is different from that of the substrate, some fraction of all the materials sputtered are returned to the target, forming a new composite surface consisting of all the bombarded materials. Some of the material is returned by simple collisions in the gas phase, and some is returned by being resputtered from the shutter after condensing there. The latter can be largely eliminated by using a "catcher" [213] such as that shown in Fig. 12. The former can only be minimized, but not eliminated in glow discharge sputtering [212]. The amount of material returned to the target and substrates is directly proportional to the sputtering gas pressure and the axial magnetic field applied (if any), and inversely proportional to the target voltage and to the sputtering yield of the materials involved [11, 212, 219]. Even at the lowest gas pressures at which a glow

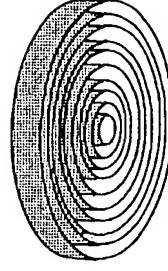


Fig. 12. Catcher (after Maissel *et al.* [213]; copy-right 1972 by International Business Machines Corporation, reprinted with permission).

discharge can operate, monolayer quantities of backscattered material are found. Radio-frequency target excitation is much more efficient in minimizing backscattering than is dc, but sputter-etch voltages of 2 kV or more must be used [200, 219]. Reactive gases similar to those used for plasma etching, reactive ion etching, etc. have been shown to produce exceptionally clean substrate surfaces, even at relatively high gas pressures and low rf voltages [220]. For example, various refractory alloys have been cleaned successfully in Ar-HCl mixtures, but cleaning in Ar-CCl₄ resulted in C deposits on the substrates. With the Ar-HCl mixtures there may have been some Cl residue remaining after etching.

In some cases, it is desirable to enhance this effect to preform an interface during sputter etching prior to film deposition. For example, ohmic contacts to Si devices have been improved by sputter etching the Si substrate with a Pt backing plate to produce PtSi in the contact regions [221]. This effect has also been used to advantage in forming graded interfacial layers to promote adhesion of the subsequently deposited film [222]. It should be noted, however, that graded interfaces are sometimes detrimental to adhesion [223]. When it is desirable to eliminate this effect, it is necessary to use backing plates made of the same material as the substrate [212]. In the case of oxide dielectric substrates, it has been shown [224] that even this approach is not effective. Sodium ions (a typical contaminant) were found to migrate down from glass and SiO₂ surfaces rather than be sputter etched away. Similar effects have been observed in other systems [225].

The structure and chemistry of single crystal Si surfaces after backscattering have been studied in detail using a variety of surface analytic techniques [214, 226, 227]. In addition to backscattered material, significant amounts of Ar were found in the substrate surfaces (2–20 at. %, depending on the bombardment potential), and crystallographic damage was propagated to a depth of 40–110 Å as the sputter-etch voltage increased from 0.5–2.5 kV. The amounts of damage produced and gas incorporated increase with increasing substrate temperature [227].

In some cases, conelike features have been observed on sputter-etched surfaces subject to backscattering [11, 111, 218], or when the substrates contain certain bulk contaminants [228]. An example is shown in Fig. 13. This effect is due to the fact that the sputtering yield of the backscattered metal or other contaminant is lower than that of the substrate or matrix. Thus, the islands of backscattered material or contaminant, act as local etch masks. Once such structures are formed, the sputter-etch rate of the surface drops markedly for geometric reasons [11, 111, 229]. In selected cases, it is possible to add reactive gases that depress the backscat-

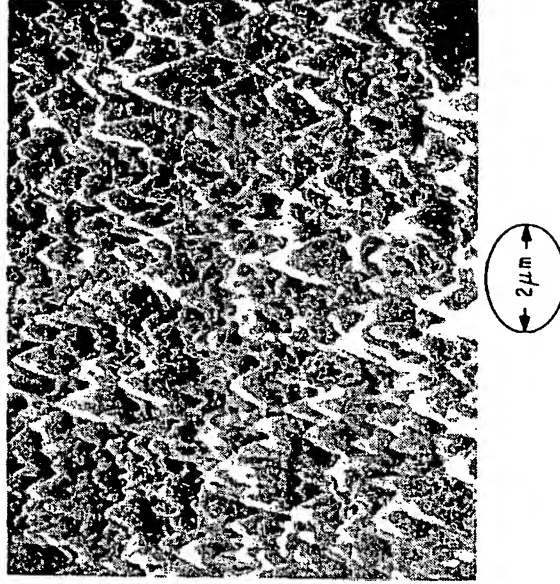


Fig. 13. Cones produced on a Si surface sputtered in contact with a Pd backing plate.

tering rate to reduce this effect [218]. The cones continue to sharpen as sputter etching proceeds [230–246]. It should also be noted that such cones can form due to initial microtopography of a substrate surface in the absence of impurities [230–246]. Structures of this sort are not always undesirable (e.g., similar structures prepared by CVD have been used as solar absorbers) [247, 248]. Still another effect occurs if the substrates are nonplanar. Since the angular distribution of material emitted from sputtered surfaces at low voltage is under cosine (i.e., there is more sidewise than normal emission), some of the sputtered material will be deposited on substrate irregularities, and become more difficult to remove from these surfaces as the irregularity becomes more vertical. While this is considered a nuisance when clean surfaces are the desired result [217, 249–251], this effect been put to beneficial use in the coating of the inside walls of through holes in substrates [252], and in enabling one to cover severe substrate topographic features by bias sputtering.

In general, all of these effects and their implications to film-substrate interfaces must be considered carefully in the design of a process involving sputter etching prior to film deposition.

VI. THE SPUTTERING GAS

A. Effects of Gas Species, Pressure, and Flow

The effects of increasing sputtering gas pressure are to increase discharge current, increase backscattering, and to slow energetic particles by inelastic collisions. The first two effects compete and largely determine deposition rates (Section VIII.B). The third effect can be used to maximize or minimize the energy of particles incident on substrates.

In general, it is desirable to use the highest possible gas flow so that impurities are constantly swept out of the sputtering chamber. Numerous workers have found that this improves the properties of thin films (e.g., Fraser and Cook [253]). This implies that the pumping system used must be operated to obtain maximum pumping speed for the gases used.

One must also be careful to ensure that no pressure gradients occur in the vicinity of the sputtering targets. Otherwise such gradients produce nonuniform bombardment and film deposition. Local pressure gradients can occur at the target surface (because of gettering), near the pumping port, or at points of high or low temperature relative to the rest of the system (e.g., near vacuum gauges with hot elements, titanium sublimation pumps, or Meissner traps). To offset these problems it is often necessary to introduce the gas at more than one point in the system. This is especially a problem in reactive sputtering and in very large systems.

As noted in Section II.A, the nature of the sputtering gas largely de-

Table IV

Metastable Neutral Energies and Lifetimes

Species	Metastable energy (eV)	Lifetime (sec)
H	10.20	0.12
H ₂	11.86	Long
He	19.82	Very long
He	20.61	Long
N	2.38	6×10^4
N	3.58	13
N ₂	6.16	0.9
N ₂	8.54	1.7×10^{-4}
O	1.97	110
O	4.17	0.78
O ₂	0.98	Very long
Ne	16.62, 16.71	Long
Ar	11.55, 11.72	Long
Kr	9.91, 9.99	—
Xe	8.31, 8.44	—

11-1. GLOW DISCHARGE SPUTTER DEPOSITION

termines the sputtering yield, and hence, the deposition rate. In addition to that, excited metastable neutrals of the sputtering gas are formed by collisions of electrons with ground-state gas atoms. The potentials required to raise some common sputtering gases from the ground state to the lowest excited state along with the lifetimes of the excited states are given in Table IV [254, 255]. It is well established [172] that sputtered neutral atoms can be ionized by the Penning mechanism (the collision of a metastable neutral with a ground-state neutral to produce an ion and return the metastable neutral to the ground state) when the first ionization potential of the sputtered atom is less than that of the metastable energy. Since the metastable energies of the noble gases are greater than the first ionization potential of most elements, this mechanism can produce a copious supply of ions which can bombard substrate surfaces and/or return to the target to cause self sputtering [212]. It is possible that some sputtered atoms can be doubly ionized by this process [256]. The amount of Penning ionization that occurs increases with increasing gas pressure.

B. Sources of Gas Contamination

The major sources of gaseous impurities in sputtering systems are residual gases (mainly H₂O) left after initial pumpout, wall desorption due to bombardment, the surface of the target (gases adsorbed when the system is vented), occluded gases in the sputtering target, backstreaming of pump fluids, leaks (real or virtual), and impurities in the gas supply itself. Many of these can be eliminated by a combination of good vacuum practice and extensive presputtering before film deposition. For example, to minimize condensation onto the target surface during venting, the cooling water should be shut off or hot water should be valved into the cooling lines to keep the target a few degrees above room temperature. Reactive impurities in inert gas sources can be reduced by passing the gas through hot Ti sponge before introducing it into the process chamber. If the pumping system must be throttled, it is preferable to put the cold trap on the chamber side of the throttling valve so that condensable gases (e.g., H₂O) can be pumped at full efficiency [257].

C. Getter Sputtering

Getter sputtering is a technique sometimes used to reduce the amount of background contamination in the vicinity of sputtering targets and substrates [257a-262]. This technique involves enclosing the target-substrate region of the vacuum system with a rather close-fitting, cooled cylinder. With a shutter closed, the target is presputtered extensively. Films

deposited onto the cylindrical enclosure and the shutter getter reactive gases and bury them; and the cylindrical enclosure acts as a conductance-limiting baffle, retarding the entry of more contaminating gases into the active region of the discharge. After all of the reactive gases are getterred, the shutter is opened and deposition proceeds.

This procedure does not eliminate inert gas incorporation in films, but does eliminate most reactive gas incorporation. The main disadvantage of this technique is that the cylindrical enclosure acts as "wall," giving rise to wall losses and excessive nonuniformity in film deposition near the target edges. If the target itself contains dissolved or occluded reactive gases in the bulk, these gases will still be incorporated into the films because they will be sputtered as negative ions and accelerated toward the substrate.

A variant of getter sputtering has been described [263], in which the solid cylindrical container is replaced by a reactive gas (e.g., SiH_4), which decomposes in the diffuse discharge region surrounding the sputtering target. The cation of the reactive gas (e.g., Si) is capable of chemically gettering reactive gases if its free energy of formation of compounds with the reactive gases is more negative than that of the target material. This eliminates the wall problem, but the reactive gas must be introduced far enough from the substrate to exclude the possibility that some of the cations of the gas are incorporated into the growing film.

Films have been numerous theoretical treatments and reviews of reactive sputtering processes [264-274]. For purposes of discussion, this topic should be subdivided. In one form of reactive sputtering, the target is a nominally pure metal, alloy, or mixture of species which one desires to synthesize into a compound by sputtering in a pure reactive gas or an inert gas-reactive gas mixture. The reactive gas either is, or contains the ingredient required to synthesize the desired compound. The second type of reactive sputtering involves a compound target that chemically decomposes substantially during inert gas ion bombardment, resulting in a film deficient in one or more constituents of the target. In this case, a reactive gas is added to make up for the lost constituent. The main difference between these two types of reactive sputtering has to do with the deposition rate dependence on partial pressure of the reactive gas.

A large number of reactive gases have been used to synthesize compounds from metal targets or to maintain stoichiometry in the face of decomposition: Air, O_2 , or H_2O (oxides), N_2 or NH_3 (nitrides), O_2 + N_2 (oxynitrides), H_2S (sulfides), C_2H_2 or CH_4 (carbides), SiH_4 (silicides), HF or

CF_4 (fluorides). As (arsenides), etc. There are obvious safety problems with some of these gases.

The question of where compounds are synthesized (at the target, in the gas, or at the substrate) is central to an understanding of reactive sputtering [264]. Reactions in the gas phase can for the most part be ruled out for much the same reasons that ions cannot be neutralized in the gas phase. The heat liberated in the chemical reaction cannot be dissipated in a two body collision. Simultaneous conservation of energy and momentum requires the reaction to occur at a surface—either the target or the substrate. At very low reactive gas partial pressure and high target sputtering rate, it is well established that virtually all of the compound synthesis occurs at the substrate and that the stoichiometry of the film depends on the relative rates of arrival at the substrate of metal vapor and reactive gas. Under these conditions, the rate of removal and/or decomposition of compounds at the target surface is far faster than the rate of compound formation at the target surface. However, as the reactive gas partial pressure is increased and/or the target sputtering rate is decreased, a threshold is reached at which the rate of target-compound formation exceeds the removal rate of compounds. For metal targets, this threshold is usually accompanied by a sharp decrease in the sputtering rate. This decrease is due partly to the fact that compounds have generally lower sputtering rates than metals and partly that compounds have higher secondary-electron emission yields than metals. As a result, more of the energy

current automatically decreases the target voltage for a fixed power setting. A third cause of the drop in sputtering rate is simply due to less efficient sputtering by reactive gas ions than by inert gas ions.

The net effect of all of this is illustrated in Fig. 14. If instead of main-

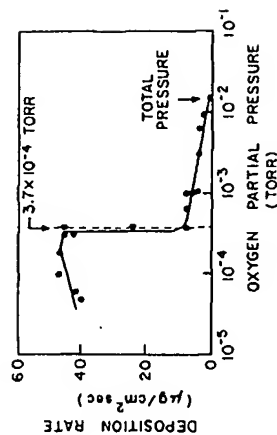


Fig. 14. Deposition rate versus oxygen partial pressure for an iron target in an Ar- O_2 mixture (after Heller [269]).

taining constant power one maintains constant voltage, the abrupt decrease in rate is smoothed out considerably. Likewise, for compound targets there is a much more gradual decrease in sputtering rate with increasing partial pressure of reactive gas which is mainly related to the less efficient sputtering ion concentration.

Clearly, the critical partial pressure depends not only on the glow discharge conditions, but on the kinetics of compound formation of the target surface itself. For example, target materials that do not oxidize readily do not show abrupt rate decrease as oxygen partial pressure increases.

It is impossible for us to review in detail all of the reactive sputtering processes that have been described in the literature. Instead, we present a bibliography of reactive sputtering and reactive ion plating processes in Table V. This table includes only processes in which the target (or evaporant in reactive ion plating) is a metal, and the desired compounds are wholly synthesized in the deposition process. Reactive sputtering of compounds to maintain stoichiometry is not included. The table is organized alphabetically by source material with elemental sources first, then binary sources, ternary sources, etc. For multielement sources, the elements are listed according to their abundance in the source.

VII. DEPOSITION WITH SIMULTANEOUS ION

BOMBARDMENT OF THE SUBSTRATE AND GROWING FILM

A. Plasma, Floating, and Bias Potentials

The true potentials on substrates in glow discharge sputtering have been studied extensively [124, 147, 454-459]. The luminous region of a glow discharge is not a true plasma in that the concentrations of electrons and ions are not equal, but plasma conditions are roughly approximated. The substrates in a glow discharge may be treated as floating-plane probes. Figure 15 shows the I - V characteristics of such a probe in somewhat idealized fashion. Any material body immersed in a glow discharge, unless it is grounded, will acquire a potential with respect to ground that is slightly negative. This is known as the floating potential V_f . This potential arises because of the higher mobility of electrons, as opposed to ions, in the discharge so that more electrons reach the surface than ions. It can be shown [460] that the floating potential is related to the electron temperature T_e and the masses of the electron m and ion M involved in the discharge:

$$V_f = -(1/2e)kT_e \ln(\pi m/2M), \quad (3)$$

where e is the electron charge and k is Boltzmann's constant.

II-1. GLOW DISCHARGE SPUTTER DEPOSITION

Table V
Bibliography of Reactive Sputtering and Reactive Ion Plating

Source	Gases	References
Ag	Air	[275]
Ag	Ar + N ₂	[272]
Ag	Ar + O ₂	[272, 273, 276, 277]
Al	Ar + N ₂	[278, 279]
Al	Ar + O ₂	[18, 261, 273, 280]
Al	O ₂	[281]
Au	Air	[275]
Au	Ar + O ₂	[276]
Bi	Ar + O ₂	[276, 277, 282]
C	N ₂	[283]
Cd	Ar + H ₂ O	[266]
Cd	Ar + H ₂ S	[266, 284, 285]
Cd	Ar + O ₂	[266, 276, 277, 286-294]
Cr	Ar + CH ₄	[295]
Co	Ar + O ₂	[269, 296, 297]
Cu	Ar + H ₂ S	[284, 285]
Cu	Ar + O ₂	[264, 298-303]
Cu	Ne + O ₂	[302]
Fe	Ar + CH ₄	[295]
Fe	Ar + O ₂	[269, 273, 276, 304-306]
Ga	Ar + As	[307]
Ge	Ar + N ₂	[308]
Hf	Ar + C ₂ H ₂	[18]
Hf	Ar + N ₂	[309]
Hf	Ar + O ₂	[309-311]
In	Ar + O ₂	[266, 286, 288, 312-318]
Mg	Ar + O ₂	[319]
Mn	Ar + O ₂	[296, 320, 321]
Mo	Ar + CH ₄	[295]
Mo	Ar + H ₂ S	[303]
Mo	Ar + N ₂	[322]
Mo	Ar + O ₂	[272, 323]
Nb	Ar + CH ₄	[324]
Nb	Ar + C ₂ H ₂	[18]
Nb	Ar + N ₂	[325-327]
Nb	Ar + O ₂	[310]
Nb	Ar + N ₂ + CH ₄	[326]
Nb	Ar + N ₂ + O ₂	[328]
Ni	Ar + CH ₄	[295]
Ni	Ar + O ₂	[277, 296, 329-331]
Pb	Ar + H ₂ O	[266]
Pb	Ar + Si ₂ S	[303]
Pb	Ar + N ₂	[308]

Table V (Continued)

Source	Gases	References
Zn	Ar + H ₂ S	[284]
Zn	Ar + O ₂	[264, 268, 410-414]
Zr	Ar + N ₂	[271, 325]
Zr	Ar + O ₂	[310, 325, 351, 415, 416]
Al-Si	Ar + O ₂	[354, 355]
Au-Ta	Ar + O ₂	[417, 418]
Au-W	Ar + O ₂	[417]
Ba-Ti	Ar + O ₂	[419, 420]
Bi-Ta	Ar + O ₂	[421]
Bi-Ti	Ar + O ₂	[421]
Cd-Cu	Ar + H ₂ S	[303]
Cd-Cu	Ar + O ₂	[287]
Cd-In	Ar + H ₂ S	[303]
Cd-In	Ar + O ₂	[287]
Cd-Zn	Ar + H ₂ S	[422]
Cr-Mo	Ar + O ₂	[423]
Cu-Fe	Ar + O ₂	[424]
Ga-Al	Ar + As	[307]
Gd-Fe	Ar + O ₂	[425]
Hf-Ta	Ar + N ₂	[426-429]
In-Sn	Ar + O ₂	[286, 294, 371, 403, 430-437]
Li-Nb	Ar + O ₂	[438]
Nb-C	Ar + N ₂	[326]
Ni-Fe	Ar + O ₂	[424, 439]
Ni-Ti	Ar + C ₂ H ₂	[440]
Pb-Te	Ar + O ₂	[354]
Pb-Ti	Ar + O ₂	[415, 441, 442]
Pt-Ta	Ar + O ₂	[417]
Pt-W	Ar + O ₂	[417]
Si-Al	Ar + N ₂	[443]
Sn-In	Ar + O ₂	[286, 362]
Sn-Sb	Ar + O ₂	[28, 362, 437, 444]
Ta-Si	Ar + O ₂	[445]
Ta-Ti	Ar + N ₂	[446]
Ti-C	Ar + O ₂	[447]
Ti-Ni	C ₂ H ₂	[448]
Zn-Cu	Ar + H ₂ S	[449]
Cd-Cu-In	Ar + H ₂ S	[303]
Fe-Cr-Ni	Ar + CH ₄	[295, 450]
Mg-Mn-Zn	Ar + O ₂	[451]
Ti-Al-V	Ar + C ₂ H ₂	[452]
Pb-Nb-Zr-Fe-Bi-La	Ar + O ₂	[453]

Table V (Continued)

Source	Gases	References
Pb	Ar + O ₂	[266, 277, 332-334]
Pb	O ₂	[334]
Pt	Air	[275]
Pt	Ar + O ₂	[276, 335]
Sb	Ar + O ₂	[276, 277]
Si	Ar + C ₂ H ₂	[336]
Si	Ar + N ₂	[280, 319, 337-350]
Si	Ar + NH ₃	[268]
Si	Ar + O ₂	[273, 276, 277, 351-358]
Si	C ₂ H ₂	[359]
Si	N ₂	[67, 360, 360a]
Si	NH ₃	[360]
Si	NH ₃ + SiH ₄	[360b]
Si	O ₂	[357, 361]
Si	Ar + N ₂ + O ₂	[312]
Sn	Air	[103]
Sn	Ar + H ₂ S	[308]
Sn	Ar + N ₂	[276, 277, 286, 288, 362-364]
Sn	Ar + O ₂	[295, 365, 366]
Ta	Ar + CH ₄	[18, 367]
Ta	Ar + C ₂ H ₂	[264]
Ta	Ar + CO	[366]
Ta	Ar + H ₂	[266, 368-370]
Ta	Ar + H ₂ O	[264, 325, 365, 366, 371-379]
Ta	Ar + N ₂	[261, 266, 267, 273, 277, 310, 325, 351, 365, 369, 380-395]
Ta	Ar + O ₂	[396-400]
Ta	Ar + O ₂ + N ₂	[330]
Ta	Ar + SiH ₄	[277, 282]
Te	Ar + O ₂	[401]
Ti	Ar + CH ₄	[18, 402]
Ti	Ar + C ₂ H ₂	[266]
Ti	Ar + H ₂ O	[18, 272, 325, 371, 401, 403]
Ti	Ar + N ₂	[18]
Ti	Ar + NH ₃	[266, 270, 272, 274, 276, 310, 319, 323, 325, 351, 383, 401, 404-407]
Ti	Ar + O ₂	[18]
V	Ar + C ₂ H ₂	[408]
V	Ar + O ₂	[295]
W	Ar + CH ₄	[276, 277, 310]
W	Ar + O ₂	[18, 408, 409]
Y	Ar + O ₂	[264]
Zn	Ar + H ₂ O	

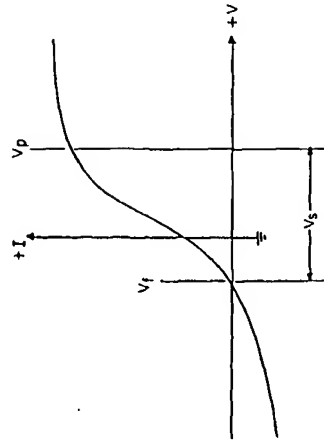


Fig. 15. Idealized $I-V$ characteristics of a Langmuir probe in a glow discharge.

At the point V_p , the probe is at the same potential as the plasma. Ideally, there are no electric fields at this point, and the charged particles migrate to the probe because of their thermal velocities. Again, because electrons are more mobile than ions, what is collected by the probe is predominantly electron current. Under ideal conditions, the plasma potential is given by

$$V_p = kT_i \ln 2/q_i, \quad (4)$$

where T_i and q_i are the temperature and charge of the ions involved [460]. The assumptions made in the derivations of these equations are by no means strictly valid in glow discharges (especially in the presence of magnetic fields), but they may be used to estimate the electron and ion temperatures in the discharge.

There are three major practical consequences to be drawn from Fig. 15. First, substrates (even if they are grounded) are at a potential that is negative with respect to the plasma. This is shown for a floating substrate in Fig. 15 as V_s . If the substrates are grounded, V_s is reduced by an amount equal to V_f . The second consequence is that *substrates in sputtering systems should rarely be grounded*. If an insulating substrate is attached to a grounded substrate support, the surface of the substrate acquires the potential V_s while its surroundings acquire the lower potential $V_s - V_f$. This leads to nonuniformity of bombardment near the edges of the substrate which, in turn, leads to variable thickness, composition or other properties as a function of distance from the edge of the substrate. The only exception to this rule is in the case of a conducting substrate onto which a conducting film is to be deposited. Finally, since target voltages and substrate voltages (in the case of bias sputtering or ion plating) are measured relative to ground, the existence of the plasma potential in-

roduces a systematic error since the true potential is the sum of the measured voltage and V_p . In some cases the error can be large.

The variation of the floating potential (V_f) with various dc glow discharge parameters is shown in Fig. 16. For rf glow discharges, the behavior is similar, except the magnitudes of the voltages involved are generally

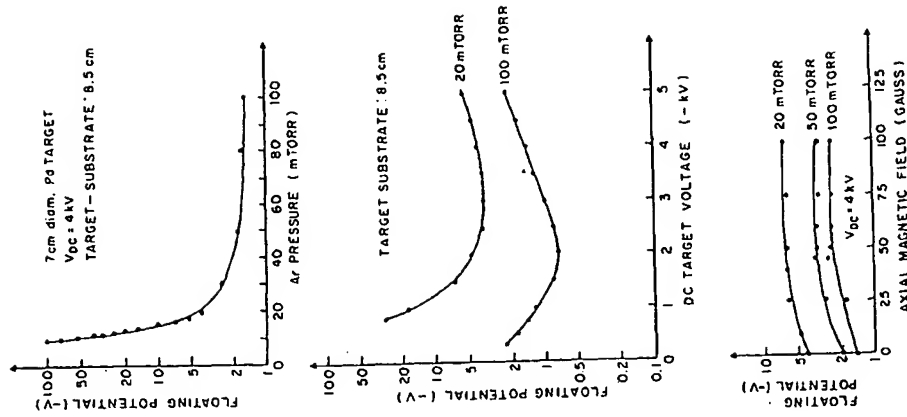


Fig. 16. The variation of the floating potential with Ar pressure, target voltage, and axial magnetic field in a dc sputtering system.

higher because the electron temperatures are higher for otherwise equivalent conditions.

The variation of the plasma potential (V_p) with dc glow discharge conditions is similar to the variation of the floating potential because parameters that increase electron temperature generally increase ion temperatures as well. For example, as the pressure is decreased, V_f and V_p , respectively, become more negative and more positive with respect to ground, leading to higher substrate potentials V_s .

The situation with rf glow discharges is somewhat more complicated because the geometry of the system becomes a major factor. As was pointed out (Eq. (1)), the ratio of the average potential on the capacitively coupled electrode (target) to that of the grounded electrode with respect to the plasma is given by $(A_d/A_c)^{1/2}$, where A_r and A_d are the areas of the capacitively coupled and grounded electrodes, respectively. These areas refer to the areas actually in contact with the glow discharge. If the discharge is confined (e.g., by placing a cylinder around the target), a limited portion of the total grounded area is actually in contact with the discharge. This has been done [454], and the plasma potentials have been measured for various confining ratios, $R = \text{target area/grounded area}$ versus the sum of the applied target potential to ground and the plasma potential (i.e., the total target potential) as shown in Fig. 17. These effects can be used to impose a negative bias on a substrate without the necessity for making a direct electrical contact, but it is clearly difficult to control.

It should be noted that the potentials described so far are *average* dc potentials. This does not imply that all ions striking substrate surfaces arrive with these potentials. In both dc and rf glow discharges, the thickness of the ion sheath at the substrates is greater than the ionic mean free paths, leading to inelastic collisions which slow many of the ions as they

charges, the potential of the ion sheath is time dependent. This leads to modulation of the ion energies depending upon exactly when the ions reach the outer edge of the ion sheath. In this case, incident ions can arrive with potentials ranging from zero to almost $2eV_s$ [123].

Negative substrate bias voltages can be applied from an external power source. If the substrate is electrically conducting, this may be accomplished with a dc power supply [461]. For insulating substrates and/or for the deposition of insulating films on conducting substrates, rf-induced substrate bias is preferred [11, 147, 462-463]. When this is done, the applied bias voltage, V_b , in effect takes the place of the floating potential, and the plasma potential remains unchanged [454]. Thus, the total negative substrate bias is $-(V_p - V_b)$.

II-1. GLOW DISCHARGE SPUTTER DEPOSITION

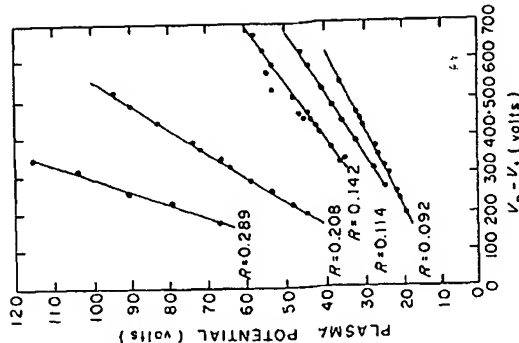


Fig. 17. Plasma potential versus total target potential for various confining ratios, R (see text) in an rf glow discharge (after Coburn and Kay [454]).

If a positive bias is applied to a substrate in a dc glow discharge, the substrate simply becomes a virtual anode, resulting in a very large electron current flow to the substrate. This, in turn, leads to a large amount of substrate heating and a very nonuniform current distribution [456]. For both dc and rf discharges, application of a positive bias to an independent

positive values of V_b , the effective substrate bias never exceeds the plasma potential. Thus, application of a positive bias is seen to have little effect on the effective substrate potential, but the relatively large increase in V_p leads to rather high levels of bombardment of all grounded surfaces in contact with the discharge. This can lead to rather large amounts of gas desorption from the walls of the chamber. Except in those instances where one might wish to clean up the grounded parts of a sputtering system, the application of positive substrate biases should be avoided.

It can be seen from this discussion that substrates in sputtering systems are nearly always subject to a negative bias (ion bombardment), whether externally applied or not. Consequently, substrates must be treated as sputtering targets, and all of the effects described in Section II

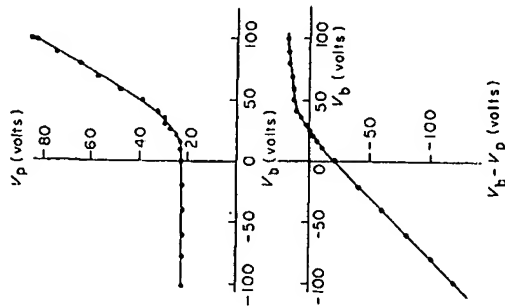


Fig. 18. The plasma potential (V_p) and total substrate potential ($V_b - V_p$) versus substrate bias in an rf glow discharge (after Coburn and Kay [454]).

apply to substrates during film growth as well as to sputtering targets. In some cases, one may wish to maximize substrate bombardment, while in other cases minimum bombardment may be desired. In all cases it should be controlled.

Bombardment of substrates is not limited to charged particles. High-energy neutrals reflected from the target and/or generated in the glow discharge by various excitation processes also bombard the substrate. Clearly these are unaffected by the substrate potential, and bombardment from this source is impossible to eliminate completely in glow discharge sputtering [464]. Recent estimates have been made of the relative contribution to substrate bombardment by ions (10%) and energetic neutrals (90%) in ion plating [465-467].

It should also be pointed out that the phenomena discussed in this section apply to substrates in *any* glow discharge. Thus, they apply not only to sputtering processes, but to all glow-discharge deposition and etching processes.

B. Gas Incorporation and Desorption

During the sputtering process, gas is incorporated in the growing film. The amount depends on target voltage [468-472], substrate bias voltage

II-1. GLOW DISCHARGE SPUTTER DEPOSITION

[469-471, 473-478], target-to-substrate distance [473, 479], sputter gas pressure [471, 473, 479], inert gas atomic volume [471, 480], substrate temperature, magnetic field, and system geometry. The interplay among these parameters is responsible for the varied results found in the literature. There are two mechanisms by which gas is incorporated: ions can be neutralized at the target surface and reflected at high energy toward the substrate where they may be implanted; and ions can bombard the substrate and be implanted because of the effective substrate bias.

1. Substrate Bias

The effective substrate bias is the most important parameter in determining gas incorporation [468-488]. At very low bias voltages, there is insufficient energy to implant gas, but some thermal desorption can occur. At higher voltages, gas contents increase as V_b^2 , where V_b is the substrate bias voltage. At very high bias voltages substrate heating leads to desorption of the implanted gas.

2. Target Voltage

The entrapment of energetic neutral sputter gas atoms reflected from the target surface has been amply demonstrated [468-472]. For example, in the incorporation of He in gold films [468], it was shown that at constant pressure and bias voltage, lower target voltages gave less gas incorporation than higher target voltages. Ar was found to increase in concentration for both triode and diode sputtered W films [478], and the amount of Ar that is incorporated in the film increases with the atomic number of the target material [489].

3. Substrate Temperature

As the substrate temperature is increased the sticking probability of inert sputter gas decreases [468, 473, 483, 487]. However, the rate of reaction increases in reactive sputtering.

4. Pressure

Increasing pressure decreases gas incorporation [471-473]. The increase in gas content with decreasing pressure is due to an increase in the plasma potential.

5. System Geometry

Geometric effects such as target-to-substrate distance have been shown to affect the amount of gas incorporated in films. The greater the distance of the target from the substrate the less gas will be incorporated in the growing films [472-473]. For example, in dc triode sputtering of W films [472] Ar was shown to decrease from about 15 at. % with a target-substrate separation of 9 cm to about 0.1 at. % at a separation of 18 cm.

Another geometric effect found that influences the film gas content is the target size for a fixed system geometry. Here we find seemingly conflicting results. For example, the inert gas concentration in rf sputtered amorphous films with rf bias voltage was found to vary inversely with the target electrode area [471], while in dc triode sputtered films it was found that the Ar concentration increased as the target area increased [473].

C. Stoichiometry of Films

The stoichiometry of films deposited from multicomponent targets when a substrate bias is applied has been addressed by a number of workers [83, 84, 92, 96a, 477, 483, 489-491]. Most of these treatments are theoretical. Rather than review them in detail, we summarize the practical consequences.

To control film stoichiometry, many conditions must be met. The target itself must be homogeneous. This is especially a problem with some alloys and mixtures in which constituents segregate out in patches. The altered surface layer must be established at steady state. There must be no bulk diffusion in the target. If sublimation occurs at the target, the target composition must be enriched in the subliming material. When targets with normally gaseous constituents (e.g., oxides) are used, chemical dissociation at the target must be compensated by reactive sputtering. Preferential resputtering must be compensated by adjusting the target composition and/or by reactive sputtering. Shutters should be biased to the same potential as substrates during deposition to prevent transients in resputtering which change the composition of the first few monolayers of film material.

D. Physical Film Properties

In the absence of problems with film stoichiometry, controlled resputtering in various bias modes often aids in producing films of high quality. Most of the studies of physical film properties as a function of substrate bias have been reviewed elsewhere [9, 11, 13, 147], and they will not be

covered in detail here. There have been reports of improved film density, electrical properties, magnetic properties, adhesion, and surface morphology, to name but a few. In addition, variations in grain size, preferred orientation, and crystal polymorphs have been observed in some materials. Ohmic contacts can be made to semiconductors without the need for sintering. Conformal coatings over severe topographic features on substrates can be achieved because of small-angle resputtering. In general, the judicious use of substrate biasing is one of the most powerful tools available in sputtering to tailor the properties of deposited films. To optimize some properties, high bias voltages are required, while to optimize others, substrate bombardment must be minimized.

In summary, there are three basic effects that occur at a substrate during glow discharge sputtering: (1) condensation of energetic vapor, (2) heating, and (3) bombardment by a variety of energetic species. The sum of all of these effects must be carefully controlled, and, since they are all interdependent [11], this is sometimes difficult.

VIII. RATE AND UNIFORMITY OF DEPOSITION

Most deposition rates quoted in the literature should more properly be called "accumulation rates," since they are really the difference between the arrival and resputtering rates of the film material at the substrate. Both the accumulation rate and the uniformity of film deposition have been thoroughly reviewed by Maissel [5, 9], so only a summary is presented here.

For a given target material both rate and uniformity are influenced by system geometry, target voltage, sputtering gas, gas pressure, and power. All other things being equal, rates are linearly proportional to power and decrease with increasing target-substrate separation. The sputtering gas influences deposition rate in the same way as it affects sputtering yields. As the gas pressure is increased the discharge current increases (increasing rate), but return of material to the target by backscattering also increases (decreasing rate). This is further complicated in some cases by increased Penning ionization at higher pressures which increases the rate by self-sputtering. The sum of all of this leads to a gas pressure or a small range of gas pressure at which the rate is a maximum, and this must be determined empirically for each application. The optimum pressure may be anywhere between a few mTorr and several tens of mTorr.

In general, for a given gas pressure there will be an optimum target-substrate separation to produce the best uniformity. For small targets

(<15-cm diameter) this separation is generally small (a few centimeters), while for larger targets, the optimum separation may be considerably larger (10–20 cm). The edges of the target, no matter how the dark-space shield is constructed, represent regions of gross nonuniformity. Under ideal conditions, the best uniformity that one can hope to achieve is ± 2 –5% over an area concentric with the deposition target, but ~ 5 cm smaller in diameter than the target. Often it is much worse than this.

IX. CONCLUSION

In this chapter we have attempted to review the rather complex interplay of the parameters involved in sputter deposition and to introduce some of the glow discharge aspects of related processes.

Unquestionably, the hallmark of the sputtering processes described is versatility, both in terms of materials that can be deposited and process parameters that can be adjusted to tailor the properties of thin films as desired. However, the sheer number of critical process parameters and their complex interrelationships can often make these processes difficult to control. For many applications, the advantages far outweigh the disadvantages, and "diode sputtering" and "ion plating" have been put to use in large-scale production in applications of a wide variety: electronics, optics, abrasion-resistant coatings, lubricating coatings, corrosion protection, and thermal insulation, to name but a few.

In general, these processes are found to be most useful in applications requiring rather thin films (generally $< 1 \mu\text{m}$ because of relatively low deposition rates) and/or in cases where the desired material simply cannot be deposited stoichiometrically any other way.

REFERENCES

1. G. K. Wehner, *Adv. Electron. Electron. Phys.* **7**, 239 (1955).
2. E. Kay, *Adv. Electron. Electron. Phys.* **17**, 245 (1962).
3. M. Kaminsky, "Atomic and Ionic Impact Phenomena on Metal Surfaces," Academic Press, New York, 1965.
4. M. H. Francombe, in "Basic Problems in Thin Film Physics" (R. Niedermeyer and H. Mayer, eds.), p. 52. Vanderhoeck & Ruprecht, Göttingen, 1966.
5. L. I. Maissel, *Phys. Thin Films* **3**, 61 (1966).
6. G. Carter and J. S. Colligon, "Ion Bombardment of Solids," Am. Elsevier, New York, 1968.
7. K. L. Chopra, "Thin Film Phenomena," McGraw-Hill, New York, 1969.
8. G. K. Wehner and G. S. Anderson, in "Handbook of Thin Film Technology" (L. I. Maissel and R. Glang, eds.), Ch. 3. McGraw-Hill, New York, 1970.
9. L. I. Maissel, in "Handbook of Thin Film Technology" (L. I. Maissel and R. Glang, eds.), Ch. 4. McGraw-Hill, New York, 1970.

II-1. GLOW DISCHARGE SPUTTER DEPOSITION

10. G. N. Jackson, *Thin Solid Films* **5**, 209 (1970).
11. J. L. Vossen, *J. Vac. Sci. Technol.* **8**, S12 (1971).
12. P. D. Townsend, J. C. Kelly, and N. E. W. Hartley, "Ion Implantation, Sputtering and Their Applications," Ch. 6. Academic Press, New York, 1976.
13. W. D. Westwood, *Prog. Surf. Sci.* **7**, 71 (1976).
14. R. J. MacDonald, *Adv. Phys.* **19**, 457 (1970).
15. I. S. T. Tsong and D. J. Barber, *J. Mater. Sci.* **8**, 123 (1973).
16. D. M. Mattox, *Electrochem. Technol.* **2**, 295 (1964).
17. D. M. Mattox, *J. Vac. Sci. Technol.* **10**, 47 (1973).
18. R. E. Bunshah and A. C. Raghuram, *J. Vac. Sci. Technol.* **9**, 1385 (1972).
19. O. Almen and G. Bruce, *Nucl. Instrum. Methods* **11**, 257 (1961).
20. O. Almen and G. Bruce, *Nucl. Instrum. Methods* **11**, 279 (1961).
21. J. L. Vossen and E. B. Davidson, *J. Electrochem. Soc.* **119**, 1708 (1972).
22. P. D. Davids and L. I. Maissel, *J. Vac. Sci. Technol.* **4**, 33 (1967).
23. G. K. Wehner, Rep. No. 2309. General Mills, Minneapolis (1962).
24. J. L. Vossen, unpublished observations (1974).
25. C. H. Weyensfeld and A. Hoogendoorn, *Proc. Conf. Ion. Phenom. Gases, 5th. Munich 1*, 124 (1961).
26. D. McKeown and A. Y. Cabezas, *Annu. Rep. Space Sci. Lab.: General Dynamics July* (1962).
27. F. Keywell, *Phys. Rev.* **97**, 1611 (1955).
28. J. Comas and C. B. Cooper, *J. Appl. Phys.* **37**, 2820 (1966).
29. D. McKeown, A. Cabezas, and E. T. Mackenzie, *Annu. Rep. Low Energy Sputtering Stud.: Space Sci. Lab.: General Dynamics July* (1961).
30. R. C. Krutnal and C. Panzera, *J. Appl. Phys.* **41**, 4953 (1970).
31. T. W. Snouse, *NASA Tech. Note D-2235* (1964).
32. H. Patterson and D. H. Tomlin, *Proc. R. Soc. A* **265**, 474 (1962).
33. M. T. Robinson and A. L. Southern, *J. Appl. Phys.* **38**, 2969 (1967).
34. P. K. Rol, J. M. Fluit, and J. Kistemaker, "Electromagnetic Separation of Radioactive Isotopes," p. 207. Springer-Verlag, Berlin and New York, 1960.
35. O. Almen and G. Bruce, *Trans. Natl. Vac. Symp., 8th, Washington, D.C.*, p. 245 (1961).
36. M. I. Guseva, *Sov. Phys.—Solid State* **1**, 1410 (1959).
37. M. T. Robinson and A. L. Southern, *J. Appl. Phys.* **39**, 3463 (1968).
38. P. A. B. Toombs, *J. Phys. D* **1**, 662 (1968).
39. L. Holland, T. Pinner, and G. N. Jackson, *J. Phys. E* **1**, 32 (1968).
40. I. Brodie, L. T. Lamont, and D. O. Myers, *J. Vac. Sci. Technol.* **6**, 124 (1969).
41. D. J. Ball, *J. Appl. Phys.* **43**, 3047 (1972).
42. B. N. Chapman, D. Downer, and L. J. M. Guimaraes, *J. Appl. Phys.* **45**, 2115 (1974).
43. Y. Shintani, K. Nakanishi, T. Takawaki, and O. Tada, *Jpn. J. Appl. Phys.* **14**, 1875 (1975).
44. Y. A. Fogel, *Sov. Phys.—Usp.* **10**, 17 (1967).
45. R. E. Honig, *J. Appl. Phys.* **29**, 549 (1958).
46. A. K. Ayukhanov and M. K. Abdullaeva, *Bull. Acad. Sci. USSR., Phys. Ser.* **30**, 2083 (1966).
47. A. Benninghoven, *Z. Phys.* **220**, 159 (1969).
48. A. Benninghoven, *Surf. Sci.* **28**, 541 (1971).
49. A. Benninghoven, *Z. Phys.* **230**, 403 (1970).
50. A. Benninghoven, *Surf. Sci.* **35**, 427 (1973).
51. H. W. Werner, *Surf. Sci.* **47**, 301 (1975).

53. V. E. Krohn, *Int. J. Mass Spectrom. Ion Phys.* **22**, 43 (1976).
- 53a. J. J. Cuomo, R. J. Gambino, J. M. E. Harper, and J. D. Kuptsis, *IBM J. Res. Dev.* **21**, 580 (1977).
- 53b. J. J. Cuomo, R. J. Gambino, J. M. E. Harper, J. D. Kuptsis, and J. C. Webber, *J. Vac. Sci. Technol.* **15**, 281 (1978).
54. E. Kay, *Colloid. Int. Pulver. Cathod., 2nd. Nitr.* 1976.
55. H. D. Hagstrum, *Phys. Rev.* **123**, 758 (1961).
56. E. V. Kornelsen, *Can. J. Phys.* **42**, 364 (1964).
57. E. R. Cawthron, D. L. Catterell, and M. Oliphant, *Proc. R. Soc., Ser. A* **314**, 53 (1969).
58. J. K. Roberts, *Proc. R. Soc., Ser. A* **135**, 192 (1932).
59. F. O. Goodman, *Surf. Sci.* **24**, 667 (1971).
60. E. P. Suurmeijer and A. L. Boers, *Surf. Sci.* **43**, 309 (1973).
61. F. W. Bingham, *J. Chem. Phys.* **46**, 2003 (1967).
62. H. Niehus and E. Bauer, *Surf. Sci.* **47**, 222 (1975).
63. E. Brown and J. H. Leck, *Br. J. Appl. Phys.* **6**, 161 (1955).
64. K. Erentis and G. Carter, *J. Phys. D* **2**, 435 (1969).
65. K. Erentis and G. Carter, *J. Phys. D* **2**, 711 (1969).
66. H. F. Winters and P. Sigmund, *J. Appl. Phys.* **45**, 4760 (1974).
67. J. L. Vossen, *J. Vac. Sci. Technol.* **8**, 751 (1971).
68. P. Bacuvier and P. Lavallee, *J. Vac. Sci. Technol.* **13**, 1101 (1976).
69. C. Snoeck and J. Kistemaker, *Adv. Electron. Electron Phys.* **21**, 67 (1965).
70. I. S. T. Tsong, *Phys. Status Solidi A* **7**, 451 (1971).
71. C. B. Kerkdijk and R. Kelly, *Surf. Sci.* **47**, 294 (1975).
72. J. P. Meriaux, R. Goutie, and C. Guiland, *Appl. Phys.* **7**, 313 (1975).
73. C. W. White, D. L. Simms, N. M. Toek, and D. V. Caughan, *Surf. Sci.* **49**, 657 (1975).
74. G. Blaise and M. Bernheim, *Surf. Sci.* **47**, 324 (1975).
75. A. Benninghoven, *Surf. Sci.* **35**, 324 (1973).
76. G. Blaise, *Surf. Sci.* **60**, 65 (1976).
77. E. P. Bertin, "Principles and Practice of X-Ray Spectrometric Analysis," 2nd Ed., pp. 960-963, 968-971, Plenum, New York, 1975.
78. J. Comas and C. A. Carosella, *J. Electrochem. Soc.* **115**, 974 (1968).
79. K. E. Manchester, *J. Electrochem. Soc.* **115**, 656 (1968).
80. J. F. Gibbons, *Proc. IEEE* **56**, 295 (1968).
81. W. Brandt, *Sci. Am.* **218**(3), 90 (1968).
82. E. Gillam, *J. Phys. Chem. Solids* **11**, 55 (1959).
83. D. B. Dove, R. J. Gambino, J. J. Cuomo, and R. J. Koblicka, *J. Vac. Sci. Technol.* **13**, 965 (1976).
84. W. L. Patterson and G. A. Shirn, *J. Vac. Sci. Technol.* **4**, 343 (1967).
85. J. W. Coburn, *J. Vac. Sci. Technol.* **13**, 1037 (1976).
86. H. J. Mathiew and D. Landolt, *Surf. Sci.* **53**, 228 (1975).
87. W. T. Ogier, N. T. Olson, and H. P. Smith, *J. Appl. Phys.* **40**, 4997 (1969).
88. H. Shimizu, M. Ono, and K. Nakayama, *Surf. Sci.* **36**, 817 (1973).
89. L. A. West, *J. Vac. Sci. Technol.* **13**, 198 (1976).
90. W. Färber, G. Betz, and P. Braun, *Nucl. Instrum. Methods* **132**, 351 (1976).
91. G. Betz, P. Braun, and W. Färber, *J. Appl. Phys.* **48**, 1404 (1977).
92. H. F. Winters and J. W. Coburn, *Appl. Phys. Lett.* **28**, 176 (1976).
93. H. W. Pickering, *J. Vac. Sci. Technol.* **13**, 618 (1976).
94. H. M. Naguib and R. Kelly, *J. Phys. Chem. Solids* **33**, 1751 (1972).
95. D. K. Murti and R. Kelly, *Thin Solid Films* **33**, 149 (1976).
96. G. S. Anderson, *J. Appl. Phys.* **40**, 2884 (1969).
- 96a. M. L. Tarn and G. K. Wehner, *J. Appl. Phys.* **42**, 2449 (1971).
97. J. L. Vossen and J. J. O'Neill, *RCA Rev.* **29**, 149 (1968).
98. W. J. Takai, N. P. Formigoni, and M. H. Francombe, *J. Vac. Sci. Technol.* **7**, 442 (1970).
99. R. Kelly, *Radiat. Eff.* **32**, 91 (1977).
100. J. L. Vossen, *Proc. Symp. Deposition Thin Films Sputter., 3rd, Univ. Rochester*, p. 80 (1968).
101. H. M. Naguib and R. Kelly, *Radiat. Eff.* **25**, 79 (1975).
102. D. K. Murti and R. Kelly, *Surf. Sci.* **47**, 282 (1975).
103. H. B. Sachse and G. L. Nichols, *J. Appl. Phys.* **41**, 4237 (1970).
104. R. Kelly and J. B. Sanders, *Nucl. Instrum. Methods* **132**, 335 (1976).
105. R. Holm and S. Storp, *Appl. Phys.* **12**, 101 (1977).
106. K. S. Kim and N. Winograd, *Surf. Sci.* **43**, 625 (1974).
107. K. S. Kim, W. E. Bainger, and N. Winograd, *Surf. Sci.* **55**, 283 (1976).
108. G. V. Jorgenson and G. K. Wehner, *J. Appl. Phys.* **36**, 2672 (1965).
109. R. E. Jones, H. F. Winters, and L. I. Maissel, *J. Vac. Sci. Technol.* **5**, 84 (1968).
110. J. B. Lounsbury, *J. Vac. Sci. Technol.* **6**, 838 (1969).
111. J. L. Vossen, *J. Appl. Phys.* **47**, 544 (1976).
112. L. Holland, *J. Vac. Sci. Technol.* **14**, 5 (1977).
113. J. J. Hanak and J. P. Pellicane, *J. Vac. Sci. Technol.* **13**, 406 (1976).
114. S. C. Brown, "Introduction to Electrical Discharges in Gases," Wiley, New York, 1966.
115. A. von Engel, "Ionized Gases," Oxford Univ. Press, London and New York, 1965.
116. T. Kihara, *Rev. Mod. Phys.* **24**, 45 (1952).
117. R. G. Fowler, in "Handbuch der Physik" (S. Flugge, ed.), Vol. 22, p. 59, Springer-Verlag, Berlin and New York, 1956.
118. W. D. Davis and T. A. Vanderslice, *Phys. Rev.* **121**, 219 (1963).
119. A. K. Brewer and J. W. Westhaver, *J. Appl. Phys.* **8**, 779 (1937).
120. H. R. Koenig and L. I. Maissel, *IBM J. Res. Dev.* **14**, 168 (1970).
121. H. S. Butler and G. S. Kino, *Phys. Fluids* **6**, 1346 (1963).
122. G. S. Anderson, W. N. Mayer, and G. K. Wehner, *J. Appl. Phys.* **37**, 574 (1966).
123. R. T. C. Tsui, *Phys. Rev.* **168**, 107 (1968).
124. J. S. Logan, J. H. Keller, and R. G. Simmons, *J. Vac. Sci. Technol.* **14**, 92 (1977).
125. J. W. Nickerson and R. Moseson, *Res/Dev.* **16**(3), 52 (1965).
126. D. Anderson, *SCP Solid State Technol.* **9**(12), 27 (1966).
127. J. Nickerson, *SCP Solid State Technol.* **8**(12), 30 (1965).
128. D. Anderson, *Res/Dev.* **19**(1), 42 (1968).
129. N. Laegreid and R. Moseson, U.S. Patents 3,324,019; 3,297,115; 3,344,054; 3,347,772 (1967).
130. W. N. Huss, *SCP Solid State Technol.* **9**(12), 50 (1966).
131. E. C. Muly and A. J. Aronson, *J. Vac. Sci. Technol.* **6**, 128 (1969).
132. E. C. Muly and A. J. Aronson, *Trans. Natl. Vac. Symp.*, 13th p. 145 (1967).
133. T. C. Tisone and J. B. Bindell, *J. Vac. Sci. Technol.* **11**, 519 (1974).
134. R. C. Sun, T. C. Tisone, and P. D. Cruzan, *J. Appl. Phys.* **46**, 112 (1975).
135. R. C. Sun, T. C. Tisone, and P. D. Cruzan, *J. Appl. Phys.* **44**, 1009 (1973).
136. B. E. Nevis and T. C. Tisone, *J. Vac. Sci. Technol.* **11**, 1147 (1974).
137. T. C. Tisone and P. D. Cruzan, *J. Vac. Sci. Technol.* **12**, 677 (1975).
138. Y. Murayama, *Jpn. J. Appl. Phys., Suppl.* **2**, Part 1, 459 (1974).
139. L. I. Maissel and J. H. Vaughn, *Vacuum* **13**, 421 (1963).
140. P. D. Davids and L. I. Maissel, *J. Appl. Phys.* **37**, 574 (1966).
141. L. A. Cambey, *Proc. Conf. Sputtering Technol. Autom. Prod. Equip., Materials Research Corp., Orangeburg, N.Y.* p. 129 (1973).

142. P. Silano and P. A. Leary, IBM Res., personal communication (1977).
143. R. Lee, "Electronic Transformers and Circuits," 2nd Ed., Ch. 8, Wiley, New York, 1955.
144. "U.S. Federal Communications Commission Rules and Regulations," Part 18, U.S. Gov. Print. Off., Washington, D.C., 1964.
145. F. E. Terman, "Radio Engineers' Handbook," Sect. 3, McGraw-Hill, New York, 1943.
146. J. S. Logan, *IBM J. Res. Dev.* 14, 172 (1970).
147. O. Christensen, *Solid State Technol.* 13(12), 39 (1970).
148. J. S. Logan, U.S. Patent 3,617,459 (1971).
149. N. M. Mazza, *IBM J. Res. Dev.* 14, 192 (1970).
150. L. J. Koche, *Rev. Sci. Instrum.* 47, 1556 (1976).
151. P. Silano, A. Halperin and L. West, *J. Vac. Sci. Technol.* 15, 116 (1978).
152. P. A. B. Toombs, *J. Phys. D* 1, 662 (1968).
153. L. Holland, T. Putner, and G. N. Jackson, *J. Phys. E* 1, 32 (1968).
154. R. B. McDowell, *Solid State Technol.* 12(2), 23 (1969).
155. R. B. McDowell, U.S. Patent 3,704,219 (1972).
156. J. L. Vossen, U.S. Patent 3,860,507 (1975).
157. J. L. Vossen and J. J. O'Neill, *J. Vac. Sci. Technol.* 12, 1052 (1975).
158. J. J. Sullivan, *Res/Dev*, 27(1), 41 (1976).
159. T. L. Thomas and E. L. Battle, *J. Appl. Phys.* 41, 3428 (1970).
160. A. Amith, *J. Vac. Sci. Technol.* 14, 803 (1977).
161. C. Misiano, E. Simonetti, and C. Corsi, *Thin Solid Films* 27, L15 (1975).
162. A. J. Stirling and W. D. Westwood, *J. Appl. Phys.* 41, 742 (1970).
163. A. J. Stirling and W. D. Westwood, *J. Phys. D* 4, 246 (1971).
164. A. J. Stirling and W. D. Westwood, *Thin Solid Films* 7, 1 (1971).
165. A. J. Stirling and W. D. Westwood, *Thin Solid Films* 8, 199 (1971).
166. H. Raitinen, *J. Appl. Phys.* 44, 2730 (1973).
167. J. E. Greene and F. Sequeda-Osorio, *J. Vac. Sci. Technol.* 10, 1144 (1973).
168. H. J. Bauer and E. H. Bogardus, *J. Vac. Sci. Technol.* 11, 1144 (1974).
169. J. Sosniak, *J. Vac. Sci. Technol.* 4, 87 (1966).
170. J. B. Lounsbury, *J. Vac. Sci. Technol.* 6, 838 (1969).
171. J. W. Coburn, *Rev. Sci. Instrum.* 41, 1219 (1970).
172. J. W. Coburn and E. Kay, *Appl. Phys. Lett.* 18, 435 (1971).
173. H. Raitinen, *Appl. Phys. Lett.* 21, 473 (1972).
174. A. B. Arthur and C. B. Cooper, *J. Appl. Phys.* 43, 863 (1972).
175. J. W. Coburn, E. Taglaier, and E. Kay, *Jpn. J. Appl. Phys., Suppl. 2, Part 1*, 301 (1974).
176. F. Shinoki and A. Itoh, *Jpn. J. Appl. Phys., Suppl. 2, Part 1*, 505 (1974).
177. K. Jensen and E. Veje, *Z. Phys.* 269, 293 (1974).
178. J. W. Coburn, E. W. Eckstein, and E. Kay, *J. Vac. Sci. Technol.* 12, 151 (1975).
179. E. W. Eckstein, J. W. Coburn, and E. Kay, *Int. J. Mass Spectrom. Ion Phys.* 17, 129 (1975).
180. J. M. Poitevin, G. Lempereire, and C. Fourier, *J. Phys. D* 9, 1783 (1976).
181. A. J. Purdes, B. F. T. Bolker, J. D. Bucci, and T. C. Tison, *J. Vac. Sci. Technol.* 14, 98 (1977).
182. D. M. Mattox, Rep. SC-R-65-997, Sandia Lab., Albuquerque, New Mexico (1966).
183. R. C. Brumfield, J. T. Naff, and A. T. W. Robinson, U.S. Patent 3,514,388 (1970).
184. G. Seeley, P. A. Totta, and G. Wald, U.S. Patent 3,507,248 (1970).
185. D. L. Chambers and D. C. Carmichael, *Res/Dev* 22(5), 32 (1971).
186. G. W. White, *Res/Dev* 24(7), 43 (1973).
- 11-1. GLOW DISCHARGE SPUTTER DEPOSITION 67
187. G. J. Hale, G. W. White, and D. E. Meyer, *Electron. Packag. Prod.* 15(5), 48 (1975).
188. S. S. Charschan and H. Westgaard, *Electrochem. Technol.* 2, 5 (1964).
189. P. Granger and C. R. D. Priestland, *Vacuum* 21, 309 (1971).
190. C. H. George, *J. Vac. Sci. Technol.* 10, 393 (1973).
191. H. J. Glaser and H. W. Brandt, U.S. Patent 3,891,536 (1975).
192. D. C. Carmichael, D. L. Chambers, and C. T. Wan, U.S. Patent 3,904,506 (1975).
193. F. H. Gillery, U.S. Patent 3,907,660 (1975).
194. J. J. Bessot, *Thin Solid Films* 32, 19 (1976).
195. A. W. Morris, *Plat. Surf. Finish.* 63(10), 42 (1976).
196. C. Altman, *Trans. Natl. Vac. Symp.*, 9th, p. 174 (1962).
197. H. Isaak, *Trans. Natl. Vac. Symp.*, 9th, p. 180 (1962).
198. J. G. Needham, *Trans. Natl. Vac. Symp.*, 10th, Boston, 1963, p. 402 (1964).
- 198a. H. J. Glaser, *Proc. Int. Vac. Congr., 7th, Int. Conf. Solid Surf.*, 3rd, Vienna p. 1575 (1977).
199. J. van Esdonk and J. F. M. Janssen, *Res/Dev* 26(1), 41 (1975).
200. J. E. Houston and R. D. Bland, *J. Appl. Phys.* 44, 2504 (1973).
201. D. M. Mattox, Rep. SAND 74-0344, Sandia Lab., Albuquerque, New Mexico (1975).
202. D. M. Mattox, "Surface Cleaning in Thin Film Technology," Thin Film Div., Am. Vac. Soc., New York, 1975.
203. H. E. Farnsworth, R. E. Schlier, T. H. George, and R. M. Burger, *J. Appl. Phys.* 29, 1150 (1958).
204. O. C. Yontis and D. E. Harrison, *J. Appl. Phys.* 31, 1583 (1960).
205. D. Haneman, *Phys. Rev.* 119, 563 (1960).
206. R. W. Roberts, *Br. J. Appl. Phys.* 14, 537 (1963).
207. F. Jona, *J. Phys. Chem. Solids* 28, 2155 (1967).
208. R. P. H. Gasser, *Q. Rev. Chem. Soc.* 25, 223 (1971).
209. L. Holland, *Br. J. Appl. Phys.* 9, 410 (1958).
210. R. B. Gillette, J. R. Hollahan, and G. L. Carlson, *J. Vac. Sci. Technol.* 7, 534 (1970).
211. J. H. Greiner, *J. Appl. Phys.* 42, 5151 (1971).
212. J. L. Vossen, J. J. O'Neill, K. McFinlayson, and L. J. Royer, *RCA Rev.* 31, 293 (1970).
213. L. I. Maissel, C. L. Stundley, and L. V. Gregor, *IBM J. Res. Dev.* 16, 67 (1972).
214. C. C. Chang, P. Petroff, G. Quintana, and J. Sosniak, *Surf. Sci.* 38, 341 (1973).
215. H. Dimigen and H. Lühje, *Thin Solid Films* 27, 155 (1975).
216. H. Dimigen and H. Lühje, *Philips Tech. Rev.* 35, 199 (1975).
217. T. C. Tison and P. D. Cruzan, *J. Vac. Sci. Technol.* 12, 677 (1975).
218. C. Misiano and E. Simonetti, *Thin Solid Films* 33, L15 (1976).
219. G. J. Kominiak and J. E. Uhl, *J. Vac. Sci. Technol.* 13, 170 (1976).
220. G. J. Kominiak and D. M. Mattox, *Thin Solid Films* 40, 141 (1977).
221. J. L. Vossen and J. H. Banfield, U.S. Patent 3,640,812 (1972).
222. G. J. Kominiak, *J. Vac. Sci. Technol.* 13, 1100 (1976).
223. J. L. Vossen, J. J. O'Neill, E. A. James, and O. R. Mesker, *J. Vac. Sci. Technol.* 14, 85 (1977).
224. D. V. McCaughan and R. A. Kushner, *Thin Solid Films* 22, 359 (1974).
225. R. R. Hart, H. L. Dunlap, and O. J. Marsh, *J. Appl. Phys.* 46, 1947 (1975).
226. G. W. Sachse, W. E. Miller, and C. Gross, *Solid-State Electron.* 18, 431 (1975).
227. J. C. Bean, G. E. Becker, P. M. Petroff, and T. E. Seidel, *J. Appl. Phys.* 48, 907 (1977).
228. G. K. Wehner, *NASA Spec. Publ.* SP-5111, 59 (1972).
229. J. F. Ziegler, J. J. Cuomo, and J. Roth, *Appl. Phys. Lett.* 30, 268 (1977).
230. M. J. Nobes, J. S. Colligon, and G. Carter, *J. Mater. Sci.* 4, 730 (1969).
231. A. P. Janssen and J. P. Jones, *J. Phys. D* 4, 118 (1971).
232. G. Carter, J. S. Colligon, and M. J. Nobes, *J. Mater. Sci.* 6, 115 (1971).

233. I. H. Wilson and M. W. Kidd, *J. Mater. Sci.* 6, 1362 (1971).
234. J. Punzel and W. Haupte, *Phys. Status Solidi A* 14, K97 (1972).
235. T. Oohashi and S. Yamashita, *Jpn. J. Appl. Phys.* 11, 1581 (1972).
236. C. Catana, J. S. Colligon, and G. Carter, *J. Mater. Sci.* 7, 467 (1972).
237. G. Carter, J. S. Colligon, and M. J. Nobes, *J. Mater. Sci.* 8, 1473 (1973).
238. R. S. Nelson and D. J. Mazey, *Radiat. Eff.* 18, 127 (1973).
239. P. Sigmund, *J. Mater. Sci.* 8, 1545 (1973).
240. M. J. Witcomb, *J. Mater. Sci.* 9, 127 (1974).
241. M. J. Witcomb, *J. Mater. Sci.* 9, 551 (1974).
242. M. J. Witcomb, *Proc. Electron Microsc. Soc. South Afr., Johannesburg* 4, 57 (1974).
243. P. G. Glöerson, *J. Vac. Sci. Technol.* 12, 28 (1975).
244. M. J. Witcomb, *J. Appl. Phys.* 46, 5053 (1975).
245. G. Carter, *J. Mater. Sci.* 11, 1091 (1976).
246. M. J. Witcomb, *J. Mater. Sci.* 11, 859 (1976).
247. J. J. Cuomo, J. F. Ziegler, and J. M. Woodall, *Appl. Phys. Lett.* 26, 557 (1975).
248. J. J. Cuomo, J. M. Woodall, and T. H. DiStefano, *Proc. Am. Electroplating Soc. Conf. Sol. Collect., Atlanta, Ga.* p. 133 (1976).
249. R. E. Chapman, *J. Mater. Sci.* 12, 1125 (1977).
250. H. W. Lehmann, L. Krausbauer, and R. Widmer, *J. Vac. Sci. Technol.* 14, 281 (1977).
251. B. L. Soporì and W. S. C. Chang, *J. Vac. Sci. Technol.* 14, 782 (1977).
252. J. L. Vossen, *J. Vac. Sci. Technol.* 11, 875 (1974).
253. D. B. Fraser and H. D. Cook, *J. Electrochem. Soc.* 119, 1368 (1972).
254. D. E. Gray, ed., "American Institute of Physics Handbook," 2nd Ed., pp. 7-13-7-15. McGraw-Hill, New York, 1963.
255. E. E. Muschitz, *Science* 159, 599 (1968).
256. K. Gerard and H. Hotop, *Chem. Phys. Lett.* 43, 175 (1976).
257. V. Hoffman, *Electron. Packag. Prod.* 13(11), 81 (1973).
- 257a. L. Holland and R. E. L. Cox, *Vacuum* 24, 107 (1974).
258. H. C. Theuerer and J. J. Hauser, *J. Appl. Phys.* 35, 554 (1964).
259. H. C. Theuerer and J. J. Hauser, *Trans. Metall. Soc. AIME* 233, 588 (1965).
260. H. C. Theuerer, E. A. Nesbitt, and D. D. Bacon, *J. Appl. Phys.* 40, 2994 (1969).
261. F. Vrainy, *J. Electrochem. Soc.* 114, 505 (1967).
262. H. C. Cooke, C. W. Covington, and J. F. Libsch, *Trans. Metall. Soc. AIME* 236, 314 (1966).
263. J. J. Cuomo and W. W. Molzen, U.S. Patent 3,892,650 (1975).
264. N. Schwartz, *Trans. Natl. Vac. Symp., 10th, Boston, 1963* p. 325 (1964).
265. G. Perny, *Vide* 21, 106 (1966).
266. J. Pompei, *Proc. Symp. Deposition Thin Films Sputter., 2nd, Univ. Rochester* p. 127 (1967).
267. E. Hollands and D. S. Campbell, *J. Mater. Sci.* 3, 544 (1968).
268. J. Pompei, *Proc. Symp. Deposition Thin Films Sputter., 3rd, Univ. Rochester* p. 165 (1969).
269. J. Heller, *Thin Solid Films* 17, 163 (1973).
270. K. G. Geraghty and L. F. Donaghy, *Proc. Conf. Chem. Vap. Dep., 5th, Electrochem. Soc., Princeton, N.J.* p. 219 (1975).
271. F. Shinoki and A. Itoh, *J. Appl. Phys.* 46, 3381 (1975).
272. T. Abe and T. Yamashita, *Thin Solid Films* 30, 19 (1975).
273. B. Goranchev, V. Orlov, and V. Popova, *Thin Solid Films* 33, 173 (1976).
274. L. F. Donaghy and K. G. Geraghty, *Thin Solid Films* 36, 271 (1976).
275. T. Suzuki, *Z. Naturforsch., Teil A* 12, 497 (1957).

276. L. Holland, "Vacuum Deposition of Thin Films," pp. 455-463. Wiley, New York, 1954.
277. M. L. Lieberman and R. C. Medrud, *J. Electrochem. Soc.* 116, 242 (1969).
278. A. J. Noreika, *J. Vac. Sci. Technol.* 6, 194 (1969).
279. Y. Hirohata, T. Abe, and T. Toshiro, *Oyo Butsuri* 5, 402 (1976).
280. C. Weissmantel, *Thin Solid Films* 32, 11 (1976).
281. R. F. Bunshah and R. J. Schramm, *Thin Solid Films* 40, 211 (1977).
282. M. Lieberman, *J. Appl. Phys.* 40, 2659 (1969).
283. J. J. Cuomo and W. Reuter, *IBM Tech. Disc. Bull.* 19, 742 (1976).
284. G. Perny and B. Laville-St-Martin, *Thin Solid Films* 6, R25 (1970).
285. T. K. Lakshmanan and J. M. Mitchell, *Trans. Natl. Vac. Symp., 10th, Boston, 1963* p. 335 (1964).
286. J. L. Vossen, *Phys. Thin Films* 9, 1 (1977).
287. T. K. Lakshmanan, *J. Electrochem. Soc.* 110, 548 (1963).
288. L. Holland and G. Siddall, *Vacuum* 3, 375 (1953).
289. J. S. Preston, *Proc. R. Soc. Ser. A* 202, 449 (1950).
290. G. Helwig, *Z. Phys.* 132, 621 (1952).
291. H. Dunschlöder, *Z. Phys.* 137, 383 (1954).
292. F. Lappe, *Z. Phys.* 137, 380 (1954).
293. J. Stuke, *Z. Phys.* 137, 401 (1954).
294. R. R. Mehta and S. F. Vogel, *J. Electrochem. Soc.* 119, 752 (1972).
295. G. L. Harding, *J. Vac. Sci. Technol.* 13, 1070 (1976).
296. J. G. Froemel and M. Sapoff, *Proc. Symp. Deposition Thin Films Sputter., 1st, Univ. Rochester* p. 62 (1966).
297. M. Hecq, A. Hecq, and J. van Cakenberghe, *Thin Solid Films* 42, 97 (1977).
298. G. Perny, *C. R. Acad. Sci., Ser. B* 256, 2160 (1963).
299. G. Perny and B. Laville-St-Martin, *J. Phys. (Paris)* 25, 5 (1964).
300. G. Perny and B. Laville-St-Martin, *J. Phys. (Paris)* 25, 993 (1964).
301. M. Samirani and G. Perny, *C. R. Acad. Sci., Ser. B* 270, 603 (1970).
302. A. J. Purdes, B. T. F. Bolker, J. D. Buccell, and T. C. Tisone, *J. Vac. Sci. Technol.* 14, 98 (1977).
303. M. Samirani, B. Laville-St-Martin, and G. Perny, *Thin Solid Films* 8, 293 (1971).
304. S. K. Banerjee, *Nature (London)* 202, 1098 (1964).
305. J. Heller, *IEEE Trans. Magn.* MAG-12, 396 (1976).
306. V. I. Orlov and G. A. Sarov, *Bulg. J. Phys.* 2, 156 (1975).
307. J. M. Berak and D. J. Quinn, *J. Vac. Sci. Technol.* 13, 609 (1976).
308. J. J. Hantzpergue, Y. Doucet, Y. Pauleau, and J. C. Remy, *Ann. Chim. (Paris)* 10, 211 (1975).
309. F. T. J. Smith, *J. Appl. Phys.* 41, 4227 (1970).
310. C. H. Lane, *Proc. Natl. Electron. Conf.* 20, 221 (1964).
311. F. Huber, W. Witt, and I. H. Pratt, *Proc. Electron. Components Conf., Washington, D.C.* p. 66 (1967).
312. J. S. Preston, U.S. Patent 2,769,778 (1956).
313. A. Thelen and H. König, *Naturwissenschaften* 43, 297 (1956).
314. V. M. Vainshtein and V. I. Fistul, *Sov. Phys.—Semicond.* 1, 104 (1967).
315. V. I. Fistul and V. M. Vainshtein, *Sov. Phys.—Solid State* 8, 2769 (1967).
316. H. K. Muller, *Phys. Status Solidi* 27, 723 (1968).
317. H. K. Muller, *Phys. Status Solidi* 27, 733 (1968).
318. V. M. Vainshtein, L. Gerashimova, and I. N. Nikolsheva, *Izv. Akad. Nauk SSSR, Ser. Mater.* 4, 357 (1968).

319. T. I. Danilina and K. I. Smirnova, *Mikroelektronika (Akad. Nauk SSSR)* 5, 286 (1976).
320. R. M. Valletta and W. A. Pliskin, *J. Electrochem. Soc.* 114, 944 (1967).
321. L. D. Locker, R. W. Landorf, C. L. Naegele, and F. Vratny, *J. Electrochem. Soc.* 119, 183 (1972).
322. F. Shoji and S. Nagata, *Jpn. J. Appl. Phys.* 13, 1072 (1974).
323. T. Abe and T. Yamashima, *Thin Solid Films* 30, 19 (1975).
324. H. J. Spitzer, *J. Vac. Sci. Technol.* 10, 20 (1973).
325. D. Gerstenberg, *Bell Lab. Res.* 42, 364 (1964).
326. J. Spitz and A. Aubert, *Proc. Conf. Chem. Vap. Dep., 5th, Electrochem. Soc., Princeton, N.J.*, p. 258 (1975).
327. H. J. Spitzer, *J. Vac. Sci. Technol.* 9, 333 (1972).
328. S. J. Ingrey and W. D. Westwood, *Appl. Opt.* 15, 607 (1976).
329. A. J. Stirling and W. D. Westwood, *Thin Solid Films* 8, 199 (1971).
330. A. E. Feuersanger, U.S. Patent 3,627,682 (1971).
331. A. E. Feuersanger, M. S. Wasserman, and I. H. Pratt, *Proc. Electron. Components Conf., Washington, D.C.*, p. 52 (1970).
332. F. Lappe, *Phys. Chem. Solids* 23, 1563 (1962).
333. F. Lappe, *Z. Phys.* 137, 380 (1954).
334. J. R. Clarke, A. K. Weiss, J. L. Donovan, J. E. Greene, and R. E. Klinger, *J. Vac. Sci. Technol.* 14, 219 (1977).
335. W. D. Westwood and C. D. Bennewitz, *J. Appl. Phys.* 45, 2313 (1974).
336. K. E. Haq, *Appl. Phys. Lett.* 26, 235 (1975).
337. P. Pileur and J. C. Viret, *C. R. Colloq. Int. Pulver. Cathod., Ist. Montpellier* p. 123 (1974).
338. C. J. Mogab and E. Lugujo, *J. Appl. Phys.* 47, 1302 (1976).
339. W. B. Pennebaker, *Br. Patent* 1,118,757 (1968).
340. A. W. Stephens, J. L. Vossen, and W. Kern, *J. Electrochem. Soc.* 123, 303 (1976).
341. G. J. Kominiak, *J. Electrochem. Soc.* 122, 1271 (1975).
342. C. J. Mogab, P. M. Petroff, and T. T. Sheng, *J. Electrochem. Soc.* 122, 815 (1975).
343. P. C. Y. Chen, *Thin Solid Films* 21, 245 (1974).
344. W. Rothmund and C. R. Fritzsche, *Thin Solid Films* 15, 199 (1973).
345. P. J. Burkhardt and R. F. Marvel, *J. Electrochem. Soc.* 116, 864 (1969).
346. A. R. Janus and G. A. Shinn, *J. Vac. Sci. Technol.* 4, 37 (1967).
347. L. F. Cordes, *Appl. Phys. Lett.* 11, 383 (1967).
348. S. M. Hu, D. R. Kerr, and L. V. Gregor, *Appl. Phys. Lett.* 10, 97 (1967).
349. S. M. Hu and L. V. Gregor, *J. Electrochem. Soc.* 113, 693 (1966).
350. S. M. Hu, *J. Electrochem. Soc.* 113, 693 (1966).
351. E. E. Smith and D. R. Kennedy, *Proc. Inst. Electr. Eng.* 109, 504 (1962).
352. M. M. Nekrasov, V. I. Dudkin, S. V. Smirnova, I. K. Mikhalova, and L. I. Avramenko, *Poluprovodn. Tekh. Mikroelektron.* 3, 20 (1969).
353. R. S. Clark, *Trans. Metall. Soc. AIME* 233, 592 (1965).
354. W. R. Sinclair and F. G. Peters, *J. Am. Ceram. Soc.* 46, 20 (1963).
355. J. C. Williams, W. R. Sinclair, and S. E. Koonce, *J. Am. Ceram. Soc.* 46, 161 (1963).
356. E. Sawatzky and E. Kay, *J. Appl. Phys.* 39, 5613 (1968).
357. S. Mirsch and J. Bauer, *Phys. Status Solidi A* 26, 579 (1974).
358. R. M. Valletta, J. A. Perri, and J. Riseman, *Electrochem. Technol.* 4, 402 (1966).
359. Y. Murayama and T. Takeo, *Thin Solid Films* 40, 309 (1977).
360. J. Chin and M. B. Elsner, *J. Vac. Sci. Technol.* 12, 821 (1975).
- 360a. M. Fukutomi, M. Kitajima, M. Okada, and R. Wanatabe, *J. Electrochem. Soc.* 124, 1420 (1977).

- 360b. D. Kropman, M. Vinnal, and P. Puk, *Vacuum* 27, 125 (1977).
361. R. I. Frank and W. L. Moberg, *J. Electrochem. Soc.* 117, 524 (1970).
362. W. R. Sinclair, F. G. Peters, D. W. Stilling, and S. E. Koonce, *J. Electrochem. Soc.* 112, 1096 (1965).
363. M. Hecq and E. Portier, *Thin Solid Films* 9, 341 (1972).
364. S. Yamanaoka and T. Ohashi, *Jpn. J. Appl. Phys.* 8, 1058 (1969).
365. D. Gerstenberg and C. J. Calbick, *J. Appl. Phys.* 35, 402 (1964).
366. D. Gerstenberg, *J. Electrochem. Soc.* 113, 542 (1966).
367. W. Grossklauß and R. F. Bunshah, *J. Vac. Sci. Technol.* 12, 811 (1975).
368. W. D. Westwood and F. C. Livermore, *Thin Solid Films* 5, 407 (1970).
369. P. R. Stuart, *Vacuum* 19, 509 (1969).
370. W. D. Westwood, D. J. Willmott, and P. S. Wilcox, *J. Vac. Sci. Technol.* 9, 987 (1972).
371. Y. Murayama, *J. Vac. Sci. Technol.* 12, 818 (1975).
372. T. Koikeda and S. Kumagai, *Proc. Symp. Deposition Thin Films Sputter., 3rd, Univ. Rochester* p. 68 (1969).
373. D. Gerstenberg and E. H. Mayer, *Proc. Electron. Components Conf., Washington, D.C.*, p. 57 (1962).
374. A. Sato, Y. Oda, and Y. Hishinuma, *Proc. Electron Components Conf., Washington, D.C.*, p. 58 (1970).
375. M. R. Wormald, B. Y. Underwood, and K. W. Allen, *Nucl. Instrum. Methods* 107, 233 (1973).
376. H. J. Coyne and R. N. Tauber, *J. Appl. Phys.* 39, 5585 (1968).
377. E. A. Buvinger, *Appl. Phys. Lett.* 7, 14 (1965).
378. J. W. Balde, S. S. Charschan, and J. J. Dineen, *Bell Syst. Tech. J.* 43, 127 (1964).
379. M. Nakamura, M. Fujimori, and Y. Nishimura, *Jpn. J. Appl. Phys.* 12, 30 (1973).
380. F. Vratny and D. J. Harrington, *J. Electrochem. Soc.* 112, 484 (1965).
381. W. J. Pendergast, U.S. Patent 3,258,413 (1966).
382. E. Krikorian and R. J. Sneed, *J. Appl. Phys.* 37, 3674 (1966).
383. Y. A. Prokhorov, V. V. Shakhmanov, L. B. Shelyakin, and V. E. Yurasova, *Fiz. Tverd. Tela (Leningrad)* 9, 1398 (1967).
384. W. D. Westwood, R. J. Boynton, and S. J. Ingrey, *J. Vac. Sci. Technol.* 11, 381 (1974).
385. P. Lloyd, *Solid-State Electron.* 3, 74 (1961).
386. W. R. Hardy and D. Mills, *Thin Solid Films* 18, 309 (1973).
387. R. S. Clark and C. D. Orr, *IEEE Trans. Parts, Mater. Packag. PMP-1*, S-31 (1965).
388. L. I. Maissel and J. H. Vaughan, *Vacuum* 13, 421 (1963).
389. W. D. Westwood and N. Waterhouse, *J. Appl. Phys.* 42, 2946 (1971).
390. W. D. Westwood and P. S. Wilcox, *J. Appl. Phys.* 42, 4055 (1971).
391. F. C. Livermore, P. S. Wilcox, and W. D. Westwood, *J. Vac. Sci. Technol.* 8, 155 (1971).
392. L. G. Feinstein and D. Gerstenberg, *Thin Solid Films* 10, 79 (1969).
393. J. Harvey and J. Corkhill, *Thin Solid Films* 6, 277 (1970).
394. N. Waterhouse, P. S. Wilcox, and D. J. Willmott, *J. Appl. Phys.* 42, 5649 (1971).
395. P. N. Baker, *Thin Solid Films* 6, R57 (1970).
396. A. Perinati and G. F. Piacenti, *J. Vac. Sci. Technol.* 14, 169 (1977).
397. S. J. Ingrey, W. D. Westwood, and B. K. MacLaurin, *Thin Solid Films* 30, 377 (1975).
398. G. L. Parisi, *Proc. Electron. Components Conf., Washington, D.C.*, p. 367 (1969).
399. W. R. Hardy, J. Schewschun, D. Kuenzig, and C. Tam, *Thin Solid Films* 8, 81 (1971).
400. W. D. Westwood, *J. Vac. Sci. Technol.* 11, 466 (1974).
401. F. Shinoki and A. Itoh, *Jpn. J. Appl. Phys., Suppl.* 2, Part 1, 505 (1974).
402. A. C. Raghuram and R. F. Bunshah, *J. Vac. Sci. Technol.* 9, 1389 (1972).

403. P. J. Clarke, *J. Vac. Sci. Technol.* **14**, 141 (1977).
404. T. K. Lakshmanan, C. A. Wysocki, and W. J. Slegosky, *IEEE Trans. Component Paris CP-11*, 14 (1964).
405. W. Grossklaus and R. F. Bunshah, *J. Vac. Sci. Technol.* **12**, 593 (1975).
406. L. Lavielle, B. Laville-St-Martin and G. Perny, *Thin Solid Films* **8**, 245 (1971).
407. K. G. Graghty and L. F. Donaghey, *Thin Solid Films* **40**, 375 (1977).
408. J. Duchene, M. Terrillon, and M. Paillly, *Thin Solid Films* **12**, 231 (1972).
409. R. M. Goldstein and S. C. Wigginton, *Thin Solid Films* **3**, 841 (1969).
410. M. Minakata, N. Chubachi, and Y. Kikuchi, *Jpn. J. Appl. Phys.* **11**, 1852 (1972).
411. N. F. Foster, *J. Vac. Sci. Technol.* **6**, 111 (1969).
412. G. A. Rosgonyi and W. J. Polito, *J. Vac. Sci. Technol.* **6**, 115 (1969).
413. D. L. Raimondi and E. Kay, *J. Vac. Sci. Technol.* **7**, 96 (1970).
414. R. A. Mickelsen and W. D. Kingery, *J. Appl. Phys.* **37**, 3541 (1966).
415. N. F. Jackson, E. Hollands, and D. S. Campbell, *Proc. J. IERE/IEEE Conf. Appl. Thin Films Electron. Eng., London* p. 13-7 (1967).
416. R. Blickensderfer, R. L. Lincoln, and P. A. Romans, *Thin Solid Films* **37**, L73 (1976).
417. C. H. Lane and J. P. Farrell, *U.S. Gov. Res. Dev. Rep.* **67**, 73 (1967).
418. J. Harvey and J. Corkhill, *Thin Solid Films* **8**, 427 (1971).
419. R. Vu Huy Dat and C. Baumberger, *Phys. Status Solidi* **22**, K67 (1967).
420. W. J. Takei, N. P. Fornigoni, and M. H. Francombe, *Appl. Phys. Lett.* **15**, 256 (1969).
421. J. G. Titchmarsh and P. A. B. Toombs, *J. Vac. Sci. Technol.* **7**, 103 (1969).
422. J. Deforges, S. Durand, and P. Bugnet, *Thin Solid Films* **18**, 231 (1973).
423. L. F. Cordes, U.S. Patent 3,703,456 (1972).
424. L. V. Kirenskiy, P. Galepov, and A. Turpanov, *Kristallografiya* **11**, 346 (1966).
425. E. Sawatzky and E. Kay, *IBM J. Res. Dev.* **13**, 696 (1969).
426. W. R. Kneib and W. C. Ballamy, *J. Electrochem. Soc.* **122**, 561 (1975).
427. R. B. Liebert and T. H. Conklin, U.S. Patent 3,723,278 (1973).
428. L. D. Locker, C. L. Naegele, and F. Vratny, *J. Electrochem. Soc.* **118**, 1856 (1971).
429. L. D. Locker and D. L. Malm, *Rev. Sci. Instrum.* **42**, 1692 (1971).
430. Y. T. Sihvonen and D. R. Boyd, *Rev. Sci. Instrum.* **31**, 992 (1960).
431. D. R. Boyd, Y. T. Sihvonen, and C. D. Woelke, U.S. Patent 3,235,476 (1966).
432. V. A. Williams, *J. Electrochem. Soc.* **113**, 234 (1966).
433. J. M. Pankratz, *J. Electrochem. Mater.* **1**, 182 (1972).
434. M. Bonnet and M. Marchal, *C. R. Colloq. Int. Pulver. Cathod., Ist. Montipellier* p. 157 (1973).
435. W. W. Molzen, *J. Vac. Sci. Technol.* **12**, 818 (1975).
436. J. A. Thornton and V. L. Hedgcock, *J. Vac. Sci. Technol.* **13**, 117 (1976).
437. H. W. Lehmann and R. Widmer, *Thin Solid Films* **27**, 359 (1975).
438. N. F. Foster, *J. Appl. Phys.* **40**, 420 (1969).
439. D. C. Lewis, W. D. Westwood, and A. G. Sadler, *J. Can. Ceram. Soc.* **33**, 153 (1964).
440. R. Nimmagadda and R. F. Bunshah, *J. Vac. Sci. Technol.* **12**, 815 (1975).
441. W. P. Beckley and D. S. Campbell, *Vide* **99**, 14 (1962).
442. C. J. Ridge, P. J. Harrop, and D. S. Campbell, *Thin Solid Films* **2**, 413 (1968).
443. J. Chin and N. B. Elsner, *Proc. Conf. Chem. Vap. Dep., 5th, Electrochem. Soc., Princeton, N. J.*, p. 241 (1975).
444. V. M. Vaynshteyn, *Sov. J. Opt. Technol.* **34**, 45 (1967).
445. T. Umezawa and S. Yajima, *Thin Solid Films* **29**, 43 (1975).
446. G. Gabor and E. Hahn, *Proc. Symp. Deposition Thin Films Sputter., 3rd, Univ. Rochester*, p. 68 (1969).
447. W. D. Sproul and M. H. Richman, *Thin Solid Films* **28**, L39 (1975).
448. V. K. Sarin, R. F. Bunshah, and R. Nimmagadda, *Thin Solid Films* **40**, 183 (1977).
- 11-1. GLOW DISCHARGE SPUTTER DEPOSITION
449. P. Bugnet, J. Deforges, S. Durand, and G. Battailier, *C. R. Acad. Sci., Ser. B* **269**, 313 (1969).
450. G. L. Harding, D. R. McKenzie, and B. Window, *J. Vac. Sci. Technol.* **13**, 1073 (1976).
451. D. S. Lo, G. F. Sauter, and W. J. Simon, *J. Appl. Phys.* **40**, 5402 (1969).
452. R. Nimmagadda and R. F. Bunshah, *J. Vac. Sci. Technol.* **12**, 585 (1975).
453. S. F. Vogel and I. C. Barlow, *J. Vac. Sci. Technol.* **10**, 381 (1973).
454. J. W. Coburn and E. Kay, *J. Appl. Phys.* **43**, 4965 (1972).
455. O. Christensen and M. Brunot, *C. R. Colloq. Int. Pulver. Cathod., Ist. Montipellier*, p. 37 (1973).
456. O. Christensen and B. J. Klein, *J. Phys. E* **7**, 261 (1974).
457. O. Christensen, *Thin Solid Films* **27**, 63 (1975).
458. L. Holland, *Thin Solid Films* **27**, 185 (1975).
459. P. C. Huang and P. M. Schabie, *Electrochem. Soc. Extend. Abstr.* **76-2**, 754 (1976).
460. F. F. Chen, *In "Plasma Diagnostic Techniques"* (R. H. Huddleston and S. L. Leonard, eds.), p. 113. Academic Press, New York, 1965.
461. L. I. Maissel and P. M. Schabie, *J. Appl. Phys.* **36**, 237 (1965).
462. J. L. Vossen and J. J. O'Neill, *RCA Rev.* **29**, 566 (1968).
463. J. L. Vossen and J. J. O'Neill, *RCA Rev.* **31**, 276 (1970).
464. I. Brodie, L. T. Lamont, and R. L. Jepson, *Phys. Rev. Lett.* **21**, 1224 (1968).
465. D. G. Teer, B. L. Delcen, and A. J. Kirkham, *J. Adhes.* **8**, 171 (1976).
466. D. G. Teer, *J. Phys. D* **9**, L187 (1976).
467. D. G. Teer, *J. Adhes.* **8**, 289 (1977).
468. D. M. Mattox and G. J. Kominiak, *J. Vac. Sci. Technol.* **8**, 194 (1971).
469. R. S. Berg, G. J. Kominiak, and D. M. Mattox, *J. Vac. Sci. Technol.* **11**, 52 (1974).
470. I. V. Mitchell and R. C. Maddison, *Vacuum* **21**, 591 (1971).
471. J. J. Cuomo and R. J. Gambino, *J. Vac. Sci. Technol.* **14**, 152 (1977).
472. W. W. Y. Lee and D. W. Oblas, *J. Appl. Phys.* **46**, 1728 (1975).
473. G. C. Schwartz and R. E. Jones, *IBM J. Res. Dev.* **14**, 52 (1970).
474. E. A. Fagen, R. S. Nowicki, and R. W. Saguini, *J. Appl. Phys.* **45**, 50 (1974).
475. A. G. Blachman, *Metal. Trans.* **2**, 699 (1971).
476. A. G. Blachman, *J. Vac. Sci. Technol.* **10**, 299 (1973).
477. J. J. Cuomo and R. J. Gambino, *J. Vac. Sci. Technol.* **12**, 79 (1975).
478. S. Riggo, G. Amsel, and M. Croset, *J. Appl. Phys.* **47**, 2800 (1976).
479. W. W. Y. Lee and D. W. Oblas, *J. Vac. Sci. Technol.* **7**, 129 (1970).
480. P. H. Schmidt, *J. Vac. Sci. Technol.* **10**, 611 (1973).
481. E. Kay, *J. Vac. Sci. Technol.* **7**, 317 (1970).
482. M. A. Frisch and W. Routhier, *Ann. Conf. Mass Spectrom. Allied Top., 23rd, Houston, Tex.*, 1975.
483. H. F. Winters, D. L. Raimondi, and D. E. Horne, *J. Appl. Phys.* **40**, 2996 (1969).
484. B. Navinsek and T. Zabkar, *Thin Solid Films* **36**, 41 (1976).
485. S. Esho and S. Fujiwara, *AIP Conf. Proc., Magn. Magn. Mater., Am. Inst. Phys., New York* p. 34 (1976).
486. G. A. N. Connell, *Phys. Rev. B* **13**, 787 (1976).
487. H. F. Winters and E. Kay, *J. Appl. Phys.* **38**, 3928 (1967).
488. W. Hoffmeister and M. Zuegel, *Thin Solid Films* **3**, 35 (1969).
489. P. K. Hoff and Z. E. Switkowski, *Appl. Phys. Lett.* **29**, 549 (1976).
490. J. E. Greene, *Surf. Sci.*, to be published.
491. R. J. Gambino and J. J. Cuomo, *J. Vac. Sci. Technol.* **15**, 296 (1978).

11-2

Cylindrical Magnetron Sputtering

JOHN A. THORNTON AND ALAN S. PENFOLD

Telic Corporation
Santa Monica, California

I. Introduction	76
II. Principles of Operation	79
A. Basic Glow Discharge Parameters	79
B. Single Particle Motion	80
C. Mobility and Diffusion	82
D. Plasma Sheaths	83
E. Plasma Waves and Stability	85
F. Cold Cathode Discharges	86
G. Discharge between Coaxial Cylinders in an Axial Magnetic Field	87
H. Formation of Electron Traps	89
I. Anode Considerations	90
III. Cylindrical Magnetron Apparatus	91
A. Cylindrical-Post Magnetrons	92
B. Cylindrical-Hollow Magnetrons	93
C. End Containment	94
D. Magnetic Materials	94
E. Cathode Fabrication	94
IV. Plasma Discharge	98
V. RF Operation	99
VI. Erosion and Deposition Profiles	100
A. Erosion Profile	101
B. Deposition Profile	102
VII. Coating Deposition	102
A. Substrate Environment	105
B. Influence of Operating Parameters on Coating Properties	107
VIII. Reactive Sputtering	109
IX. Summary	110
References	

I. INTRODUCTION

We define magnetrons as diode sputtering sources in which magnetic fields are used in concert with the cathode surface to form electron traps which are so configured that the $E \times B$ electron drift currents close on themselves.

The role of magnetrons in sputtering technology can best be understood by reviewing the limitations of conventional planar diodes. Figure 1 shows a typical planar diode (see Chapter II-1, Sections III and IV). A low pressure abnormal negative glow discharge [1, 2] is maintained between the cathode (target) and an adjacent anode (substrate mounting table). Electrons emitted from the cathode by ion bombardment are accelerated to near the full applied potential in the cathode dark space, and enter the negative glow as so-called primary electrons, where they collide with gas atoms and produce the ions required to sustain the discharge. The primary electron mean free path (mfp) increases with increasing electron energy and decreasing pressure. At low pressures, ions are produced far from the cathode where their chances of being lost to the walls are great; and also many primary electrons hit the anode with high energies, causing a loss that is not offset by impact-induced secondary emission. Therefore, ionization efficiencies are low, and self-sustained discharges cannot be maintained in planar diodes at pressures below about 10 mTorr (1.3 Pa) [3]. Currents are limited because an increase in voltage increases the electron mfp and reduces the ionization efficiency. As the pressure is increased at a fixed voltage, the mfp decreases and larger currents are possible, as shown in Fig. 2. However, at high pressures the sputtered atom transport is reduced by collisional scattering [4]; improvements in deposition rate cease above about 120 mTorr, as shown in the figure. Typical deposition conditions for Ni sputtered in Ar are: cathode-to-substrate separation 4.5 cm, voltage 3000 V, pressure 75 mTorr (10 Pa), current density ~ 1 mA/cm², and deposition rate 360 Å/min.

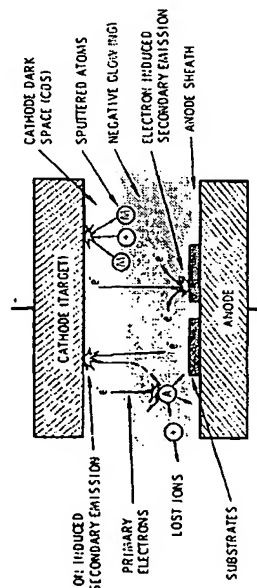


Fig. 1. Schematic representation of the plasma in planar diode sputtering.

II-2. CYLINDRICAL MAGNETRON SPUTTERING

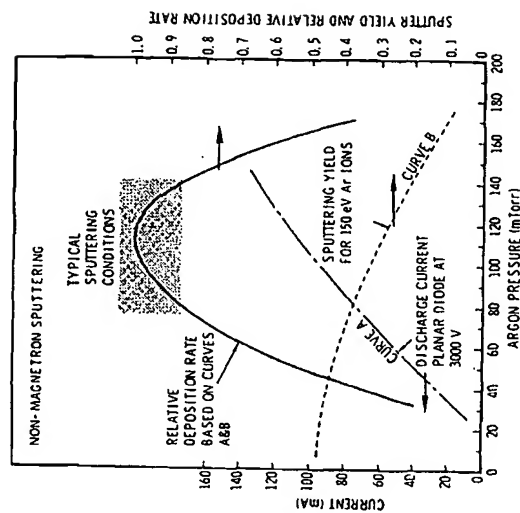


Fig. 2. Influence of working gas pressure on deposition rate for a nonmagnetron sputtering source. The relative deposition rate is calculated for illustrative purposes from the 3000 V discharge current data (curve A) of Kay [3], for a nickel planar diode, and the sputtered atom transport (net yield) data (curve B) of Laegreid and Wehner [4], for a triode with a spherical nickel target.

A magnetic field parallel to the cathode surface can restrain the primary electron motion to the vicinity of the cathode and thereby increase the ionization efficiency. However, the $E \times B$ motion causes the discharge to be swept to one side [5]. This difficulty can be overcome by using cylindrical cathodes which allow the $E \times B$ drift currents to close on themselves. This is the general magnetron geometry. Both post [6-12] and hollow [13] cathodes have been investigated for sputtering. However their performance is limited by end losses.

Remarkable performance is achieved when end losses are eliminated. High currents can be obtained, nearly independent of voltage, even at low pressures. This characterizes what we shall define as the *magnetron mode* of operation. This operation may be achieved with electron-reflecting surfaces which result in the formation of an intense uniform plasma sheet over the cathode, as shown in Figs. 3a and b, or with curved magnetic fields which form a series of plasma rings over the cathode, as shown in Figs. 3c and d. These are all cylindrical magnetrons but the hollow cathode types (Figs. 3b and d) are often called inverted magnetrons. We will

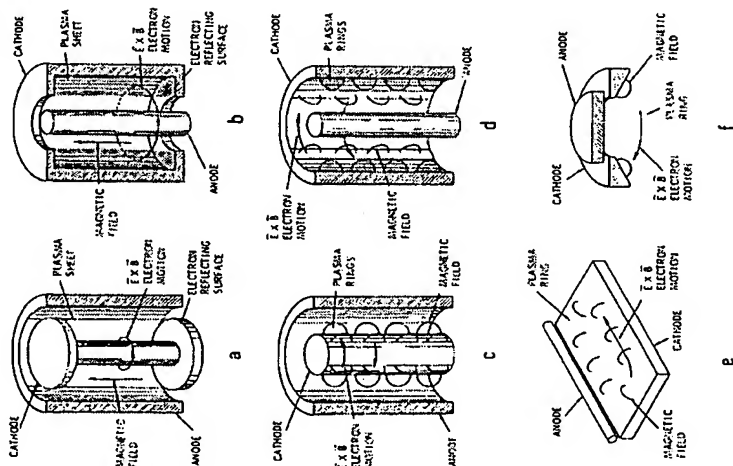


Fig. 3. The configuration of various magnetron sputtering sources: (a)–(d) are cylindrical magnetrons; (b) and (d) are often called inverted magnetrons and sometimes hollow cathodes; (a) is referred to here as a cylindrical-post magnetron and (b) as a cylindrical-hollow magnetron; (e) is the planar magnetron; (f) is often referred to as a sputter gun. In figures vectors are indicated by arrows over the vector quantities.

use the term cylindrical-post magnetron to describe type 3a, and the term cylindrical-hollow magnetron to describe type 3b. The magnetron mode of operation may also be obtained from plasma rings sustained over planar surfaces, as shown in Fig. 3e. These planar magnetrons are discussed in Chapter II-3. When the magnetron mode is obtained from plasma rings sustained on short cylinders or within cylindrical surface cavities, as shown in Fig. 3f, the devices are known as sputter guns. They are discussed in Chapter II-4. The emphasis in this chapter is on cylindrical-post and cylindrical-hollow magnetrons, but the general principles which will be discussed have application to all the devices.

Typical magnetron-mode operating conditions for a cylindrical magnetron are voltage 800 V, magnetic field 150 G, pressure 1 mTorr (0.13 Pa), current density 20 mA/cm², cathode erosion rate 12,000 Å/min, and deposition rate 2000 Å/min. The power is generally dc, but rf may be used. Large cathode sizes are possible. This is an important attribute. Furthermore, substrates are not subject to the plasma bombardment common in planar diodes.

As early as 1921 [14], work on the transport of thermionically emitted electrons in cylindrical magnetrons established the importance of plasma oscillations in both the vacuum [15–17] and plasma cases [18–21] and led to their use in microwave oscillators [22–24]. Townsend discharges have been sustained in the geometries shown in Figs. 3a and b to form pressure gauges [25–28], and low pressure negative space charge discharges have been used in geometries 3a–d to form sputter ion pumps [29–31].

The first operation in the magnetron mode for sputtering appears to have been achieved by Penning and Moubis using configurations 3a [32] and 3b [33]. Very active development of cylindrical magnetron technology has occurred over the period from 1969 to the present [34–40a]. Types of apparatus with the general configurations shown in Figs. 3a–d have been operated. Direct current cathodes have ranged in length from 10 to 200 cm. Both cylindrical-post and cylindrical-hollow magnetrons have been operated with rf power. Direct current magnetron sputtering has recently been reported using configurations 3a [41–43], 3c [42, 44], and 3d [44].

II. PRINCIPLES OF OPERATION

This section reviews certain fundamental concepts of plasma physics relevant to plasma magnetrons and describes the principles of operation of the cylindrical magnetron. These same principles apply to the more complex geometries of the planar magnetron and sputter gun described in Chapters II-3 and II-4.

A. Basic Glow Discharge Parameters

A glow discharge plasma can be defined as a region of relatively low temperature gas which is sustained in an ionized state by energetic electrons. The negative glow, shown in Fig. 1, and the positive column (Section II.F) are examples of glow discharge plasmas [1, 2]. The state of a glow discharge plasma can be characterized by the density of neutral atoms (or molecules) n_A , the electron density n_e , and the electron energy distribution, which can often be approximated by an electron temperature T_e (electrons are frequently maintained in a near-thermal velocity distribu-

tion by electron-electron collisions and the randomizing effects of plasma oscillations [44a]. Electron energies and temperatures are often specified in electron volts, where $1 \text{ eV} = 11600 \text{ K}$ [45]. Average electron energies in glow discharges are typically several electron volts.

Plasmas differ from nonionized gases by their propensity for undergoing collective behavior [45, 46]. Three parameters (derived from n_e , T_e , and n_A) provide useful measures of the tendency toward collective behavior.

The Debye length

$$\lambda_D = 743(T_e/n_e)^{1/2} \text{ cm}, \quad (1)$$

where T_e is in electron volts and n_e in (cubic centimeters) $^{-1}$, is a measure of the distance over which significant departures from charge neutrality can occur. A plasma cannot exist in a space of size L much less than λ_D . The plasma frequency,

$$f_p = \omega_p/2\pi = 9000 (n_e)^{1/2} \text{ Hz}, \quad (2)$$

provides a measure of the tendency for electrostatic waves to develop. Waves can form if $\omega_p \gg \nu$, where ν is the electron collision frequency and ω_p the plasma angular frequency.

A critical degree of ionization [47] can be written as

$$\alpha_c \sim 1.73 \times 10^{13} \sigma_{eA} T_e^{-1/2}, \quad (3)$$

where σ_{eA} (centimeters 2) is the electron-atom collision cross section at the average electron energy. When $n_e/n_A \gg \alpha_c$, long-range Coulomb collisions dominate and the charged particles behave as though they were in a fully ionized gas.

In magnetron plasmas $\lambda_D \ll L$, $\omega_p \gg \nu$, and n_e/n_A is often greater

B. Single Particle Motion

The equation of motion of a particle of charge e , mass m , and velocity \mathbf{v} in an electric field \mathbf{E} and magnetic field \mathbf{B} is [45-46, 48-50]

$$\frac{d\mathbf{v}}{dt} = \frac{e}{m} (\mathbf{E} + \mathbf{v} \times \mathbf{B}). \quad (4)$$

Only the electron motion is influenced by magnetic fields of the strengths used in sputtering sources operating in the magnetron mode.

When \mathbf{B} is uniform and \mathbf{E} is zero, the electrons drift along the field

11-2. CYLINDRICAL MAGNETRON SPUTTERING

81

lines with a speed v_{\parallel} which is unaffected by the magnetic field, and orbit the field lines with a gyro or cyclotron frequency

$$\omega_c = eB/m_e = 1.76 \times 10^7 B \text{ rad/sec}, \quad (5)$$

and at the gyro or Larmor radius

$$r_L = \frac{m_e}{e} \left(\frac{v_{\perp}}{B} \right) = 3.37(W_L)^{1/2}/B \text{ cm}, \quad (6)$$

where B is in Gauss and W_L is the energy associated with the electron motion perpendicular to the field in electron volts. The motion is a helix, as shown in Fig. 4a.

When \mathbf{B} and \mathbf{E} are uniform and \mathbf{E} is parallel to \mathbf{B} , the particles are freely accelerated and the helix pitch increases continuously. When there is an electric field component E_{\perp} (volts per centimeter) perpendicular to \mathbf{B} , a drift of speed

$$v_E = 10^8 E_{\perp}/B \text{ cm/sec} \quad (7)$$

develops in a direction perpendicular to both E_{\perp} and \mathbf{B} and combines with the orbiting motion as shown in Fig. 4b. This is the $\mathbf{E} \times \mathbf{B}$ drift. For a particle created at rest in uniform and perpendicular \mathbf{E} and \mathbf{B} fields, the trajectory becomes the cycloid generated by a circle of radius r_L [given by

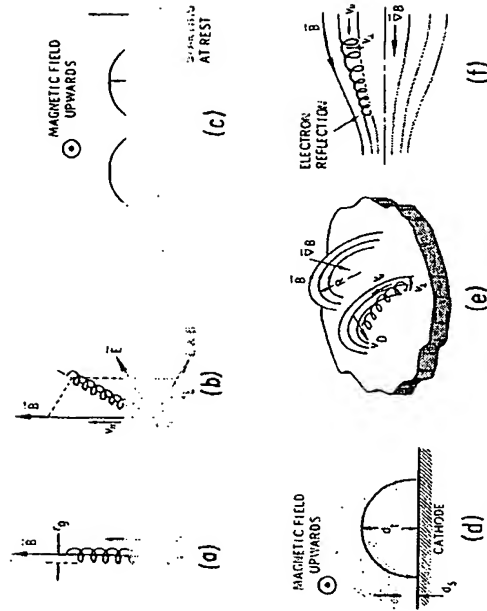


Fig. 4. Electron motion in static electric and magnetic fields.

Eq. (6) with $v_1 = v_E$ from Eq. (7)] moving with velocity v_E as shown in Fig. 4c.

Electrons are emitted from a cold cathode with an initial energy (~ 5 eV) that is small compared to the energy acquired as they are accelerated in the cathode dark space (CDS). Their motion is not exactly cycloidal because the CDS electric field is nonuniform. However, for a planar cathode the distance d_1 to the turning point is given by Eq. (6), with W_1 equal to the total energy which the electrons have gained from the electric field in passing to the turning point [14]. When d_1 exceeds the sheath thickness d_s , as is generally the case in sputtering systems, W_1 is equal to the voltage drop in the CDS (approximately the discharge voltage) and d_1 is easily estimated. The trajectory is shown in Fig. 4d. In the case of thin sheaths ($d_s \ll r_d$) over cylindrical cathodes of radius R_0 , the turning distance d_1 varies from r_s when $R_0 \gg d_1$ to $2r_u$ when $R_0 \ll d_1$ [14].

Curved magnetic fields of the type shown in Figs. 3c-f have an inwardly directed gradient ∇B . Such a gradient is largely perpendicular to \mathbf{B} . It induces a $\nabla B \times \mathbf{B}$ drift that is perpendicular to both \mathbf{B} and ∇B and proportional to v_1^2 . This combines with an identically directed drift caused by the centrifugal force associated with the speed u_0 along the curved field lines [51]. See Fig. 4e. For the circular field lines shown, the total drift can be approximated as

$$v_D \sim (v_1^2 + \frac{1}{2}v_1^2)/\omega_e R, \quad (8)$$

where R is the field radius.

In the region where the magnetic field lines in the magnetrons shown in Figs. 3c-f enter the cathode, there is a gradient ∇B parallel to \mathbf{B} (see Fig. 8c). Electrons moving in such a field tend to conserve their magnetic moment μ_M [52]:

$$\mu_M \equiv m_e v_1^2 / B. \quad (9)$$

Therefore v_1 must increase as they move in the direction of increasing field strength. Conservation of energy then requires that $v_{||}$ decrease, and an electron may be reflected, as indicated in Fig. 4f.

C. Mobility and Diffusion

The current density J_1 which flows across a magnetic field because of a perpendicular electric field E_1 is

$$J_1 = en_e \mu_e E_1 + en_i \mu_i E_1. \quad (10)$$

The electron and ion mobilities are given by [53]

$$\mu_1 = \frac{\mu}{1 + (\omega_e/\nu)^2}, \quad (11)$$

where $\mu = \mu_0 = e/m\nu$ is the mobility in the absence of a magnetic field or along a field line and ν is the collision frequency for the species in question. The diffusion coefficients, which can be written as $D = \mu kT/e$ (where k is the Boltzmann constant), therefore obey similar relationships [54].

Operation in the positive space charge (PSC) magnetron mode (Section I) requires that $\mu_e \gg \mu_i$. In the presence of a sufficiently strong magnetic field so that $\omega_e/\nu \gg 1$ for both the electrons and ions, it can be shown by substituting $\nu_i = e/m\mu_i$ into Eq. (11) that $\mu_e/\mu_i = \mu_i/\mu_e$. Thus $\mu_{e1} < \mu_{i1}$. A typical cylindrical magnetron operates at a pressure of 1 mTorr with a magnetic field strength of 100 G. From Eq. (5), $\omega_{e1} = 2.4 \times 10^4$ rad/sec and $\omega_{e1} = 1.8 \times 10^4$ rad/sec. At 1 mTorr, and an electric field of a few volts per cm, the ion mobility for Ar^+ in Ar is about 10^6 cm²/volt-sec [55, 55a], and $\omega_{e1}/\nu_i = \omega_{e1} m_i \mu_i / e \sim 1$. Thus, from Eq. (11) we see that the ion mobility is only slightly reduced by the magnetic field. Consider electrons with an energy of 10 eV. For degrees of ionization of a few per cent or less, their motion will be dominated by collisions with gas atoms; see Eq. (3). Collision cross sections are shown in Fig. 5. For an electron energy of 10 eV the total cross section is $\sim 2 \times 10^{-19}$ cm² and the collision frequency $\nu_e = n_A \sigma \nu_e$ is about 10^7 sec⁻¹. Thus the calculated mobility μ_e is $\sim 1.5 \times 10^8$ cm²/volt-sec, which is in good agreement with experiment [58a]. However, $\omega_{e1}/\nu_e \sim 180$; consequently, the magnetic field reduced the electron mobility by a factor of more than 10^4 , so that $\mu_{e1} \sim 5 \times 10^3$ cm²/volt-sec and $\mu_{e1} \ll \mu_{i1}$. However, despite this prediction, operation in the PSC magnetron mode still occurs. The transition to a negative space charge mode in cylindrical discharge tubes with central cathodes is not observed until fields of several thousand gauss are used (see Section II.G and [6-12, 59-60]). We ascribe this sustained PSC operation to collective behavior, in the form of plasma oscillations, which fortunately allow the low energy electrons to migrate effectively across fields strong enough to restrain the motion of the primary electrons. Similar anomalous electron transport observed in Penning discharge tubes is also attributed to plasma instabilities [61-64].

D. Plasma Sheaths

Because of their different masses, electrons and ions tend to pass from a plasma to an adjacent surface at different rates. Thus a space charge region, in which one species is largely excluded, forms adjacent to such surfaces. The potential variation between the surface and the plasma is largely confined to this layer, called a sheath [65]. The nature of the sheath depends on the current density passing across it. Except for cases

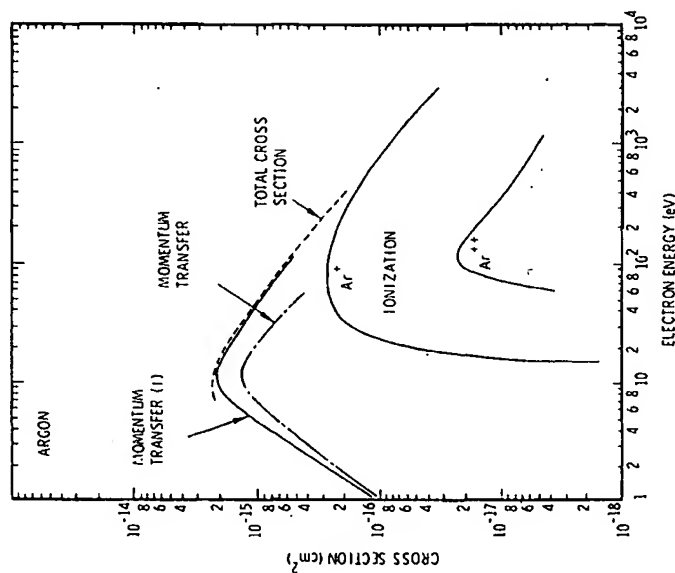


Fig. 5. Collision cross sections for electrons in argon gas. The data are total cross section, Delcroix [47]; momentum transfer (1), Christophorou [56]; momentum transfer (2), Huxley and Crompton [57]; ionization, Kieffer and Dunn [58].

involving very high current densities to anodes, the space charge region will contain primarily particles of the low-mobility species. Thus, for typical magnetron plasmas where $\mu_{e1} \gg \mu_{i1}$ (Section II.C), electrically isolated surfaces within the plasma develop a positive space charge sheath and float at a negative potential relative to the plasma. Substrates surrounding a cylindrical-post magnetron may assume a positive potential of 1 or 2 V_s , probably because of the relatively low electron mobility outside of the intense plasma region.

The cathode dark space is a positive space charge sheath. Such a sheath is shown schematically in Fig. 6. The thickness d_s is taken to be that of the region where the electron density is negligible and where the potential drop V_s occurs. The ion current density J_1 is related to d_s and V_s by the Child-Langmuir law [1, 45]

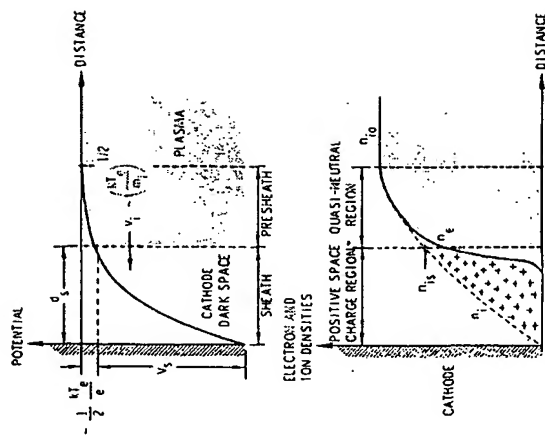


Fig. 6. Schematic representation of the positive space charge sheath that develops over a cathode.

$$J_1 = 27.3(40/M)^{1/2}(V_s^2/d_s^2) \text{ mA/cm}^2, \quad (12)$$

where V_s is in kilovolts and d_s is in millimeters. M is the ion molecular weight. It is difficult to relate J_1 to the density n_{i0} of ions in the bulk plasma, because there is a quasi-neutral presheath region where a potential drop V_0 of the order of $\frac{1}{2}(kT_e/e)$ occurs [45, 66]. For estimates, the presheath density can be assumed to obey a Boltzmann distribution so that $n_{i0}/n_0 = \exp(-eV_0/kT_e)$ and

$$J_1 \sim 0.6en_{i0}(kT_e/m_i)^{1/2}. \quad (13)$$

E. Plasma Waves and Stability

The plasma state is rich in wave phenomena, particularly when a magnetic field is present [45, 46, 67, 68]. The electrons in a magnetron plasma can be pictured as drifting through a sea of relatively stationary atoms and ions in response to the various electric and magnetic field interactions described in Section II.B. Severe departures from charge neutrality, capable of generating waves, can occur in the form of charge bunching and separation over distances of the order of the Debye length. Thus, for example,

charge separation associated with the azimuthal electron drift in a cylindrical magnetron can give rise to plasma oscillations and an azimuthal perturbation electric field which interacts with the axial magnetic field to produce radial $E\rho_z$ electron drift waves [69–72]. A similar effect (diocotron instability) can occur if the radial variation in electron density has a strong maximum within the plasma region [64, 73, 74]. Electron electrostatic waves generated by such charge inhomogeneities can propagate along field lines with frequencies of the order of ω_p , or across field lines with a frequency of the order of $(\omega_p^2 + \omega_{ce}^2)^{1/2}$. Ion electrostatic waves can propagate in all directions at a velocity of the order of $(kT_e/m_i)^{1/2}$. If feedback mechanisms are present, oscillations of the type described above can grow into macroscopic instabilities capable of enhancing electron transport across the magnetic field, as discussed in Section II.C.

Plasma instabilities can also be important in permitting a collisionless exchange of energy between particles within the plasma. Examples are the two-stream instability and Landau damping [45, 46]. Evidence of such energy transfer has been seen between the primary electrons and the negative glow over thermionic cathodes [75, 76]. Electric field oscillations can negate the static field conservation relations that were used, for example, in developing the turning radius criteria discussed in Section II.B. Such oscillations are believed to play an important role in the primary electron energy exchange and in the operation of plasma magnetrons (see Section II.G).

F. Cold Cathode Discharges

A low pressure cold cathode discharge is one which is maintained primarily by secondary electrons emitted from the cathode because of the bombardment by ions from the plasma. These secondary electrons are accelerated in the cathode dark space and enter the negative glow as shown in Fig. 1, where, known as primary electrons, they must produce sufficient ions to release one further electron from the cathode [2]. This requirement can be expressed by the following relationship for the minimum potential to sustain such a discharge [77]:

$$V_{\min} = \frac{\mathcal{E}_0}{\gamma_i \epsilon_e} \quad (14)$$

where γ_i is the number of electrons released per incident ion [the secondary electron coefficient: typically 0.1 for low-energy Ar^+ incident on metals [78]], \mathcal{E}_0 the average energy required for producing ions [about 30 eV for Ar^+ [79]], ϵ_e the ion collection efficiency, and ϵ_e the fraction of the full complement of ions (V/\mathcal{E}_0) that is made by the average primary electron before it is lost from the system. In conventional sputtering systems

II-2. CYLINDRICAL MAGNETRON SPUTTERING

V_{\min} is large because ϵ_i and ϵ_e are small. In magnetron sources, ϵ_i and ϵ_e are near unity but γ_i is believed to be reduced to an effective value of about $\frac{1}{2}\gamma_i$ by electron recapture at the cathode (Section II.G). As a result, $V \approx 2 V_{\min} \approx 20\mathcal{E}_0$.

The negative glow (NG) is the energy exchange region for the primary electrons, and its extent corresponds to the extent of their travel [1, 2]. The electron distribution in the NG consists of primary electrons, ultimate electrons (primaries that have transferred their energy), and much larger numbers of low energy ionization products. In the classical glow discharge a positive column (PC) extends from the NG to the anode. The electric field in the PC is just sufficient to transport the low energy electrons from the NG to the anode and to produce sufficient ionization to make up for wall losses. In conventional sputtering sources the substrates generally intercept the NG, as shown in Fig. 1, and there is no PC. In magnetrons the magnetic field restricts the primary electrons and the NG to the vicinity of the cathode, and a PC-like region can be identified (Section II.G).

A positive or negative space charge sheath will form at the anode, depending on whether the electron thermal flux is greater or less than the discharge current [65]. Thus the anode sheath potential drop, which determines the plasma potential relative to the anode, is strongly dependent on the placement of the anode within the magnetic field.

G. Discharge between Coaxial Cylinders in an Axial Magnetic Field

Consider a cold cathode discharge between a central cathode and a surrounding anode separated by distance D , as shown in Fig. 7, with a magnetic field of such strength that $d_i < d_e < D$ and $\omega_c \gg \nu$. Cylindrical coordinates are used. We neglect end effects (they are considered in the next section) and consider particle motion in the r - θ plane.

The primary electrons are emitted from the cathode with energies of a few electron volts [78] and move in cycloidlike orbits. There is a strong probability of recapture at the cathode. (Electron bombardment-induced secondary emission is generally negligible, since most electrons returning to the cathode have insufficient energy.) It is believed that the recapture probability is reduced by interactions with plasma oscillations [18, 24]. On a random phase basis about one-half will escape recapture and enter the negative glow. One defines an effective secondary emission coefficient Γ_i equal to γ_i times a factor which accounts for the probability of recapture [61, 80, 81]. Thus Γ_i is perhaps close to $\frac{1}{2}\gamma_i$. Secondary emission from the end reflectors (which is unaffected by the magnetic field) is of little signifi-

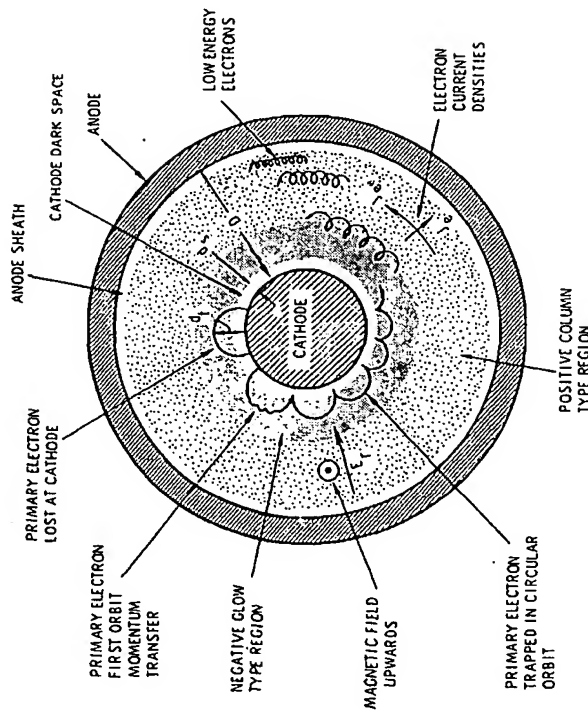


Fig. 7. Schematic representation of electron transport processes in a cold cathode discharge between a cylindrical cathode and a coaxial anode in a uniform axial magnetic field.

cance in most geometries because of the relatively small end reflector area in contact with the intense plasma.

Primary electrons which enter the NG are believed to become trapped on similar cycloidlike paths which orbit, but do not reach, the cathode, as shown in Fig. 7. Collisions in the radial E field beyond the sheath [Eq. (10)] and plasma oscillations cause the electrons to migrate to the anode, but with decreasing azimuthal speed because of a weakening electric field [Eq. (7)] and with reduced gyro radii [Eq. (5)] because of the concurrent energy loss. The azimuthal drifts produce an azimuthal (Hall) current density J_θ equal to $(\omega_c/\nu) J_z$ [82]. The total Hall current is typical an order of magnitude larger than the discharge current and constitutes a solenoidal current that can cause a 10% reduction in magnetic field strength in the vicinity of the cathode.

Such discharges exhibit a bright glow extending a distance of about $2d_1$ from the cathode and a dimmer glow from there to the anode. These regions can be identified as having NG- and PC-like characteristics, respectively.

11-2. CYLINDRICAL MAGNETRON SPUTTERING

89

Essentially identical discharges can be formed in cylindrical-hollow magnetrons. The primary differences are the stronger radial E field in the PC adjacent to the anode (in configurations with axial anodes) and the formation of a negative space charge (NSC) anode sheath if the anode diameter is small.

If the magnetic field is made very strong, the electron mobility can be decreased to the point where a strong electric field and considerable ionization occurs in the vicinity of the anode [6, 8, 9, 59, 60]. A mode of this form (NSC) is particularly pronounced in inverted magnetrons with axial anodes [13]. These conditions have been suggested for sputtering [6, 8, 9], but the magnetron mode (Section I) is vastly superior. Numerous plasma instabilities have been reported when using strong magnetic fields [60, 83–85].

H. Formation of Electron Traps

Effective sputtering requires that the primary electrons be used efficiently ($\epsilon_e \sim 1$) to produce a copious supply of ions in the vicinity of the cathode ($\epsilon_i \sim 1$) [see Eq. (14)]. The ionization collision cross sections are small for the primary electrons (Fig. 5), so that these electrons must be trapped in orbits that permit long travel distances adjacent to the cathode. For cylindrical magnetrons this requirement can be satisfied in the r - θ plane by a magnetic field parallel to the cathode surface. Electrons can thus cross field lines and pass from the cathode only by making the desired energy exchange. However, the electrons can move freely along field lines (Fig. 4a). End losses can be eliminated by installing reflecting surface wings maintained at cathode potential (Figs. 3a,b) or by causing the magnetic field lines to intersect the cathode (Figs. 3c–f). Primary and ultimate electron trajectories for several trap configurations are shown in Fig. 8.

I. Anode Considerations

The low-energy electrons must be removed from the trap to complete the electrical circuit. The anode should be placed within the magnetic field so that it terminates the trap at a point where the primary electrons have dissipated their energy. Plasma oscillations are believed to assist in the migration of low energy electrons across field lines to the anode. Anode placement is further aided by the fact that $\mu_{e\parallel} > \mu_{e\perp}$. Thus in the configuration shown in Fig. 8a, all electrons reaching the radius R are swept into the annular anode located at the end of the cathode; i.e., a virtual anode that does not disrupt the sputtered flux separates the substrates

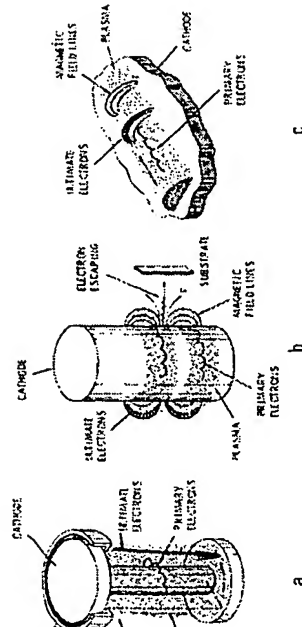


Fig. 8. Schematic representation of primary and ultimate electron trajectories for several electron trap configurations. (Ultimate electrons are defined as primary electrons which have given up most of their energy. Low energy electrons which are the products of the ionization will have identical trajectories.)

from the plasma and removes plasma substrate heating (ions are electrostatically forced to stay in the vicinity of the electrons). Heating can result at substrate positions that intersect field lines, as shown in Fig. 8b.

An anode of insufficient size or with poor placement can cause a significant anode voltage drop. Poor placement can also improperly terminate the trap and permit electrons to reach the substrates. Anode design should take into account the poor mobility of the low-energy electrons in the θ direction in Fig. 8a and the z direction in Fig. 8c.

III. CYLINDRICAL MAGNETRON APPARATUS

Engineering design details affect the operational stability, the profile of substrate coating thickness, and the ability to have long-time trouble-free operation [34, 36-38]. Proper anode placement and design can greatly reduce spurious electrical activity. Proper design of the field coil system allows adjustment of the field shape for optimum performance and allows the shape to be held accurately. The shape of the field is very important in this application, particularly when the ratio of cathode length to electron trap diameter is large. In many cases it is essential that the designer have access to some means for determining and plotting the contours of magnetic flux. With axial symmetry, as in this case, these contours show the shape of the field, and the values determine the degree of saturation in the various magnetic materials which may be present.

11-2. CYLINDRICAL MAGNETRON SPUTTERING

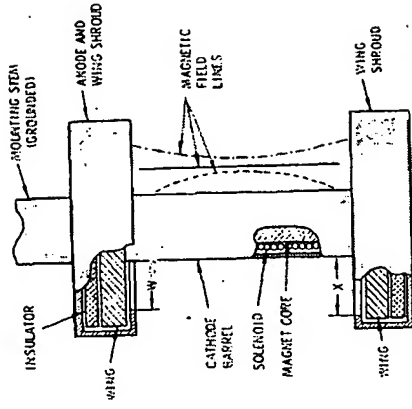


Fig. 9. Representative design of a cylindrical-post magnetron sputtering source.

A. Cylindrical-Post Magnetrons

A cylindrical-post magnetron cathode is a spool formed from a cylindrical barrel and two disklike wings. Figure 9 shows a representative design wherein the dimension of one wing W is smaller than that of the other X . If the magnetic field lines are straight, an intense plasma will form uniformly along the barrel and will extend outward a distance W , whereupon it is terminated abruptly by the anode action of the shroud on the smaller wing, as shown in Fig. 8a. Because electrons in the plasma move with ease along field lines, a virtual anode is projected along the length of the barrel from the smallest wing shroud (Section 11.1). The water cooling means for the barrel, the wings, and the anode are not shown in Fig. 9.

Any metal surface which is at cathode potential but does not face the intense plasma between the wings sputters very slowly. Such a surface receives a net coating which may become oxidized, yielding a surface layer with relatively poor electrical conductivity. This layer is susceptible to intermittent spurious electrical activity in the form of small sparks and occasional power arcs. A power arc constricts the entire discharge current into a small cathode spot which moves rapidly over the surface because of the $E \times B$ motor action. The discharge voltage falls to a small value like 30 V. Metal will be melted at the attachment spot if the current is too high. This type of melting has been found to occur above about 8 A for Al and above 25 A for higher melting point materials like Cr. The power supply must be capable of handling arc conditions and must pre-

vent uncontrolled current flow. The wing shrouds shield the wing insulators (which may be pyrex) from coating material. Small gaps located between the insulators and their metal surroundings prevent degradation of the insulators by the spurious electrical activity. The wing shrouds also prevent material from the sides and edges of the wings from reaching the substrates.

The smallest wing size W should be at least three times larger than the gyro radius of the primary electrons emitted from the cathode. With this criterion the field strength, wing size, and operating voltage are related to each other in the following way [compare with Eq. (6)]:

$$BW = 10V^{1/2} \quad (\text{G-cm}). \quad (15)$$

Fields from 30 to 200 G are usually employed.

A solenoid placed coaxially and externally to the cathode may be used as the field generator. Careful attention must be paid to field curvature resulting from end effects. A solenoid, wound on a core of good magnetic material, may be located within the cathode as shown in Fig. 9. If this solenoid is in contact with cooling water, it must be operated at a negative potential with respect to the cathode to avoid corrosion through pinholes in the insulation. A cathode solenoid by itself will generate a field which is strongly bowed outward (dashed line). The plasma will concentrate toward the midplane of the barrel and the sputter erosion will not be uniform. External and internal solenoids can act in concert to produce bowed in, bowed out, or straight field lines as shown. A field which is straight and parallel to the barrel results in uniform barrel erosion up to within a small distance from the wings. The use of an internal solenoid for field shaping is particularly important for cathodes with a large length to wing size ratio.

The power-weight product for a solenoid of copper wire designed to produce a field of B (gauss) over a diameter D (centimeters) and a length L (centimeters) when operating at a temperature T (degrees Celsius) is

$$PW = (BLD/108)^2(1 + (T/234)) \quad (\text{W-g}). \quad (16)$$

b. Cylindrical-Hollow Magnetrons

The schematic arrangement of a typical cylindrical-hollow magnetron cathode is shown in Fig. 10. Two useful aspects of design are shown. First, the anodes are joined to a tubular backstrap and both are made from magnetic material. This greatly reduces field curvature near the ends and also increases the field strength in the plasma inside the cathode. Second, the solenoid is divided into three or more coils whose current ratios may

11-2. CYLINDRICAL MAGNETRON SPUTTERING

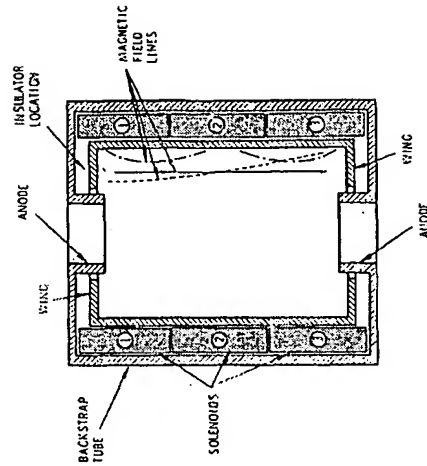


Fig. 10. Schematic arrangement of a typical cylindrical-hollow magnetron sputtering source.

be controlled to provide a wide variety of field shapes including wedges and double traps, as shown. The solenoid sections should be operated in electrical series connection to eliminate changes in field shape caused by unequal heating of the sections. Similar techniques can be used with post cathodes.

C. End Containment

Cylindrical magnetron cathodes may employ end containment which is electrostatic, magnetic, or a combination of the two, depending on how the field is shaped. With straight field lines, electrostatic end containment is used at both ends. Then the cathode sheath thickness at the wings is small. With bowed-out field lines, the ion current drawn to the wings is a small fraction of that drawn to the barrel. Variations of field shape cause other forms of containment to occur. A bowed-out shape causes magnetic containment at both ends. A wedge shape (Fig. 10, dashed line) causes magnetic containment at one end and electrostatic at the other. A multiply bowed field creates multiple traps (see Figs. 3c and d). It is also possible to create multiple traps enclosed by a single trap where the latter has electrostatic end containment [39].

D. Magnetic Materials

Magnetic materials can be sputtered using cylindrical magnetrons. To provide the cathode cylinder is uniformly saturated with magnetic field. To accomplish this with a cylindrical-post cathode the core of the internal solenoid is provided with flanges which make close mechanical contact with the cathode barrel so as to form a closed magnetic structure. Then the barrel can be saturated and the field lines outside the barrel can be accurately straight and parallel to the surface. Great care must be taken to achieve uniform erosion so that the wall thickness of the barrel remains uniform. Variations of voltage with field shape can be used as a diagnostic tool for achieving the required uniformity.

E. Cathode Fabrication

Cathodes of common engineering metals can be easily fabricated from commercially available tube and rod stock. Cathodes of higher purity metals can be formed by vacuum casting or hot pressing. Soft metals such as In, Pb, Sn, and Cd have been cast over tubular sections that contain the vacuum seals. Electroplated or plasma sprayed cathodes can be used when coatings are thin and purity is not critical. Cathodes can also be formed by wrapping sheet on a tubular support. Compounds may be fabricated in cathode shapes by hot pressing. If the compound is porous it may be mounted on a tubular vacuum shell.

IV. PLASMA DISCHARGE

The current-voltage (I - V) characteristic reveals a great deal about the ionization processes in a plasma discharge. Discharges operating in the magnetron mode (Section I) obey an I - V relationship of the form $I \propto V^n$, where n is an index to the performance of the electron trap and is typically in the range 5-9. Thus, with appropriate magnetic field strengths, discharges operate in the magnetron mode at a voltage that is nearly constant and is related to the basic ionization mechanisms by Eq. (14) with $\gamma_i = \Gamma_i$ (see Section II.G). Typical I - V curves for cylindrical-post magnetron operation at various pressures and magnetic field strengths are shown in Fig. 11. If the magnetic field is too weak, the voltage will increase abruptly as shown by A in Fig. 11. Discharges can be stably operated on this part of the characteristic using a constant voltage power supply (41). However, operation in the magnetron mode using a constant current power supply is generally preferred for sputtering.

At a fixed voltage and magnetic field strength the current increases

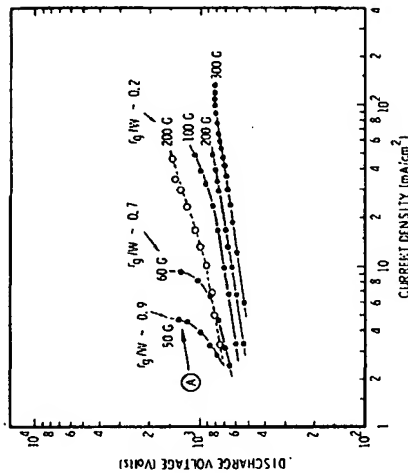


Fig. 11. Typical current-voltage characteristics for a cylindrical-post magnetron sputtering source operating under various conditions of pressure and magnetic field strength. Copper cathode, argon: \bullet , 10 mTorr; \square , 0.5 mTorr.

with pressure (more collision targets to make ionization). At a fixed voltage and pressure the current increases with the magnetic field strength (higher ϵ_i). With proper choice of magnetic field, magnetron mode operation with a near common I - V characteristic has been achieved for a wide range of apparatus sizes in both the cylindrical-post and cylindrical-hollow magnetron configurations, as shown in Fig. 12.

Figure 13 shows the variation of discharge voltage with pressure at constant currents and magnetic fields. The discharge will fail to operate in the magnetron mode if the primary electrons do not exchange sufficient momentum with the plasma during their first cycloidal orbit and are lost at the cathode (Section II.G), or if after entering the trap, they escape without producing the required ionization. The latter action causes the abrupt voltage increase shown at A in Fig. 11 and at B in Fig. 13. The abrupt extinction of the discharge at C in Fig. 13 is believed to result from the first action.

Figure 14 shows the conditions of pressure and magnetic field strength that permitted stable operation of a cylindrical-post magnetron at a current density of 10 mA/cm². The criterion of Eq. (15) establishes a minimum magnetic field strength that must be exceeded even at relatively high pressures, as shown at D in Fig. 14. High field strengths apparently permit lower pressure operation until the magnetic field decreases the cycloidal path to the point where Γ_i is too low to permit the discharge to sustain itself.

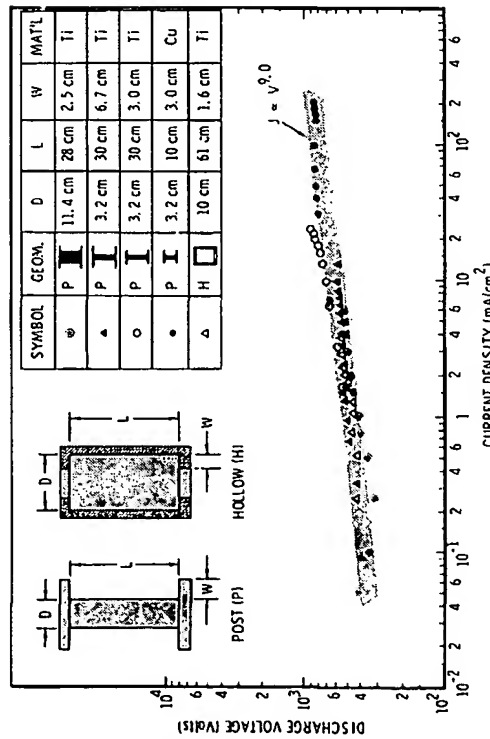


Fig. 12. Current-voltage data for magnetron mode operation of cylindrical-post and cylindrical-hollow magnetron sputtering sources with various geometries.

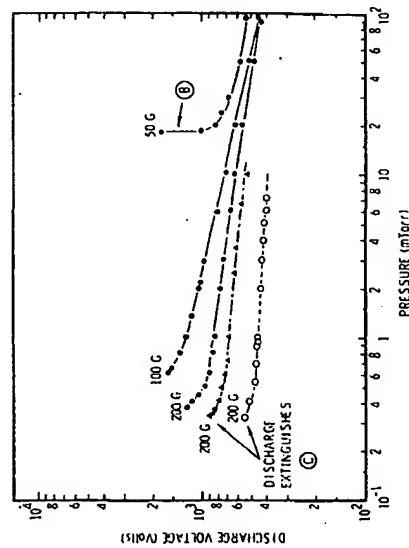


Fig. 13. Operating characteristics of a cylindrical-post magnetron sputtering source, showing the variation of discharge voltage with pressure at constant discharge current and magnetic field strength. Copper cathode (3.2 cm diam. x 30 cm long): ●, current, 3 A, argon; ▲, current, 1 A, argon; ○, current, 1 A, oxygen.

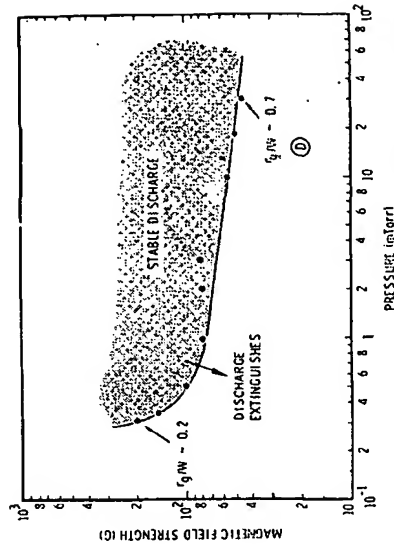


Fig. 14. Conditions of pressure and magnetic field strength for stable operation of a representative cylindrical-post magnetron at fixed current. Copper cathode (3.2-cm diam. x 30 cm long). argon: current density, 10 mA/cm².

Figure 13 shows that operation at the low pressure limit is surprisingly independent of the gas species (compare argon and oxygen data). This behavior is attributed to the role of plasma oscillations in establishing T_e (Section II.G). Oscillations in voltage with amplitudes approaching the applied potential are observed at low pressures just prior to extinguishing of the discharge. Oscillations at frequencies in the range 50–500 kHz, with a maximum frequency that varies inversely with the square root of the working gas atomic mass, have been detected using plasma probes in cylindrical magnetron sputtering sources operating with Ar, O₂, and He [86]. This frequency range is consistent with electrostatic waves oscillating in the discharge cavity, and is about equal to the ion-ion collision frequency. The amplitude tended to increase with increasing magnetic field strength and significantly increased with decreasing pressure.

Electrostatic probe ion density measurements indicate that the degree of ionization in the electron trap is a few percent or less. These measurements are generally consistent with estimates based on the cathode current density using Eq. (13). Gas flux calculations indicate that to allow the observed operating conditions, an Ar atom passing through the discharge must have a 1–30% chance of being ionized, depending on the discharge current and the size of the plasma column.

Typical magnetron operation is at a potential of 700 V (Fig. 11). Measurements with an electrostatic probe placed over the anode of a cylindrical magnetron indicate that the primary electrons exchange essentially all

of their energy in the discharge, implying that $\epsilon_e \sim 1$ [44a, 86]. Γ_i is believed to be equal to approximately $\frac{1}{2}$ (Section II.G). Letting $\%_0 = 30$ eV/ion [79] and using Eq. (13), we obtain $\epsilon_i \sim 0.9$. This collection efficiency for the ions is generally consistent with electrostatic probe measurements at positions beyond the virtual anode.

V. RF OPERATION

Cylindrical magnetrons of various types have been operated successfully as rf devices. Most experience has been with two cylindrical-hollow cathodes placed end to end and driven as a balanced double-ended system. Ion sheaths appear over both cylinders and also over the surfaces of the vacuum envelope. The latter sheath can be eliminated by appropriate electrical adjustment of the system. Operation is best if the magnetic field forms separate traps over each electrode with a common trap joining the two [39].

The voltage on an electrode can rise only slightly above the plasma potential [6, 7, 87–89]. Therefore, on a time-average basis, each electrode is at a negative potential with respect to the plasma. This is the induced bias [87]. The vacuum chamber walls are similarly biased [90]. In a proper system the bias is negligibly small over all surfaces which should not be sputtering.

The action in an rf system is complicated and it is helpful to have a simple model to aid understanding. Suppose the time required for an ion to cross the sheath is large compared to an rf cycle time. This is a reasonable viewpoint for frequencies above a few megahertz. The ions are then unable to follow rf variations of voltage and are accelerated across the sheath by the time-average voltage they experience. This is equal to the negative bias across the sheath. The ions are thus collected at the electrode at a constant rate throughout the cycle. Even though the ion density is independent of time, the sheath thickness is not. It varies as electrons move among the ions. The sheath thickness is maximum when the electrode is most negative with respect to the plasma and is zero when there is no voltage difference. This is a probelike behavior [87]. Thus the electrodes, and the vacuum chamber wall, are cathodes throughout most of the rf cycle and are anodes for relatively brief fractions of the cycle. The total applied voltage is shared among the various sheaths.

Assuming a square wave of line current gives mathematical simplification to the equations of the model and allows solutions to be obtained in closed form [91]. The sheath size is governed by a Child–Langmuir law, just as in the dc case. In the limit of ion current small compared to dis-

placement current, it is found to be

$$JD^2 = 46(40/M)^{1/2}(V/1000)^{3/2}, \quad (17)$$

where D is the maximum size of the sheath during the cycle (millimeters), J the collected ion current density (milliamperes per centimeter²), M the ion mass in atomic units, and V the sheath bias voltage. The latter decreases as the ratio of ion current to displacement current rises and is always less than $\frac{1}{2}$ of the peak voltage which appears between the plasma and the electrode. The constant 46 is 1.7 times larger than that for a dc Child–Langmuir law [Eq. (12)]. The electrode voltage (with respect to the plasma) is a clipped triangular wave. The effective sheath capacity is the ratio of the maximum ion charge in the sheath to the maximum voltage across the sheath. It is found to be $1.1/D$ Pf/cm².

In diode rf sputtering systems without magnetron action, the vacuum chamber forms a giant hollow cathode with electrostatic containment at the walls. This action, along with the fact that the wall area is usually large compared to the target electrode, forms an efficient electron trap at the walls and results in a voltage division which places most of the applied voltage on the target sheath. Thus wall sputtering is effectively suppressed.

The corresponding situation for cylindrical-post magnetrons has not been investigated in detail. However, the foregoing arguments suggest that each magnetic, electric, and geometrical situation must be examined with care to ensure that the action is desirable in all respects. In making judgments the following points may help.

1. Each electrode has a dc bias and tends to act like a dc magnetron sputtering cathode.
2. Ions in front of a given electrode may be produced by primary electrons from some other electrode.
3. An rf probelike behavior is superimposed on the dc picture. This can modify the efficiency of an electron trap during one rf cycle.
4. Magnetic fields offer a strong impedance to the motion of electrons across field lines.
5. Plasma oscillations may play an important role and structured discharge forms may appear [92].

VI. EROSION AND DEPOSITION PROFILES

Agreement is usually obtained between a measured profile of coating thickness and the corresponding calculated one. This gives confidence to predictions made concerning altered configurations. The operating

pressure is usually so low that sputtered material is not gas scattered. Thus, a substrate placed a short distance behind a small pinhole in a plate receives an image of the cathode which pictures in detail the sputter emission rate, as shown in Fig. 15 (note: cathode did not have wing shrouds). A small object placed between the cathode and the pinhole is imaged as a sharp shadow. The law of angular emission of sputtered material may not be a cosine law, but the practical effect on the calculation of profiles is negligible. Sputtering from the cathode wings is too small to require consideration in most cases (see Fig. 15).

A. Erosion Profile

An erosion profile which is uniform along the length of the cathode is usually wanted. Figure 16 shows a representative erosion profile for a cylindrical-post magnetron. Variations in erosion rate around the barrel do not occur (so substrates do not have to be rotated around the cathode).



Fig. 15. Pinhole camera image of a chromium cylindrical-post magnetron cathode formed by sputtered chromium landing on a glass plate placed a small distance behind a mask with a small aperture. The cathode did not have wing shrouds.

II-2. CYLINDRICAL MAGNETRON SPUTTERING

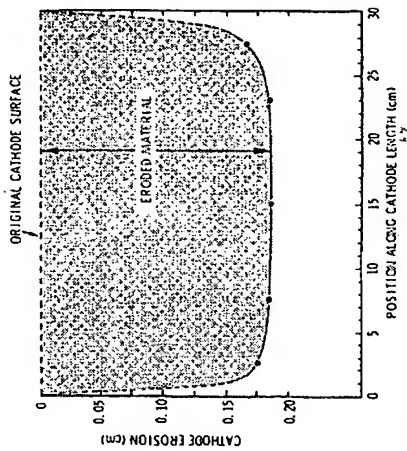


Fig. 16. Sputter erosion of material along the length of a titanium cylindrical-post magnetron cathode (3.2 cm diam. \times 30 cm long). (Note the larger scale for the radial direction.)

With a magnetic material like iron, 3.2-mm thick cathode walls have been employed and over 2 mm have been eroded before wall thickness variations gave rise to deleterious changes of field shape. Thick-walled cathodes can be used with nonmagnetic materials of good thermal conductivity. Aluminum barrels with walls 2.5-cm thick have been employed successfully.

B. Deposition Profile

Consider a substrate whose normal is parallel to the midplane of a post cathode and inclined at an angle θ with respect to the radial direction. Let the substrate be a distance X from the cathode axis and a distance Z from one end of the cathode. Let the cathode have a radius R , length L , and erosion rate C_0 . If the erosion rate is uniform, and the transport is collisionless, the coating rate can be represented by the following formula:

$$C = C_0(R/X)^2 F(X, Z) \cos \theta. \quad (18)$$

The R/X term describes a coating rate which falls off inversely with distance, as expected for a cylindrical system. The function F gives the departure from this ideal behavior because of end losses. The exact equation for F is quite complicated, so an approximation is usually used instead [93]. The approximation has an error smaller than 2% if X/R is larger than

2. The equation approximating F is

$$F = G(a, b_1) + G(a, b_2), \quad (19)$$

where $a = R/X$, $b_1 = Z/X$, and $b_2 = (L - Z)/X$. In terms of a general value b , the function G is given by

$$G(a, b) = G_0(b) + aG_1(b)[1 + aG_2(b)], \quad (20)$$

where

$$G_0(b) = \frac{1}{\pi} \left[\tan^{-1} b + \frac{b}{1 + b^2} \right], \quad (21)$$

$$G_1(b) = \frac{1}{2} \left[\frac{b}{1 + b^2} \right]^2, \quad (22)$$

and

$$G_2(b) = \frac{2}{\pi} \left[\frac{8}{3(1 + b^2)} - 1 \right]. \quad (23)$$

Figure 17 shows a contour map of the function F for a cathode whose length is ten times its diameter. It displays the end effect correction as a function of radial and axial position near the cathode. An auxiliary contour (the dashed line labeled 80%) shows the contour on which the values of F fall to 80% of their values at the midplane of the cathode. This contour is of minimum axial extent at the radial position $X = \frac{1}{2}L$. Roughly speaking, the cathode acts as a line source when the radial position is less than this, and as a point source when it is more than this.

A representative comparison of a measured profile to one which was calculated is shown in Fig. 18.

A hollow cathode whose wall erosion rate is uniform has a special characteristic which makes it well suited for coating objects of complex shape. The coating rate is independent of the orientation of the substrate and is equal to the erosion rate of the walls. This holds true when two conditions are met. First, the substrate surface must be far enough from the ends so that end losses can be ignored. Second, it must have an unobstructed view of the cathode surface [94].

VII. COATING DEPOSITION

A. Substrate Environment

The environment at substrate locations surrounding a cylindrical-post magnetron is considerably different from that in a conventional planar diode sputtering source (see Chapter II-1). Of particular importance is the

II-2. CYLINDRICAL MAGNETRON SPUTTERING

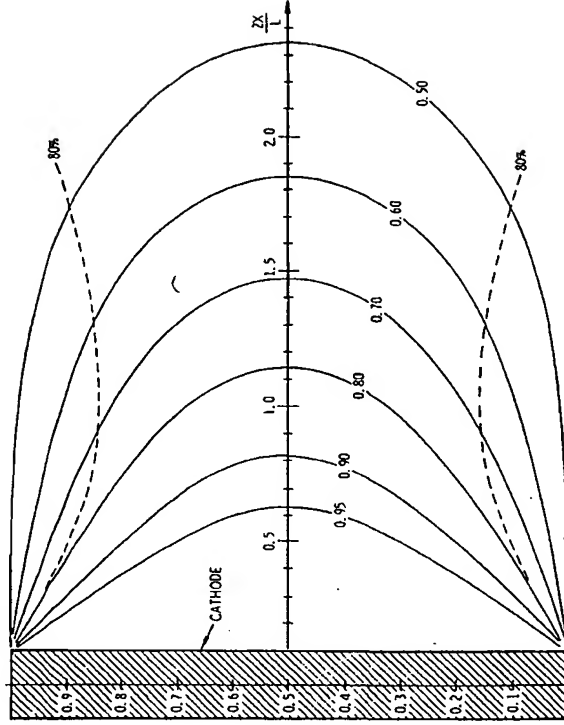


Fig. 17. Contour map for the function F [Eq. (18)] which gives the departure of the deposition rate from ideal inverse- R behavior, due to end losses; based on the assumption of uniform cathode current density, cosine emission, and collisionless transport. Solid lines are contours of constant F . Dashed lines are contours on which F values fall to 80% of their values on the cathode midplane.

fact that the substrates are not in direct contact with the intense plasma (see Fig. 19). Substrates are generally located at radii beyond the virtual anode where the charged particle density due to escaping ions is typically $\frac{1}{10}$ that in the discharge. In the case of a cylindrical-hollow magnetron the charged particle density on the axis is typically about $\frac{1}{3}$ that adjacent to the target wall. (Similar charge particle densities are found in the region of the virtual anode of a cylindrical-post magnetron.)

A second important difference is the wide range of working gas pressures that are possible with magnetrons. Magnetrons can be effectively operated at such low pressures that the mean free path of both the working gas and the sputtered atoms is of the same order of magnitude as the source-to-substrate distance (see Fig. 15). Thus mechanical masks can be effectively used to define deposition areas. Furthermore, the sputtered atoms pass to the substrates with little loss of kinetic energy, as do energetic neutral atoms (ions that are neutralized and reflected at the target surface [95-99]). Atom reflection (Chapter II-1) is believed to be particu-

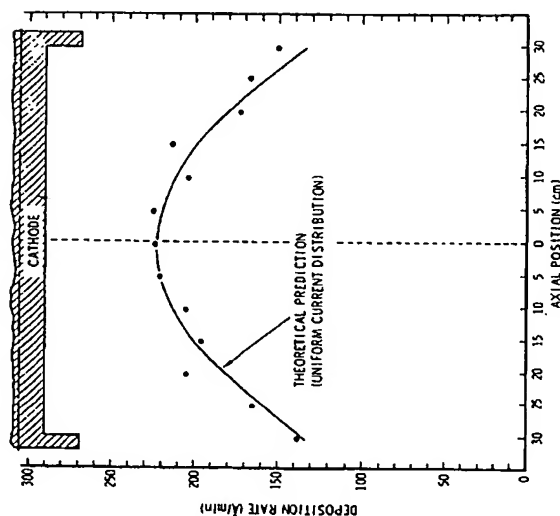


Fig. 18. Comparison between calculated and measured deposition profiles for a chromium cylindrical-post magnetron sputtering source. Argon pressure, 2.5 mTorr; current 8 A; voltage, 830 V; magnetic field, 65 G; and substrate radius, 40 cm.

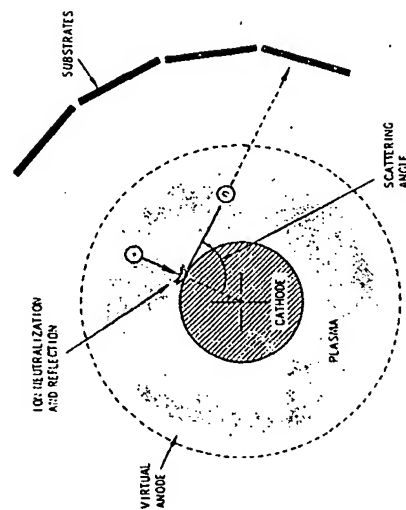


Fig. 19. Schematic representation showing substrate location and atom reflection in a cylindrical-post magnetron sputtering system.

larly important in cylindrical-post magnetrons because atoms undergoing considerably less than 180° reflections pass in the direction of substrates, as indicated in Fig. 19. For binary collisions the cross section and the reflected atom energy increase with decreasing scattering angle [98, 100–102].

The substrate heating is much reduced in magnetrons by the absence of plasma bombardment. Thus plastics, including heat-sensitive membranes, have been effectively coated with metals by using cylindrical-post magnetrons [103]. The heating flux has been found to be proportional to the sputtered flux and to vary from 15 to 25 eV/atom for metals such as Ti, Cr, and Cu to ≈ 50 eV/atom for heavy metals such as Mo, Ta, and W where ion reflection and sputtered atom kinetic energy become more significant and where sputtering yields are moderate [104]. Heating rates can be predicted in most cases. Typical contributions are heat of condensation, 5 eV/atom; kinetic energy of sputtered atom, 10 eV/atom; radiation from plasma discharge, 5 eV/atom; and reflected neutrals, 10 eV/atom. The heating rate per atom increases with decreasing intrinsic sputtering yield. Thus heating rates several times larger are found for dielectric compounds sputtered by rf- or dc-reactive methods. Heating rates per atom are typically a factor of two larger for cylindrical-hollow magnetrons because of the higher plasma density adjacent to the substrates.

Electrically isolated substrates on the axis of a cylindrical-hollow magnetron generally assume a potential of -20 – -50 V relative to the anode. When metals are sputtered, the ion component of the diffusion flux [45, 54] is typically $\frac{1}{4}$ to $\frac{1}{3}$ of the sputtered atom flux. Relatively high potentials (1000–3000 V) are required to achieve current densities effective for bias sputtering because of the low plasma density. In the case of cylindrical-post magnetrons, ion bombardment fluxes are typically only about $\frac{1}{4}$ to $\frac{1}{3}$ of the deposition flux even with an applied negative substrate bias. Substrate sputter cleaning and bias sputtering can often be executed effectively in magnetron devices by designing the substrate holders to form, in concert with the substrates, an effective magnetron electrode that can operate in the existing magnetic field to provide a magnetron-type discharge and a controlled ion flux to the substrate [40].

B. Influence of Operating Parameters on Coating Properties

Figure 20 shows a schematic representation of the influence of substrate temperature and argon working pressure on the structure of metal coatings [105]. The diagram was formulated from thick coating data accumulated using both cylindrical-post and cylindrical-hollow magnetron sources [106]. Zone I is associated with coating flux shadowing due to

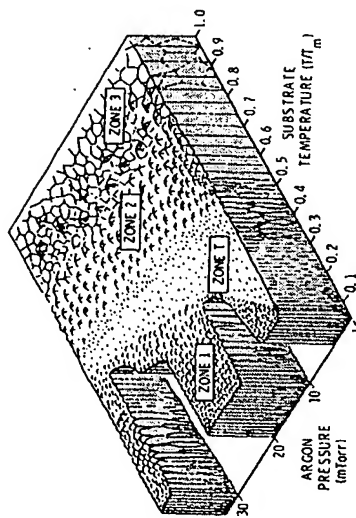


Fig. 20. Schematic representation of the influence of substrate temperature and argon working pressure on the structure of metal coatings deposited by sputtering using cylindrical magnetron sources. T_m is the substrate temperature and P_m is the melting point of the coating material in absolute degrees (from Thornton [106]).

roughness of the substrate and growing coating, and consists of tapered crystals which are poorly bonded [106, 107]. Zone 2 is a transition structure consisting of a dense array of poorly defined fibrous grains [106]. Zone 2 is characterized by evolutionary growth due to adatom diffusion and consists of columnar grains separated by distinct dense intercrystalline boundaries [105, 107, 108]. Zone 3 consists of equiaxed grains and results from bulk diffusion processes such as recrystallization [107]. The exact mechanism by which an inert gas promotes the open Zone 1 structure (see Fig. 20) is not known but is believed to involve a reduction in adatom mobility [106]. The oblique component of the sputtered flux in a cylindrical-hollow magnetron also tends to promote Zone 1 characteristics [106]. The Zone 1 structure may be suppressed by ion bombardment yielding a Zone 2-like structure [109, 110].

Thin films also exhibit the general characteristics of the zone model. Coatings of a number of metals (Al, Ti, V, Cr, Ni, Cu, Zr, Nb, Mo, Ta, and W) deposited using cylindrical-post magnetrons in the thickness range 500–5000 Å have been found to have high optical reflectance, moderate electrical resistivities, and to be in a state of compression when deposited in the Zone 2 region [111–113]. Transition pressures have been identified above which the coatings are in tension, and the resistivity and reflectance become strongly dependent on working gas pressure, increasing and decreasing, respectively, with increasing pressure. The transition pressures, although not exactly the same for the different properties, may signal passage (at constant T/T_m) into Zone 1. Of particular interest is the

observation that the transition pressure increases with atomic mass, varying from about 1 mTorr for Ti to more than 10 mTorr for Ta and W. This dependence is believed to be related to the kinetic energy of the sputtered atoms and to reflected neutrals. The general occurrence of compressive stresses in low-pressure sputtered deposits may be a fundamental characteristic of sputtered metal film growth. It was first observed in cylindrical magnetrons because they can operate below the transition pressure for even the low-mass metals. A few reports of compressive stresses in heavy elements have been made for other devices capable of operating below the transition pressure for heavy materials [114, 115].

VIII. REACTIVE SPUTTERING

Reactive sputtering (see Chapter II-1, Section VI.D) can be effectively done in both cylindrical-post and cylindrical-hollow magnetrons. Working pressures are generally sufficiently low so that gas phase reactions involving the reactive species are unimportant. However, the high circulating electron currents in the plasma (Section II.G) are believed to play an important role in the process chemistry by causing dissociation, excitation, and ionization of the reactive gas molecules. The nonionized active species pass to the substrates and onto the cathode where they have a high probability of chemisorption [116–119] and of being sputtered by the bombardment ions [120]. Ionized reactive gas species have a high probability of being neutralized and reflected as energetic atoms because their mass is generally low [121]. Such scattering is believed to be particularly important in cylindrical-post magnetrons, as shown in Fig. 19. Thus an intense flux of energetic free radicals is generated at the cathode and accompanies the sputtered metal atoms to the substrate, where they are generally capable of overcoming the activation energies associated with film growth. (The cathode-to-substrate transport of these species may be virtually collisionless at low pressures.) This flux, and the species arriving at the substrates directly from the gas phase, may be operative in forming the final compound. An example is copper oxide, where substrate holder rotation has been found to affect the coating composition.

When a reactive-gas-argon mixture is used, an increase in reactive-gas injection causes an increase in the density of reactive species present on the cathode surface and incorporated within the deposited coatings. At a critical injection rate, for otherwise constant sputtering conditions, a transition in operating conditions is generally observed which, for many metal-reactant combinations, is abrupt and involves a significant decrease in deposition rate (see Fig. 21). Such transitions have also been reported by investigators using a variety of conventional apparatus configurations

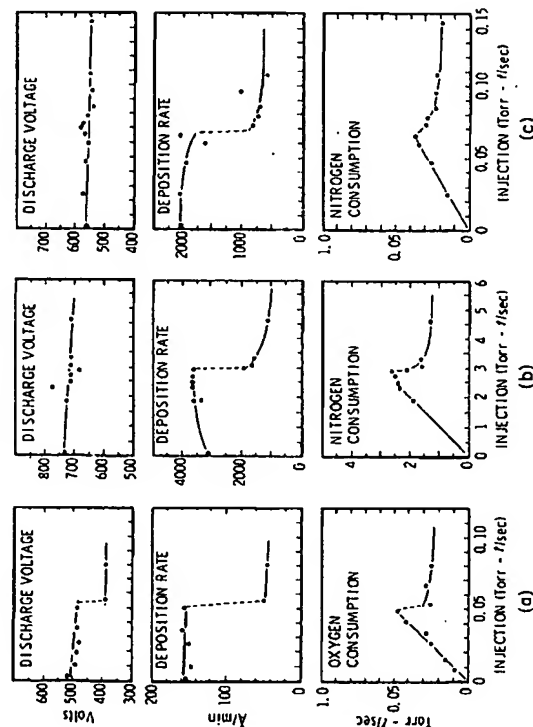


Fig. 21. Discharge voltage, deposition rate, and reactive gas consumption as a function of reactive gas injection rate for reactive sputtering in cylindrical-post and -hollow magnetron sources. The data show abrupt transitions in performance that occur with increasing injection rate at otherwise constant sputtering conditions. Consumption is defined as that injected reactive gas which does not pass into the vacuum pumps. The relatively small consumption at high currents in hollow cathode is due to the small substrate area. (a) cylindrical-post magnetron, chromium-oxygen, current, 1 A, argon pressure, 1 mTorr; (b) cylindrical-cal-post magnetron, niobium-nitrogen, current, 10 A, argon pressure, 1.5 mTorr; (c) cylindrical-hollow magnetron, niobium-nitrogen, current, 10 A, argon pressure, 1.5 mTorr.

[122-127]. The uniformity of the cathode current density and chemistry, and the symmetry, facilitate the interpretation of data from cylindrical-post magnetrons. The transition for a large number of cases has been found to occur when the atomic flux of injected reactive gas is of the same order of magnitude as the total sputtered metal atom flux. Scaling studies for several metals [128] show that over a surprising range of conditions the transition is independent of current density (factor of 10), reactive gas partial pressure (factor of 3), and deposition surface area (factor of 5). The studies imply that the plasma formation of constituents such as radicals is rate limiting under many conditions. The decrease in deposition rate is believed to be associated largely with an increase in the cathode secondary emission coefficient (causing a lowering of voltage) and the formation of cathode surface compounds [124, 129] with low sputtering yields [130].

Similar behavior has been observed in cylindrical-hollow magnetrons (see Fig. 21). An important aspect of these devices is the sputtering of reactive constituents back and forth across the cylinder until they are finally incident on the substrate and incorporated into the coating.

A wide range of materials have been formed using cylindrical-post magnetrons. A few of these include Al_2O_3 , AlN (using N_2), TiO_2 , TiC (using C_2H_2), Cr_2O_3 [131], Fe_2O_3 , Cu_3S (using H_2S), ZrN , NbN [132], CdS (using H_2S), In_2O_3 [133], InP (using PH_3) [134], Ta_2O_5 , TaN , and WO_3 . Similar materials have been formed using cylindrical-hollow magnetrons.

IX. SUMMARY

An operation defined as the magnetron mode can be achieved in diode sputtering sources configured so that magnetic fields, in concert with the cathode surface, form electron traps such that the $\mathbf{E} \times \mathbf{B}$ electron drift currents close on themselves. Primary electrons are injected into such traps by the electric field in the cathode dark space and can escape only by undergoing energy exchange processes of the type required to sustain the discharge. Accordingly, the ionization process is very efficient. High currents and sputtering rates can be achieved, at moderate (~ 1000 V) and near constant voltages, even at low pressure.

This chapter has primarily discussed cylindrical magnetrons that are formed with uniform axial magnetic fields and reflecting surfaces to remove end losses. These have been called cylindrical post- and cylindrical-hollow magnetrons. They can be configured in a wide range of sizes, provided certain requirements on magnetic field strength and uniformity, and reflector size, are satisfied. Post devices with lengths from 10 to 200 cm have been operated with dc. Uniform current densities of over 200 mA/cm² have been achieved. Both post and hollow devices have been operated with rf power.

Long cathodes can provide uniform coatings over large areas. Hollow cathodes are effective for coating complex shaped objects. Substrate plasma bombardment is much reduced, particularly with cylindrical-post magnetrons. A large inventory of coating material can be stored on a cylindrical cathode and used efficiently because of the uniform current density. For applications involving exotic materials, difficulty may be encountered in fabricating cylindrical sputtering targets. When sputtering magnetic materials, the cathode must be of sufficient size to incorporate internal magnetic field coils. Special magnetic field considerations are generally required for in-line systems where the substrates pass by one or more cathodes.

Considerable experience has been accumulated using cylindrical magnetrons in production situations. For example, a cylindrical-post magnetron 10 cm in diameter and 40 cm long has been used to deposit photo-mask quality chromium on glass for over seven years with virtually no maintenance. A cathode of similar size has been used to reliably produce iron oxide coatings by reactive sputtering at a current density of 14 mA/cm².

REFERENCES

1. J. D. Cobine, "Gaseous Conductors," pp. 205-248. Dover, New York, 1958.
2. A. von Engel, "Ionized Gases," pp. 217-253. Oxford Univ. Press, London and New York, 1965.
3. E. Kay, *Tech. Met. Res.* 1, Part 3, 1269 (1968).
4. N. Laegreid and G. K. Wehner, *J. Appl. Phys.* 32, 365 (1961).
5. L. Maissel, in "Handbook of Thin Film Technology" (L. J. Maissel and R. Glang, eds.), p. 4-1. McGraw-Hill, New York, 1970.
6. K. Wasa and S. Hayakawa, *Proc. IEEE* 55, 2179 (1967).
7. K. Wasa and S. Hayakawa, *Microelectron. Reliab.* 6, 213 (1967).
8. K. Wasa and S. Hayakawa, *IEEE Trans. Part. Mater. Packag. PMP-3*, 71 (1967).
9. K. Wasa and S. Hayakawa, *Rev. Sci. Instrum.* 40, 693 (1969).
10. R. F. Tischler, *Soc. Vac. Coaters, Proc. Annu. Tech. Conf. 14th, Cleveland, Ohio* p. 71 (1971).
11. L. Lamont, *NASA Spec. Publ. SP-5111*, 139 (1972).
12. S. Aoshima and T. Asamaki, *Jpn. J. Appl. Phys., Suppl. 2*, Part 1, 253 (1974).
13. W. D. Gill and E. Kay, *Rev. Sci. Instrum.* 36, 277 (1965).
14. A. W. Hull, *Phys. Rev.* 18, 31 (1921).
15. R. L. Jepsen, in "Cross-Field Microwave Devices" (E. Okress, ed.), Vol. 1, p. 251. Academic Press, New York, 1961.
16. J. M. Osepchuk, in "Cross-Field Microwave Devices" (E. Okress, ed.), Vol. 1, p. 275. Academic Press, New York, 1961.
17. K. Mouthaan and C. Susskind, *J. Appl. Phys.* 37, 2598 (1966).
18. J. E. Drummond, in "Plasma Physics" (J. E. Drummond, ed.), p. 332. McGraw-Hill, New York, 1961.
19. S. Saito, N. Sato, and Y. Hatta, *Appl. Phys. Lett.* 5, 46 (1964).
20. S. Saito, N. Sato, and Y. Hatta, *J. Phys. Soc. Jpn.* 21, 2695 (1966).
21. S. Saito and Y. Hatta, *J. Phys. Soc. Jpn.* 26, 175 (1969).
22. J. B. Fisk, H. D. Hagstrum, and P. L. Hartman, *Bell Syst. Tech. J.* 25, 167 (1946).
23. G. B. Collins, in "Microwave Magnetrons" (G. B. Collins, ed.), p. 1. McGraw-Hill, New York, 1948.
24. R. Latham, A. H. King, and L. Rushforth, "The Magnetron," Chapman & Hall, London, 1952.
25. A. H. Beck and A. D. Brisbane, *Vacuum* 11, 137 (1952).
26. J. P. Hobson and P. A. Redhead, *Can. J. Phys.* 36, 271 (1958).
27. P. A. Redhead, *Can. J. Phys.* 37, 1260 (1959).
28. P. A. Redhead, in "Advances in Vacuum Science Technology" (E. Thomas, ed.), p. 410. Pergamon, Oxford, 1960.
29. W. Knauer and E. R. Stack, *Trans. Natl. Vac. Symp., 10th, Boston, 1963* pp. 180-184 (1964).
30. D. Andrew, *Proc. Int. Vac. Congr., 4th, Manchester, England* p. 325 (1968).
31. M. Wutz, *Vacuum* 19, 1 (1969).
32. F. M. Penning and J. H. A. Moubis, *Proc., K. Ned. Akad. Wet.* 43, 41 (1940).
33. F. M. Penning, *Physica (Utrecht)* 3, 873 (1936).
34. A. S. Penfold and J. A. Thornton, U.S. Patent 3,884,793 (1975).
35. A. S. Penfold, U.S. Patent 3,919,678 (1975).
36. A. S. Penfold and J. A. Thornton, U.S. Patent 3,995,187 (1977).
37. A. S. Penfold and J. A. Thornton, U.S. Patent 4,030,996 (1977).
38. A. S. Penfold and J. A. Thornton, U.S. Patent 4,031,424 (1977).
39. A. S. Penfold and J. A. Thornton, U.S. Patent 4,041,353 (1977).
40. J. A. Thornton, U.S. Patent Appl. No. 821,698 (1977).
- 40a. J. A. Thornton, *J. Vac. Sci. Technol.* 15, 171 (1978).
41. K. I. Kirov, N. A. Ivanov, E. D. Atansova, and G. M. Minchev, *Vacuum* 26, 237 (1976).
42. N. Hosokawa, T. Tsukada, and T. Misumi, *J. Vac. Sci. Technol.* 14, 143 (1977).
43. F. R. Arcidiacono, *Proc. Electron. Components Conf., 27th, IEEE, New York* p. 232 (1977).
44. U. Heisig, K. Goodieck, and S. Schiller, *Proc. Int. Symp. Electron Ion Beam Sci. Technol., 7th, Washington, D.C.* p. 129 (1976).
- 44a. J. A. Thornton, *J. Vac. Sci. Technol.* 15, 188 (1978).
45. F. Chen, "Introduction to Plasma Physics," Plenum, New York, 1974.
46. N. A. Krall and A. W. Trivelpiece, "Principles of Plasma Physics," McGraw-Hill, New York, 1973.
47. J. L. Dellecroix, "Introduction to the Theory of Ionized Gases," pp. 128-130. Wiley (Interscience), New York, 1960.
48. L. Spitzer, Jr., "Physics of Fully Ionized Gases," Wiley (Interscience), New York, 1956.
49. J. G. Linhart, "Plasma Physics," North-Holland Publ., Amsterdam, 1960.
50. H. Alfven and C. G. Fälthamar, "Cosmical Electrodynamics," Oxford Univ. Press, London and New York, 1963.
51. Reference 45, pp. 25-26; ref. 46, p. 626.
52. Reference 45, pp. 27-31; ref. 46, pp. 622-623.
53. Reference 46, pp. 328-330.
54. S. Glasstone and R. H. Lovberg, "Controlled Thermonuclear Reactions," pp. 451-469. Van Nostrand, New York, 1960.
55. Reference 2, pp. 114, 124.
- 55a. E. W. McDaniel and E. A. Mason, "The Mobility of Ions in Gases," p. 275. Wiley, New York, 1973.
56. L. G. Christophorou, "Atomic and Molecular Radiation Physics," p. 283. Wiley (Interscience), New York, 1971.
57. L. G. H. Huxley and R. W. Crompton, "The Diffusion and Drift of Electrons in Gases," p. 611. Wiley, New York, 1974.
58. L. J. Kieffer and G. H. Dunn, *Rev. Mod. Phys.* 38, 1 (1966).
- 58a. A. Gilardini, "Low Energy Electron Collisions in Gases," p. 336. Wiley, New York, 1972.
59. S. Hayakawa and K. Wasa, *Electr. Eng. in Jpn (Engl. transl. of Denki Gakka Zasshi)* 83, 36 (1963).
60. S. Hayakawa and K. Wasa, *J. Phys. Soc. Jpn.* 20, 1692 (1965).

61. J. C. Helmer and R. L. Jepson, *Proc. IRE* 49, 1920 (1961).
62. W. Knauer, *J. Appl. Phys.* 33, 2093 (1962).
63. E. H. Hirsch, *Br. J. Appl. Phys.* 15, 1535 (1964).
64. R. F. Mukhamedov, *Sov. Phys.—Tech. Phys.* 18, 1057 (1974).
65. M. H. Mittleman, in "Symposium of Plasma Dynamics" (F. H. Clauser, ed.), p. 54. Addison-Wesley, Reading, Massachusetts, 1960.
66. D. Bohm, E. H. S. Burhop, and H. S. W. Massey, in "The Characteristics of Electrical Discharges in Magnetic Fields" (A. Guthrie and R. K. Wakerling, eds.), p. 13. McGraw-Hill, New York, 1949.
67. J. F. Denisse and J. L. Delcroix, "Plasma Waves," Wiley (Interscience), New York, 1963.
68. T. H. Stix, "The Theory of Plasma Waves," McGraw-Hill, New York, 1962.
69. F. C. Hoh, *Phys. Fluids* 6, 1184 (1963).
70. D. M. Kerr, Jr., *Phys. Fluids* 9, 2531 (1966).
71. E. B. Hooper, Jr., *Phys. Fluids* 13, 96 (1970).
72. D. B. Illic, T. D. Rognien, S. A. Self, and F. W. Crawford, *Phys. Fluids* 16, 1042 (1973).
73. R. H. Levy, *Phys. Fluids* 8, 1288 (1965).
74. W. Knauer and R. L. Poessel, *Proc. Int. Conf. Phenom. Ion. Gases*, 7th, Belgrade, 2, 719 (1966).
75. T. K. Allen, R. A. Bailey, and K. G. Emeleus, *Br. J. Appl. Phys.* 6, 320 (1955).
76. A. B. Cannara and F. W. Crawford, *J. Appl. Phys.* 36, 3132 (1965).
77. A. S. Penfold and J. A. Thornton, in preparation (1978).
78. E. S. McDaniel, "Collision Phenomena in Ionized Gases," Ch. 13. Wiley, New York, 1964.
79. Reference 56, p. 35.
80. P. A. Redhead, *Can. J. Phys.* 36, 255 (1958).
81. R. L. Jepsen, *J. Appl. Phys.* 32, 2619 (1961).
82. G. W. Sutton and A. Sherman, "Engineering Magnetohydrodynamics," p. 394. McGraw-Hill, New York, 1965.
83. S. Hayakawa and K. Wasa, *J. Phys. Soc. Jpn.* 19, 1990 (1964).
84. K. Wasa and S. Hayakawa, *J. Phys. Soc. Jpn.* 20, 1219 (1965).
85. K. Wasa and S. Hayakawa, *J. Phys. Soc. Jpn.* 20, 1732 (1965).
86. J. A. Thornton, in preparation (1978).
87. H. S. Butler and G. S. Kino, *Phys. Fluids* 6, 1346 (1963).
88. P. D. Davids and L. J. Maissel, *J. Appl. Phys.* 37, 574 (1966).
89. R. T. C. Tsui, *Phys. Rev.* 168, 107 (1968).
90. J. S. Logan, J. H. Keller, and R. G. Simmons, *J. Vac. Sci. Technol.* 14, 92 (1977).
91. A. S. Penfold and J. A. Thornton, in preparation (1978).
92. L. T. Lamont, Jr. and J. J. Delone, Jr., *J. Vac. Sci. Technol.* 7, 155 (1970).
93. A. S. Penfold and J. A. Thornton, *Soc. Vac. Coaters, Proc. Annu. Tech. Conf.*, 19th, Toronto p. 8 (1976); *Met. Finish.* 75, 33 (1977).
94. J. A. Thornton and V. L. Hedgcock, *J. Vac. Sci. Technol.* 12, 93 (1975).
95. H. F. Winters and E. Kay, *J. Appl. Phys.* 38, 3928 (1967).
96. I. Brodie, L. T. Lamont, Jr., and R. L. Jepson, *Phys. Rev.* 21, 1224 (1968).
97. W. W. Lee and D. Oblas, *J. Vac. Sci. Technol.* 7, 129 (1970).
98. W. W. Y. Lee and D. Oblas, *J. Appl. Phys.* 46, 1728 (1975).
99. G. Helm and E. Kay, *J. Appl. Phys.* 46, 4006 (1975).
100. F. W. Bingham, Res. Rep. SC-RR-66-506. Sandia Lab., Albuquerque, New Mexico (1966), available from Clearinghouse Fed. Sci. Tech. Inf., Springfield, Virginia.

II-2. CYLINDRICAL MAGNETRON SPUTTERING

101. D. P. Smith, *J. Appl. Phys.* 38, 340 (1967).
102. G. Carter, *J. Vac. Sci. Technol.* 7, 31 (1970).
103. J. A. Thornton, *Soc. Vac. Coaters, Proc. Annu. Tech. Conf.*, 18th, Key Biscayne, Fla., p. 8 (1975); *Met. Finish.* 74, 46 (1976).
104. J. A. Thornton, *Thin Solid Films* to be published (1978).
105. J. A. Thornton, *Ann. Rev. Mater. Sci.* 7, 239 (1977).
106. J. A. Thornton, *J. Vac. Sci. Technol.* 11, 666 (1974).
107. B. A. Movchan and A. V. Demchishin, *Phys. Met. Metall. (USSR)* 28, 83 (1969).
108. J. A. Thornton, *J. Vac. Sci. Technol.* 12, 830 (1975).
109. D. M. Mattox and G. J. Kominiak, *J. Vac. Sci. Technol.* 9, 528 (1972).
110. J. A. Thornton, *Thin Solid Films* 40, 335 (1977).
111. D. W. Hoffman and J. A. Thornton, *Thin Solid Films* 40, 355 (1977).
112. J. A. Thornton and D. W. Hoffman, *J. Vac. Sci. Technol.* 14, 164 (1977).
113. D. W. Hoffman and J. A. Thornton, *Thin Solid Films* 45, 387 (1977).
114. P. R. Stuart, *Vacuum* 19, 507 (1969).
115. R. G. Sun, T. C. Tisone, and P. D. Cruzen, *J. Appl. Phys.* 46, 112 (1975).
116. W. R. Ott and W. L. Fite, *J. Appl. Phys.* 40, 3402 (1969).
117. M. Nagasaka and T. Yamashina, *J. Vac. Sci. Technol.* 8, 605 (1971).
118. R. O. Adams and L. E. Musgrave, *J. Vac. Sci. Technol.* 9, 539 (1972).
119. M. Nagasaka and T. Yamashina, *J. Vac. Sci. Technol.* 9, 543 (1972).
120. H. F. Winters, *J. Vac. Sci. Technol.* 8, 17 (1971).
121. H. F. Winters and D. E. Horne, *Surf. Sci.* 24, 587 (1971).
122. E. Hollands and D. S. Campbell, *J. Mater. Sci.* 3, 544 (1968).
123. J. Harvey and J. Corkhill, *Thin Solid Films* 6, 277 (1970).
124. A. J. Stirling and W. D. Westwood, *Thin Solid Films* 7, 1 (1971).
125. J. Heller, *Thin Solid Films* 17, 163 (1973).
126. T. Abe and T. Yamashina, *Thin Solid Films* 30, 19 (1975).
127. F. Shinoki and A. Itoh, *J. Appl. Phys.* 46, 3381 (1975).
128. J. A. Thornton, *Soc. Vac. Coaters, Proc. Annu. Tech. Conf.*, 20th, Atlanta, Ga., p. 5 (1977).
129. H. F. Winters, *J. Appl. Phys.* 43, 4809 (1972).
130. O. Almen and G. Bruce, *Trans. Natl. Vac. Symp.*, 8th p. 245 (1962).
131. J. A. Thornton, *Proc. Am. Electroplating Soc. Coat. Sol. Collect. Symp.*, Atlanta, Ga., p. 63 (1976).
132. J. A. Thornton and F. M. Kilbane, in preparation (1978).
133. J. A. Thornton and V. L. Hedgcock, *J. Vac. Sci. Technol.* 13, 117 (1976).
134. J. A. Thornton and A. D. Jonath, *Conf. Rec., IEEE Photovoltaic Spec. Conf.*, 12th, Baton Rouge, La., p. 549 (1976).

//-3

The Sputter and S-Gun Magnetrons*

DAVID B. FRASER

Bell Telephone Laboratories
Murray Hill, New Jersey

I. Introduction	115
II. Description	116
III. Operational Characteristics	117
IV. Bias Operation	121
V. Film Deposition	126
VI. Conclusions	128
References	128

I. INTRODUCTION

The Sputter Gun and S-Gun are circular magnetrons invented by Clarke [1]. As in other magnetrons, an intense plasma region is formed near the cathode due to the $E \times B$ field configuration (Fig. 3, Chapter II-2). In common with other magnetrons these sources are high current-low voltage devices operating at relatively low pressures while conventional diode sources tend to be high voltage-low current sources operating at higher pressures. To maximize film deposition rates in conventional sputtering diodes, the cathode is placed close to the substrates which are on the anode, and a maximum potential is applied to the cathode. However, bombardment of the substrate will occur due to the flux of electrons, and thermal degradation of the substrates can result. Magnetrons have high cathode erosion rates and yield useful film deposition rates with substrates supported in planetary or other movable support systems. The cir-

* Sputter Gun® and S-Gun® are registered trademarks of Sloan Technology and Varian Associates, respectively.

cular magnetrons have proven to be very useful for a variety of film deposition requirements.

II. DESCRIPTION

Both of these magnetrons utilize circular cathodes and concentric central anodes. Cross-sectional views are shown in Figs. 1 and 2. The cathodes are clamped without bonding into water cooled housings and in each, contact to the cooled metal surface is achieved through thermal expansion of the cathode during sputtering operation. The anodes are also water cooled and insulated, permitting them to be electrically biased. The cathodes are shown schematically in Figs. 3 and 4 with the B field and the plasma ring. Permanent magnets are used to obtain the magnetic field and values of 0.015 T are typical of the flux density near the cathode. In the S-Gun power densities of about 50 W/cm² are utilized in the erosion zone of the cathode when depositing Al or its alloys with Ar discharges powered at 700 V and 10 A. The dc power supplies are high, constant current devices capable of shutting off and restarting when arcs occur. In sputtering, arcs may occur during start up due to an oxide film or particles on the target surface and also, during operation when a flake of detached film material enters the plasma zone. Conventional dc high current supplies are generally inadequate as a power source for the magnetrons since they lack the necessary arc-suppression characteristics. The effect of power supply output characteristics has to be carefully considered during design in order to achieve efficient operation of the magnetron sputter source. This will be pointed out when specific examples of source operation are discussed.

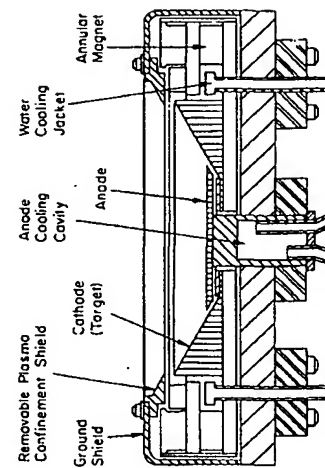


Fig. 1. Cross-section view of the 12.5 cm S-Gun (courtesy Vanian Associates).

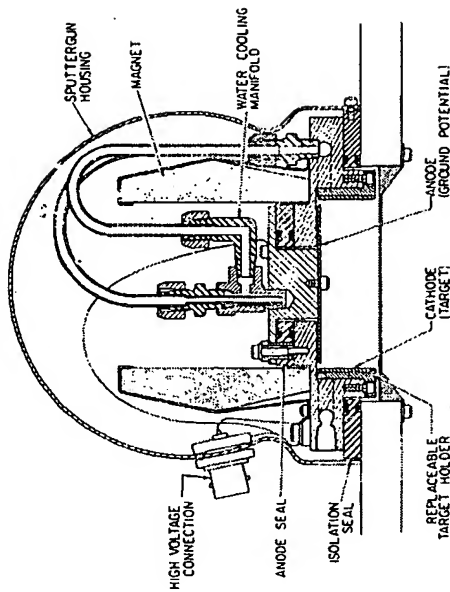


Fig. 2. Cross-section view of the 7.5 cm Sputter-Gun (courtesy of Sloan Technology).

Operation of the circular magnetrons may be accomplished with rf generators as energy sources. The S-Gun may be obtained in an rf model (also capable of being operated in the dc mode) which has shield and insulator differences compared to the dc model. Operation with rf substrate bias is also possible, permitting sputter etching of the substrates *in situ* prior to film deposition.

III. OPERATIONAL CHARACTERISTICS

The current-voltage relationship for a magnetron is dictated by the electron trap [2] formed by the configurations of the electrodes and the magnetic field. In Fig. 5 a typical set of three *I-V* curves is shown for an

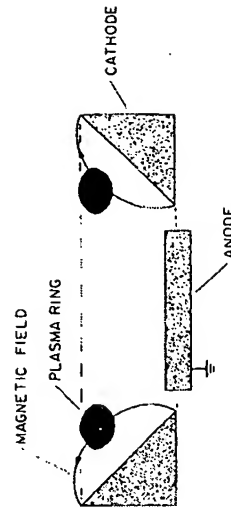


Fig. 3. Cross-section view of the 12.5 cm S-Gun electrodes with B field and plasma ring.

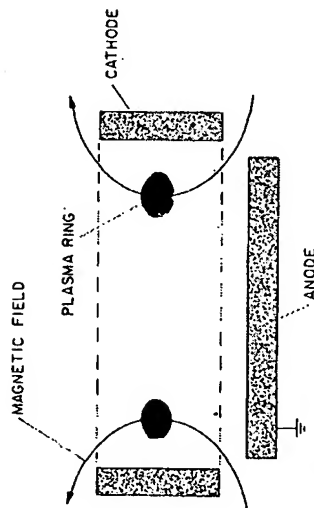


Fig. 4. Cross-section view of the 7.5 cm Sputter-Gun electrodes with B field and plasma ring.

Al target with anode grounded and three different Ar pressures. As the pressure is decreased, the nearconstant voltage characteristic of the high pressure $I-V$ curve is replaced at low pressure by one with an increasing voltage for increasing current. At low pressure, the discharge current is limited by the ionization determined by the magnetic field and electrode configuration. Note that since the target erodes with use, the magnitude of

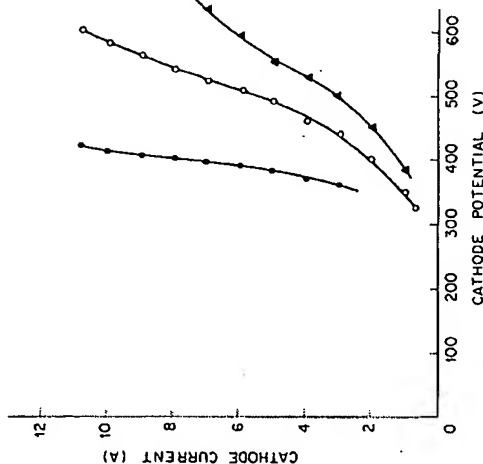


Fig. 5. Current versus cathode potential for 12.5 cm S-Gun with Al cathode, anode grounded and three Ar pressures. Δ , 2.5 mTorr; \circ , 4 mTorr; \square , 10 mTorr.

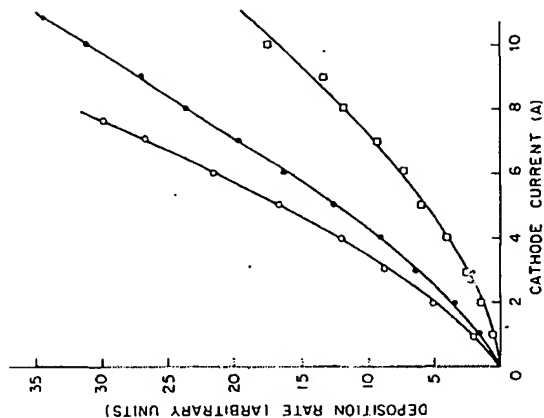


Fig. 6. Deposition rate versus cathode current for 12.5 cm S-Gun with Al cathode, anode grounded, and three Ar pressures. \circ , 2.5 mTorr; \square , 4 mTorr; Δ , 10 mTorr.

the magnetic field increases near the target surface. Hence, the $I-V$ characteristics will change with target use and the target is capable of operating at successively lower pressure. It is for this reason that the design of the S-Gun target was changed from its initial uniform conical surface to one that has a step. This step "breaks in" the target and permits immediate operation of the source at normal pressure and voltages. At pressures of 2 mTorr and above, the S-Gun operates with $I \propto V^n$ with n in the range of 6-7.

In Fig. 6 a set of curves relating Al deposition rate to S-Gun cathode current is shown for three Ar pressures. The anode was grounded in each case. At 2.5 mTorr, the Ar appears to be twice as efficient as at 10 mTorr in producing film deposition; e.g., it takes a current of 8 A to produce at 10 mTorr the same deposition rate obtained at 2.5 mTorr with a current of 4 A. Thus, it is of interest to consider the operation of the S-Gun over a range of Ar pressure in two modes: (a) constant current and (b) constant power. In Fig. 7 the deposition rates in a 48 cm planetary system of Al-2% Si are shown for the two modes over a range of Ar pressures. The source was operated with anode biased at +40 V relative to ground. Note that for small pressure changes, the deposition rate change is less in a con-

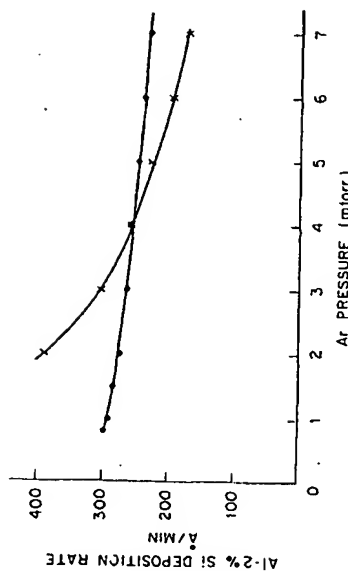


Fig. 7. Deposition rate versus Ar pressure for 12.5 cm S-Gun with Al cathode, anode at +40 V relative to ground and two modes of operation. X, 5 A constant current; ●, constant power.

stant power mode of operation. As the pressure is decreased, the voltage required to sustain a given current increases and the sputtering efficiency increases [3] yielding a higher deposition rate. Reduced gas scatter also occurs at lower Ar pressures and increases the deposition rate in both modes of operation.

The sputter deposition efficiency is determined by the impedance of the magnetron and the characteristics of the power supply. As an example, an Al-0.5% Cu S-Gun target was used to deposit films in a 48 cm planetary system at different Ar pressures with the power supply set at maximum power output and a +40 V bias applied to the anode. Three variables are shown in Fig. 8 as a function of Ar pressure, deposition rate, input power to the cathode, and deposition efficiency. The latter variable is simply the deposition rate divided by the power input to the cathode. Maximum values of deposition rate and power input occurred at 3 mTorr pressure. However, efficiency increased as pressure decreased due to increased cathode potential [3] and reduced gas scatter. In summary, the current output at high pressure and voltage output at low pressure limit the deposition rate achieved with targets possessing excellent heat transfer.

The use of poor thermal conductors as targets may lead to excessive heating and target degradation. Materials with low melting points such as In or In-Sn alloys will melt and fragile materials such as polycrystalline Si and hot-pressed ceramics, crack under the severe thermal stressing of high power input. An unusual effect has been noted in a 99.999% Al S-Gun target with 2 cm and larger grains. Extended operation of this target

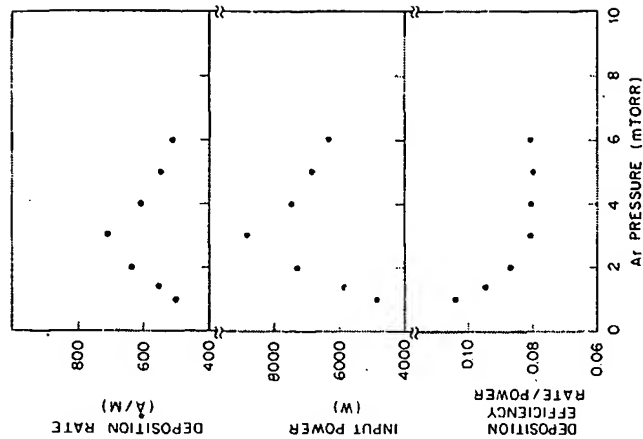


Fig. 8. Deposition rate, input power and deposition efficiency versus Ar pressure for a 12.5 cm S-Gun with Al-0.5% Cu cathode, power supply set at maximum output, and anode at +40 V relative to ground.

at 7 kW (40–50 W/cm²) with adequate cooling water flow led to uniform target shrinkage such that after 60% target use, the diameter had shrunk by 2%. Dilute alloys of Si and Cu in Al have also exhibited shrinkage [4]. Contact with the water cooled jacket may eventually be lost and severe target heating may occur. It is believed that a mass transfer of metal into the bombardment zone occurs, leading to uniform shrinkage of the target. Use of small grained targets appears to reduce the effect.

IV. BIAS OPERATION

Bias may be applied either electrically or magnetically in both types of circular magnetron. Magnetic bias has been used with the 7.5 cm source either to increase or decrease the substrate bombardment during film deposition [5]. Both magnetrons have been biased electrically by use of a pos-

itive potential (relative to ground) applied to the anode. The plasma potential in these sources is a few volts negative with respect to the anode; thus, the use of a high positive potential on the anode causes the magnetron to act as a source of positive ions as well as neutrals.

The use of an auxiliary bias magnet beneath the stationary substrate is shown in Fig. 9 for three cases: an opposing magnet, no magnet, and a magnet in the field aiding configuration. The effect of the bias may be seen in the plot of temperature at the substrates versus time (Fig. 10). From the initial temperature versus time curve slopes, the flux of energy to the substrates may be estimated. These values plus electrical probe data are presented in Table I with deposited Cu film resistivity. All films were deposited in 15 min and were 5000 Å thick. The current at -40 V bias of the electrical probe is an indication of the positive ion flux to the substrate. The highest current corresponds to the highest film resistivity (no bias magnet) and may indicate more entrapped Ar in the Cu film. The fact that

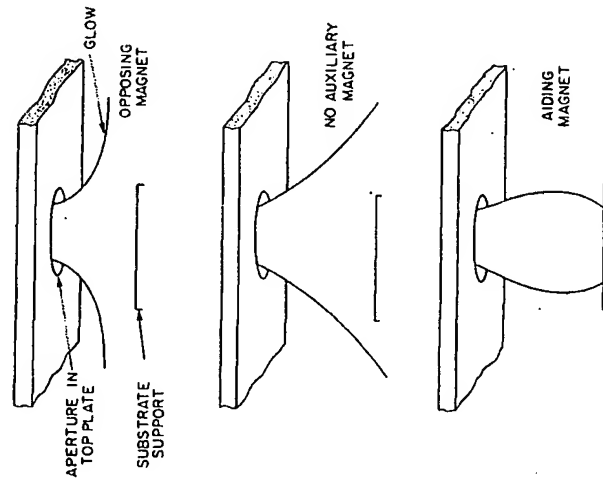


Fig. 9. Influence of a circular auxiliary magnet beneath the substrate support upon the glow extending from a 7.5 cm Sputter Gun. Three cases are shown: (a) opposing magnet, (b) no magnet, and (c) aiding magnet (Fraser and Cook [5]).

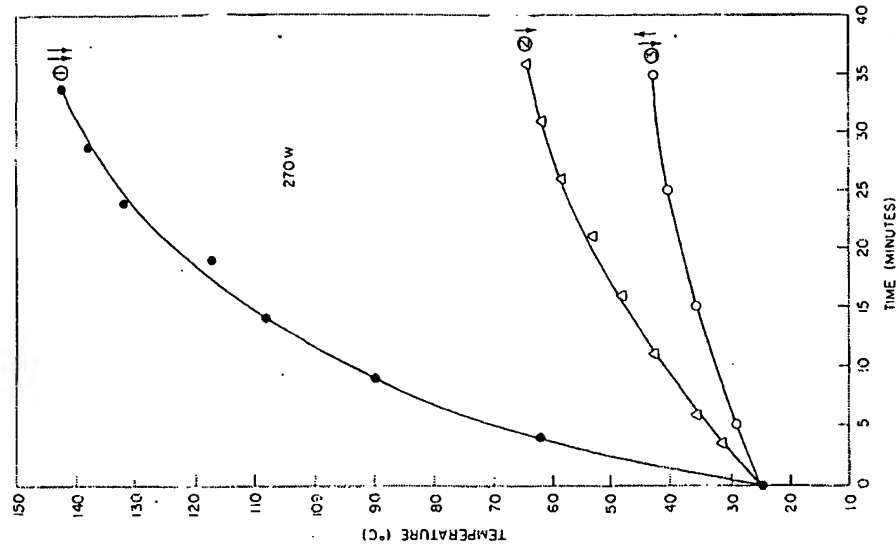


Fig. 10. Temperature versus time as a function of auxiliary magnet orientation for a 7.5 cm Sputter Gun. A power input of 270 W was used in each case (Fraser and Cook [5]).

the Cu film deposition rate was the same in each case indicates that film growth proceeds primarily from the neutral particle flux.

Deposition of indium-tin oxide (ITO) was also performed with and without auxiliary magnets at a power input of 175 W. The results are summarized in Table II. Briefly, the increased energy flux to the substrate with an aiding magnet yields the lowest resistivity while the opposing

Table I
Operating Characteristics and Film Properties for Cu Deposited with Various Magnetic Bias Configurations^a

Magnets	T_f (°C)	Energy flux (W/cm ²)	Probe current (mA/cm ²)	Wall potential (V)	Deposition rate (Å/M)	Resistivity (μΩ cm)	Current Resistivity (at -40 V) (mA/cm ²)
↓ ↓	142	1.4×10^{-1}	1.38	-10.3	330	3.5	0.061
↓ ↓	64	2.6×10^{-2}	0.75	-7.1	330	38	0.084
↓ ↑	42	5.1×10^{-4}	0.05	-3.6	330	13	0.028

^a See Fraser and Cook [5].

magnet yields films of only about 3.5 times higher resistivity. The opposing magnet mode has been used to deposit ITO on 6 μm stretched plastic materials, on emulsion photo masks, and on Cr and iron oxide coated photomasks without thermally degrading the substrates. All of the preceding experiments with the auxiliary bias magnet were performed with the magnetron anode grounded. If the anode is biased positively with respect to ground, the wall potential will rise to a value somewhat lower than the anode potential. For example, when an indium-tin oxide target in 5 mTorr of Ar was biased at -250 V and the anode at +150 V (anode current 0.2 A), the wall potential was +127 V and the grounded probe current was +0.08 mA/cm² at a distance of 19 cm beneath the magnetron aperture. Auxiliary external electrodes may also be used to help confine the discharge. A ring electrode, 18 cm in diameter, centered on the 7.5 cm magnetron axis and just below the magnetron has been used as a plasma potential-determining anode. The experimental layout is shown schematically in Fig. 11. The current to a 1.5 cm² Pt probe, 14 cm below the bottom edge of the ring electrode (19 cm below the magnetron), is shown in Fig.

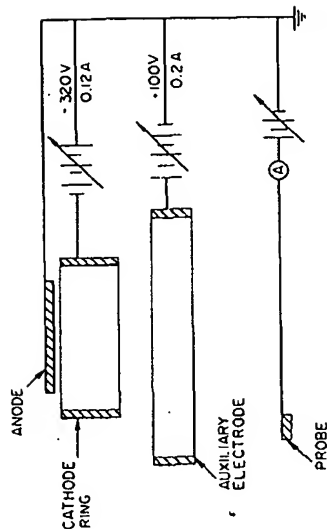


Fig. 11. Schematic view of 7.5 cm Sputter Gun used with an auxiliary external ring electrode.

Fig. 12 for two positions in the chamber as a function of probe voltage. By adjusting the relative removal and deposition rates, film deposition or etching was obtained at the substrate.

In the 12.5 cm magnetron, the use of positive bias of +100 V or more on the anode has led to surface roughening of deposited Al films. Also, the

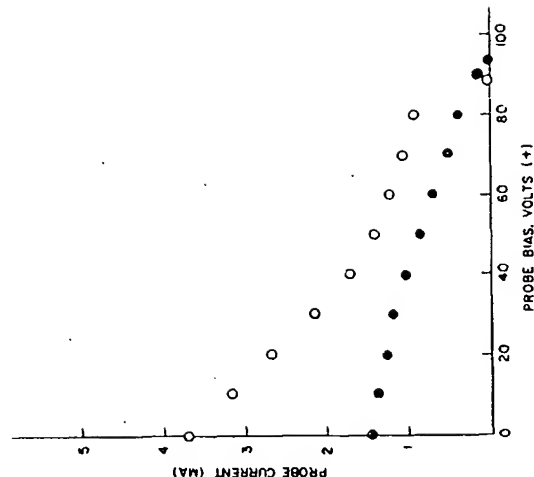


Fig. 12. Current to a 1.5 cm² Pt probe as a function of probe potential (relative to ground) for two positions of the probe. O, centered 19 cm under Sputter Gun; ●, 5 cm off center.

Table II
Deposition Rate and Film Resistivity for ITO Films Deposited under Various Magnetic Bias Conditions^a

Magnets	Deposition rate (Å/M)	Sheet resistance (Ω/□)	Resistivity (μΩ cm)
↓ ↓	573	3.75	215
↓ ↓	459	11	505
↓ ↑	495	14	693

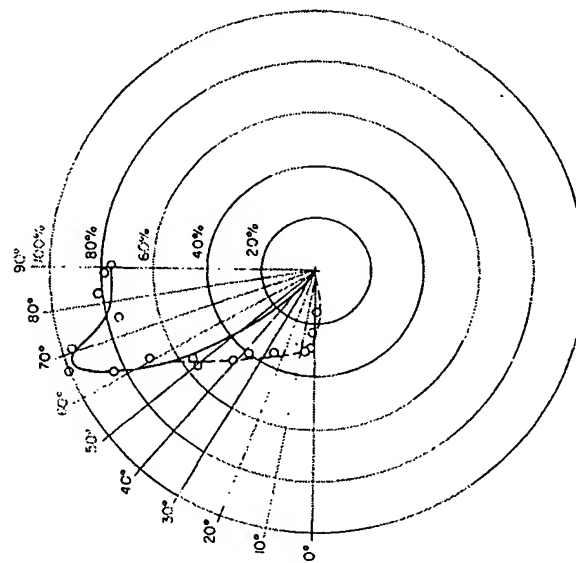
^a See Fraser and Cook [5].

planets used to support the substrates and the stainless steel bell jar became hot ($> 60^\circ\text{C}$) as a result of the energetic bombardment. Thus, bias sputter deposition may be accomplished with both magnetrons and may find application in film step coverage problems [6] and in reactive sputter deposition.

Recently, the application of rf bias to sputter etch planetary-mounted substrates has become available; this feature may find application in bias deposition processes as well as sputter etching.

V. FILM DEPOSITION

In common with other magnetrons, the S-Gun and the Sputter Gun have high target erosion rates and can yield high deposition rates. However, the sources yield a lobe of vapor of sputtered material that requires substrate motion during deposition. As an example, the distribution from an S-Gun obtained by Turner [7] is shown in Fig. 13 with the distribution



$P = 6 \times 10^{-3}$ Torr

Fig. 13. Angular distribution of sputtered material from a 12.5 cm S-Gun; the solid line is the calculated flux from a ring source and the broken line is the measured flux (Turner [7]).

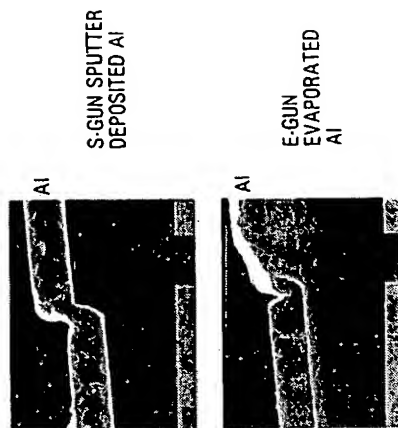
II-3. THE SPUTTER AND S-GUN MAGNETRONS

calculated from an annular source. For low angles, the flux is over cosine and in the side lobes there is a large flux of material in excess of that calculated for the ring source. This characteristic permits the use of domed rotating planetary fixtures with the S-Gun source to achieve deposited film thickness uniformity of $\pm 6\%$ over all substrates. However, the substrate angle relative to the planet shell may have to be changed from that normally used in film deposition with evaporation sources [7].

Flat rotating planetaries are often used with the Sputter Gun to achieve similar film thickness uniformity. Although, power and time parameters can be used to predict deposited film thickness, quartz crystal thickness monitors may be used conveniently with these magnetrons.

Because of the extended source geometry and gas scattering, the circular magnetrons do yield better step coverage in integrated circuit metallization than in single evaporation sources. A comparison of step coverage of electron beam evaporated Al and of S-Gun sputtered Al over similar oxide steps is shown in Fig. 14. The crack evident in the evaporated film is not present in the sputtered film. In the case of the sputter deposited film, the metal thins to 50% of the flat surface thickness at the step. Both films were deposited without any heating before or during deposition. Extreme step geometries such as those involving reentrant angles may require the use of bias sputter deposition [6] to ensure adequate film coverage of the step.

The ionizing radiation present in the plasma of the magnetrons such as long wavelength UV or x-ray photons can cause radiation damage when



COMPARISON OF STEP COVERAGE

Fig. 14. A comparison of step coverage from Al-0.5% Cu films deposited by electron beam evaporation and by S-Gun sputter deposition onto SiO_2 steps.

MOS integrated circuit silicon wafers are metallized. Test wafers Al metallized by filament evaporation, electron beam evaporation, and S-Gun magnetron sputter deposition yielded similar C-V characteristics of temperature and voltage stressed MOS capacitors following high temperature annealing (475°, 30 min) [8]. Similar tests at these laboratories have corroborated the latter results.

In the metallization of integrated circuits, the use of Al-Si alloys to prevent shallow junction penetration [9, 10] or Al alloys containing Cu, Mg, or Cr to retard electromigration and suppress hillock growth is well known [11]. Some of the difficulty in preserving alloy composition in the deposited film is avoided by using magnetron sputter deposition from a single target rather than simultaneous electron beam evaporation from multiple sources. The sputtered films essentially reproduce the composition of source target [8].

Magnetic materials may be deposited by using targets which have been thinned by machining. The thinning operation permits sufficient magnetic field strength to be maintained near the target surface such that magnetron operation is achieved [12].

Reactive sputter deposition of TiN using a Ti target and Ar-N₂ sputtering gas and of ITO using an In-Sn alloy target and Ar-O₂ gas have been performed using dc magnetron operation [13].

VI. CONCLUSIONS

The S-Gun and Sputter Gun, circular magnetrons provide flexible sputter deposition capability for a wide variety of film materials. As for other magnetrons these sources also permit practical film deposition on thermally sensitive substrates.

ACKNOWLEDGMENTS

The author wishes to thank R. E. Kerwin, H. J. Levinstein, A. K. Sinha, and R. S. Wagner for their discussions and encouragement and J. L. Fink for his assistance.

REFERENCES

1. P. J. Clarke, U.S. Patent 3,616,450 (1971).
2. J. A. Thornton and A. S. Penfold, Ch. 11-2.
3. N. Laegreid and G. K. Wehner, *J. Appl. Phys.* **32**, 365 (1961).
4. T. N. Fogarty, D. B. Fraser, and W. J. Valentine, *J. Vac. Sci. Technol.* **15**, 178 (1978).
5. D. B. Fraser and H. D. Cook, *J. Vac. Sci. Technol.* **14**, 147 (1977).
6. J. L. Vossen, *J. Vac. Sci. Technol.* **8**, S12 (1971).

11-3. THE SPUTTER AND S-GUN MAGNETRONS

7. F. T. Turner, *Varian Seminar Proc.: Thin Film Coat., Ion Implant. Auger Surf. Anal., Palo Alto, Calif.* 1975.
8. R. W. Wilson and L. E. Terry, *J. Vac. Sci. Technol.* **13**, 157 (1976).
9. J. R. Black, *J. Electrochem. Soc.* **115**, 242C (1968).
10. P. A. Totta and R. P. Sopher, *IBM J. Res. Dev.* **13**, 226 (1969).
11. A. Gangulee and F. M. d'Heurle, *Appl. Phys. Lett.* **19**, 16 (1971).
12. V. Hoffman, Varian Associates, personal communication (1976).
13. P. J. Clarke, *J. Vac. Sci. Technol.* **14**, 141 (1977).

11-4

Planar Magnetron Sputtering

ROBERT K. WAITS

Data Systems Division
Hewlett-Packard Company
Cupertino, California

I. Introduction	131
II. DC Planar Magnetron Sputtering	134
A. System Configuration	134
B. Thickness Uniformity Control	142
C. Voltage, Current, and Pressure Relationships	148
D. Deposition Rate	150
E. Substrate Effects	157
F. Power Supplies	160
G. Miscellaneous Techniques	162
III. RF Planar Magnetron Sputtering	163
A. Comparison of RF and DC PM Sputtering	164
B. Power Density, DC-Self-Bias, and Pressure Relationships	164
C. Rate Limitations and Rate Control	165
D. Power Supplies and Matching Networks	166
E. Deposition Rates	166
IV. Applications	167
A. Industrial Coating	167
B. Thin Film Electronics	167
C. Miscellaneous Applications	169
V. Conclusions	170
References	170

I. INTRODUCTION

The planar magnetron (PM) has emerged as an elegant embodiment of the long-sought [1, 2] high-rate sputtering source. In essence, it is the classic dc or rf sputtering arrangement consisting of a planar cathode and its

131

surrounding dark-space shield (Chapter II-1) with the essential addition of permanent magnets directly behind the cathode. The magnets are arrayed so that there is at least one region in front of the cathode surface where the locus of magnetic field lines parallel to the cathode surface is a closed path. Although there are many variations in geometry, all have in common a closed path or region in front of a substantially flat cathode surface where the magnetic field is normal to the electric field. Bounding this region, the magnetic field lines enter the cathode surface. Ideally, at the point of entry the field lines are normal to the cathode face. The magnetic field can be supplied by electromagnets, but at the loss of simplicity.

The discharge plasma (ionization region) is constrained to an area adjacent to the cathode surface by one or more endless toroidal electron-trapping regions bounded by a tunnel-shaped magnetic field. The same principle can be applied to tubular and other nonplanar surfaces, but this discussion will be limited to planar structures. The basic principle of all magnetically enhanced sputtering techniques was discovered by Penning [3] and further developed by Kay and others [4-8], ultimately spawning the Sputter Gun (Chapter II-3) and cylindrical magnetron (Chapter II-2) sources. Penning's work had led earlier to the invention of the getter-ion pump [9], the development of which also indirectly contributed to the understanding [10, 11, 11a] and evolution of magnetically enhanced sputtering sources [12].

The planar magnetron structure is an example of an embarrassingly "obvious" solution to a technological problem that eluded discovery and implementation for more than 30 years. One of the first descriptions of a planar magnetron device may have been that of Kesaev and Pashkova [13] who, in mercury arc lamp studies, used an electromagnet to stabilize a plasma on the surface of a mercury pool (Fig. 1). Striking photographs of circular and square (!) plasma regions were published. The use of permanent magnets inside a tubular cathode for an ion pump application was reported by Knauer and Stack [11]. Once again, photographs clearly showed multiple toroidal plasma rings surrounding the cylindrical cathode. This work led to a patent [11a] for ion pump structures that included two disk planar magnetron configurations. These devices were either overlooked or ignored by those intent on developing high-rate sputtering.* Some 15 years later the principle was reintroduced in the form of the planar magnetron by Chapin [14]. This work was not overlooked. Within one year PM sputtering was included in a review of deposition technology

* In 1969 research at the CVC division of Bendix Company led to a planar magnetron sputtering source in the form of a long rectangle. The plasma was thermionically supported and the magnetic field, supplied by permanent magnets, did not form a closed "tunnel" [13a].

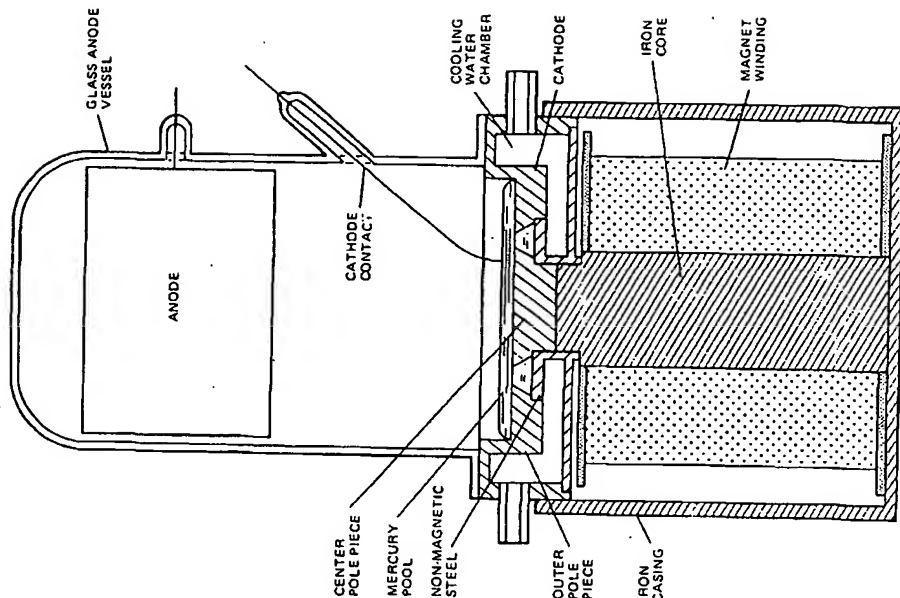


Fig. 1. Cross section of device for electromagnetic (planar magnetron) anchoring of cathode spot in mercury-discharge lamp (after Kesaev and Pashkova [13]).

[15], further developed [16, 17], and independently reported [18, 19]. By early 1975, versions of the PM sputtering source were available commercially from several manufacturers [17, 20]. By 1976, if not earlier, both rf and dc planar magnetron sputtering were being used in daily production. Planar magnetron sputtering has recently been reviewed [21], and was briefly mentioned in a recent review of glow discharge sputtering [22].

For a general discussion of the theory of operation of magnetron sputtering sources, see Chapter II-2, Section II. The applications of PM sputtering are wide ranging and are discussed in Section IV.

Schiller *et al.* [23] have used the term "ring gap plasmatron" to describe PM sputtering sources. However, the words "plasmatron" and "duoplasmatron" have been used previously to describe certain gas discharge tubes and particular classes of ion-beam sources [23a]. "Magnetron" has generally evolved as an inclusive term describing devices operating with crossed electric and magnetic fields (including microwave electron tubes, some ionization vacuum gauges, and sputtering sources).

II. DC PLANAR MAGNETRON SPUTTERING

A. System Configuration

A typical sputtering system would be similar to those discussed in Chapter II-1, Section IV. A planar cathode (sputtering source or target) is parallel to an anode surface, usually grounded, that serves as a substrate holder or carrier. One simple geometry is a disk-shaped cathode having a toroidal plasma ring facing and parallel to a fixed planar substrate holder [14, 23]. An alternative arrangement is a rectangular (or oval) cathode in conjunction with a means whereby the substrates are moved continuously in a direction perpendicular to the cathode width during deposition [16, 17, 24]. The plasma region is in the shape of an elongated ring which, in the case of a long cathode, behaves as two parallel line sources. The two configurations are shown in Fig. 2.

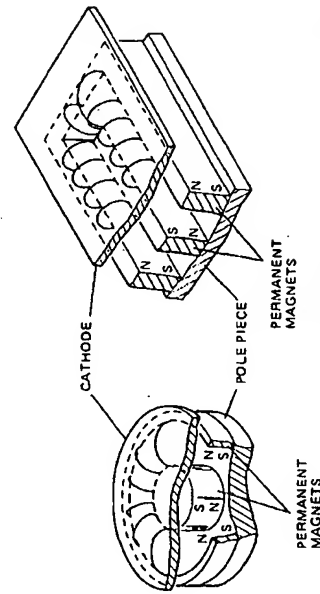


Fig. 2. Circular and rectangular planar magnetron sputtering sources. Curved lines represent magnetic field lines.

1. Cathode and Magnet Geometry

Magnet arrangements can be varied substantially, the only constraints being those of geometry and the requirement that there be at least one closed path where the magnetic field lines are parallel to the cathode surface. For example, the paths may be single or multiple circles or ovals, concentric circles or ovals, or cloverleaf or multilobed [11] patterns. Permanent magnets, electromagnets [14], or a combination of both [25] have been used. Although electromagnets add complexity to the system (e.g., power supply and control, insulation, cooling), their use may be justified if it is desired to alternate easily between conventional and magnetron sputtering.

The maximum transverse component of magnetic field in front of the target is typically in the range 200–500 G (0.02–0.05 T), although the threshold flux density for the magnetron discharge may be as low as 80–90 G [26].

Various permanent magnet materials and pole piece arrangements have been used. Suitable magnet materials are barium (or barium-strontium) ferrites, alnico alloys, and cobalt rare-earth alloys [27]. All of these materials have a high coercive force and residual induction and do not readily demagnetize by being "open circuited," which is the normal situation for a magnetron cathode. Ferrites do not corrode, which allows them to be placed within a water-cooled cathode assembly. Cobalt rare-earth magnets, although expensive, may be of use in sputtering ferromagnetic materials where the target must be magnetically saturated in order to achieve a useful field beyond the cathode face. The choice of magnetic material determines the pole piece geometry. Ideally the magnetic field should enter and leave the target normal to the target face to avoid sputtering from the target edges and maximize the transverse field component. It is preferable to have the magnet material adjacent to the target surface rather than to the pole pieces, since there will be greater limb leakage from the pole piece material (soft iron or cold-drawn steel) than from the magnet material [28]. Since ferrite magnets are magnetized along their thickness (generally 2–3 cm), they can be placed behind the cathode and backed by a flat pole piece, as in Fig. 2. Alnico magnets are magnetized along their length and have been used in a radial arrangement behind a round cathode having a center cylinder and an outer ring as pole pieces, as in Fig. 3a [29]. Long alnico magnets can also be used adjacent to the cathode, but more space is required behind the cathode (see Fig. 3b). A slight oval pattern of U-shaped magnets has also been reported [25]. A slight amount of sputtering occurs along the corners and sides of targets due to fringing magnetic field lines from the limbs of the outer magnets or pole

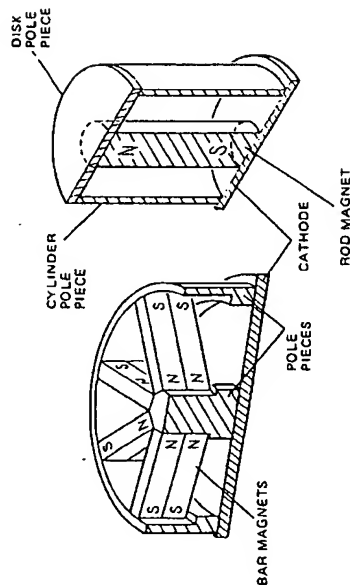


Fig. 3. Disk cathode bar magnet arrangements: (a) radial magnets, (b) central rod magnet.

pieces. This can be minimized—at the cost of less efficient use of target material—by moving the pole faces farther in from the edge of the target. A convex target surface [19] or modified pole faces may minimize the fringe effect. Computer-aided magnetic circuit design should allow the optimization of magnet-pole piece geometry for a given cathode design and magnetic material.

The advantages of permanent magnets over electromagnets can be summarized as no dc power required, no additional heat to dissipate, no field interruption, no danger of magnet insulation failure, and less weight and volume for equivalent magnetic field. The disadvantages are the field cannot readily be varied or turned off and the target will continually attract magnetic "dirt" [28].

2. Cathode Shielding and Insulation

Two basic designs have been used: (1) The cathode and shielding are entirely within the deposition vacuum chamber with power and coolant brought in via vacuum feedthroughs [16, 24]. (2) The cathode and surrounding electrical insulator form part of the vacuum chamber wall so that high-voltage connections and coolant seals are outside the vacuum chamber [14].

The advantages of the first design are that the cathode can be readily retrofitted to an existing vacuum system as, for example, a replacement for an electron-beam deposition source, and it can be placed to deposit in any direction. The disadvantages are that it requires vacuum feedthroughs for coolant and high voltage and may, depending on the de-

11-4. PLANAR MAGNETRON SPUTTERING

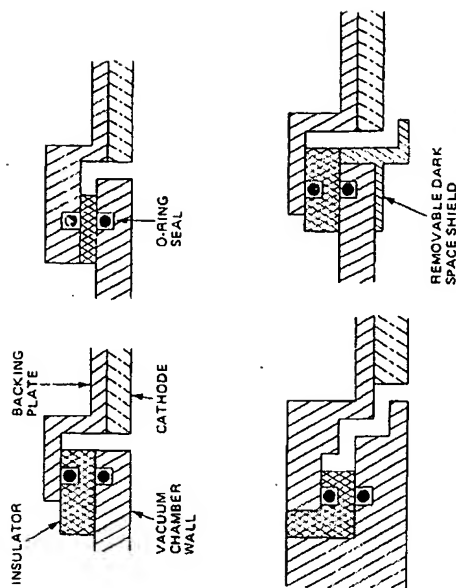


Fig. 4. Examples of cathode isolation geometries.

sign, have vacuum-to-coolant O-ring seals. Slight leakage through such seals may not be detected, and total seal failure can be catastrophic.

The second design has the advantage of not requiring vacuum-to-coolant seals if a cathode backing plate is used. A disadvantage is that some portion of the deposition chamber wall must be designed to receive the cathode assembly.

Cathode isolation details can vary from a simple stacked arrangement of the chamber wall-insulator-cathode to a reentrant or stair-step profile. Dark-space or ground shielding may be flush with the cathode surface or it may extend beyond or in front of the cathode surface. It has been reported that arcing along the cathode surface can be suppressed by a ground shield extending slightly over the outside edge of the cathode [14, 24]. A removable dark-space shield is advantageous when frequent clean up of sputtered deposits is necessary. An alternative would be to make that portion of the vacuum chamber wall surrounding the cathode easily removable. Various insulator-shield arrangements are illustrated in Fig. 4. The concept of the dark-space shield loses some meaning in the context of magnetron sputtering, since outside the magnetic field region at 5–10 mTorr argon pressure the dark-space thickness is several centimeters [30].

The insulating material may be polytetrafluoroethylene (Teflon®), acetal resin (Delrin®)* or a similar insulator having suitable mechanical

* Teflon and Delrin are registered trademarks of E. I. duPont de Nemours and Co., Wilmington, Delaware.

and vacuum characteristics, i.e., low permeability, low water absorption, and low outgassing rate [31]. Glass or ceramic may be used in some applications (e.g., small cathodes), but a more flexible material is preferable to brittle ceramic because the mating surfaces may not be absolutely flat or coplanar and a slight amount of "give" may be necessary to effect a vacuum-tight seal. Under such conditions a ceramic may crack. The plastic material used for cathode insulation fabrication should be free of seams that may be gas permeable.

3. Cathode Construction

The cathode assembly consists of the source material, generally 3–10 mm thick, bonded to a backing plate which in turn forms one wall of a coolant plenum. The magnet assembly may be within or external to the coolant channel. Source material and target fabrication techniques are similar to those used for conventional sputtering targets (Chapter II-1, Section V-A). Ferromagnetic targets such as Ni or Co must be thin enough to be saturated by the magnetic field; for ferrite magnets this is 2–3 mm. Targets should be free of voids or bubbles because at the high power densities and erosion rates typical of magnetron sputtering, local melting and cathode "spitting" can occur as these voids are uncovered. Targets should be stress free.

The backing plate material must not be ferromagnetic; it should have good thermal conductivity through its thickness; and the backing plate and coolant plenum must be designed to withstand atmospheric pressure plus coolant pressure without deformation. The total pressure may exceed 3 atm. Both copper and nonmagnetic stainless steel have been used, however, stainless steel is a very poor thermal conductor.

Cathode cooling in PM sputtering is critical because of the high power dissipation at the cathode. In conventional sputtering an estimated 55–70% [30, 32] of the power delivered to the cathode is dissipated in the coolant. For PM operation, cooling limitations will generally determine the maximum operating power of the cathode (Section D-2). In high-power applications, cathode bonding is essential. Disk targets bonded to a stud-mounted backing plate, as sometimes used for conventional rf sputtering targets less than about 30 cm in diameter, may be marginal at high power densities. In lower-power usage with targets that can operate at higher temperatures, it may be feasible to bolt or clamp the target to the backing plate, preferably with a malleable foil intermediate layer [33].

An innovative nonbonded aluminum cathode design has recently been developed [33a]. Four aluminum bars (the source material) approximately 2.5-cm-wide and 2.5-cm-thick, having mitered corners, are arranged as a

rectangular frame and held in place by channeled magnetically soft pole pieces within and surrounding the frame. The pole pieces are clamped to a water-cooled copper backing plate by magnets behind the backing plate. The faces of the pole pieces are approximately coplanar with the aluminum target surface.

Target bonding details are rarely given. A relatively simple technique [34] applicable to Cu and many other materials is to use a low melting-point solder such as 50:50 In–Sn (m.p. 117°C, Table I). Ga can be used at room temperature to wet the (precleaned) surfaces to be joined. This allows the bonding operation to be carried out with minimum oxidation of the surfaces to be bonded. The absolute minimum amount must be used because Ga forms a brittle alloy with In–Sn. Ga cannot be used with materials such as Al in which rapid Ga diffusion occurs at room temperature. Solder bonding [38] is preferable to the use of metal-filled organic adhe-

Table I
Low Melting-Point Solders^a

Bi ^b	Composition (wt %)			Temperature (°C)	
	In	Pb ^c	Sn	Liquid	Solid
49	21	18	12	58	58
56	—	22	22	104	95
—	52	—	48	117	117
—	50	—	50	127	117
—	25	37.5	37.5	138	—
58	—	—	42	138	—
—	42	—	58	145	117
—	80	15	—	149	141
—	—	(Ag 5)	—	—	—
—	99	—	—	153	153
—	(Cu 1)	—	—	—	—
—	100	—	—	157	157
—	12	18	70	174	150
—	70	30	—	174	160
—	—	37	63	182	—
—	—	30	70	186	183
—	—	40	60	188	183
—	—	50	50	214	183
—	—	50	40	238	183 ^c

^a Data from Rosebury [35], Kohl [36], and Manko [37] and Indium Corporation of America, Utica, New York.

^b Bi and Pb have vapor pressures $<10^{-4}$ Torr at 300°C; In and Sn have substantially lower vapor pressures.

^c Most ductile of Sn–Pb solders.

sives [39, 40] where low thermal resistance and minimum outgassing are required. Vacuum brazing of sputtering targets has also been described [38]. Joining processes suitable for vacuum applications including brazing, soldering, and glass- and ceramic-metal sealing have been reviewed previously [36].

Some early planar magnetron designs sealed the target directly to the coolant plenum with no backing plate. This is very risky due to the high differential pressure exerted on the cathode (which may not be a suitable structural material), the possibility of diffusion through the target [41], possible electrolytic corrosion at the O-ring seal, and finally, the likelihood of the target bursting and flooding the vacuum chamber with coolant when the erosion depth reaches some critical point.

Water cooling is the most common method of maintaining a low cathode temperature, although gas flow or even oil cooling [42] have been used. The flow rates required are relatively high. Systems should be designed conservatively for a water-temperature rise of 10°C or less. Table II lists required minimum water flow versus power dissipated for a 10°C ΔT [43]. High flow rates require that the cathode cooling channels offer minimum flow resistance if high water pressures are to be avoided. The thermal characteristics of the cathode are important; they are discussed in Section II.D. The use of chilled water at some temperature above the dew point of the room air will afford an extra margin of safety. The electrical conductivity of the cooling water should be low enough to minimize current leakage to ground when maximum voltage is applied. If 0.5 m or more of 1-cm inner diameter insulating water line (for example, polyvinyl chloride) is inserted between the cathode and ground, a water resistivity of about 10 k Ω cm would reduce leakage to less than 1 mA at 600 V.

One disadvantage of PM sputtering is that the target erodes only in the transverse magnetic field region; as the erosion proceeds, the bombarding ions are focused into an increasingly narrow region leading to a V-shaped

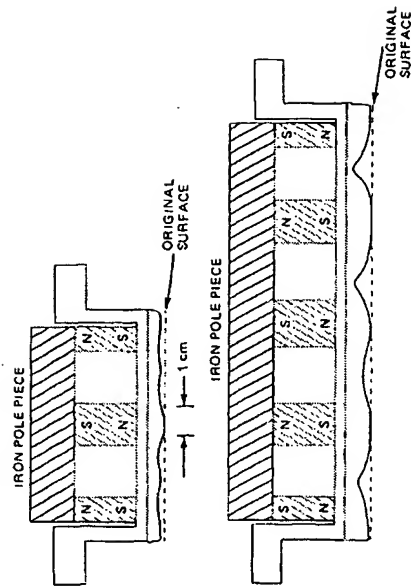


Fig. 5. Relation of cathode erosion profile to magnet position: (a) Al_2O_3 cathode, 10×25 cm, single plasma ring, operated at 7 W/cm^2 rf, $\sim 1 \text{ mTorr}$ Ar pressure; (b) Al-4% Cu cathode, 19×25 cm, dual plasma rings, operated at 5.6 W/cm^2 dc, $\sim 9 \text{ mTorr}$ Ar pressure. Note unequal erosion rates for the two plasma regions due to unequal magnetic field strengths.

erosion profile as shown in Fig. 5. End-of-life for the target occurs as soon as this groove reaches the backing plate. Reported material utilization at this point ranges from 26–45% [14, 23, 24, 43]. Various means have been employed to improve material utilization: increased target thickness in the erosion region, an oscillating electromagnetic field to modulate the position of the permanent magnet field [25], and mechanical movement of the magnet array [44, 45]. Mechanical movement is more amenable to the cylindrical-cathode internal-magnet magnetron [46] than to a planar cathode. Expensive target materials may warrant the complexity necessary to increase the erosion area.

4. Anode Placement

An auxiliary anode has been reported to be effective in preventing electron bombardment of the substrate [14, 17, 23] (see Section II.E). Configurations have included a peripheral anode ring between the cathode and the dark-space shield of a disk target [23]; a water-cooled tube connected to the positive side of the floating-cathode power supply and located slightly in front of and surrounding the circular cathode surface [14]; and anode rod or rods along the sides of a rectangular cathode [16]. The relative effectiveness of these arrangements has not been reported. It may be that the magnetron discharge acts much like a conventional rf or dc

Table II
Water Flow Rates for $\Delta T = 10^\circ\text{C}$

Power dissipated (kW)	Water flow rate (liter/min)	Water flow rate (gal/min)	Power dissipated (kW)	Water flow rate (liter/min)	Water flow rate (gal/min)
2	2.8	0.74	15	21	5.6
4	5.6	1.5	20	28	7.4
6	8.4	2.2	25	35	9.3
8	11.2	3.0	30	42	11
10	14	3.7			

plasma in that the position of a positively biased auxiliary electrode is not critical [47]. The placement of the anode with respect to the magnetic field lines may be important, however (see Chapter II-2). The most effective anode placement should be near the regions where the magnetic field enters the cathode, as in the Sputter Gun (Chapter II-3).

It has been suggested [48, 49] that both the annular shield surrounding the target and the center of the target (where the magnetic field is normal to the target surface) must be anodes. If a central anode is not provided and an easily oxidizable material such as Al is used as a source, the center of the target may form an insulating layer that will charge up to the cathode potential. If this potential exceeds the oxide film breakdown potential, arcs can occur that can contaminate the growing film (Section II.F.3). A planar disk cathode source having a grounded central anode (akin to a flattened Sputter Gun) has been compared with a conical cathode Sputter Gun [41] and found to give equivalent deposition rates for Cu and Al targets for a given power input. It was noted that even with a central anode it was more "difficult" to apply high dc power levels to the flat cathode structure than to the conical structure. There was no problem when rf power was used with the flat cathode.

5. Substrate Heating

Substrate heating poses a problem in PM sputtering. Tubular quartz lamps are often used as radiant heaters; the close source-substrate distance typically used in PM sputtering prevents uniform surface heating during deposition by a conventional quartz-lamp radiant heater array. In an in-line system, radiant heaters can be used to preheat the substrates prior to entering the deposition zone. Deposition will then occur on a cooling substrate. This may or may not be a disadvantage. The effect would be less for a planar or cylindrical rotating substrate carrier system (see Section II.B.2). If constant uniform heat is necessary, radiant surface preheating combined with some type of backside substrate carrier heating to minimize thermal conductive losses may be an effective technique. In any substrate heating arrangement it is difficult to avoid heating extraneous portions of the deposition chamber and fixturing, resulting in desorption of residual gases and ubiquitous low-vapor-pressure contaminants (e.g., alkali metals). This is especially true for radiant heating. The determination of actual substrate surface temperature for calibration or temperature control purposes is not trivial and is discussed in Chapter II-1.

B. Thickness Uniformity Control

A planar magnetron is inherently a nonuniform deposition source because the sputtered material originates from the regions of high plasma

density. Since these regions are dependent on magnet location and field strength, the PM technique allows adjustment of the effective source geometry by modifying the magnet arrangement and the resultant erosion pattern on the target. Substrate motion appropriate to the source geometry, with or without shaped shields, is another method that can improve film thickness uniformity.

Actual sputtering thickness distributions usually agree with calculations based on a cosine emission of sputtered material from the erosion area [50]. However, such calculations may be inaccurate at high deposition rates because of considerable self scattering of emitted material in the high source-material flux region above the erosion area. This may result in a "virtual source" in front of the cathode surface and an "under-cosine" distribution [51, 52]. It should be recognized that thickness distribution can change as the erosion depth increases and the effective emission width narrows [34].

1. Magnet Pattern

a. Disk Source. The thickness distribution from the planar disk magnetron has been reported to agree with that calculated for a ring source having a cosine emission characteristic [14, 23]. For such a source, best film uniformity is obtained when the source inner radius is about 0.7 of the source-to-substrate distance h and the outer ring radius is about $0.8h$ [53]. If we assume a plasma ring width of 2 cm and a minimum source-substrate spacing of 5 cm,* the optimum plasma ring outside diameter would be ~ 9.5 cm. Larger single-ring disk sources would have to be proportionately farther away from the substrates. A better magnet geometry for a large disk source would be n concentric rings [54, 55] of opposite magnetic polarity resulting in $n-1$ toroidal plasma regions. In any source utilizing multiple independent closed plasma regions, it is important to have equal magnet strengths and field intensities in each individual plasma region to equalize cathode erosion rates for maximum material utilization. Figure 5b illustrates the effect of unequal magnetic field strengths for two independent oval patterns on a 19×25 cm cathode. Concentric-ring cathodes up to 61 cm in diameter with six equally spaced plasma rings have been constructed and 80% target utilization realized [56]. Figure 6 illustrates calculated thickness distributions for a single-ring source and for concentric-ring sources having from two to six rings, based on the analysis of Glang [53]. A source-substrate distance of 5 cm was chosen, and each ring was assumed to have uniform cosine emission from an effective width of 2 cm. The ring radius in centimeters at midwidth was $4n$,

* Generally the minimum source-substrate distance for magnetron sputtering is 5-6 cm in order to be outside the plasma region.

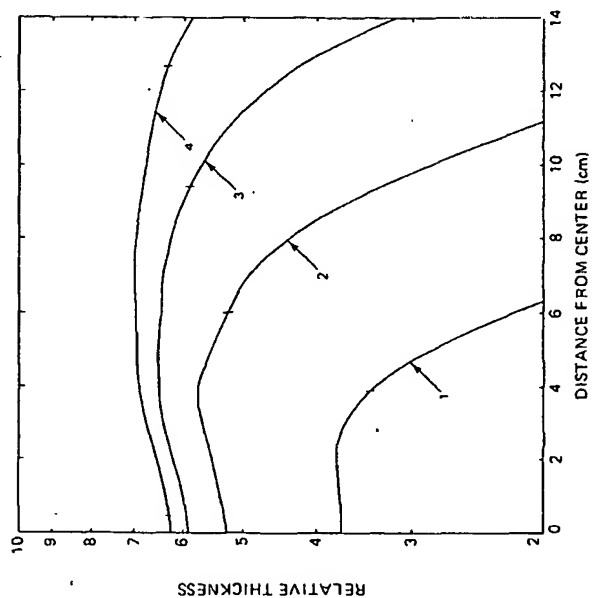


Fig. 6a. Calculated thickness distribution for multiple concentric ring sources. Relative thickness is plotted versus distance from center for (a) one to four rings and (b) four to six rings. The source-substrate spacing was taken as 5 cm. The effective ring width was assumed to be 2 cm; ring spacing is 2 cm. Short vertical lines indicate approximate boundaries for $\pm 5\%$ uniformity. Based on ring source analysis of Glang [53].

where n is the ring number. This results in an array of 2-cm-wide rings with 2 cm spacing between rings. As Table III indicates, uniformity efficiency over a circular region improves for three or more concentric rings.

gated ring plasma pattern. Good deposition uniformity requires substrate motion perpendicular to the cathode width. For a cathode length/width ratio of about 2.5 and a source-substrate distance one-half the target width, the deposition profile is thick in the center [16, 43]. Figure 7 shows two examples of magnet arrangements for improved uniformity from a rectangular cathode [57]. Increasing the length/width ratio to ≥ 3 can also improve uniformity of a rectangular magnet arrangement. Obviously, a long narrow cathode having the end semicircular plasma regions beyond the substrate region will give uniformity distribution approximating an in-

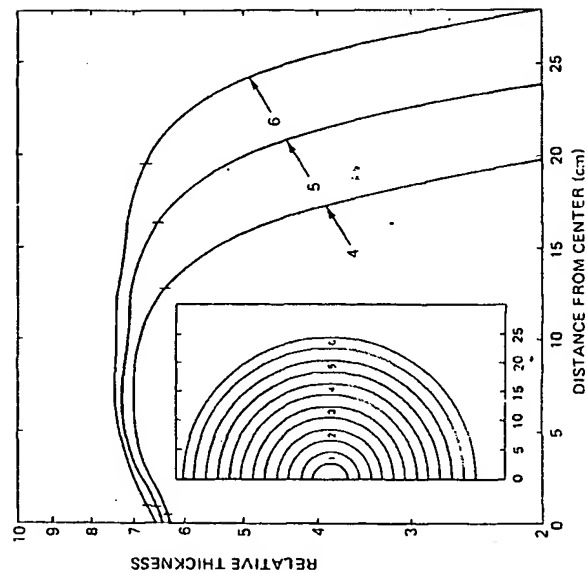


Fig. 6b. See legend for Fig. 6a.

finite line source. Cathodes as long as 150 cm and 20 cm wide have been reported [24, 58].

Other than magnet rearrangement, the plasma intensity can be modified by varying the spacing between the magnets and the cathode surface [45], by modifying the magnets or pole faces with gaps, or by varying pole face widths or angles. Special closed-curve geometries can be devised to

Table III

Single and Concentric Ring Source Efficiencies^a

No. of rings	Target radius (cm)	Efficiency %	No. of rings	Target radius (cm)	Efficiency %
1	6	42	4	18	50
2	10	36	5	22	55
3	14	45	6	26	57

^a Efficiency is the substrate area for $\pm 5\%$ uniformity divided by target area (see Fig. 6).

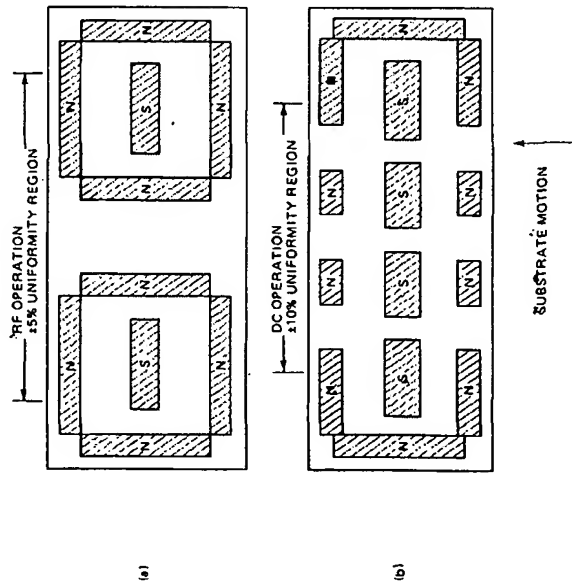


Fig. 7. Magnet arrangements for improved deposition thickness distribution from rectangular cathodes: (a) dual rings, (b) magnet gaps. Experimentally determined uniformities are indicated (Muto *et al.* [57]).

2. Substrate Motion

Various types of substrate motion relative to the sputtering source are shown in Fig. 8. Sputter sources can be mounted to sputter in any direction. When used with planetary motion (Fig. 8a), as in replacing an existing electron-beam source, the source-substrate distance is large and the effective deposition rate is lowered. Planetary motion implies multiple rotation of the substrates and continuously varying angles of incidence, instantaneous deposition rates, and source-substrate distance. If a disk source is used with planar rotation (Fig. 8b), the source-substrate distance can be less but an aperture shield [59] is required for good deposition uniformity. However, modification of the cathode and magnet arrangement to get a wedge-shaped source distribution may be possible.* Figure 8c shows substrates located on the interior of a drum-shaped substrate holder rotating around a planar cathode. A cylindrical cathode

* For example, the Perkin-Elmer Ultek "delta source" [59a].

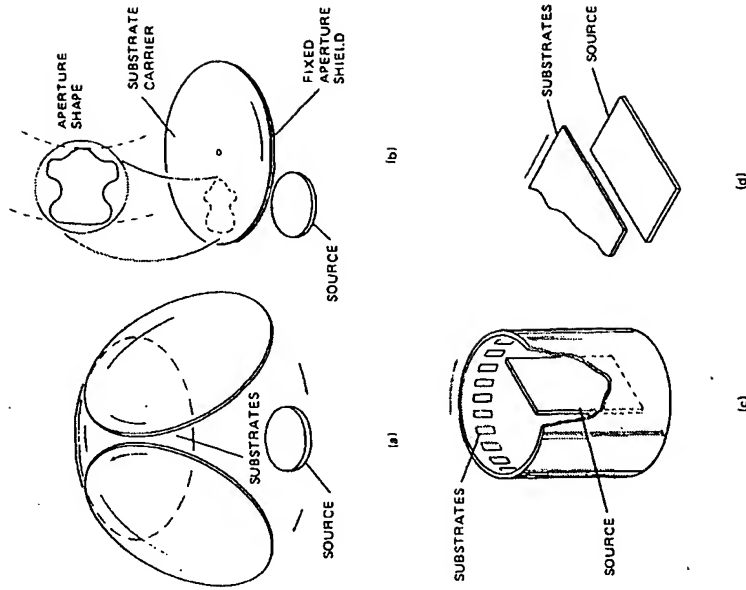


Fig. 8. Planar magnetron deposition with substrate motion: (a) planetary motion, (b) planar rotation with aperture shield, (c) drum rotation, (d) linear motion.

(Chapter II-2) would be more appropriate unless multiple sources (different materials) are required [60]. Substrates can also be placed on the exterior of a drum-shaped carrier and single or multiple PM sources located outside the drum. Planar rotary motion, as in Fig. 8b or c, results in a nearly constant source-substrate spacing; but if multiple passes are required, the deposition rate varies. The linear motion arrangement in Fig. 8d is, in effect, similar to Fig. 8c but is easily adapted to continuous substrate motion from and to a magazine chamber or air-to-vacuum load lock.

The substrate exposure time for linear substrate motion from an extended oval plasma ring having semicircular end regions has been calcu-

lated [45]; the optimum arrangement was a wide plasma region with a minimum end radius.

Linear motion makes optimum use of the high-rate capability of the rectangular magnetron source by allowing minimum source-substrate spacing and maximum throughput. All substrate motion, however, results in time-varying instantaneous deposition rates and incident angles. Such variation can affect the structure and properties of the deposited films.

3. Cathode Shielding for Uniformity Control

Shaped aperture shields have been used to achieve uniform deposition from a magnetron disk source with planar substrate rotation (Perkin-Elmer Ultek, Inc. [59] and Fig. 8b) and from a rectangular source with linear motion [17]. Because the emission from the source is nonuniform, the shield profiles were empirically determined. Such shields have the disadvantages of (1) collecting deposited material that must be periodically removed and (2) reducing the effective deposition rate for a given cathode erosion rate. In most cases, modification of magnet geometry is preferable to aperture shielding. An exception would be for rate or angle-of-incidence control; for example, single or stacked aperture shields can be

C. Voltage, Current, and Pressure Relationships

Planar magnetron sources usually are operated in argon at a pressure of 1–10 mTorr and at cathode potentials of 300–700 V. Under these conditions, current densities can vary from 4 to 60 mA/cm²; power densities are in the range 1–36 W/cm².

Typical voltage-current characteristics are shown in Fig. 9a for various pressures.* For an optimum magnetic field shape and intensity, these curves follow the relation:

$$I = kV^n \quad (1)$$

where I is the cathode current (or current density) and V is the cathode potential (Chapter II-2, Section IV). The more efficient the electron trapping in the plasma, the higher the exponent n . Thus, for a given cathode material and configuration the magnetron operates at some characteristic, nearly constant voltage.

Figure 9b displays the same data as Fig. 9a in terms of the voltage re-

* The current density in the erosion area of the target may be up to four times the average current densities given.

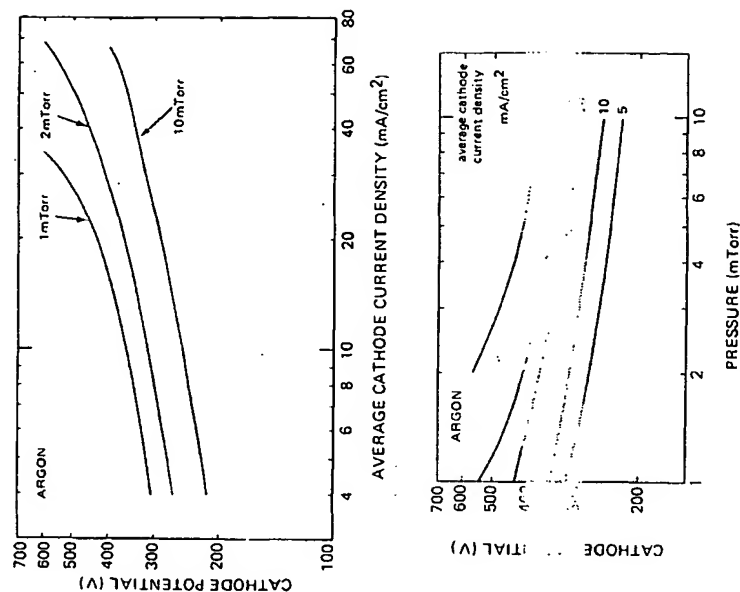


Fig. 9. (a) Current-voltage characteristics for rectangular planar magnetron cathode at various pressures. (b) Cathode voltage versus pressure for constant average cathode current density. Target size 37.5×12.1 cm, oval ring plasma geometry (data from Van Vorous [24] and Materials Research Corp. [62]).

quired to maintain a constant average current density at various pressures. Almost no data have been published concerning the effect of parameters such as magnetic field geometry, target material, and pressure on the constants of Eq. (1). Since the power (P) is the product of cathode potential and current, Eq. (1) becomes

$$P = kV^{n+1} \quad (2)$$

where k and n are the same constants as in Eq. (1). For the 10 mTorr curve of Fig. 9a, $n = 4.6$ and $k = 9.0 \times 10^{-13}$ for average power density in W/cm² and cathode potential in volts.

For a given cathode configuration, a family of current-voltage curves versus pressure can be obtained that enable a suitable operating point to be chosen for a given power input. Similar or argon-calibrated gauges must be used when transferring a process from one deposition system to another. Sputtering gas pressure as measured with thermal-conductivity gauges, ionization gauges, and capacitance manometers are not directly comparable because these gauges are usually calibrated in terms of nitrogen-equivalent pressure and all except the capacitance manometer have differing calibration factors or response curves for various gases [63]. Pressures given in the literature may be nitrogen- or argon-equivalent readings. Since the distinction is rarely made, direct comparison of data is uncertain.

D. Deposition Rate

1. Factors Determining Deposition Rate

Sputtering rates are determined primarily by the ion-current density at the target and secondarily by the ion energy (voltage). In practice, for magnetron sputtering, deposition rates have been found to be directly proportional to the power delivered to the target. The factors determining deposition rates are power density in the erosion area, size of the erosion area, source-substrate distance, source material, and pressure. Other factors such as sputtering gas composition will not be considered here. The above parameters are listed in approximate order of importance but some are interrelated, such as pressure, power density, and size of the erosion area. Also, as will be discussed later, the thermal and mechanical properties of the target may limit the maximum deposition rate attainable.

For maximum deposition rate, the substrate should be as close as possible to the source while remaining outside the plasma region. Typical minimum spacings are 5–7 cm. Source-substrate distance and deposition rate will vary with time when substrate motion is used to improve uniformity or increase capacity.

Substrate motion complicates the definition of deposition rate. For planetary or other rotary motion of substrates, the deposition rate reported is usually the average rate determined by dividing thickness by deposition time. For static deposition with PM sources, the thickness is usually nonuniform, so a thickness average (or even maximum thickness) is used to calculate reported deposition rates.

For linear motion of substrates under a rectangular target, an average deposition rate (R) can be defined by

$$R = tS/W, \quad (3)$$

where t is the average film thickness for one pass of the substrate at speed S under a target of width W measured in the direction of substrate motion. The rate, R , will have the unit thickness/time.

A deposition rate efficiency (R_E) can be defined as the slope of the linear deposition rate versus power density curve, or

$$R_E = R \text{ (Å/min)} / P \text{ (W/cm}^2\text{)}. \quad (4)$$

Deposition rate efficiency is a useful concept for optimizing deposition conditions, magnet arrangement, source-substrate spacing, etc. Table IV summarizes some deposition rates and calculated rate efficiencies reported for dc PM sputtering. Average power densities are 10–30 W/cm² and rate efficiencies are 800–1200 Å-cm²/W-min for copper and 200–650 Å-cm²/W-min for aluminum. For a constant cathode size, magnet configuration, and power density, the deposition efficiencies vary with material. For nonferromagnetic materials, this is partly due to differences in sput-

Table IV
DC PM Sputtering—Deposition Rates and Efficiencies

Cathode material	Reported rate (Å/min)	Calculated efficiency (Å-cm ² /W-min)	Av. power density (W/cm ²)	Source-substrate distance (cm)	Argon pressure (mTorr)	Cathode dimensions (cm)	Reference
Cu	10.7	1020					
Al	5.5	520	10.5	5	4	9 × 21	[16]
Ti	3.9	370		(static)			
Au	20	1250					
Cu	20	1250		not reported (static)	not reported	15 × 41	[17]
Cr	10	630	16				
Al	7	440					
Ti	4	250					
Cu	25	780		5		diam. 14	[23]
Al	11	340	30	(static)	3–5	(est.)	
Au	17	1100					
Cu	13	840		not reported (linear)	not reported	13 × 30	[24]
Cr	10	650	15.5				
Al	10	650					
Ti	3.3	210					
Al	2	185	10.8	7	11	10 × 25	[64]
				(linear)			

tering yield. If the deposition rate or efficiency of a given material of yield A is known, then the expected rate for another material of yield B under the same conditions can be estimated by multiplying the rate for A by the ratio B/A . Sputtering yields at 600 V have been tabulated [65].

Sputtering yields increase with voltage in the 300–800 V range used for dc PM sputtering. Thus part of the rate versus power dependence is due to sputtering yield increasing with voltage. The sputtering yield for many metals doubles or triples between 200 and 600 V. Following the reasoning of Lamont and Turner [66], we can show, assuming a linear relation between sputtering yield and voltage between 300 and 800 V, that for PM sputtering the deposition rate should be proportional to power. Deviations occur due to effects such as gas scattering of sputtered material, re-emission from the substrate, and the presence of inefficient sputtering gas species such as hydrogen [67] that contribute to ion current but not to sputtered material flux.

Sputter gas pressure has less influence on deposition rate for dc PM sputtering than for conventional sputtering. As shown in Fig. 9b, as gas pressure decreases, the effective plasma resistance increases, requiring a slightly higher voltage to maintain a given current density. Therefore if the deposition rate for a given current is plotted versus pressure, the rate will increase with decreasing pressure. If power is held constant, the deposition rate versus pressure curve will exhibit a maximum (Fig. 10). For the conditions of Fig. 10, the deposition rate changes less than 10% between 3 and 15 mTorr. The decreasing rate at high pressures is caused by gas scattering of the sputtered material; the reduction at lower pressure was suggested to be due to less efficient ion collection by the cathode [23].

The magnetron discharge is a very efficient sputtering source: it has been estimated that the sputter rate per watt of discharge power may exceed 60% of the theoretical limit set by the ratio of sputtering yield to mean ion energy [23]. In comparison to conventional sputtering, planar magnetron sputtering has been reported to result in three times the cathode erosion rate efficiency, e.g., for copper sputtered in argon, 2 mg/sec-kW for PM sputtering versus 0.7 mg/sec-kW for conventional sputtering [23].

2. Rate Limitations

The major factor limiting deposition rate is the maximum power flux that can be applied to the cathode without causing cracking, sublimation, or melting (if a molten target is used, then in most cases we are dealing more with thermal evaporation than with sputtering).

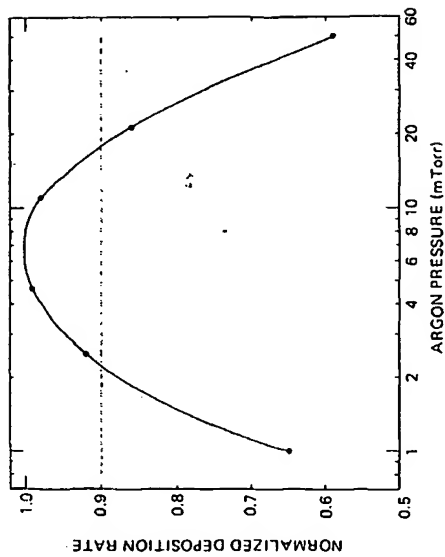


Fig. 10. Normalized deposition rate versus argon pressure. Chromium disc cathode; source-substrate distance 5 cm; estimated power density 18 W/cm² (data from Schiller *et al.* [23]).

If we assume that the coolant flow channels are properly sized so that the necessary minimum flow rates are possible (see Table II), the cooling rate of the target depends on the thermal conductances of the backing plate, the target backing-plate interface, and the target itself. These conductances depend on the thermal resistance (thickness \times thermal conductivity) of the materials involved.

Table V lists calculated maximum power densities that can be applied to various materials for a 100°C temperature gradient through the material thickness for a thickness of 1.0 cm. Assumptions in the calculations are only conductive heat transfer, uniform distribution of power flux at the target surface, and no thermal resistance at the target backing-plate coolant interfaces—obviously an ideal situation. These values are equal numerically to the thermal conductivity of the material in the units W/m K, i.e., watts per meter per degree Kelvin. (See Rosebury [69] for a tabulation of thermal conductivities of many metals and alloys.)

For good thermal conductors, the allowable power density can easily exceed the ability of water cooling to remove the heat from the back of the target. If we assume 1 liter/sec (16 gal/min) as an upper limit for cooling water flow and 30°C as the maximum tolerable water-temperature rise, then the power limit for a water-cooled cathode is 125 kW [70]. For an

aluminum cathode having an area of 360 cm² (a 21-cm-diameter disk or a 12 x 30 cm rectangle), the power limit for a 100°C cathode temperature gradient is 85 kW and the required water flow is 40 liter/min (11 gal/min) for a 30°C water-temperature rise.

For poor thermal conductors, for example, glass or quartz, the maximum power density (total power divided by erosion area) would be a safer number to use than the average power density (total power divided by target area). A stress-free low thermal expansion material such as fused quartz can support a much higher temperature gradient than a target having internal stresses or a high thermal expansion coefficient. For example, successful operation of an SiO₂ target in a magnetically enhanced, high-rate rf mode at 72 W/cm² has been reported [71]. At this power density the target surface was near its melting point and the authors concluded that evaporation as well as sputtering was occurring. In contrast, Table VI lists some results for rf sputtering of aluminum oxide targets.

The data of Table V also allow determination of the conditions when a poor thermal conductor such as stainless steel can be used as a backing plate. In all cases, we have neglected the target backing-plate interface (Section II.A.3). For solder-bonded targets, this is not a significant thermal barrier unless voids or discontinuities are present [38].

3. Rate and Thickness Control

If all the factors affecting deposition rate can be held constant, then the rate will be constant and reproducible. The power supply should be

Table VI
Aluminum Oxide Targets—Power Density Comparison

Target type	Thickness (cm)	Av Power Density (W/cm ²)	Av Power Density for $\Delta T = 100^\circ\text{C}$ ^a (W/cm ²)	Time to Failure (min)	Reference(s)
Polycrystalline ^b	~0.5	72	16	5	[71]
Sintered	~0.5	120	60	15	[71]
Sintered ^c	0.64	7 ^d	50	>10 ^d	[72, 73]

^a Gradient through target thickness for uniform power density (Table IV).

^b General Electric Co. Lucalox[®].

^c Western Gold and Platinum Co. AL-995.

^d rf PM; maximum power density in erosion area ~20 W/cm².

Power Density (W/cm²) for a 100°C Temperature Gradient through a 1 cm Cathode Thickness^a

Metals/ semiconductors	Power density	Classes	Power density	Conducting compounds	Alloys	Data from Weast [68] and Rosebury [69]
Ag	427	dielectrics	2-4	glasses and most borosilicate, aluminosilicate, and soda-lime glasses	80:20 PbO-SiO ₂ oxides (polycrystalline) BeO Al ₂ O ₃ MgO	
Cu	398			oxides (single crystal) sapphire (Al ₂ O ₃) quartz (SiO ₂)	In-Sn 50:50 Pb-Sn 60:40 Pb-Sn 50:50	
Au	315					
W	178					
Si	149		0.6			
Mo	138		51			
Cr	94		30			
Ni	91		8.7			
Fe	80		7.7-8.3			
Ge	76		1.4-2.6			
Pt	73					
Pd	72					
Sn	67		70 (est)			
Ta	58		47			
Pb	35		43			
Ti	22		13.4-15.5			
			31			
			21			

Table V

capable of maintaining a constant power. For PM sputtering, the power supply is usually operated in a constant-current mode with voltage limiting. Since the plasma erosion area depends on the magnetic field intensity and shape, this field should be constant or varied in a reproducible manner. Electromagnets require a high-current power supply—another source of variation.

Pressure can be held constant by servo-controlling a leak valve with an ionization gauge or a capacitance manometer [74]. In practice, this is rarely necessary if the diffusion pump throttle-valve mechanism is capable of reproducing its orifice area (conductance) in the throttle position. Turbomolecular pumps do not require a throttle valve if a sufficiently high-capacity backing pump is used. To take advantage of the pumping speed of the liquid-nitrogen trap, the throttle orifice should be located between the diffusion pump and the liquid-nitrogen trap [75]. Usually a micrometer-type needle valve can be used to set the argon flow rate for a foreline pressure below the diffusion-pump forepressure tolerance or at the foreline pressure for maximum throughput [76]. The throttle mechanism then is adjusted to give the approximate sputtering pressure desired. Lastly, the argon needle valve is readjusted for the exact pressure required. If both throughput and pressure are to be set accurately, then a vernier control on the throttle is helpful. An ion gauge designed for the pressure range 1–10 mTorr is preferable to a thermal-conductivity vacuum gauge for reproducing the pressure setting. As indicated by Fig. 10, precision pressure reproducibility is not required unless unusually accurate rate control is needed. However, sputtering gas composition and purity should be controlled (see Chapter II-1, Section VI).

For reproducible film thickness, all that remains is to control deposition time. In a linear-motion system, the substrate-carrier speed determines deposition time.

An effect peculiar to magnetron sputtering is the nonuniform erosion of the cathode surface leading to V-shaped grooves. As these grooves deepen, the discharge impedance changes and the voltage required for constant current may change slightly. If power level is critical, a power-feedback control could be used. In most cases, deposition thickness or rate monitors are not necessary for rate-thickness control during sputter deposition. Rate monitors are useful, however, for rapidly determining the effects of sputtering parameters, e.g., pressure, on deposition rate. Care must be taken to distinguish between changes in rate and changes in distribution pattern. Quartz-crystal oscillator monitors, shielded from rf, can be used.

For reactive sputtering, gas composition and throughput must be reproducible (see Chapter II-1, Section VI.D).

E. Substrate Effects

1. Electron and Ion Bombardment

In conventional rf or dc sputtering, secondary electrons emitted by the cathode are accelerated across the dark space and, unless the substrate is shielded or negatively biased in some manner, will bombard the substrate with almost the full energy of the dc cathode potential [30]. It has been estimated that for conventional rf sputtering, of the 5–10% of the cathode power dissipated at the substrate about 60% is due to electron bombardment [77]. For conventional dc sputtering, of an estimated 40% of the applied power dissipated at the substrate, virtually all was transmitted by secondary electrons [30].

In a planar magnetron the secondary electrons are accelerated to the potential difference between the cathode and the plasma, but those electrons under the influence of the transverse magnetic field will be given a curved trajectory of the order of 1-cm radius so that they cannot bombard the substrate directly (see Chapter II-2). By ionization and collision processes, the plasma becomes populated with more or less thermalized electrons having energies of about 1 eV [23]. These electrons are readily collected by an anode adjacent to the region where the magnetic field lines enter the cathode surface (Section II.A.4). Figure 11 shows how an escaping electron can follow magnetic field lines emerging from the cathode.* These electrons can impinge directly on the substrate.

It has been reported [23] that an anode surrounding the cathode at a positive potential of 20–35 V will reduce the current to a grounded substrate to near zero for a cathode potential of –450 V. Without an anode, a total current equal to the discharge current will be about equally divided between a grounded substrate and adjacent grounded chamber walls [23]. An ungrounded or nonconducting substrate will quickly charge up to a potential sufficient to prevent further electron bombardment; ion bombardment will then occur until some equilibrium “floating” substrate potential is reached.

If a negative bias is applied to the substrate, then ions can be extracted from the plasma and large substrate ion currents can be produced.† The identity of these ions is not known; presumably the majority are discharge gas ions but a significant fraction may be ionized cathode material [46] and residual gas ions [78, 79]. Schiller *et al.* [23] have measured substrate cur-

* If an rf glow discharge (positive column) is present in the same vacuum chamber with a nonoperating magnetron target, the discharge glow will graphically delineate the magnetic field pattern in front of the magnetron cathode.

† This is in contrast to cylindrical magnetrons; Chapter II-2, Section VII.A.

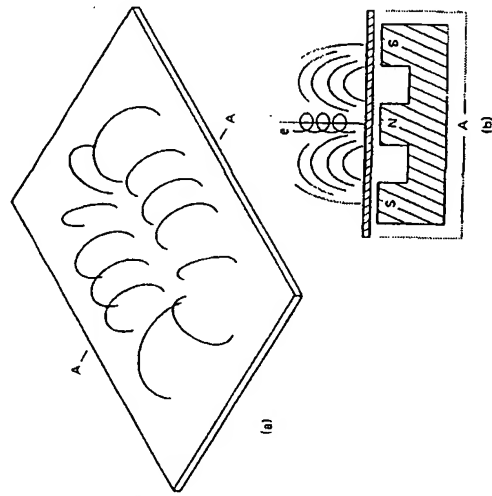


Fig. 11. Rectangular magnetron cathode: (a) magnetic field lines and plasma region, (b) cross section through section A-A showing field lines and escape path for electrons.

rents for substrate bias voltages from 0 to -400 V for disk planar magnetron cathode potentials of 350 – 485 V, $+35$ V on a concentric-ring anode, and a 5 cm cathode–substrate separation. They found that at 5 mTorr argon pressure for substrate bias potentials between -100 and -400 V, the substrate current was nearly independent of bias potential, especially at the lower cathode potentials. The substrate current saturated at about 8% of the target current. They concluded that for a given pressure, the energy of the bombarding ions could therefore be varied without substantially altering the total ion current or the ratio of ions to sputtered atoms at the substrate. For a given substrate bias, the ion current to the substrate decreased with increasing pressure. The highest ion/sputtered atom ratios at the substrate occurred at pressures slightly below 1 mTorr. The resistivity of Cr films sputtered at 5 mTorr in commercial grade Ar (about 0.2% O_2) at zero bias was $80 \mu\Omega$ cm. At -400 V bias voltage the resistivity was lowered to nearly $30 \mu\Omega$ cm. The deposition conditions were 485 V cathode potential and 6 A target current, resulting in about 500 mA substrate current. The substrate area was not given, but if it were equal to the cathode area (estimated to be 150 cm 2) then the ion current density at the substrate would have been about 3 mA/cm 2 . This is several times times

greater than cathode current densities during conventional dc sputtering. As Vossen [80] has pointed out, substrates can indeed be treated as sputtering targets. In this case, considerable resputtering of the depositing film must have occurred.

Since relatively small bias potentials can lead to large ion bombardment currents, the control of substrate bias is important in many applications of PM sputter deposition. Insulating substrates pose a particular problem in this regard. No data have been reported to date on PM magnetron sputtering with rf bias on insulating substrates.

2: Neutral Bombarding Species

As previously indicated, there is a significant ionization of sputtered species in a magnetron discharge [46]. Many of these ions may be neutralized and reflected from the target surface as atoms. At energies less than 1000 eV, reflection fractions can be as high as 0.4 and the particles can retain a substantial amount of their original energy [80]. Thus, in PM sputtering we might expect a significant flux of reflected high-energy sputtered atom bombardment of the substrate in addition to atoms arriving directly from the target. These same processes can cause high-energy neutral atom bombardment by the sputtering gas and residual gases. Ions of the sputtered species can also drift to the substrate and recombine with electrons at the substrate surface, thus releasing energy. These mechanisms may lead to higher surface mobility for atoms deposited by PM sputtering. Measurements of the energy distribution of PM sputtered atoms have not been reported.

3. Temperature

Manufacturers of PM sputtering equipment have claimed that for a given deposition rate the substrate temperature for PM sputtering is significantly lower than for rf sputtering. Details of the temperature-measurement technique are usually not given, but one example quotes for Cu deposition at 2000 Å/min a peak substrate temperature of $\sim 90^\circ\text{C}$ for PM sputtering versus $\sim 400^\circ\text{C}$ for conventional rf sputtering [24]. The temperature reached by a substrate depends on the heat capacity of the substrate, as well as the balance between the energy carried to it by the processes listed in Table VII and the energy lost by radiation and conduction. The total energy dissipated at the substrate for conventional sputtering has been variously estimated to be 4 – 5% of the total power delivered by the power supply for rf deposition [32] or 40% for dc sputtering [30]. These effects are discussed in Chapter 11-1.

Table VII
Substrate Heating Processes—Conventional Sputtering from
Water-Cooled Cathode

Mechanism	Approximate contribution (%) to substrate heating	
	rf ^a	dc ^b
Secondary electron bombardment	58	98
Argon ion bombardment		
Ion-electron recombination at substrate	22	negligible
Neutral and metastable atom bombardment		
Sputtered atom kinetic energy	15	1.5
Heat of condensation	5	0.5

^a Lau *et al.* [32] and Lamont and Lang [77].

^b Bail [30].

Lower substrate heating during PM sputtering is thought to be caused by reduced high-energy electron bombardment of the substrate. Even if all charged-particle bombardment and radiation input were eliminated, it may still be possible to get significant substrate heating by the condensing atoms—the heat of condensation plus their kinetic energy [49, 81] (see Section IV.B). The kinetic energy of PM sputtered atoms is not known, but the average energy may be higher than that generated by conventional dc sputtering due to the high percentage of ionization of the sputtered species [46]. In addition, the lower pressures and short source-substrate distances employed in PM sputtering will result in less kinetic energy loss by collision with sputtering gas atoms.

F. Power Supplies

1. Requirements

In conventional dc sputtering, power supplies are usually operated in a constant-voltage mode at 1000–3000 V and seldom operate at cathode current densities greater than a few milliamperes per square centimeter. In contrast, PM sputtering requires power supplies to operate in a constant-current mode at 300–700 V and at total currents to 25 A or greater. The output may be filtered or unfiltered dc; the latter may be advantageous in some applications [24]. The PM power supply must be able to survive high-voltage (several kilovolts) rf transients generated by the magnetron plasma, as well as by major and minor arcing along the cathode face and

II-4. PLANAR MAGNETRON SPUTTERING

161

from cathode to ground. Power supplies developed for cylindrical or conical magnetrons are also suitable for PM sputtering but are generally not rated above 10 kW. Higher power ratings are required for large-area PM sources.

2. Power Supply Design

A typical magnetron power supply [14, 43] employs a silicon-controlled rectifier dc drive for the control winding of a three-phase saturable reactor. A feedback signal derived from the voltage drop is detected in the dc output circuit to provide essentially constant current output. The power supply must also be provided with adequate short-circuit and rf high-voltage transient protection. In addition, a practical power supply should have the following features on a remote control panel: interlocks with status indicators for cathode water flow, cathode temperature (or output water temperature), vacuum, and others as required for operator protection; variable power output control, e.g., voltage control until an adjustable upper limit is reached—then constant-current control; and meters for output voltage and current. Useful optional features would include: panel control settings for maximum (controlled) power and maximum available voltage, automatic ramping to preset power level, digital power-output meter or digital voltage and current meters, adjustable anode voltage output (0–50 V dc), plasma ignition capability, e.g., tesla coil, and floating (nongrounded) output connections.

3. Arcing

Even though the operating voltage for PM dc sputtering is lower than that for conventional sputtering, the magnetron source is more susceptible to various types of arcing. This is probably caused by the electron current to various adjacent shields and anodes and by the considerable rf component in the discharge plasma (Chapter II-2, Section II.E). Present PM shield arrangements are borrowed from conventional sputtering; improvements related to the PM configuration should reduce cathode-shield arcing problems. Arcing between points on the face of the cathode, which usually occurs with a new cathode or one that has been exposed to air, is believed to be caused by charge build-up on locally insulating areas [14, 48, 49]. Easily oxidizable metals such as Al are prone to surface arcing. By slowly increasing the power on new or air-exposed targets, this arcing can be controlled until the sputtered area cathode surface is clean and the unsputtered region is covered by a backscatter conducting layer. Extreme cathode surface arcing ("racetrack arcs") can be extinguished by sensing a low-voltage, normal-current condition and interrupt-

ing the power source for 100 msec or so. A similar technique is used for arc suppression in electron-beam evaporation source power supplies (Hill [43], pp. 27-35).

G. Miscellaneous Techniques

1. Reactive Sputtering

Reactive dc PM sputtering of tantalum nitride films has been investigated [82]. Compared to conventional dc sputtering of Ta in Ar/N_2 , PM sputtering required a higher nitrogen concentration for equivalent film resistivities and temperature coefficients of resistance. Similar increased reactive gas concentrations (> 25%) were reported necessary for conical-magnetron dc reactive sputtering of titanium nitride and indium-tin oxide [83]. Reactive dc PM sputtering of TiO_2 from a Ti target in an 85:15 $\text{Ar}-\text{O}_2$ mixture has been used to deposit the high refractive-index layer of a multilayer dielectric coating on an Al mirror [60]. Optical dispersion of the films was measured for the 0.3-1.1 μm wavelength range. The deposition rate was 240 $\text{\AA}/\text{min}$ at 4.8 cm source-substrate spacing and a pressure of 2 mTorr. Deposition power was not given. Generally, rf is preferable to dc for PM reactive sputter deposition of nonconducting films because of problems caused by the formation of an insulating film on the target, e.g., igniting the discharge.

2. Ion Plating

The combination of substrate ion bombardment and deposition by evaporation in rapid repetitive sequence, termed "alternating ion plating," has been described [84]. A PM arrangement was used to ion bombard a negatively biased moving strip-steel substrate. Nickel was evaporated onto the substrate as it moved through the plasma region. A multipass planar rotating substrate arrangement was also described, again employing a PM plasma at the substrate and electron-beam evaporation. The resulting films were equivalent—in terms of porosity—to those deposited by conventional ion plating.

The use of a PM source for plasma plating, that is, simultaneous ion-beam thermal evaporation and sputtering from a molten PM source combined with a negatively biased substrate, has also been reported [85]. At 5 kW the thermal evaporation rate for Cu was 8 g/min. It is possible that such a source, once started and if sufficiently ionized, could be self-sustaining without an inert gas ambient [86].

II-4. PLANAR MAGNETRON SPUTTERING

3. Composite Targets

Ta/Al resistive films have been deposited by PM sputtering from a 9.5-mm-thick, 10-cm-wide, and 25-cm-long Al target inlaid with 5-mm-thick, 5.2-mm-wide Ta strips spaced 3.2 mm apart across the target width [64]. An oval ring plasma pattern was used. It was found that this Ta to Al area ratio (approximately 1.68:1 for the total cathode area) resulted in 53 at. % Ta in films deposited on substrates moving parallel to the Ta strips at 2.5 cm/min. Assuming a 2:1 Al:Ta sputtering yield ratio, a 59.5 at. % Ta film would be expected. Film resistivity and temperature coefficient of resistance uniformity was better than $\pm 10\%$ across a 20-cm width, indicating good uniformity of composition. The deposition rate at 300 W (280 V) was about 640 $\text{\AA}/\text{min}$ at 11 mTorr argon pressure.

4. Sputter Cleaning

Schiller *et al.* [45] have investigated the efficiency of sputter-cleaning sheet steel in a continuous linear-feed system employing a PM discharge in Ar. In this application, an electromagnet array was located above the grounded moving substrate. A water-cooled anode and surrounding ground shield were located below the substrate and facing the surface to be cleaned. It was found that even with ferromagnetic substrates up to 2-mm thick, a sufficient magnetic field could be generated adjacent to the substrate surface. By switching off the electromagnets, conventional glow discharge plasma cleaning could be compared with PM discharge cleaning. A 5- μm -thick Ni film was evaporated onto the moving substrate subsequent to discharge cleaning. Planar magnetron discharge cleaning was found to be superior to glow discharge cleaning in terms of energy consumption for equal Ni-film adherence. Methods of obtaining uniformity of discharge exposure by varying the magnet arrangement and substrate-magnet spacing were evaluated in terms of the temperature uniformity achieved. The best uniformity obtained was 3% over the 13-cm width of the steel strip.

It is possible that a similar positive anode, grounded substrate PM arrangement could be used for sputter etching or reactive ion etching of conducting materials.

III. RF PLANAR MAGNETRON SPUTTERING

Chapin [14] described a disk cathode rf PM source employing an electromagnet. No operating data were given other than that the discharge had a low impedance and that insulators could be sputtered at high rates.

Subsequently, rf PM deposition of Al_2O_3 [72] and SiO_2 [29, 60] were reported.

A. Comparison of RF and DC PM Sputtering

Planar magnetron sputtering with an rf potential on the cathode (usually 13.56 MHz or 27 MHz) enables the use of nonconducting materials as targets and allows direct or reactive deposition of dielectric films in the same manner as conventional rf sputtering. However, because of other considerations, such as the additional complexity of the rf power supply and impedance matching network, extraneous plasma generation within the deposition chamber [29], the difficulty of ensuring an efficient rf ground, and the possibility of rf radiation and rf electromagnetic interference (RFI/EMI), dc PM sputtering remains the better choice for deposition of electrically conducting materials.

Planar magnetron rf sputtering is somewhat similar to PM dc sputtering in that, because of low plasma impedance, high power densities are possible at low applied rf potentials. For example, at a power density of 2 W/cm² the dc self-bias on the target is about 360 V for PM rf sputtering compared to about 3500 V for conventional rf sputtering [66].

As Fig. 5 shows, the erosion areas of an rf target differ from those of a dc PM target. Instead of a single erosion groove approximately midway between the magnet faces of opposite polarity, there are two regions of deepest erosion near the edges of the magnet pole faces with a raised area approximately where the groove was for dc sputtering. The cause of this peculiar erosion pattern is not known. The rf target was isostatically pressed and sintered 99.5% Al_2O_3 ; the dc target was vacuum-cast Al-4% Cu.

B. Power Density, DC-Self-Bias, and Pressure Relationships

Figure 12 shows the relation between dc self-bias potential [66] and average power density for PM operation of a 6-mm-thick Al_2O_3 cathode in argon in the pressure range 10-20 mTorr. (Operation at 1 mTorr follows the same curve within the measurement error.) For comparison, the curve for dc PM operation of a 9-mm-thick aluminum cathode is also shown. The targets were identical in size and magnet configuration. The rf curve is approximately linear above 2 W/cm² and follows the relation of Eq. (2), Section II.C, with $n = 0.9$ and $k = 2.8 \times 10^{-3}$. For a conventional rf plasma, $n = \frac{1}{2}$ [66]. For the dc curve, $n = 4.6$ and $k = 1.9 \times 10^{-14}$. As previously mentioned, the larger the value of the voltage exponent n , the more efficient the plasma electron trapping (see Chapter II-2, Section IV).

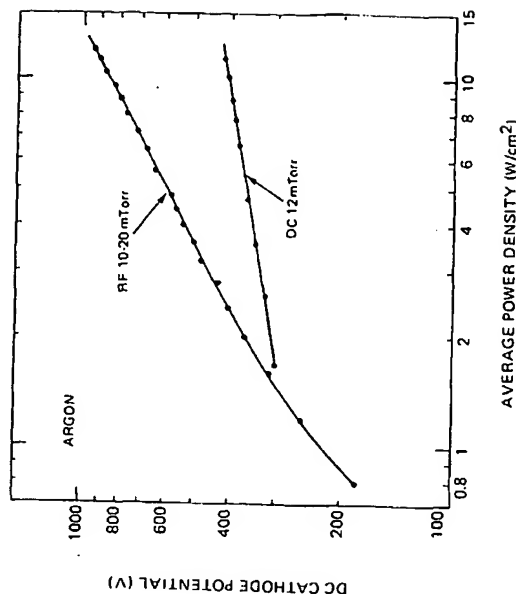


Fig. 12. Direct current self-bias versus average power density for rf PM operation of 10 x 25 cm Al_2O_3 cathode, argon pressure 10-20 mTorr. Cathode potential versus power density for dc PM operation of similar aluminum target having same magnet configuration shown for comparison.

The rf PM discharge is not as sensitive to pressure as is the dc PM magnetron. The deposition rate also appears to be constant ($\pm 10\%$) for a given power independent of pressure from 1-20 mTorr.

C. Rate Limitations and Rate Control

As discussed in Section II.D, the low thermal conductivity or high internal stresses of many targets, e.g., glass, Si, and sintered metallic oxides, will limit the maximum power density and hence the deposition rate. Targets having a relatively high coefficient of expansion combined with poor thermal conductivity may crack because of localized ion-bombardment heating. In non-PM high-rate sputtering of Al_2O_3 (a fairly good heat conductor), power densities of 120 W/cm² were attained but target life was limited to 15 min (Table VI). For targets having a high dielectric constant or high rf dissipation factor (dielectric loss tangent), rf bulk heating may be a consideration [80]. Reactive sputtering from a metallic target may be a way of circumventing these power limitations to achieve high rates.

Deposition rates for rf PM sputtering have been reported to be proportional to power [29, 72], so it is reasonable to assume that PM rf rates can be controlled in the same manner as in conventional rf deposition. The dc self-bias at the target may be useful for rate indication and control [66].

D. Power Supplies and Matching Networks

In contrast to dc PM sputtering, rf power supplies developed for conventional 13.56 MHz rf sputtering are also suitable for rf PM sputtering. Commercial rf sputtering supplies can tolerate the occasional arcs and transient high voltage pulses of rf PM sputtering. Conventional rf power supply/discharge plasma matching networks can also be used if the range of the variable components (either capacitors or capacitor and inductor) is sufficient to compensate for the lower PM plasma impedance. Matching network design for rf sputtering has been described previously [66, 87-90a].

Proper rf grounding of the power supply, vacuum chamber, and internal shielding is important to prevent unwanted substrate-plasma interaction and RFI/EMI. In many applications the substrates must be electrically isolated so that they can be biased or electrically "floated" to control charged-particle bombardment [80].

E. Deposition Rates

For a given average power density (power divided by cathode area), the deposition rates for rf PM sputtering are comparable to conventional rf sputtering, i.e., the slopes of the deposition rate versus power density curves are similar. Table VIII compares reported rf deposition rates for

Al_2O_3 and SiO_2 . These rates are lower than those for metals due to lower sputtering yields [65].

The addition of O_2 to the Ar sputtering gas has been reported to reduce deposition rates for PM rf sputtering of Al_2O_3 [72] and SiO_2 [29, 60], as is the case for conventional rf sputtering of oxides. Since the oxygen effect is partial-pressure rather than total-pressure dependent [92, 93], and PM rf sputtering pressures are typically lower than those for conventional rf sputtering, the percentage of O_2 required to reduce the sputtering rate is greater.

IV. APPLICATIONS

A. Industrial Coatings

Planar magnetron deposition offers obvious advantages in coating large surface areas and could replace or supplement electron-beam deposition for plastic film metallization and for antireflection and thermal-barrier coating of architectural glass [42, 43, 94, 94a]. Planar magnetron sources are advantageous in such applications because cathode size (usually length) can be scaled up, cathodes can be run side-by-side or sequentially in continuous coating machines, and they can be placed to deposit in any direction [24]. Other applications include decorative coatings on plastic [94b], functional coatings on plastic (antireflective lens coatings, video disk metallization), and anticorrosion or abrasion-resistant coatings on metals.

B. Thin Film Electronics

1. Integrated Circuits

a. Al metallization. The evolution and status of Al and Al-alloy metallization have recently been reviewed [95], and magnetron sputtering was characterized as a promising deposition technique that is amenable to process automation. An acceptable integrated circuit metallization process must deposit rapidly about $1 \mu\text{m}$ of Al alloy, usually containing 3-4% Cu and/or 1-2% Si with a reproducibility and uniformity of $\pm 5\%$ or better. The resulting film must form a continuous layer over the various Si, SiO_2 , and Si_3N_4 steps that abound on large-scale integrated circuits. In addition, the deposition process must not cause radiation damage to the underlying interfaces or dielectric layers by x-ray, electron, or ion bombardment, nor contaminate the metal-dielectric interface with mobile alkali-metal ions [95]. Typically, substrate heating ($\sim 300^\circ\text{C}$) is used during electron-beam

Table VIII
RF Sputtering—Deposition Efficiency Comparison

Target	Sputtering method	Power density range (W/cm ²)	Rate Power density ($\frac{\text{\AA}}{\text{min}} \frac{\text{cm}^2}{\text{W}}$)	Source-substrate spacing (cm)	Reference
Al_2O_3	conventional	1.2-2.4	50	3	[91]
Al_2O_3	PM ^a	3-8	51	7	[72]
Al_2O_3	high rate	20-120	52	2.5	[71]
SiO_2	PM	1-9	110	9	[29]
SiO_2	PM ^b	26	93	4.8	[60]
SiO_2	high rate	<20	~100	3.3	[71]

^a Linear substrate motion.

^b Drum rotation of substrates.

deposition to promote surface diffusion of the Al in order to achieve adequate step coverage; heating, however, increases the likelihood of mobile ion contamination. Electron-beam evaporators have been retrofitted with single or multiple conical-magnetron sputtering sources that simplify Al-Cu-Si or Al-Si alloy deposition, but substrate heating is still required for vertical step coverage [96].

A theoretical analysis of deposition from an extended sputtering source with translational motion suggests that such motion "will not drastically change the propensity for microcrack formation" [97]. The applicability of this analysis to magnetron sputtering seemed to be confirmed by the results of aluminum deposition with a PM source with linear substrate motion, since substrate heating was required for adequate step coverage [61]. However, other work has indicated that excellent step coverage can be achieved with PM sputtering without substrate heating [98]. The substrates were 7 cm from a 19×25 cm cathode with transverse substrate motion perpendicular to the long dimension of the cathode.

The reason for conflicting results with PM sputtering is not understood. It may be simply that the step contours tested were different; but it is tempting to speculate whether substrate heating, substrate bias, or both, may play a role. It is easy to show [49, 81] that the heat flux due to condensation of Al atoms having an average kinetic energy of 6 eV will be 0.142 W/cm^2 at a deposition rate of $1 \mu\text{m/min}$. If we assume that the average kinetic energy of PM sputtered aluminum atoms is 12 eV (or that 12 eV represents the average energy imparted to the substrate per Al atom by the first five processes listed in Table VII), then the heat flux will be 0.242 W/cm^2 . For a thermally isolated $300\text{-}\mu\text{m-thick}$ Si wafer, this represents a temperature rise rate of either 2.8°C/sec (6 eV) or 4.7°C/sec (12 eV). Thus, starting at 25°C the substrate will reach $\sim 190^\circ\text{C}$ in 1 min in the former case and over 300°C in the latter case. The critical point for microcrack formation occurs when self-shadowing starts. This depends on step geometry, but one can conclude that heat flux from the impinging atoms may not get the substrate hot enough, soon enough, to heal a microcrack unless the substrates are $\sim > 100^\circ\text{C}$ at the start of the deposition.

A negative substrate bias of the proper magnitude can promote microcrack healing by resputtering of the growing film [80, 99, 100]. If, in addition, the incoming Al is ionized, then conformal coating would be enhanced by self-sputtering and ion-plating effects. Any such unintentional bias effect would be sensitive to the degree of electrical isolation of the substrate, the position (and motion) of the substrate in relation to the cathode [72], the cathode power [23, 72], and the source-substrate spacing. An auxiliary anode would reduce or eliminate electron bombardment of the substrate and thus influence the floating bias. If bias effects are in-

deed responsible for enhanced step coverage during dc PM Al deposition, then variance in the reported experimental results would be expected.

A comparison of electron-beam deposited pure Al with PM sputtered Al indicated that the PM deposited Al, having smaller more randomly oriented grains, was more resistant to grain growth during heat treatment but the median time to failure due to electromigration was less [101].

b. Passivation. A low-temperature hermetic passivation process employing Al_2O_3 or Si_3N_4 is desirable [95]. Previously mentioned studies indicate that good step coverage can be achieved on aluminum metallization by rf PM sputtering of Al_2O_3 [72] or SiO_2 [29]. It has been shown that for conventional rf sputtering, an rf substrate bias of $\sim 60 \text{ V}$ is sufficient for vertical-wall step coverage with SiO_2 and a -100 V bias enables Al_2O_3 to cover a reentrant step [100]. Thus, PM rf sputtering offers an alternative low-temperature deposition technique.

2. Thin-film Thermal Printhead Fabrication

Thermal printheads employing a matrix of thin-film resistor elements to develop an image on thermally sensitive paper [102-104] are being used on computers and portable and hand-held printing calculators. The printing element requires an abrasion- and chemically-resistant overlay to prevent premature wearout. A $6\text{-}\mu\text{m-thick}$ Al_2O_3 layer deposited by the PM sputtering process previously described [72] has provided an effective printhead wear-resistant layer. The resistive element (Ta-Al) and the low-resistance interconnections (Al-Cu) are also deposited sequentially from dual independent cathodes in an in-line dc PM sputtering system [104].

C. Miscellaneous Applications

Table IX lists recent PM sputtering applications. In many applications, PM sputtering has the potential for continuous automated processing [105, 107].

On a smaller scale, dc sputter deposition from $5\text{-}7\text{-cm}$ diameter disk PM sources has been found advantageous for coating heat-sensitive biological samples with Au, Au-Pd, or C prior to examination by scanning electron microscopy. For example, not until soil fungi samples prepared by PM sputtering of Au were observed were the obliterative effects of filament evaporation coating noted. The conclusion was that vacuum evaporation was an unreliable coating technique for retention of microorganism surface structure detail [108].

Table IX
PM Sputtering Applications

Application	Materials	Purpose	Reference(s)
Sputter deposition	Al-1% Si	Integrated circuit metallization	[43]
	Al	Integrated circuit metallization	[97, 101, 101a]
	Al-SiO ₂ -TiO ₂	Coated Al mirror	[60]
	Cr-Au, Cr-Cu	Ceramic metallization	[106, 107]
	Ta-Al	Resistor film	[102, 64]
	TaN	Resistor film	[82]
	Al ₂ O ₃	Evaluation of film properties	[72]
	SiO ₂	Evaluation of film properties	[29]
Sputter cleaning	Cr alloy	Evaluation of film properties	[101b]
		Plastic metallization	[94b]
	Sheet steel	Clean prior to Ni evaporation	[45]
Ion plating	Ni	PM cathode at substrate during Ni evaporation	[84]
	Cu	PM as sputter/evaporation source	[85]

^arf PM.

V. CONCLUSIONS

Planar magnetron sputtering can deposit metallic films over large areas at rates comparable to electron-beam evaporation without the degree of radiation heating typical of thermal sources. The deposition rates for dielectric films are higher than those for conventional rf sputtering but are lower than the rates achievable by chemical vapor deposition; however, a wider range of materials may be deposited.

At the present stage of development of PM sputtering there are more questions than answers. For example, what is the energy distribution of the sputtered atoms? What percentage is ionized? How can the magnetic field pattern be optimized? What is the effect of controlling the substrate bias? In rf sputtering, what is the effect of an anode? Can direct reactive sputtering of dielectrics produce high-quality films at high rates?

The details of competitively advantageous production processes are often proprietary and this is becoming true for planar magnetron technology. Developments may be several years old or even obsolete before being published. Nevertheless, dissemination of information inevitably occurs to the general benefit of industry.

REFERENCES

1. L. I. Maissel, in "Handbook of Thin Film Technology" (L. I. Maissel and R. Glang, eds.), p. 4-1. McGraw-Hill, New York, 1970.

II-4. PLANAR MAGNETRON SPUTTERING

2. S. D. Dahlgren and E. D. McClanahan, *Proc. Symp. Deposition Thin Films*, 3rd. Univ. Rochester p. 20 (1969); S. D. Dahlgren, E. D. McClanahan, J. W. Johnston, and A. G. Graybeal, *J. Vac. Sci. Technol.* 7, 398 (1970).
3. F. M. Penning, *Physica (Utrecht)* 3, 873 (1936); U.S. Patent 2,146,025 (1939).
4. E. Kay, *J. Appl. Phys.* 34, 760 (1963).
5. W. D. Gill and E. Kay, *Rev. Sci. Instrum.* 36, 277 (1965).
6. E. Kay and A. P. Poenisch, U.S. Patent 2,282,815 (1966).
- 6a. P. D. Davids and L. I. Maissel, U.S. Patent 3,369,991 (1968).
7. J. R. Mullaly, *Res/Dev*, 22(2), 40 (1971).
8. K. Waga and S. Hayakawa, *Rev. Sci. Instrum.* 40, 693 (1969); U.S. Patent 3,528,902 (1970).
9. A. M. Gurevitch and W. F. Westendorf, *Rev. Sci. Instrum.* 25, 389 (1954); L. D. Hall, *Rev. Sci. Instrum.* 29, 367 (1958); *Science* 128, 279 (1958).
10. J. C. Helmer and R. L. Jepsen, *Proc. IRE* 49, 1920 (1961).
11. W. Knauer and E. R. Slack, *Trans. Natl. Vac. Symp.*, 10th, Boston, 1963 p. 180 (1964).
- 11a. W. Knauer, U.S. Patent 3,216,652 (1965).
12. K. M. Welch, U.S. Patent 4,006,073 (1977).
13. I. G. Kesaev and V. V. Pashkova, *Sov. Phys.—Tech. Phys.* 4, 254 (1959).
- 13a. J. P. Argana, CVC Products, Inc., Rochester, New York (private communication).
14. J. S. Chapin, *Res./Dev.* 25(1), 37 (1974); U.S. Patent Appl. 438,482 (1974).
15. H. R. Smith, *Proc. Electron Beam Process. Semin.*, 3rd, Stratford, England; *Universal Technology Corp.*, Dayton, Ohio p. 21 (1974).
16. R. L. Cormia, P. S. McLeod, and N. K. Tsujimoto, *Proc. Int. Conf. Electron Ion Beam Technol.*, 6th, *Electrochem. Soc., Princeton, N.J.* p. 248 (1974).
17. S. Hurwitz, *Trans. Conf. Prod. Sputter., Materials Research Corp., Orangeburg, N. Y.* p. 3.1 (1974).
18. A. M. Dorodnov, in "Fizika i Primenenie Plasmennich Uskorielej" (A. I. Morosov, ed.), p. 330. Nauka Tehnika, Minsk, 1974.
19. J. F. Corbani, U.S. Patent 3,878,085 (1975).
20. T. Van Vorus, *Circuits Manuf.* 15(6), 6 (1975).
21. G. N. Jackson, *Electrocomponent Sci. Technol.* 3, 254 (1977). Abstr.
22. W. D. Westwood, *Prog. Surf. Sci.* 7, 71 (1976).
23. S. Schiller, U. Heisig, and K. Goedicke, *Thin Solid Films* 40, 327 (1977).
- 23a. J. Markus, "Electronics and Nucleonics Dictionary," 3rd Ed. McGraw-Hill, New York, 1966.
24. T. Van Vorus, *Solid State Technol.* 19(12), 62 (1976).
25. P. S. McLeod, U.S. Patent 3,956,093 (1976).
26. F. A. Green and B. N. Chapman, *J. Vac. Sci. Technol.* 13, 165 (1976).
27. E. A. Nesbitt and J. H. Wernick, "Rare Earth Permanent Magnets." Academic Press, New York, 1973.
28. R. J. Parker and R. J. Studders, "Permanent Magnets and Their Application." Wiley, New York, 1962.
29. K. Urbanek, *Solid State Technol.* 20(4), 87 (1977).
30. D. J. Ball, *J. Appl. Phys.* 43, 3047 (1972).
31. W. G. Perkins, *J. Vac. Sci. Technol.* 10, 543 (1973).
32. S. S. Lau, R. H. Mills, and D. G. Muth, *J. Vac. Sci. Technol.* 9, 1196 (1972).
33. L. I. Maissel and J. H. Vaughn, *Vacuum* 13, 421 (1963).
- 33a. Materials Research Corp., Data Sheet 1057-AMD, Orangeburg, New York (1978). Unpublished.
34. S. Muto, Hewlett-Packard Co., personal communication (1975).
35. F. Rosebury, "Handbook of Electron Tube and Vacuum Techniques." Addison-Wesley, Reading, Massachusetts, 1965.

36. W. H. Kohl, "Handbook of Materials and Techniques for Vacuum Devices," p. 333. Reinhold, New York, 1967.
37. H. H. Manko, "Solders and Soldering," McGraw-Hill, New York, 1964.
38. J. van Esdonk and F. M. Janssen, *Res./Dev.* 26(1), 41 (1975).
39. J. A. Seichon and B. F. Stein, *Rev. Sci. Instrum.* 39, 1062 (1968).
40. A. K. Gupta, K. V. Kurup, J. Smanthanam, and P. Vijendran, *Vacuum* 27, 61 (1977).
41. P. J. Clarke, *Solid State Technol.* 19(12), 77 (1976).
42. N. Veigel, U.S. Patent 4,009,090 (1977).
43. "Physical Vapor Deposition" (R. J. Hill, ed.), pp. 114-149. Airco-Temescal, Berkeley, California, 1976.
44. E. Soxman, personal communication (1976); Anonymous, *Res./Dev.* 27(9), 63 (1976).
45. S. Schiller, U. Heisig, and K. Steinfelder, *Thin Solid Films* 33, 331 (1976).
46. N. Hosokawa, T. Tsukada, and T. Misumi, *J. Vac. Sci. Technol.* 14, 143 (1977).
47. J. W. Coburn and E. Kay, *J. Appl. Phys.* 43, 4965 (1972).
48. L. T. Lamont, Jr., *Varian Vac. Views* 9(3), 2 (1975).
49. L. T. Lamont, Jr., *J. Vac. Sci. Technol.* 14, 122 (1977) (Abstr).
50. G. K. Wehner and G. S. Anderson, in "Handbook of Thin Film Technology" (L. I. Maissel and R. Glang, eds.), p. 3-1. McGraw-Hill, New York, 1970.
51. K. H. Behndt, *J. Vac. Sci. Technol.* 9, 995 (1972).
52. E. B. Graper, *J. Vac. Sci. Technol.* 10, 100 (1973).
53. R. Glang, in "Handbook of Thin Film Technology" (L. I. Maissel and R. Glang, eds.), p. 1-3. McGraw-Hill, New York, 1970.
54. L. Holland, "Vacuum Deposition of Thin Films," p. 152. Wiley, New York, 1956.
55. J. Stroop, H. V. Neher, A. F. Whitford, C. H. Conner, and D. Heywood, "Deposition of Thin Films and Related Engineering," personal communication (1976).
57. S. Muto, W. Ebert, and R. S. Nowicki, Hewlett-Packard Co., unpublished observations (1976).
58. Reference 43, photograph following p. 102.
59. Perkin-Elmer Ultek, Inc., Sales Inf. Bull. No. 700-12. Palo Alto, California (1976). Unpublished.
- 59a. Perkin-Elmer Ultek, Inc., Engineering Note EN 1007. Palo Alto, California (1977). Unpublished.
60. L. D. Hartsough and P. S. McLeod, *J. Vac. Sci. Technol.* 14, 123 (1977).
61. P. S. McLeod and L. D. Hartsough, *J. Vac. Sci. Technol.* 14, 263 (1977).
62. Materials Research Corp., Data Sheet 1002-PED. Orangeburg, New York (1976). Unpublished.
63. S. Dushman and J. M. Lafferty, "Scientific Foundations of Vacuum Technique," 2nd Ed., Ch. 5. Wiley, New York, 1962.
64. W. Sperry and R. K. Waits, unpublished observations (1975).
65. Reference 1, p. 440.
66. L. T. Lamont, Jr. and F. T. Turner, *J. Vac. Sci. Technol.* 11, 47 (1974).
67. G. Sten and H. L. Caswell, *J. Vac. Sci. Technol.* 4, 128 (1967).
68. R. C. Weast, ed., "Handbook of Chemistry and Physics," 57th Ed. CRC Press, Cleveland, Ohio, 1976.
69. Reference 35, pp. 521-525.
70. Reference 43, p. 121.
71. D. H. Grantham, E. L. Paradis, and D. J. Quinn, *J. Vac. Sci. Technol.* 7, 343 (1970).
72. R. S. Nowicki, *J. Vac. Sci. Technol.* 14, 127 (1977).
73. R. K. Waits, unpublished observations (1976).

11-4. PLANAR MAGNETRON SPUTTERING

74. R. J. Ferran and J. J. Sullivan, *J. Vac. Sci. Technol.* 12, 560 (1975).
75. V. Hoffman, *Electron. Packag. Prod.* 13(11), 81 (1973).
76. M. Hablanian and P. Forant, *Varian Vac. Views* 11(1), 4 (1977); 11(2), 3 (1977).
77. L. T. Lamont, Jr. and A. Lang, *J. Vac. Sci. Technol.* 7, 198 (1970).
78. J. W. Coburn, *Rev. Sci. Instrum.* 41, 1219 (1970).
79. J. W. Coburn and E. Kay, *Solid State Technol.* 14(12), 49 (1971); *Appl. Phys. Lett.* 18, 435 (1971).
80. J. L. Vossen, *J. Vac. Sci. Technol.* 8(5), S12 (1972).
81. G. Gafer, *Philos. Mag.* 58, 1041 (1960).
82. J. Joly and J. B. Ranger, *C. R. Int. Colloq. Pulver. Cathod. Appl.* 2nd, Nice 1976 (1976).
83. P. J. Clarke, *J. Vac. Sci. Technol.* 14, 141 (1977).
84. S. Schiller, U. Heisig, and K. Goedicke, *J. Vac. Sci. Technol.* 12, 838 (1975).
85. S. Schiller, U. Heisig, and K. Goedicke, *J. Vac. Sci. Technol.* 14, 815 (1977).
86. R. C. Krutnal and W. R. Gesick, *J. Vac. Sci. Technol.* 7(6), S40 (1970).
87. D. J. Healy and M. Lauriente, *Proc. Natl. Vac. Symp., 13th, San Francisco, Calif.* p. 55 (1966).
88. J. S. Logan, N. M. Mazza, and P. D. Davidse, *J. Vac. Sci. Technol.* 6, 120 (1969).
89. N. M. Mazza, *IBM J. Res. Dev.* 14, 192 (1970).
90. E. C. Rock and C. W. Smith, *J. Vac. Sci. Technol.* 12, 943 (1975).
- 90a. A. Halperin, P. Silano, and L. West, *J. Vac. Sci. Technol.* 15, 116 (1978).
91. C. A. T. Salama, *J. Electrochem. Soc.* 117, 913 (1970).
92. R. E. Jones, H. F. Winters, and L. I. Maissel, *J. Vac. Sci. Technol.* 5, 84 (1968).
93. J. B. Lounsbury, *J. Vac. Sci. Technol.* 6, 838 (1969).
95. A. J. Leam, *J. Electrochem. Soc.* 123, 894 (1976).
96. V. Hoffman, *Solid State Technol.* 19(12), 57 (1976).
97. J. B. Bindell and T. C. Tison, *Thin Solid Films* 23, 51 (1974).
98. D. Chun, Hewlett-Packard Co., personal communication (1977).
99. J. L. Vossen and J. J. O'Neill, Jr., *RCA Rev.* 31, 276 (1970).
100. T. N. Kennedy, *J. Vac. Sci. Technol.* 13, 1135 (1976).
101. K. Kauchi, H. Maeda, S. Kishi, and Y. Haneta, *Electrochem. Soc. Extend. Abstr.* 77-1, 316 (1977).
- 101a. C. Ladas, *Trans. Conf. Sputter. Electron. Components; Materials Research Corp., Orangeburg, N.Y.* p. 6-1 (1976).
- 101b. R. Kossovsky, *Electrochem. Soc. Extend. Abstr.* 77-2, 429 (1977).
102. F. Ura, U.S. Patent 4,007,352 (1976).
103. S. Shibata, K. Murasugi, and K. Kaminishi, *IEEE Trans. Parts, Hybrids Packag. PHP* 12, 233 (1976).
104. R. B. Taggart and B. E. Musch, *Hewlett-Packard J.* 28(3), 9 (1976).
105. M. Hutt, *Solid State Technol.* 19(12), 74 (1976).
106. A. J. Aronson, *C. R. Int. Colloq. Pulver. Cathod. Appl.* 2nd, Nice p. 175 (1976).
107. A. Aronson and S. Weinig, *Vacuum* 27, 151 (1977).
108. S. Draggan, *Appl. Environ. Microbiol.* 31, 313 (1976).

Ion Beam Deposition

JAMES M. E. HARPER

IBM Thomas J. Watson Research Center
Yorktown Heights, New York

I. Introduction	175
II. Ion Beam Generation	176
A. Production of Ions	177
B. Ion Sources	177
C. Beam Extraction and Control	183
D. System Requirements	186
E. Measurement of Beam Properties	188
III. Secondary Ion Beam Deposition	189
A. Source and Beam Characteristics	189
B. Target Processes	191
C. Film Properties	192
D. Reactive Ion Beam Sputtering	195
IV. Primary Ion Beam Deposition	198
A. Deposition Systems	198
B. Beam Energy Limitations	199
C. Beam Size Limitations	200
D. Film Properties	201
V. Concluding Comments	203
References	204

I. INTRODUCTION

Ion beams are used in thin film deposition in two basic configurations. In primary ion beam deposition (Fig. 1a) the ion beam consists of the desired film material and is deposited at low energy (around 100 eV) directly onto a substrate. In secondary ion beam deposition (Fig. 1b), or ion beam sputter deposition, the ion beam is usually an inert or reactive gas at

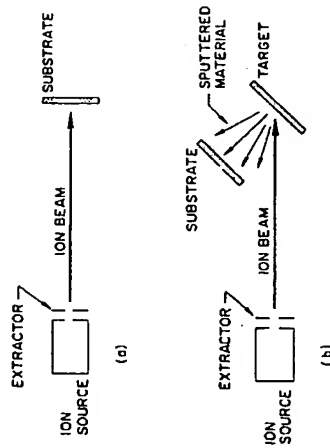


Fig. 1. Ion beam deposition configurations. (a) Primary ion beam deposition, with ion beam deposited directly onto substrate. (b) secondary ion beam deposition, with inert or reactive ion beam sputtering target material onto substrate (also called ion beam sputter deposition).

higher energy (hundreds to thousands of electron volts). The beam is directed at a target of the desired material, which is sputtered and collected on a nearby substrate.

Ion beam deposition allows greater isolation of the substrate from the ion generation process than is found in the conventional diode sputtering configuration. This enables control over the substrate temperature, gas pressure, angle of deposition, and the type of particle bombardment of the growing film, as well as independent control over the ion beam current and energy. This flexibility characterizes ion beam deposition as a useful technique in the study of thin film growth processes and has led to unique film properties not obtained in conventional deposition methods.

In this chapter the two techniques of ion beam deposition will be described, with the emphasis on the major controlling parameters which affect the deposition process. First an introduction will be given to ion source types and the basic processes of ion beam formation and control.

II. ION BEAM GENERATION

Two types of ion source will be described which are used in practical thin film deposition, the Kaufman source and the duoplasmatron. The Penning ion source will also be described to introduce some of the concepts of ion generation. Several other ion sources will be included which have particular characteristics which may be useful in future deposition applications. For further details on ion sources and ion beam transport the reader is referred to the book by Wilson and Brewer [1] and its references, and to conference proceedings [2].

A. Production of Ions

The ionization mechanism used in most ion sources is electron impact ionization in a low voltage gas discharge. The cross section for electron impact ionization has a maximum at low electron energy, about 70 eV for argon [3], therefore high electron energies are not needed for efficient ionization. More important are the electron supply rate and gas pressure, since the mean free path for ionization is inversely proportional to gas pressure (about 0.1 cm at 1 Pa) [4].

Almost any species can be introduced into a gas discharge as a vapor or by sputtering from the solid. The discharge may consist primarily of the desired species, for example argon for secondary ion beam deposition, or it may use an inert gas to support the discharge while the desired material is introduced to be ionized, as in primary ion beam deposition of a metal. The types of discharge have been described elsewhere [5]. Some discharge parameters will be mentioned here for orientation, not as a description of a particular configuration. Source pressures range from 10^{-2} to 10^{-3} Pa, giving mean-free-paths for atomic collisions of 0.01–100 cm. The neutral atom density is several times the ion density [4], but since extraction is more efficient for ions, the ionization efficiency can be high, up to 50–90%. Multiple ionization is usually a few percent of single ionization [4, 6]. The mean-free-path for electron–electron collisions is longer than the size of the source, so the electron and atom populations are usually not in thermal equilibrium [4]. Other mechanisms of ion production used in ion sources are thermal ionization [7], surface contact ionization [8], and field ionization [9, 10].

B. Ion Sources

1. Penning Ion Source

The configuration of a Penning ion source [11, 12] is shown in Fig. 2, consisting of a cylindrical anode with two cathodes forming the end plates. A magnetic field of several hundred gauss is applied parallel to the cylinder axis. With an argon pressure of about 15 Pa and a discharge voltage of several hundred volts, a plasma fills the chamber. Electrons repelled from the cathodes are attracted to the anode but the magnetic field constrains the electrons to follow helical trajectories, causing them to oscillate between the cathodes and increasing their path length, enhancing the ionization efficiency. Ions formed by collisions between fast electrons and gas atoms are attracted to the cathodes, where they bombard the surface, generating more electrons by secondary electron emission. As the discharge voltage is raised, the discharge current increases approximately

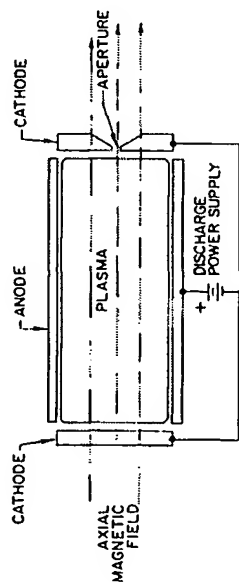


Fig. 2. Penning ion source with aperture in cathode.

linearly at first, indicating that the rate of secondary electron emission is not changing with ion energy. However, the ions bombarding the cathodes heat the surfaces, and if the discharge voltage is further increased, the cathodes become hot enough to emit electrons thermionically. At this point the electron emission increases rapidly, and the discharge changes to a negative resistance characteristic [12], as shown in Fig. 3.

Two points are illustrated here. First, the discharge has different modes of operation depending on the rate at which electrons are supplied to the plasma, as secondary electrons or by thermionic emission. Electron supply rate is therefore a primary control over the ion density. In a Pen-

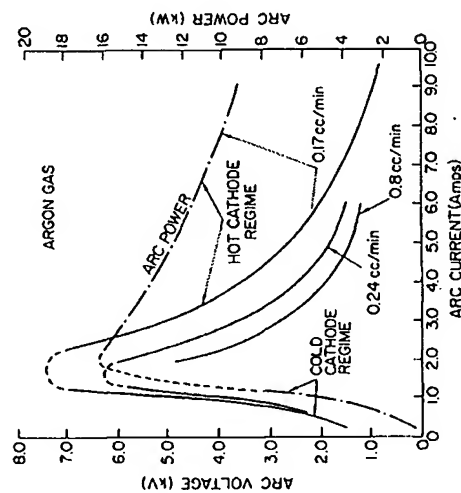


Fig. 3. Current-voltage characteristic of a Penning ion source showing transition from cold cathode regime to hot cathode regime. Argon flow rate is given in cm^3/min (from Bennett [12]).

ning discharge, the discharge current is not independent of the discharge voltage, limiting the degree of control, and this is one reason why many ion sources use a separately heated thermionic cathode to supply electrons at a rate essentially independent of the discharge voltage. The thermionic cathode supports the discharge at lower discharge voltages, minimizing heating of the source and sputtering of cathode material into the discharge. The second point is the role of the magnetic field in constraining the electron orbits. The cyclotron radius of a 1000 eV electron in a magnetic field of 10^{-2} T (100 G) is about 1 cm [13]. Thus fields on the order of hundreds of gauss are sufficient to constrain the electron trajectories in a Penning source and allow operation at lower pressures than with no magnetic field.

The ion and electron density in the plasma is high enough to shield electric fields over distances typically less than 0.01 cm (the Debye length [4, 14]). This shielding isolates the plasma from external fields, thus ions are extracted from the plasma only when they diffuse to the plasma boundary, which may be considered as an ion emitting surface. An aperture in the anode or cathode (Fig. 2) is used to extract ions into a beam. The energy of ions in the beam is determined by the potential at which the ions originate. Since the plasma is highly conductive, it is approximately an equipotential region and may be characterized by a plasma potential, a few volts positive with respect to the anode [4]. The ions originate at close to plasma potential, with an energy spread determined primarily by the discharge voltage. For accurate focusing, mass separation, and energy control it is important that the initial ion energies have a narrow spread. In a cold-cathode Penning source this is in the range 10–50 eV [15]. Thermionically supported Penning sources have an energy spread of a few electron volts [16].

2. Kaufman Ion Source

The Kaufman source is an extension of the Penning source concept to include a thermionic cathode and multiple aperture extraction. This broad-beam ion source was originally developed in 1960 for use in space propulsion as an ion thruster [17]. A review of ion thruster technology is given by Kaufman [4], and sources optimized for uniform large area ion milling are described by Reader and Kaufman [18] and Robinson and Kaufman [19].

The cross section of a Kaufman source is shown in Fig. 4 [20]. The anode forms one end of the cylindrical discharge chamber and the screen grid (at cathode potential) the other end. The thermionic cathode circles the chamber wall, supported by four clamps, and the discharge gas is in-

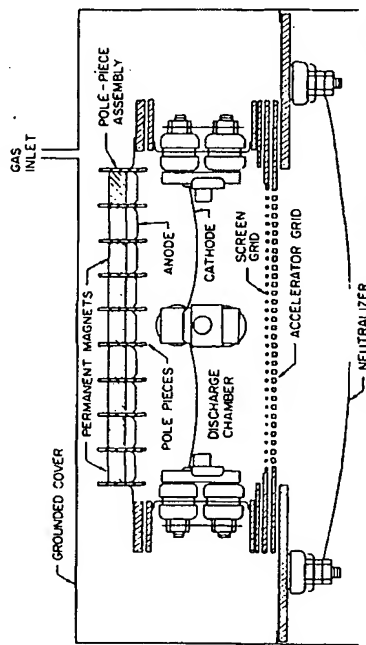


Fig. 4. Cross section of a Kaufman ion source which generates a 10 cm diameter beam (courtesy of Ion Tech, Inc. [20]).

roduced through the anode. Behind the anode is an array of permanent magnets which produce a multipole or "picket fence" field configuration across the anode surface. In some configurations an axial magnetic field is used, with both end surfaces at cathode potential (an example is given in Section III.A). The function of the magnetic field is to keep electrons emitted by the cathode from traveling directly to the anode. The screen grid contains about 1400 holes of 0.21-cm diameter. Aligned with this grid at a separation of 0.1 cm is an extraction or acceleration grid of similar structure [18]. A potential difference between the two grids shapes the plasma boundary into a meniscus at each aperture in the screen grid. The shape and control of this ion emitting surface will be discussed in the section on extraction.

The heated cathode allows operation at lower pressure (0.1 Pa) and discharge voltage (50 V) than a cold cathode Penning source, minimizing multiple ionization and reducing the ion energy spread to 1–10 eV [4, 15]. The discharge current is typically 1–2 A. Primary control over the ion density is through the rate of electron emission, which has two regimes of behavior. For low emission the ion density is proportional to the emission

on pressure is determined by arcing in the source. An important advantage of independent cathode control is that the beam current may be varied independently of the discharge voltage and beam energy. The extracted argon ion current density from a 10-cm diameter source is in the

range 1–2 mA/cm² at a beam energy of 500–2000 eV [18]. The ionization efficiency is in the range 50–75% [4].

Various magnetic field configurations have been tested for ionization efficiency and beam uniformity. The multipole configuration [18, 19, 21] (Fig. 4), with about 0.01 T (100 G) at the pole pieces, produces a more uniform beam profile than an axial or diverging field [4].

3. Duoplasmatron

The duoplasmatron, developed in 1956 by von Ardenne [22], is a versatile ion source used to generate high intensity narrow ion beams. The name refers to the dual manner of constricting the plasma in an arc discharge by both electric and magnetic fields to form a small region of high ion density adjacent to the extraction aperture. The configuration is shown in Fig. 5 [23]. With an argon pressure of 1–100 Pa in the source, the hot cathode filament supports a discharge of 1–2 A between the cathode and anode (with 80 V discharge voltage). Between these electrodes is the intermediate or *zwischen* ("in-between") electrode held at a potential intermediate between that of the cathode and anode (40 V). The canal-shaped aperture in the intermediate electrode confines the discharge electrically and an intense magnetic field (0.1–0.3 T) (1000–3000 G) between the intermediate electrode and anode constricts the plasma axially. The anode region is shown in Fig. 6 [23]. The diverging magnetic field region shapes a plasma meniscus next to the anode aperture, which becomes the emitting surface for ion extraction. Argon ion currents of 2 mA [24] and

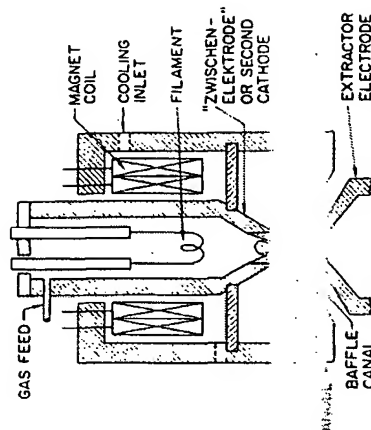


Fig. 5. Cross section of a duoplasmatron ion source showing location of plasma in baffle canal (from Brewer *et al.* [23]).

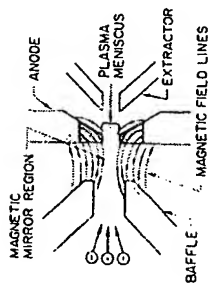


Fig. 6. Anode region of duoplasmatron showing constriction of plasma and plasma meniscus (from Brewer *et al.* [23]).

higher [15, 25] are obtained at about 20 keV beam energy through an aperture of 0.03-cm diameter with an energy spread of 10–50 eV [15]. The converging region of magnetic field lines acts as a magnetic mirror to reflect electrons back to the cathode region [23], enhancing ionization efficiency.

4. Other Ion Sources

Several additional ion source types will be mentioned, with references, to indicate the variety of approaches to generating ions. These are listed with the hope of stimulating novel applications to thin film deposition processes. The *glow discharge* ion source is simply a glow discharge between two plane electrodes with no magnetic field or thermionic cathode. One variation of this configuration is the *hollow anode* ion source in which the beam is extracted through a hole in the cathode plate [26, 27]. The *hollow cathode* ion source, of the same basic type, may be used in place of a thermionic cathode in applications where lifetime or contamination from the cathode are important [4, 28]. The *twin anode* or *electrostatic* ion source uses the geometrical arrangement of the anode surfaces within a surrounding cathode to produce long oscillatory electron trajectories, gaining enhanced ionization with no magnetic field [29].

The term *arc discharge* ion source applies to several configurations. In one type the desired material is vaporized from a crucible directly into a low voltage thermionically supported arc discharge. With some materials the arc is self sustaining with no support gas [30, 31]. No magnetic field is used. Ions are extracted with a low energy spread of 0.1–1.0 eV [31].

The *electrohydrodynamic* ion source [10] is a liquid-metal field emitting tip which generates a very high brightness, low current ion beam. A strong electric field pulls the liquid into a cusp-shaped tip less than 10⁻⁴-cm diameter.

A vapor stream of atoms may be ionized by direct electron bombardment from a hot filament [32]. A variation of this technique, the *ionized cluster* source [33], vaporizes the desired material through a small orifice, inducing cluster formation as the vapor stream expands.

High multiply-charged ion states, for example Ar¹⁴⁺, Kr¹⁷⁺, Xe²¹⁺,

have been obtained by constraining the ions long enough for sequential ionization [34]. *Negative ion* beams may be generated by sputtering the desired material with a beam of low ionization potential material such as cesium [35], and may also be extracted from an off-axis aperture in a duoplasmatron [36]. *Very high current* hydrogen ion beams (several amperes) have been generated with a combined duoplasmatron and Penning ion source [37].

C. Beam Extraction and Control

1. Ion Extraction

Ions in the interior of the plasma diffuse to the plasma boundary, where they are extracted by an electric field. The rate of ion extraction is determined by Child's law of space charge limited current flow [4, 38]. In a planar geometry the space charge limited current density between two planes a distance d apart with potential difference V is

$$j = (4\epsilon_0/9)(2q/m)^{1/2}(V^{3/2}/d^2),$$

where ϵ_0 is the permeability of free space and q/m is the charge-to-mass ratio of the particles. This relationship determines the upper limit for planar current flow and demonstrates two important controls on the current density. Ion extraction from the plasma increases rapidly with increased extraction voltage and with decreased spacing between the plasma boundary and extraction electrode. For nonplanar geometries only the proportionality constant changes in Child's law, thus a given geometry may be characterized by the ratio $j/V^{3/2}$, the *perveance* [4].

Acceleration takes place mainly in the extraction region, since this is usually where the greatest potential drop occurs. However, the ion energy at the target is determined only by the potential difference between the target and the point of origin of the ion, which is usually within a few volts of anode potential. The usual arrangement is to have the target at ground potential and raise the entire source chamber to the desired beam voltage, with the extraction electrode at ground potential or lower.

As an example of extraction geometry, Fig. 7 shows the potential distribution through the extraction region of a Kaufman source [4]. The screen electrode is at the source potential (positive) and the accelerator or extraction electrode is negative. The screen voltage is lower than the anode voltage by the discharge voltage, with the difference between plasma potential and anode voltage not indicated. The extraction electrode is held negative, typically –200 V for source voltage of 1000 V, for two reasons. The rate of ion extraction is increased by a larger potential

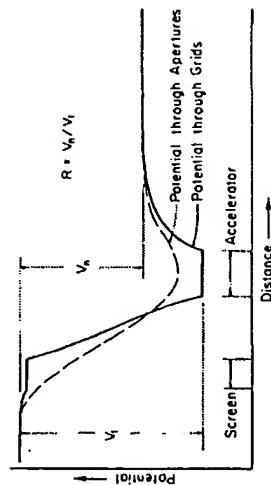


Fig. 7. Potential distribution through the extraction region of a Kaufman source (from Kaufman [4]).

difference between screen and accelerator electrodes, and the extraction electrode serves as a barrier to keep electrons (added to the beam downstream for neutrality) from backstreaming into the source and effectively shoring out the extraction field. The potential distribution is characterized by the net-to-total voltage ratio $R = V_n/V_i$, which is typically between 0.5 and 0.8 [4], the upper limit being determined by electron backstreaming and the lower limit by increased divergence of the beam.

The plasma meniscus adjusts its position such that the ion current density across the plasma boundary satisfies the space charge limited condition for the electric field at that location. In the desired operating condition (Fig. 8a) [4] the ion beam passes through the extraction electrode without impingement. As the ion density is increased, the meniscus moves downstream to a position of higher electric field, closer to the extraction electrode. If the ion density is too high, or extraction voltage too low, the meniscus can move to the position of Fig. 8b in which direct impingement on the extractor occurs, causing sputtering of this electrode. The normally concave shape of the meniscus forms an ideal ion emitting surface which gives the beam an initial convergence to counteract the de-

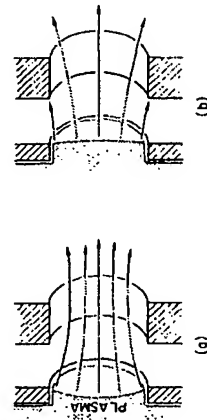


Fig. 8. Location of plasma meniscus in one aperture of a Kaufman source. (a) Normal extraction condition. (b) with excessive ion production (from Kaufman [4]).

focusing tendency of the accelerate-decelerate sequence. Thus, the beam may be extracted with a low divergence half-angle, typically $5-10^\circ$ in a Kaufman source [4]. Beam divergence may also be decreased by increasing the separation between screen and extractor grids or by adding a third grid at ground potential [18, 39, 40]. The tradeoffs between extracted current, grid voltages, beam divergence, and extraction geometry have been studied in detail in the development of ion thrusters [4, 39, 41]. In addition to direct impingement of the beam, which is to be avoided, a second form of ion current to the accelerator grid arises from charge exchange collisions between ions and neutral atoms in the extraction region producing fast neutrals and slow ions. The slow ions are attracted to the accelerator grid and sputter its surfaces. This erosion is visible on the downstream side of the grid [4] but is serious only for very long term operation.

If the aperture diameter and grid spacing are scaled together, the ion current per aperture is independent of aperture size. This enables large beam currents to be extracted through grids containing a large number of closely spaced apertures. The upper limit on current is determined by the difficulty in maintaining a small gap between thin large diameter grids. The ion current density profile is shown in Fig. 9 for several distances from a 10-cm diameter Kaufman source operating at 500 eV [18], indicating uniformity of $\pm 5\%$ across the inner half of the beam.

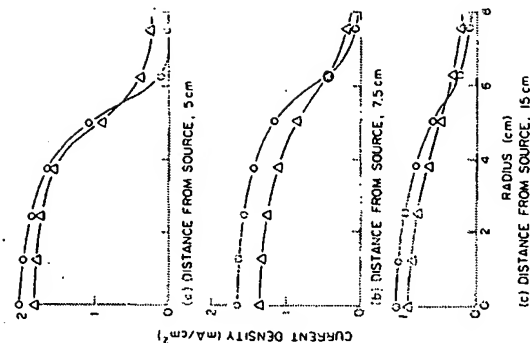


Fig. 9. Current density profile of 500 eV argon ion beam from 10-cm diameter Kaufman source at several distances from source and at two values of chamber gas pressure. O, 5×10^{-4} Torr; Δ , 15×10^{-4} Torr (from Reader and Kaufman [18]).

The beam profile from a duoplasmatron or other single aperture source is usually close to Gaussian, determined more by the range of transverse velocities and the ion transport optics than by the initial profile at the extractor.

2. Beam Transport

Beam deflection is accomplished by transverse electric fields [42] and mass separation by magnetic fields [43]. If mass separation is desired with a straight trajectory, crossed electric and magnetic fields will select a particular velocity and deflect all others, acting as a mass separator [31, 44].

One type of focusing lens will be mentioned briefly. The Einzel, or unpotential, lens consists of a decelerate section followed by an accelerate section back to the initial beam energy [24]. The field distribution defocuses the beam while it is at high energy and focuses while it is at low energy, resulting in a net focusing of the beam. Examples of using the Einzel lens to focus the beam from a single aperture source are given in Sections III.A and IV.A.

3. Neutralization

The above methods of deflecting and focusing an ion beam apply to a nonneutralized beam. With the broad beam from a Kaufman source, neutralization is necessary to avoid beam spreading by space charge repulsion. This is accomplished by adding electrons from a thermionic filament (Fig. 4) and monitoring the net current to the target or a beam probe. When the net current is zero, the arrival rate of ions equals that of electrons, but the ions are not neutralized by recombination since the mean free path for this process is much larger than the beam diameter [4]. The beam is itself a plasma, in which the electrons rapidly distribute to cancel net charge, thus electron injection does not have to be uniform. The neutralizer filament is sputtered by the beam, and contributes to contamination unless suitable masking is provided. An alternate method of injecting electrons into the beam is from a hollow cathode source (the plasma bridge neutralizer) which may be located outside the beam [4, 44a].

D. System Requirements

1. Materials

Materials in the ion source must be stable at the temperatures involved (several hundred degrees Celsius), have low sputtering yield if subjected to ion bombardment, and low susceptibility to corrosive gases, if used.

II-5. ION BEAM DEPOSITION

Particularly important components are the cathode filaments and electrode apertures. Thermionic cathodes are tantalum or tungsten wire [18], or barium oxide coated mesh [24]. Thermal cycling leads to embrittlement and failure, with exposure to oxygen or more reactive gases shortening filament life greatly. Magnetic fields may be supplied by an external solenoid, usually air cooled, or by permanent magnets, which do not have to be exposed to the plasma. Other surfaces may be molybdenum for thermal stability. In the Kaufman source the screen and accelerator grids span a large diameter, with a small separation, typically 0.1 cm. Thermal expansion leads to distortion, directly affecting extracted ion density and uniformity. These problems are minimized in ion thrusters by using dish-shaped molybdenum grids [4], such that thermal distortion occurs uniformly across the grids, but these are difficult to make accurately. Pyrolytic graphite provides the best combination of low thermal expansion, high thermal conductivity, and mechanical stiffness in flat grids [18]. For high-purity films it may be necessary to fabricate parts of the ion source out of materials that are compatible with the desired film [27, 45].

The lifetime of the source is limited by the hot cathode burning out or by buildup of sputtered material in the source, leading to shorting or to insulating coating of electrodes. Flaking of accumulated sputtered material may also cause shorts and insulating supports must be shielded from sputter coating. Lifetimes range from hours to months depending on operating conditions.

2. Vacuum and Gas

The gas pressure in the ion source is determined by the type of source and the ion density needed for the desired ion current. Therefore the pressure at the target is determined by the conductance of the ion source apertures and the pumping speed of the pump, assumed to be in the target region. Background gas in the path of the beam has two effects in addition to the effect of gas pressure on the source itself. Large angle collisions contribute slightly to beam divergence, and charge exchange collisions which result in fast neutrals and slow ions contribute to the sputtering rate at the target without registering as ion current to a probe [18]. The pressure must be below about 1 Pa to sustain a beam without excessive scattering, but is usually maintained around 0.1 Pa or lower to minimize divergence and contamination.

3. Electrical and Other Requirements

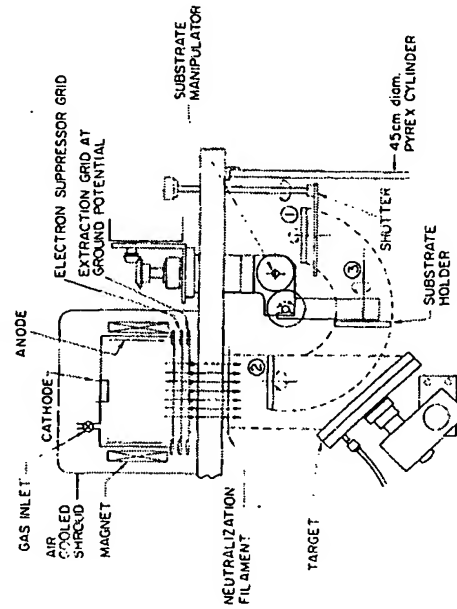
The electrical power requirements of the ion sources described above are straightforward. The filaments may be heated with ac or dc current of

III. SECONDARY ION BEAM DEPOSITION

Several aspects of secondary ion beam deposition (or ion beam sputter deposition, Fig. 1b) differ from other sputtering processes: *low background pressure* gives less gas incorporation and less scattering of sputtered particles on their way to the substrates; *directionality of beam* allows variable angle of incidence of beam on target, and angle of deposition on substrate; *almost monoenergetic beam* with narrow energy spread allows study of the sputter yield and deposition process as a function of ion energy, and enables accurate beam focusing and scanning; *beam independent of target and substrate processes* allows changes in target and substrate materials while maintaining constant beam characteristics; *target and substrate not part of rf circuit* minimizes substrate heating [51]; and *independent control of beam energy and current density*. Some applications of secondary ion beam deposition are reviewed by Weissmantel and Gautherin [51a] and uses of ion beams for device fabrication are discussed by Spencer and Schmidt [51b].

A. Source and Beam Characteristics

Two examples of secondary ion beam deposition systems will be illustrated. A Kaufman source [52] is shown in Fig. 10, equipped with a water-



several amperes at low voltage. The discharge power supply is relatively low voltage, but may need to deliver several amperes in some sources. The extraction voltage power supply is high voltage, low current, and should be protected against arcing or shorting which may occur between the electrodes. Feedback control of the beam current may be applied to the cathode heater power supply.

Heat inputs to the system include the hot cathode in the source, electron and ion bombardment of source surfaces, neutralizer filament, if used, and magnet current if electromagnets are used. The source is cooled by forced air cooling of the magnet coil and chamber, cold water cooling of the source electrodes or surrounding shroud, or more localized cooling on high-power sources, including glycol or liquid-nitrogen cooling of single aperture electrode structures. Multiaperture grids are thin and cannot be effectively cooled, thus they must be stable at their operating temperature of several hundred degrees Celsius. Heat input to the target is primarily from the energy of the ion beam if the target is far enough from the source to neglect radiation. A 1000 eV, 1 mA/cm² beam supplies 1 W/cm² to the target. Thus the total power input to the target may be 100 W or higher. Water cooling is needed to keep target temperatures to less than about 200°C [46]. One of the advantages of secondary ion beam deposition is that these heat loads are essentially confined to the source and target, and the substrates do not experience a high heat input. In primary ion beam deposition the beam energy and current density are significantly lower, and heat input to the substrate is not a problem.

E. Measurement of Beam Properties

Positive ion current density from a Kaufman source is measured with a probe biased to about -20 V to repel the low-energy electrons in the beam. Secondary electron emission from the probe surface contributes to a high reading, but is a relatively small contribution (a few percent) at low beam energies with refractory metal probes [47]. The secondary electrons may be collected in a Faraday cup with a negatively biased entrance aperture. Beam profile and divergence are measured with an array of Faraday probes [41] or a scanning wire [48]. Ion energy distribution is measured with an electrostatic analyzer [49, 50]. Degree of neutralization is measured with an unbiased probe to sample the net beam current. The beam composition and charge state [6] may be determined by mass separation

ionizer-mass spectrometer combination [50].

cooled target and rotating substrate holder which can be positioned for substrate precleaning in the beam, film deposition, and target precleaning. The beam diameter is 7 cm, target diameter 13 cm, and substrate holder diameter 6.5 cm. Argon ion energy is variable at 200–2000 eV, with current density up to 1 mA/cm², total beam current about 30 mA. Higher current sources are also available [18].

A duoplasmatron ion source with Einzel lens [53] is shown in Fig. 11. This system produces a 20 keV argon ion beam focused to 0.4-cm diameter at the target with total beam current of 2 mA, corresponding to a current density of about 20 mA/cm². The narrow beam allows deposition of thin films from milligram amounts of target material. Early studies of secondary ion beam deposition were made by Chopra and Randlett [54] using a modified duoplasmatron and by Schmidt *et al.* [27] using a hollow anode source.

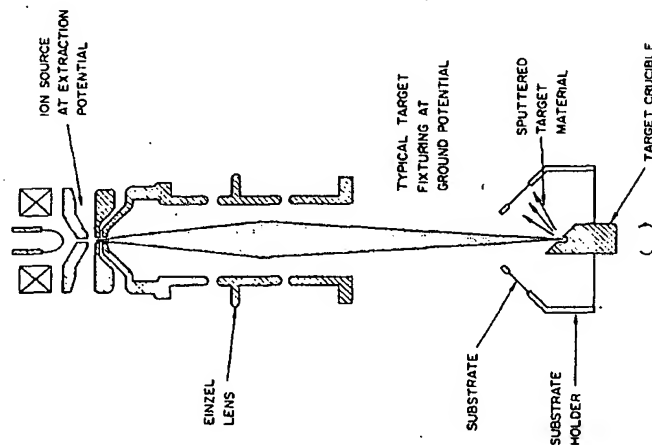


Fig. 11. Secondary ion beam deposition system using a duoplasmatron with Einzel lens to focus the beam (courtesy of General Ionex Corp. [53]).

B. Target Processes

1. Sputter Yield

The sputter yield, s , is the ratio of ejected target atoms to incoming beam ions. Only a summary of the aspects of sputter yield important in ion beam deposition will be given here. More complete descriptions of sputter yield are given by Winters [54a] and Oechsner [54b].

- (1) s increases with ion energy E approximately proportional to $E^{1/2}$ from a threshold of a few tens electron volts to a maximum around 10–20 keV, then decreases at higher energy due to implantation [55]. s is of the order of unity in the energy range considered here [56].
- (2) s generally increases with mass of ion [54b, 55, 57].
- (3) s increases with angle of ion incidence away from normal incidence, to a maximum at an angle which depends on ion and target species and energy, then decreases to zero at grazing incidence [54b, 58].
- (4) s depends on the target material, but differences are generally within an order of magnitude [56].
- (5) the energy of sputtered particles is in the range of tens of electron volts, with a small fraction at higher energies [59].

The sputtering rate for an ion beam of current density 1.0 mA/cm² with $s = 1$ corresponds to 6×10^{15} atoms/sec/cm² removal rate, which gives about 7 Å/sec for copper, on the order of several monolayers per second. Since the ion density is low enough to treat each ion-target collision independently, the sputtering rate is proportional to current density. The duoplasmatron source in Fig. 11 operates at 20 keV to optimize the sputter yield for high deposition rates. The Kaufman source in Fig. 10 operates at lower energy, 500–2000 eV, to minimize heating of substrates in its complementary use as an ion milling system.

Argon is the commonly used source gas, although some gains may be found by using heavier gases for higher yields. Some dependence of film properties on sputtering gas species has been reported [27, 60].

The increase of sputter yield with angle of ion incidence allows gains by tilting the target. This also directs the sputtered material away from the beam direction, decreasing the rate of accumulation of material in the source. Typically an angle near 45° is used. The maximum sputtered flux is directed normal to the target surface for high ion energy (> 10 keV) and increasingly towards the angle of reflection of the beam for low energy [54b, 60a]. This is because at low ion energy the first ion-target collision becomes dominant as contrasted with the collision cascade at higher energy [54b]. The angular distribution of sputtered material may also be affected by severe erosion and cone formation on the target surface [61].

2. Target Types

In addition to deposition from single element and compound targets, alloy films may be deposited from composite targets with different sectors made of different materials [46]. The relative areas are determined from the relative yields of the materials. In multicomponent targets a difference in sputter yield of target constituents leads to altered layer formation [62] in which the target surface is enriched in the lower sputter yield constituent. After this layer reaches equilibrium, the sputtered flux usually matches the target composition [46, 62a]. A dependence of sputtered film composition on angle of ejection has however been reported [62b] with Ni-Fe and Ni-Cu alloy targets. It is necessary to presputter the target for a period of time before exposing the substrates, to stabilize the ion source and beam characteristics, outgas surfaces by heating, clean the target surface, and establish the altered layer.

Sputtering of insulators requires neutralization of the beam to avoid charging of the target surface, leading to beam deflection and sparking. Neutralization is less of a problem with metals, where secondary electrons from the target help to neutralize the beam. To avoid ion bombardment of unwanted surfaces it may be necessary to collimate the beam with an aperture [45].

3. Effects of Target on Ion Source

The main interaction of the target with the ion source is through the flux of sputtered material which accumulates in the source. This leads eventually to flaking, shorting, or contamination of the target surface. Accumulation of insulating material in the source may lead to difficulty maintaining constant beam conditions or extinguish the source and cause difficulty restarting. These problems are eliminated by removing excess material from the source. The sputtered flux may also modify the discharge slightly by becoming a constituent of the plasma and the beam.

C. Film Properties

Since the substrates in an ion beam sputtering system are essentially isolated from the source and target processes, substrate temperature may be independently controlled, enabling deposition on temperature sensitive materials. Normally the substrate is at ground potential and receives no bombardment by energetic electrons as in diode sputtering. Some bombardment by energetic reflected beam atoms occurs [62c,d]. Substrate size and location are limited somewhat by the conflicting requirements of being close to the target for high deposition rates and also not obstructing the ion beam:

1. Deposition Rate and Uniformity

The primary controls on deposition rate are ion current density, ion energy, and geometrical collection efficiency. The order of magnitude of deposition rate for the systems described above is several hundred angstroms per minute. The deposition profile of Ti deposited in the duoplasmatron system shown in Fig. 11 is given in Fig. 12 [24]. The profile is somewhat narrower than the cosine distribution which would be expected from a simple point source. Uniformity of $\pm 5\%$ is obtainable over a region of $\pm 15^\circ$ about the target normal, and may be improved by rotating the substrates. The effects of angle of incidence and ion energy on the deposition profile are discussed by Oechsner [54b].

2. Purity

With an inert gas pressure of 10^{-3} Pa at the substrate, the growing film is bombarded by inert gas at the rate of about 4 monolayers/sec. However, the sticking coefficient of these thermal atoms is very low, leading to little incorporation in the film. Schmidt *et al.* [27] made a detailed study of the purity of ion beam sputtered films prepared with a hollow anode ion source using various inert gas ion beams at 0.1 mA/cm², 1200 eV. Inert gas incorporation was on the order of 0.1–1.0 at. % in Cr, Mo, Ti, W, and Zr, with less than 100 ppm atomic fraction in Ta and Au. Hinneberg *et al.* [63] report <0.1 at. % Ar with traces of Ta, Fe, and W in ion beam sputtered Si. For reactive gases such as oxygen, however, maintaining a low partial pressure is more crucial. With deposition rates of several monolayers per second, oxygen incorporation to several atomic percent is not unlikely with reactive metal films. Getter pumping, liquid-nitrogen trapping, and bakeout of the system help reduce oxygen incorporation. Castellano *et al.* [46] report 0–1.2 at. % oxygen in Al films, the higher concen-

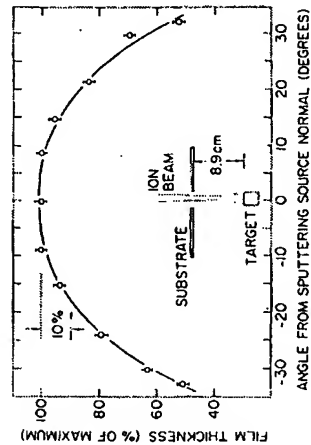


Fig. 12. Thickness profile of Ti deposited in system shown in Fig. 11 using 22 keV, 2.5 mA argon ion beam. The substrate location is shown (from Scaife *et al.* [24]).

trations found in obliquely deposited films, also up to 2 at. % oxygen in Ni and Au. Schmidt *et al.* [27] found oxidation of Ta films to be a problem. Further oxygen measurements were reported by Westwood and Ingreby [45].

Major metal contaminants can be traced to components of the system subjected to ion bombardment, such as the cathode plate in a hollow anode ion source [27] or a current probe exposed to the beam [46]. Contamination from the source is decreased by operating at a low discharge voltage to minimize energetic particles in the source, optimizing extraction for minimum ion bombardment of extraction apertures, locating the neutralizer out of sight of the target and substrates, using low sputter yield system components, and in critical applications by fabricating source structures from materials compatible with the desired film. Another approach is to mass analyze the beam, but this is usually not feasible in deposition systems which need a reasonably high deposition rate. Schmidt *et al.* [27] found higher purity films sputtered by Xe than by Ar.

3. Structure and Mechanical Properties

Small ion beam deposition systems have been installed in electron microscopes to study the early stages of sputtered film growth [64]. The qualitative features of film growth are found to be similar to evaporated films.

Weissmantel [65] finds Si films to be amorphous when deposited below 500°C and epitaxial on spinel above 750°C. Epitaxial Au and Ag on NaCl were obtained at room temperature by Chopra and Randlett [54]. Crystal structure and orientation are usually the same as obtained by other deposition techniques, although some unusual structures have been observed. Chopra and Randlett [54] obtained fcc modifications of normally bcc Ta, Mo, and W, and normally hcp Re, Hf, and Zr in an intermediate temperature range of substrates using argon ion beam sputtering. The refractory metal films were amorphous when deposited at room temperature. Schmidt *et al.* [60] observed impurity stabilized bcc Zr from an improperly cleaned target. Increases in lattice constant up to several percent were found by Schmidt *et al.* [60] in transition metal films due to gas incorporation. Texture is found to depend on angle of deposition [46], becoming more porous at glancing angles, similar to observations for evaporated films. Some measurements of grain size have been reported [46, 54, 60, 64].

Adhesion of ion beam sputtered films is reported to be superior to evaporated films [60], the improvement attributed to the higher energy of arrival of the sputtered particles. The arriving particle energy (tens of

electron volts) helps to clean the substrate by sputtering away adsorbed gases, gives greater mobility to condensing atoms, and provides implantation into the substrate, enhancing chemical bonding and localized rearrangement. Hudson [66] reports improved adhesion of SiO₂ and Al₂O₃ films by depositing at a substrate temperature of 400°C.

Ion beam sputtered films were found by Schmidt *et al.* [27] to have lower internal stress than evaporated films. No curling was observed when removing Au and Ta films from various substrates. Castellano *et al.* [46] found low values of intrinsic stress in Al films. When substrates were exposed to the perimeter of the ion beam, however, subjecting the growing film to ion bombardment, the stress was found to change from tensile to compressive, and correlated with increased porosity and oxygen content of the films.

4. Electrical Properties

Schmidt *et al.* [60] studied the superconducting transition temperature T_c of ion beam deposited transition metals, and found increases over bulk values for Mo, Ti, Zr, and W. Cr was found to be superconducting for the first time. Decreases in T_c were found for Nb, Ru, Ta, and V. The changes in T_c are attributed to lattice expansion, correlating with the atomic size of the sputtering gas used. In all cases films sputtered with Xe gave the highest T_c . Preliminary results in ion beam sputtering of superconducting Nb-Ti films are given by Gautherin *et al.* [62a]. Values of mobility in ion beam deposited Si are discussed by Hinneberg *et al.* [63], and some results on ion beam sputtered GaAs and InSb were reported by Weissmantel *et al.* [65].

D. Reactive Ion Beam Sputtering

Secondary ion beam deposition may also be used to deposit compounds of reactive species, such as oxides and nitrides. Several methods are shown in Fig. 13 for depositing an element (usually a metal) in combination with a gaseous component with which it reacts. Method (a) uses an inert gas ion beam to sputter either the metal or compound target, with reactive gas added to the deposition region. Even in sputtering the compound directly it is usually necessary to add the reactive gas to compensate for the loss of reactive component by dissociation [40]. Method (b) uses an ion beam of the reactive gas itself or a mixture of inert and reactive gas. Usually a mixture is preferable to the pure reactive gas in the beam to maintain a reasonable sputtering rate. Method (c) is a dual ion beam method in which the inert gas ion beam sputters the metal target and a reactive gas ion beam is directed at the substrate surface.

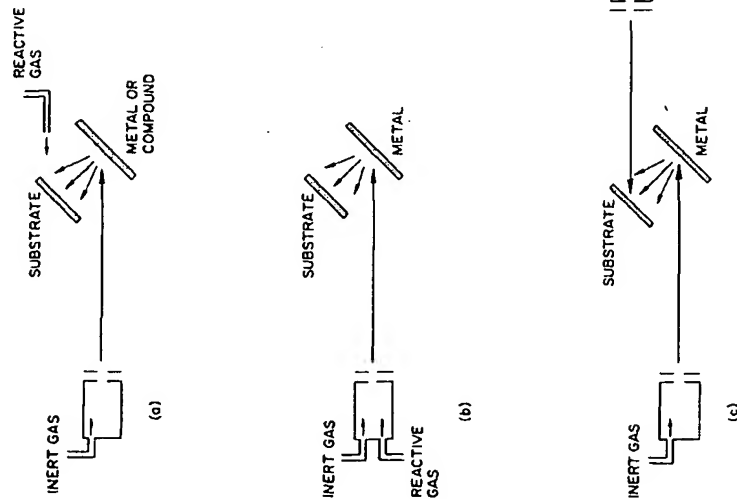


Fig. 13. Reactive secondary ion beam deposition methods. (a) Inert gas ion beam, reactive gas added to substrate region, (b) reactive and/or inert gas ion beam, (c) dual ion beam method using inert gas ion beam to sputter metal target and reactive gas ion beam to bombard growing film.

In reactive ion beam sputtering the compound formation may take place either at the target or substrate, depending on the technique used. The deposition rate of Ti and Zr as a function of oxygen partial pressure using method (a) is shown in Fig. 14, as measured by Castellano [67]. The rapid drop in deposition rate occurs when the oxide begins to form on the target surface faster than it is sputtered away, and the deposition rate becomes characteristic of the oxide, which has a lower sputter yield than the pure metal. At this point the deposited film becomes a transparent oxide film. The transition pressure is shifted to higher pressure as the beam current density is increased, since the arrival rate of oxygen at the target will

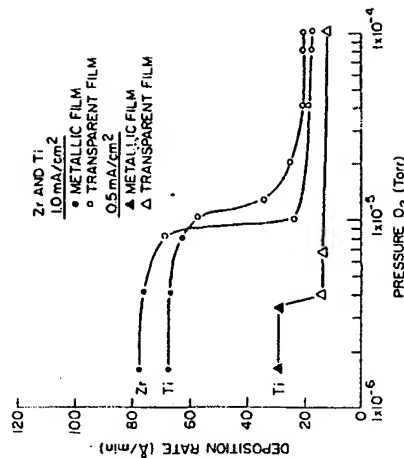


Fig. 14. Deposition rate of Zr and Ti films versus oxygen partial pressure in Kaufman ion source system using 2 keV argon ion beam at 0.5 mA/cm² and 1.0 mA/cm² (from Castellano *et al.* [46], reprinted by permission of Bell Telephone Laboratories, Inc.).

also find evidence of oxide formation at the target in reactive sputtering of Ta with method (b). Incompletely oxidized films were attributed to the lack of a chemically active substrate region which is found in glow discharge sputtering. Using a single beam of N₂⁺ ions to sputter a Si target with method (b), Weissmantel [68] found stoichiometric Si₃N₄ films only at the lowest beam energy and deposition rate. At higher beam energy the films are deficient in nitrogen, and display poor electrical properties compared with glow discharge sputtered films. In this configuration the nitride forms on the target surface.

With the dual beam technique of method (c), Weissmantel [68] used an Ar⁺ ion beam to sputter a Si target while the substrate surface was bombarded simultaneously by a N₂⁺ beam. Above a minimum level of N₂⁺ flux, stoichiometric Si₃N₄ films were always formed. By shadowing a portion of the substrate from the N₂⁺ beam it was found that a Si film condensed in the region not exposed to N₂⁺ (only 2–3 wt % N in Si). These results show that in this dual beam method the reaction takes place at the substrate. The impact of the reactive ion beam on the substrate dissociates N₂ to atoms enabling reaction with the condensing Si atoms and local rearrangement. Films prepared by the dual beam technique display the same electrical characteristics as rf sputtered films. Thus, the flexibility of ion beam techniques allows unusual conditions to be established at the target and

substrate surfaces. The fabrication of efficient photovoltaic heterojunctions of indium-tin oxides on silicon by ion beam sputtering is reported by DuBow *et al.* [69].

IV. PRIMARY ION BEAM DEPOSITION

Deposition of a charged particle beam (Fig. 1a) has several advantages over neutral particle deposition: control over *deposition energy*; ability to *deflect* and *focus* the beam; ability to *mass analyze* the beam to yield a highly pure deposit. Primary ion beam deposition has been used in two areas of interest. The first is the attempt to fabricate microcircuit elements by maskless deposition. The second is the investigation of the dependence of film properties on deposition energy.

A. Deposition Systems

In 1965, Wolter [70] first investigated the properties of Ag, Cu, and Cr films deposited as ions from a low voltage arc discharge between a thermionic cathode and the molten metal. A versatile arc discharge source is described by Amano *et al.* [31], in which the arc is self sustaining for Mg and Pb without an inert support gas. This source produces a beam of 10^{-6} A with an extraction voltage of 4–5 kV with an energy spread of several tenths of 1 eV. The beam is subsequently focused through an Einzel lens and decelerated to the substrate in the system shown in Fig. 15 [31].

A different approach is represented by the source used by Aisenberg and Chabot [71] to deposit carbon films of diamondlike structure. In this

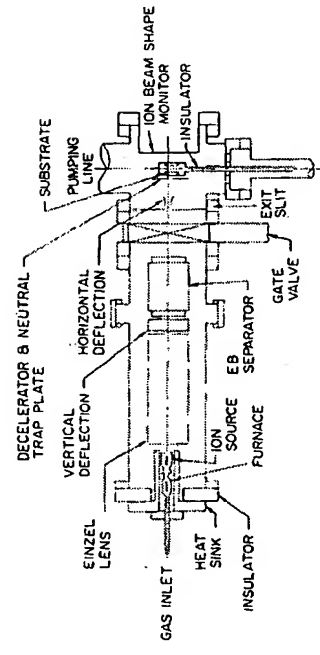


Fig. 15. Primary ion beam deposition system using extraction at high voltage (4 kV) followed by mass separation and deceleration to the substrate (from Amano *et al.* [31]).

II-5. ION BEAM DEPOSITION

source a Penning discharge arc is maintained between carbon electrodes using argon support gas, and the beam consists of carbon ions and neutrals and argon ions and neutrals. Spencer *et al.* [72] reported further work on diamondlike films with a similar source.

B. Beam Energy Limitations

In primary ion beam deposition the useful energy range of the beam is limited at low energies by low deposition rates and space charge spreading and at high energies by self-sputtering of the growing film or sputtering of the substrate. To determine the beam energy for maximum deposition rate, the dependence of self-sputter yield on energy for the material must be considered. The self-sputter yield s for Al, Cr, Cu, Au, and Ag [73] is shown in Fig. 16. The energy at which $s = 1$, E_1 , varies from a few hundred to nearly 1000 eV, depending on the material. Above this energy no material accumulates and the beam sputters the substrate. Hayward and Wolter [73] found that self-sputter yields may be calculated approximately from inert gas yields using the mass conversion factor of Almen and Bruce [73a]. Further discussion of the ion mass dependence of sputter yield is given by Winters [54a], Oechsner [54b], and Sigmund [55]. For maximum deposition rate, self-sputtering yield must be minimized, thus deposition at the lowest energy is required. However, in a deposition system the beam current which can be delivered to a given area of the substrate increases with beam energy approximately linearly [74]. Therefore the combination of factors results in an optimum beam energy of about $\frac{1}{2}E_1$ [74]. Thus the maximum deposition rate occurs when approximately half of the incoming beam ions are being sputtered away. This is a very different environment at the growing film surface compared with most

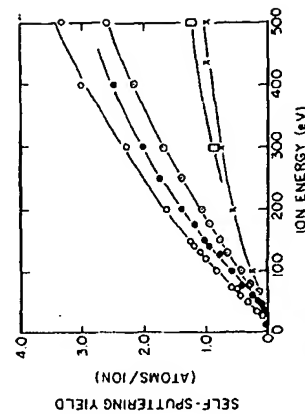


Fig. 16. Self-sputtering yield versus ion energy for several metals. \square , Aluminum; \square , chromium; \circ , copper; \bullet , gold; \times , silver (from Hayward and Wolter [73]).

other deposition processes, and is approached only by bias sputtering at high substrate bias. Operating the ion beam at an energy greater than E_1 may be used to pre-clean the substrate [71] or to ion mill.

If an inert support gas is accelerated with the desired material, the inert gas component of the ion beam will also sputter the growing film, changing the deposition rate and modifying the properties of the film [72]. If beam purity is critical, mass separation may be carried out [31]. Neutrals which form in the beam may be removed by deflecting the ion beam prior to deposition [31, 75]. The low deposition energies involved in primary ion beam deposition make it difficult to extract ample current directly from an ion source. For this reason extraction is usually performed at a high voltage with subsequent beam focusing and deceleration [31, 74, 75].

C. Beam Size Limitations

Attempts at maskless deposition have aimed at determining the minimum beam size obtainable with a useful deposition rate. An analysis by Fair [74] identified several factors which limit the beam size in the operation of an indium deposition system. These factors are summarized here.

Space charge repulsion is the most fundamental limit to beam size, because it remains even in a perfect optical system fed by a perfect ion source. Wilson and Brewer [76] discuss the regimes in which space charge repulsion dominates beam size. The effect increases for low ion energy, high current, and high mass. Thus the condition for minimizing space charge repulsion is the opposite of that required for efficient film deposition.

In the system analyzed by Fair, however, the beam size was limited by *chromatic aberration* [74] caused by the energy spread of ions in the source producing a distribution of axial velocities in the beam. An energy spread of 5 eV was sufficient to dominate the attainable spot size. While theoretically capable of depositing a 100 eV indium beam of 0.01-cm diameter at 6×10^{-8} A, the system actually gave 0.075 cm at 1×10^{-8} A, 100 eV. Fair attributed the energy spread to collisions in the source.

Thermal velocity spread perpendicular to the beam axis is due to the temperature of the source [74]. Fair found a crossover between thermal velocity limiting of beam size and space charge limiting in the region of interest. For an indium ion beam of 30–400 eV, current $< 3 \times 10^{-8}$ A and minimum diameter $< 10^{-2}$ cm, thermal velocity dominates. For larger diameter or current, space charge dominates.

Spherical aberration due to nonparallel trajectories is determined primarily by the ratio of beam diameter to lens diameter, and may usually be

D. Film Properties

1. Deposition Rate and Uniformity

The dependence of deposition rate on beam energy has been discussed. The optimum beam energy is around half of the energy of unity self-sputter yield. Some examples of demonstrated rates will be given without describing each system. Amano *et al.* [31, 77] deposited 1000–3000 Å of Pb and Mg in 7 hr at 24 eV and 10^{-5} A, with 1.5-cm spot size. The energy E_1 was found to be 200 eV for Pb and 500 eV for Mg. Wolter [70] deposited Cr and Cu at 25 Å/min at 200 eV, 5×10^{-6} A, 0.03-cm spot size. Other results are reported by Probyn [78] and by Colligon *et al.* [75]. Hayward and Wolter [73] studied the transition from deposition to self sputtering for Au, Cu, Ag, Cr, and Al films.

With these low beam currents, uniform coverage is not achieved. The beam current distribution is determined by the ion optics and is usually close to a Gaussian profile. The deposited film, however, may depart from the beam profile depending on the extent of resputtering of the film. The beam current profile and the deposited film profile are compared in Fig. 17 for In deposited by Fair [74] at 5×10^{-8} A for 30 min at 300 eV. The flat top

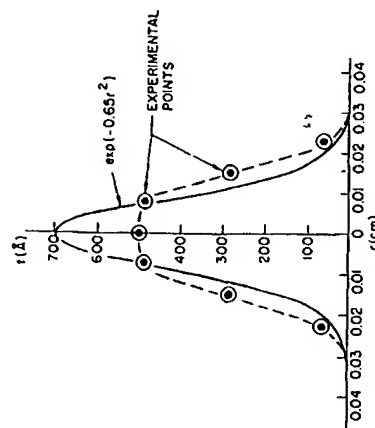


Fig. 17. Ion beam profile (solid line) and deposited film profile (dashed line and points) for primary ion beam deposition of indium at 300 eV, 5×10^{-8} A (from Fair [74]).

of the deposit indicates self-sputtering and possibly lateral migration due to the high surface mobility of the film. Scanning the beam improves uniformity, but the scan rates are very low, on the order of 0.01 cm/min for a 200-Å-thick film of In at 100 eV [74]. Thus, a narrow beam maskless deposition system does not look attractive.

2. Purity

Amano *et al.* [77] found <0.1 at. % heavy mass contamination and <10 at. % light mass by Rutherford backscattering analysis in Pb films deposited at 24–200 eV using a velocity mass filter. Similar purity was obtained for Mg [77]. Thus, high purity may be obtained with a mass analyzed beam. With argon present in the beam, Spencer *et al.* [72] found evidence of superlattice ordering of Ar in diamond structure C films deposited at 50 eV, with no oxygen or metals detected. Simultaneous sputtering of the film by the inert gas may help clean the surface of loosely bound impurities, similar to bias sputtering.

3. Structure and Mechanical Properties

Amano *et al.* [77] studied the morphology of Pb and Mg films deposited over a range of energies. With Pb films deposited at 24 eV, coverage of the surface was not achieved until a thickness of 2500 Å. However, films deposited at 48 and 72 eV were continuous at lower thicknesses. Grain size was also found to increase with increased deposition energy from 48 to 120 eV for Pb on C. With Mg, films deposited at 48 eV were smooth, but at 100 and 150 eV craters due to self-sputtering appeared. Colligon *et al.* [75] found 150 Å Pb films deposited at 50–60 eV to be discontinuous, and continuous when deposited above 600 eV. Wolter [70] found the crystal structure of Cr, Cu, and Ag films to be the same as vacuum evaporated films. Aisenberg [79] reports epitaxial growth of Si on Si by primary ion beam deposition.

Adhesion is also expected to depend on the energy of deposition. Wolter [70] found Ag very adhesive when deposited at 100 eV or higher. Amano and Lawson [77] report that Pb films deposited on graphite at 24–169 eV pass the adhesive tape test. Mg deposited at <100 eV failed the adhesive tape test, while films deposited at >120 eV passed. The adhesion is attributed to a higher degree of implantation at higher energy. Aisenberg and Chabot [71] report diamondlike C films adherent to Si and to stainless steel.

4. Metastable Phases

The demonstration by Aisenberg and Chabot [71] and by Spencer *et al.* [72] that carbon may be deposited in the diamond phase by primary ion

beam deposition shows that under some circumstances metastable phases may be formed. This is a consequence of the highly dynamic state of the growing film surface which experiences a combination of deposition and sputtering. If a range of bond types is available to an incoming ion it may be possible to preferentially resputter those of lower energy and selectively leave a desired bond type, thereby growing a particular phase. Normally one would expect the thermodynamically stable phase to form, but if two or more structures are of competing stability, the possibility arises of preferentially retaining one type. Spencer *et al.* [72] attribute the preferential formation of diamond bonds to the variation of bond energy with crystal orientation, which correlates with the observed (111) orientation perpendicular to the film surface. The charge state of the incoming ion may also affect the growth process and film structure, although this has not been shown to be a controlling factor.

5. Compounds and Reactive Species

Aisenberg and Chabot [80] deposited Al_2O_3 by primary ion beam deposition of Al with oxygen support gas, but the source was hampered by the buildup of insulating coatings on the electrodes. ZnS has been deposited by Van den Berg and Armour [81] by evaporating ZnS powder into an argon ion beam from a duoplasmatron. Hayward and Wolter [73] examined the effects of oxygen on deposition and self-sputtering of Al. Another approach is to create a compound surface layer by ion bombardment with a reactive ion beam, which is more closely related to ion implantation [82].

V. CONCLUDING COMMENTS

While ion beam deposition does not compete with high rate sputtering processes for coverage of large areas, it does offer unique capabilities for studying the sputtering process under controlled conditions. It can be used to shed light on the processes occurring in other deposition methods, for example the study of reactive sputtering by Weissmantel [68]. The ability to control the deposition energy in primary ion beam deposition has been shown to lead to unusual film structures, such as the direct deposition of diamondlike films by Aisenberg and Chabot [71] and by Spencer *et al.* [72]. This capability may be extended into precise control of film growth similar to molecular beam epitaxy.

As larger ion sources are developed [19, 83] for ion milling applications, their application to primary and secondary ion beam deposition will be stimulated. Also the imaginative use of ion beams in creating novel deposition environments appears to be an area only beginning to be explored.

ACKNOWLEDGMENTS

The author thanks R. J. Gambino, H. R. Kaufman, and R. S. Robinson for helpful comments in preparing the manuscript and R. N. Castellano for permission to use his results prior to publication.

REFERENCES

1. R. G. Wilson and G. R. Brewer, "Ion Beams with Applications to Ion Implantation," Wiley, New York, 1973.
2. *Proc. Symp. Ion Sources Form. Ion Beams*, BNL 50310 Brookhaven Natl. Lab., Upton, N.Y., 1971; *Proc. Int. Conf. Ion Sources*, 2nd, Vienna, 1972. Österreichische Studiengesellschaft für Atomenergie, Ges. m.b.h. (SGAE) Vienna, 1972.
3. W. Lotz, *Asrophys. J., Suppl. Ser.* 14, No. 128, p. 207 (1967).
4. H. R. Kaufman, *Adv. Electron. Electron. Phys.* 36, 265-273 (1974).
5. S. C. Brown, "Introduction to Electrical Discharges in Gases," Wiley, New York, 1966; A. von Engel, "Ionized Gases," Oxford Univ. Press (Clarendon), London and New York, 1965; R. G. Jahn, "Physics of Electric Propulsion," Gordon & Breach, New York, 1970.
6. R. P. Vahrenkamp, *AIAA Pap. No.* 73-1057 (1973).
7. Reference 1, pp. 35-36.
8. Reference 1, pp. 26-32.
9. Reference 1, pp. 36-39.
10. J. F. Mahoney, A. Y. Yahiku, H. L. Daley, R. D. Moore, and J. Perel, *J. Appl. Phys.* 40, 5101 (1969); V. E. Krohn and G. R. Ringo, *Appl. Phys. Lett.* 27, 479 (1975).
11. F. M. Penning, *Physica (Utrecht)* 4, 71 (1937); J. P. Flemming, *J. Vac. Sci. Technol.* 12, 1369 (1975).
12. J. R. J. Bennett, *IEEE Trans. Nucl. Sci.* NS-19, 48 (1972).
13. D. Halliday and R. Resnick, "Physics," Part 2, p. 816, Wiley, New York, 1968.
14. Reference 5, pp. 62-63.
15. Reference 1, p. 100.
16. K. Witmaack and F. Schulz, *J. Vac. Sci. Technol.* 10, 918 (1973); C. E. Carlston and G. D. Magnuson, *Rev. Sci. Instrum.* 33, 905 (1962); B. L. Crowder and N. A. Penbre, *Rev. Sci. Instrum.* 40, 170 (1969).
17. H. R. Kaufman and P. D. Reader, *Am. Rocket Soc. [Pap.] No.* 1374-60 (1960).
18. P. D. Reader and H. R. Kaufman, *J. Vac. Sci. Technol.* 12, 1344 (1975).
19. R. S. Robinson and H. R. Kaufman, *AIAA Pap. No.* 76-1016 (1976).
20. Ion Tech, Inc., Fort Collins, Colorado.
21. W. D. Ramsey, *J. Spacecr.* 9, 318 (1972).
22. M. von Ardenne, "Tabellen der Elektronenphysik. Ionenphysik und Ultramikroskopie," p. 554, Disch. Verlag Wiss., Berlin, 1956.
23. G. R. Brewer, M. R. Currie, and R. C. Knechtli, *Proc. IRE* 49, 1789 (1961).
24. W. A. Scaife, P. R. Hanley, and K. H. Purser, *Proc. Int. Conf. Nucl. Target Dev. Soc., 4th, Argonne, Ill.*, p. 75 (1975).
25. B. S. Burton, Jr., in "Electrostatic Propulsion" (D. B. Langmuir, E. Stuhlinger, and J. M. Sellen, Jr., eds.), Progress in Astronautics and Rocketry, Vol. 5, pp. 21-50, Academic Press, New York, 1961; M. G. Beigeri, M. S. Bhatia, and T. P. David, *Nucl. Instrum. Methods* 128, 29 (1975); N. B. Brooks, P. H. Rose, A. B. Wittkower, and R. P. Bastide, *Rev. Sci. Instrum.* 35, 894 (1964).

II-5. ION BEAM DEPOSITION

26. R. A. Dugdale, *Proc. Int. Conf. Phenom. Ioniz. Gases*, 7th, Belgrade 3, 334 (1965).
27. P. H. Schmidt, R. N. Castellano, and E. G. Spencer, *Solid State Technol.* 15, 27 (1972).
28. R. Schnitzer and F. C. Engesser, *Rev. Sci. Instrum.* 47, 1219 (1976).
29. R. K. Fitch, T. Mulvey, W. J. Thatcher, and A. H. McIlraith, *J. Phys. D* 3, 1399 (1970); R. K. Fitch, A. M. Ghander, G. J. Rushon, and R. Singh, *Jpn. J. Appl. Phys., Suppl.* 2, Part 1, 411 (1974).
30. H. G. Mattes, *Rev. Sci. Instrum.* 45, 1030 (1974).
31. J. Amano, P. Bryce, and R. P. W. Lawson, *J. Vac. Sci. Technol.* 13, 591 (1976).
32. Y. Namba and T. Mori, *J. Vac. Sci. Technol.* 13, 693 (1976); T. Terada, *J. Phys. D* 5, 756 (1972); Y. Murayama, *J. Vac. Sci. Technol.* 12, 876 (1975).
33. T. Takagi, I. Yamada, and A. Sasaki, *J. Vac. Sci. Technol.* 12, 1128 (1975).
34. J. Anier, E. Baron, M. Briant, A. Cabrespine, A. Liebe, A. Serafini, and T. Thon, *Nucl. Instrum. Methods* 124, 157 (1975); E. D. Donets, *IEEE Trans. Nucl. Sci.* NS-23, No. 2, 897 (1976); R. Geller, *IEEE Trans. Nucl. Sci.* NS-23, No. 2, 904 (1976).
35. R. Middleton and C. T. Adams, *Nucl. Instrum. Methods* 118, 329 (1974).
36. A. S. Kuchero, L. S. Lebedev, and A. V. Orlovskii, *Prib. Tech. Eksp.* 4, 21 (1975).
37. C. C. Tsai, W. L. Stirling, and F. M. Ryan, *Rev. Sci. Instrum.* 48, 651 (1977); R. C. Davis, O. B. Morgan, L. D. Stewart, and W. L. Stirling, *Rev. Sci. Instrum.* 43, 278 (1972).
38. C. D. Child, *Phys. Rev.* 32, 492 (1911).
39. H. R. Kaufman, *AIAA Pap. No.* 75-430 (1975).
40. W. Laznovsky, *Res. Dev. August*, p. 47 (1975).
41. G. Aston, *NASA Contract. Rep. CR-135034* (1976).
42. Reference 1, pp. 156-158.
43. Reference 1, pp. 207-213.
44. Reference 1, pp. 213-227.
- 44a. P. D. Reader, D. P. White, and G. C. Isaacson, *Symp. Electron. Ion Photon Beam Technol. 14th, Palo Alto, Calif.*, 1977.
45. W. D. Westwood and S. J. Ingrej, *J. Vac. Sci. Technol.* 13, 104 (1976).
46. R. N. Castellano, M. R. Notis, and G. W. Simmons, *Vacuum* 27, 109 (1977).
47. L. Maissel, in "Handbook of Thin Film Technology" (L. I. Maissel and R. Glang, eds.), p. 4-3, McGraw-Hill, New York, 1970.
48. J. H. Ormond, *Rev. Sci. Instrum.* 40, 1247 (1969).
49. G. A. Harrower, *Rev. Sci. Instrum.* 26, 850 (1955).
50. J. W. Coburn, *Rev. Sci. Instrum.* 41, 1219 (1970).
51. J. J. Hanak and J. P. Pellicane, *J. Vac. Sci. Technol.* 13, 406 (1976).
- 51a. C. Weissmantel and G. Gauthern, "Ion Beam Etching, Sputtering and Plating," Elsevier, Amsterdam, 1978; C. Weissmantel, *Proc. Int. Vac. Congr. 7th, Vienna, 1977*.
- 51b. E. G. Spencer and P. H. Schmidt, *J. Vac. Sci. Technol.* 8, S52 (1971).
52. Veeco Instruments, Inc., Plainview, New York.
53. General Ionex Corp., Ipswich, Massachusetts.
54. K. L. Chopra and M. R. Randlett, *Rev. Sci. Instrum.* 38, 1147 (1967); K. L. Chopra, M. R. Randlett, and R. H. Duff, *Philos. Mag.* 16, 261 (1967).
- 54a. H. F. Winters, *Adv. Chem. Ser.* 158, 1 (1976).
- 54b. H. Oechsner, *Appl. Phys.* 8, 185 (1975).
55. P. Sigmund, *Phys. Rev.* 184, 383 (1969).
56. N. Laegreid and G. K. Wehner, *J. Appl. Phys.* 32, 365 (1961).
57. H. H. Andersen and H. L. Bay, *Radiat. Eff.* 19, 139 (1973).
58. H. Oechsner, *Z. Phys.* 261, 37 (1973).
59. G. K. Wehner and G. S. Anderson, in "Handbook of Thin Film Technology" (L. I. Maissel and R. Glang, eds.), p. 3-23, McGraw-Hill, New York, 1970.

60. P. H. Schmidt, R. N. Castellano, H. Barz, A. S. Cooper, and E. G. Spencer, *J. Appl. Phys.* **44**, 1833 (1973).
- 60a. B. M. Gurmin, Y. A. Ryzhov, and I. I. Skharban, *Bull. Acad. Sci. USSR, Phys. Ser.* **33**, 752 (1969).
61. B. Navinsek, *Prog. Surf. Sci.* **7**, 49 (1976).
62. E. Gillam, *J. Phys. Chem. Solids* **11**, 55 (1959).
- 62a. G. Gautherin, C. Schwebel, and C. Weissmantel, *Proc. Int. Vac. Congr. 7th, Vienna, 1977*.
- 62b. R. Olson and G. K. Wehmer, *J. Vac. Sci. Technol.* **14**, 319 (1977).
- 62c. E. V. Kornelsen, *Can. J. Phys.* **42**, 364 (1964).
- 62d. H. F. Winters and D. Horne, *Phys. Rev. B* **10**, 55 (1974).
63. H. J. Hanneberg, M. Weidner, G. Hecht, and C. Weissmantel, *Thin Solid Films* **33**, 29 (1976).
64. D. M. Sherman and T. E. Hutchinson, *Rev. Sci. Instrum.* **43**, 1793 (1972); D. M. Sherman, J. S. Maa, and T. E. Hutchinson, *J. Vac. Sci. Technol.* **10**, 155 (1973).
65. C. Weissmantel, O. Fiedler, G. Hecht, and G. Reisse, *Thin Solid Films* **13**, 359 (1972).
66. W. R. Hudson, *NASA Tech. Memo. TM X-73511* (1976).
67. R. N. Castellano, *Thin Solid Films* **46**, 213 (1977).
68. C. Weissmantel, *Thin Solid Films* **32**, 11 (1976).
69. J. B. DuBow, D. E. Burk, and J. R. Sites, *Appl. Phys. Lett.* **29**, 494 (1976).
70. A. R. Wolter, *Proc. Microelectron. Symp.*, 4th, IEEE, St. Louis, Mo. p. 2A-1 (1965).
71. S. Aisenberg and R. Chabot, *J. Appl. Phys.* **42**, 2953 (1971).
72. E. G. Spencer, P. H. Schmidt, D. C. Joy, and F. J. Sansalone, *Appl. Phys. Lett.* **29**, 118 (1976).
73. W. H. Hayward and A. R. Wolter, *J. Appl. Phys.* **40**, 2911 (1969).
- 73a. O. Almen and G. Bruce, *Nucl. Instrum. Methods* **11**, 257 (1961).
74. R. B. Fair, *J. Appl. Phys.* **42**, 3176 (1971); R. B. Fair, Ph.D. Thesis, Duke Univ., Durham, North Carolina, 1969.
75. J. S. Colligon, W. A. Grant, J. S. Williams, and R. P. W. Lawson, *Inst. Phys. Conf. Ser.* No. 28, p. 357 (1976).
76. Reference 1, p. 141.
77. J. Amano and R. P. W. Lawson, *J. Vac. Sci. Technol.* **14**, 831 (1977); J. Amano and R. P. W. Lawson, *J. Vac. Sci. Technol.* **14**, 836 (1977).
78. B. A. Probyn, *J. Phys. D* **1**, 457 (1968).
79. S. Aisenberg, *J. Vac. Sci. Technol.* **5**, 172 (1968).
80. S. Aisenberg and R. W. Chabot, *AFCRL-TR-73-0176*. Air Force Cambridge Res. Lab., Bedford, Massachusetts (1973).
81. J. A. Van den Berg and D. G. Armour, *Vacuum*, **27**, 27 (1977).
82. M. Watanabe and A. Tōoi, *Jpn. J. Appl. Phys.* **5**, 737 (1966); V. P. Asakhov, T. B. Karashev, and R. M. Aranovich, *Sov. Phys.—Semicond.* **4**, 1826 (1971); B. Strizker and W. Buckel, *Z. Phys.* **257**, 1 (1972).
83. J. S. Sovey, *NASA Tech. Memo. TM X-73509* (1976).